Università degli Studi di Cagliari

Ph.D. DEGREE
Ph.D. in Industrial Engineering
Cycle XXXIV

Ph.D. THESIS

NONLINEAR ACOUSTIC TECHNIQUES FOR IMPACT DAMAGE DETECTION IN COMPOSITE MATERIALS

S.S.D ING-IND/14 Mechanical Design and Machine Construction

Ph.D. student: Gabriela Loi

Supervisor: Prof. Francesco Aymerich;
                          Prof. Lukas Pieczonka

Final examination academic year 2020/2021

Thesis defense: April 2022 Session

Introduction

Abstract

Due to their high stiffness–to–mass ratio and good resistance to fatigue and corrosion, fiber-reinforced materials have been intensively used in several engineering branches, such as the automotive and aeronautic industries. Nevertheless, their low resistance to low-velocity impacts may question their wide use in critical load-bearing structures and components. Events like the drop of a maintenance tool, hailing, or bird strikes may result in the emergence of small and barely visible levels of internal damage. Although not severe enough to lead to the immediate failure of the inspected component, the impact-induced damage may entail a decrease in its stiffness and strength and, thus, compromise its load-bearing capability. The need to detect the onset of internal damage has led to an ever-rising interest in Structural Health Monitoring (SHM), i.e., an emerging engineering field that keeps the promise of a continuous assessment of the component health and its remaining service life. Nowadays, although the underlying physics is still not clear, the SHM approaches based on nonlinear acoustic phenomena and, thus, exploiting the perturbation induced by internal cracks on the propagation of an impinging wave (e.g., the emergence of additional spectral components, phase shift, and scattering) are widely used to provide information on the structural integrity of composite materials. In this perspective, this thesis focuses on two nonlinear acoustics techniques, namely the Scaling Subtraction Method (SSM) and the Nonlinear Vibro-Acoustic Modulation (VAM), to further assess their effectiveness in detecting the occurrence of impact damage in composite beams.

The Scaling Subtraction Method accounts for the global nonlinear content of the response of the inspected component to infer information on its integrity and ability to withstand critical loads. Mainly applied to granular materials, the Scaling Subtraction Method was proven to be effective in identifying the onset of internal damage also in metals and composite materials. However, the quality of the indication provided was highly affected by the selection of the interrogating frequency, usually chosen among the resonance frequencies of the inspected system. The need for preliminary modal analysis and, at once, the lack of a robust algorithm to pick the resonance with the highest sensitivity to damage prevent the SSM from

being a viable and reliable NDT tool. In an attempt to overcome both these limitations, this thesis proposes a novel SSM-based approach relying on the use of a broadband impulsive excitation. By alternatively driving a composite laminated beam through impulsive or pure-tone harmonic excitations tuned at different natural frequencies in both pristine and damaged conditions, the pulse-based SSM approach was shown to be a rather promising option for identifying the nonlinearities arising from the occurrence of low-velocity impact damage in composite materials.

The Nonlinear Vibro-Acoustic Modulation (VAM) relies upon simultaneously driving the inspected structure with two waves of distinct frequencies and amplitudes. The presence of material discontinuities perturbates the propagation of the two impinging waves leading to the emergence of modulation sidebands that are exploited to infer information on the structural integrity of the monitored sample. In recent years, the analysis of modulation sidebands has been successfully applied to detect the onset of internal damage in both metal and non-metallic structures. Nonetheless, since some critical issues still have to be faced, this thesis aims to further assess whether the selection of some testing parameters, e.g., the choice of the frequency of both the pump and the probe frequency, the sensing-actuation scenario, and boundary conditions, may affect the effectiveness and the sensitivity of the Nonlinear Vibro-Acoustic Modulation. For this purpose, an experimental campaign in which three laminated composite beams have been subjected to multiple low-velocity transverse impact loads to induce the emergence of a pattern of modulation sidebands around the probe frequency peak has been conducted. The obtained results showed that the amplitude of the modulation sidebands tends to increase with the damage severity, confirming the overall ability of the Nonlinear Vibro-Acoustic Modulation to detect the onset of impact-induced damage and rank its severity. However, the trial of a set of pump frequencies revealed the Nonlinear VAM to be highly sensitive to the selected natural frequency. Similarly, the pump excitation amplitude was shown to affect the quality of the provided indications. In addition, the method capability to characterize the changes in the inspected sample integrity slightly varied with the considered sensing-actuation scenario, even though it was the sensor positioning to be found the factor susceptible to affect the method performance to a greater extent.

Introduction

Index

Introduction

Introduction

Introduction

Multilayered fiber-reinforced materials offer many advantages over more conventional materials, such as good resistance to fatigue and corrosion and high flexibility in design, which translates in the chance to tailor the material to withstand preferentially loads along specific directions. Moreover, the high stiffness–to–mass ratio makes them the primary choice in those applications in which lightweight structures lead to a significant reduction of maintenance, fuel, and operational costs. Nevertheless, their high susceptibility to impact damage may question their use in critical load-bearing applications. In contrast to metallic (i.e., steel and aluminum) structures, low-velocity impacts generated through contact with objects during flights or routine maintenance may result in some level of damage. Therefore, events like hailing, bird strikes, or a tool drop might trigger the onset of delaminations and cracks, which will also entail a stiffness or strength decrease and a reduction of the load-bearing capability. If not detected in due time, flaws and cracks may spread out during service operations. As a result, structural failures may occur. The poor and deficient quality of both the inspection and maintenance programs were recognized to be the reasons behind several aircraft accidents, like the Japan Airlines Flight 123 (figure 1, [1]) in 1985, the Aloha Airlines Flight 243 (figure 2, [2]) in 1988 and the China Airlines Flight 611 [3], that occurred in 2002.

Figure 1. Debris of the Japan AirLines Flight 123.
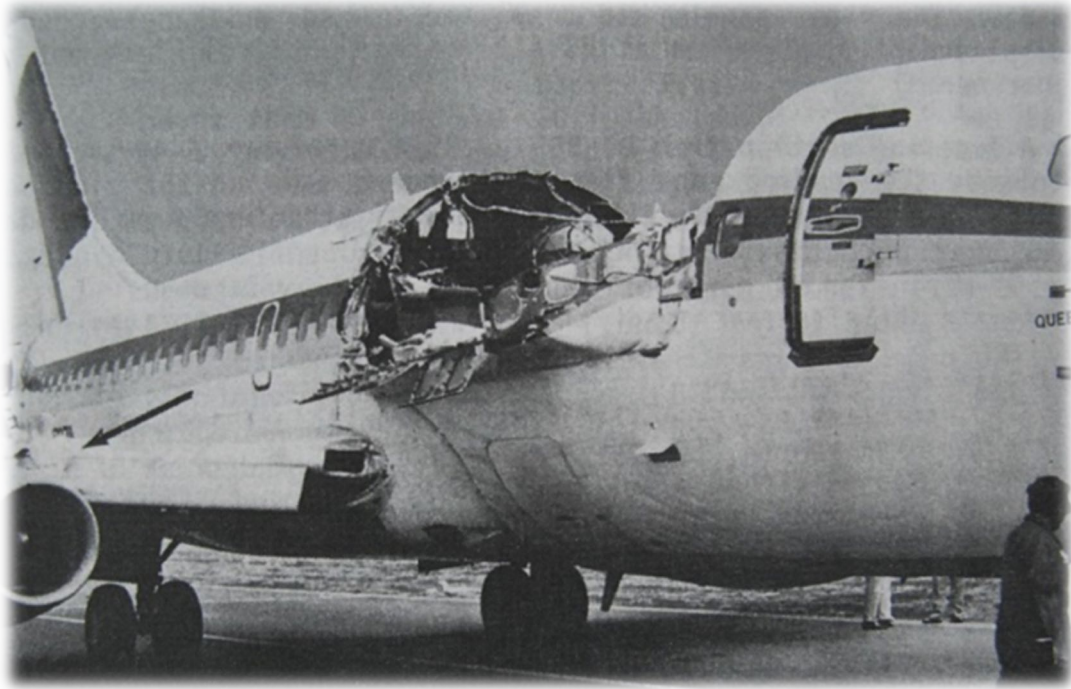
Figure 2. Fuselage remains after the emergency landing of the *Aloha Airlines Flight 243* [2]*.*

The wide use of composite materials in primary structures has brought out the problem of assessing the integrity of load-bearing structures and their ability to bear service loads. Assuring the desired performance and safety requirements is an extremely complex task that concerns both new and existing aging structures and infrastructures. To address this problem many Non-Destructive Testing (NDT) techniques have been proposed, e.g., liquid penetrant testing, eddy current, visual inspection, x-ray, radiography, ultrasonic testing, and shearography [4] [5]. Nevertheless, these techniques are still time-consuming, labor-intensive, and expensive. Furthermore, the extensive application of advanced materials helped to increase both the complexity and the accuracy of the damage detection process due to the material anisotropy, the insulating properties of the matrix, the fibers conductivity, and the occurrence of damage beneath the laminate surface, making it not easily detectable. Therefore, the need to prevent catastrophic failures has led several branches, such as the aeronautic and chemical industry, automotive, and civil engineering, to gain interest in Structural Health Monitoring.

Introduction

Based on sensors embedded within a structure, Structural Health Monitoring (SHM) is an emerging engineering field that aims to detect the presence of damage and, at one time, to continuously assess the structural integrity [6] [7] [8]. By providing a real-time diagnosis/prognosis on the component status, the SHM methods keep the promise to reduce the maintenance costs, the machine service downtime, and, above all, to enhance both the reliability and the safety of critical structures and components. Nowadays, the SHM techniques based on guided ultrasonic waves are the most adopted when dealing with composite materials on account of their ability to inspect large structural areas with a relatively small number of transducers.

The presence of internal cracks may perturbate the propagation of an impinging wave, leading to the onset of specific features that can be used for damage detection. Wave attenuation, reflection, refraction, and scattering are just some of the signal features that can be monitored to provide information on the presence of internal damage. Nevertheless, the obtained results are often ambiguous, making it difficult to assess whether the observed wave alterations are triggered by the presence of damage or other factors (i.e., varying thicknesses or changes in operational/environmental conditions). Consequently, a baseline measurement representing the system response in undamaged conditions is required for reference. The application of the linear acoustic analysis generally allows to relate the changes in wave scattering pattern and wave attenuation to the crack geometry. However, even if large defects may significantly affect the system response, early-stage defects may not result in any detectable effect and may subsequently go undetected. Thus, it can be stated that both the efficiency and the sensitivity of the linear methodologies are not sufficient to retrieve the presence of microscopic defects and different approaches are needed.

In light of these challenges, nonlinear acoustic and ultrasonic phenomena have proven to be more sensitive to the presence of early-stage damage than their linear counterparts. Small severity damage might generate nonlinear effects whose amplitude can be orders of magnitude higher than that of the pristine material inherent nonlinearities. Even though the physics underlying the mechanisms involved is still not clear, these nonlinear methodologies rely on the failure of the superposition

principle, according to which two waves occupying the same space at the same time superimpose without one wave affecting the other. Therefore, material nonlinearity may cause wave distortion, leading to the onset of additional frequency components that are not part of the original excitation signal and that may infer useful information about the integrity of the inspected component or structure.

This thesis aims to further investigate and to assess the reliability and the efficiency of a couple of nonlinear acoustic methods, i.e., scaling subtraction method, and nonlinear vibro-acoustic modulation, to detect and characterize low-velocity impact damage in composite laminated. Hence, the primary objectives of this thesis are to:

- Identify literature gaps associated to the selected nonlinear approaches to drive the research effort on pertinent areas.
- Further understand the current limitations of the selected nonlinear methods.
- Apply the considered nonlinear approaches for damage detection and characterization in laminated composite beams, to exploit the effects of low-velocity impact damage on the generation of nonlinear effects.
- Investigate the influence of different analysis parameters, such as the shape of the excitation signal, measurement methodologies, actuating system, and transducer positioning, that may affect the reliability and the sensitivity of these nonlinear methods.

Chapter 1

Damage and failure in composite materials

The application of composite materials dates backs to ancient times. As early as 3000 B.C., the African civilizations (i.e., Egyptians) used to embed straw into mud bricks to prevent shrinkage cracks and, at once, improve their tensile strength. Although mud-straw bricks still remain one of the first applications of composite materials, they could not be further from the current high-performance composites, which mainly consist of a fibrous reinforcement (i.e., long carbon fibers) embedded within a polymeric matrix (i.e., a toughened epoxy resin). In the last few decades, due to significant progress in material science and technology, the use of advanced composites as a primary structural material has sharply increased (figure 1.1), ending
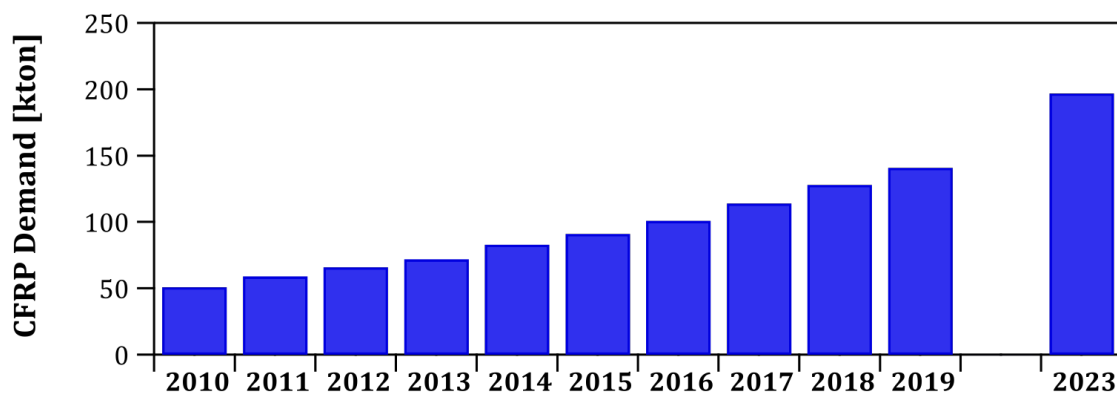
Figure 1.1 – Development of the global demand for CFRP (from *Composite Market Report 2019 – The global CF- und CC-market 2019*. M. Sauer, Carbon Composites e.V.).
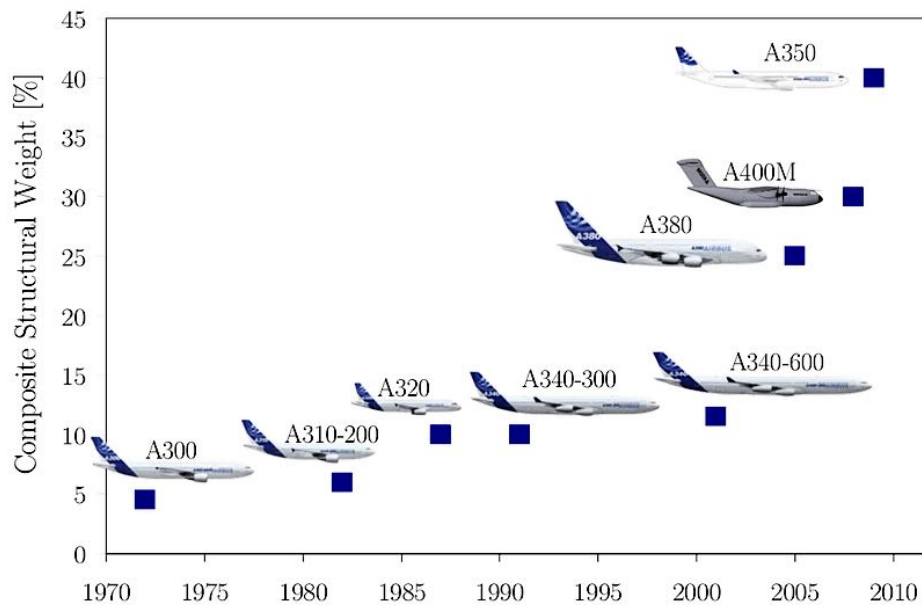
Figure 1.2 – Evolution of the Airbus aircrafts: relative composite weight [9].

up including a wide range of application fields, such as architecture, automotive, energy, infrastructure, and medicine. Nonetheless, the benefits of the massive use of high-performance composites became immediately evident in the aerospace field, in which an ever-rising fraction of the total weight of an aircraft is manufactured from advanced composites materials (figure 1.2). In fact, in the aerospace industry, the high mechanical properties of composites (i.e., high stiffness and good resistance to fatigue and corrosion) allowed the design of lightweight structures and components, whose constituent materials were tailored to achieve the optimum strength along the primary load paths. However, the high susceptibility of aerospace composites to low-velocity impact damage may question their usage in critical load-bearing applications. Impact events (e.g., the drop of a hand tool, hail impact, and bird strike) might trigger the onset of barely visible impact damage (BVID), which results in a sharp degradation of the material properties. In this context, the need to satisfy the stringent security requirements of the aerospace industry to prevent human losses and ensure an adequate residual strength at the end of the composite structures service-life resulted in an extensive research effort to characterize both the damage

initiation and its progression. Unlike metallic components whose failure mainly occurs due to the initiation of a fatigue crack that under in-service cycling-loads propagates up to critical dimensions, composite materials fail accordingly to a multiscale process consisting of a succession of several events that gradually spread over an increasing volume of material. Thus, the failure of a composite structure or component arises from the emergence of different damage mechanisms, which are not still completely understood.

1.1   Composite materials

Composite materials result from the combination of two phases, which mutually contribute to determine mechanical and physical properties that, impossible to be achieved with either of the constitutive phase alone, best fit the requirements of the specific loading conditions. Despite their intimate bond, the two constitutive elements retain both their physical and chemical identity owing to the presence of a distinct interface between them. As a matter of fact, that is the chance to easily recognize the material constitutive phases to distinguish aerospace composites from metallic alloys, in which the alloying elements are so intimately linked to make it impossible to identify them.

In a composite structure, the matrix and the reinforcement accomplish specific functions. In fact, if the load-carrying capacity of a composite component almost relies upon the fibers that, pursuant to the high volume fraction, constitute almost the entire structure volume, the matrix keeps the fibrous reinforcement located and oriented along the desired directions, enabling the load transfer between adjacent fibers, and, at once, provides a barrier against adverse environments (i.e., chemicals, moisture, elevated temperatures) and mechanical degradation (e.g., by abrasion). Moreover, by providing lateral support to the fibers and, thus, preventing them from buckling when compressive loads are applied, the matrix may considerably influence the compressive strength, the interlaminar and the in-plane shear properties of the composite material. Hence, the two constitutive phases, namely the fibers and the polymeric matrix, equally govern the overall properties of advanced composites and their failure behavior.
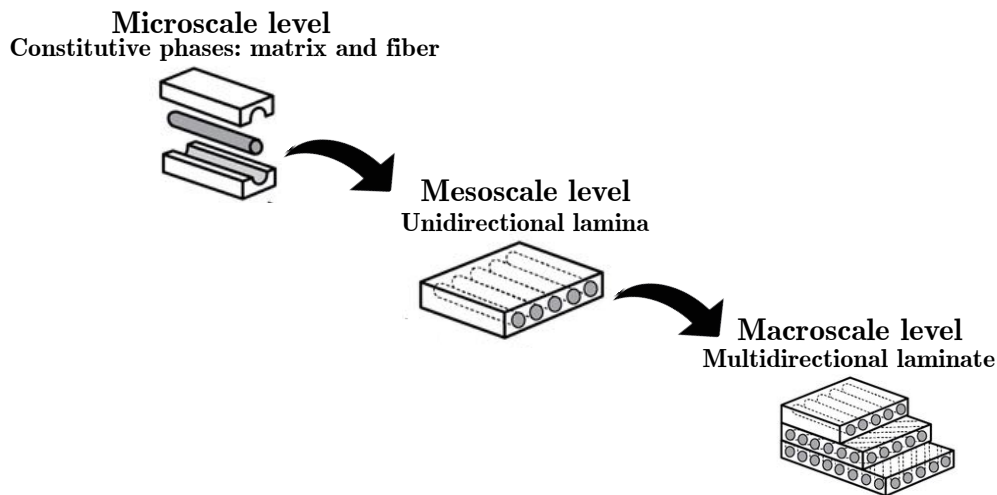
Figure 1.3 – Multiscale representation of fiber-reinforced composites (adapted from: https://compositeskn.org/KPC/index.php?title=A245&veaction=edit&section=4)

1.2   Damage in composite materials

In composite structures and components, both the emergence and the growth of internal damage rely upon the mechanisms governing the failure of its constituents and the damage progression at the fiber-matrix interfaces. Therefore, since internal damage of composite structures initiates at the length scale of the fiber diameter and then propagate over an increasing material volume, a detailed description of the failure process of a composite laminate requires a macroscale approach to provide an equally accurate description of the mechanisms, that, occurring at different length scales (figure 1.3), underlie the fracture of both the constituents and their interactions.

1.2.1 Microscale level: constitutive phases

Unlike thermosetting epoxy matrix, whose nonlinear stress-strain curve reveals a ductile response with a gradually reducing slope and high ultimate strain (figure 1.4a), the fibers behave almost linearly without undergoing significant plastic deformation before the ultimate failure occurs (figure 1.4b). However, the tensile
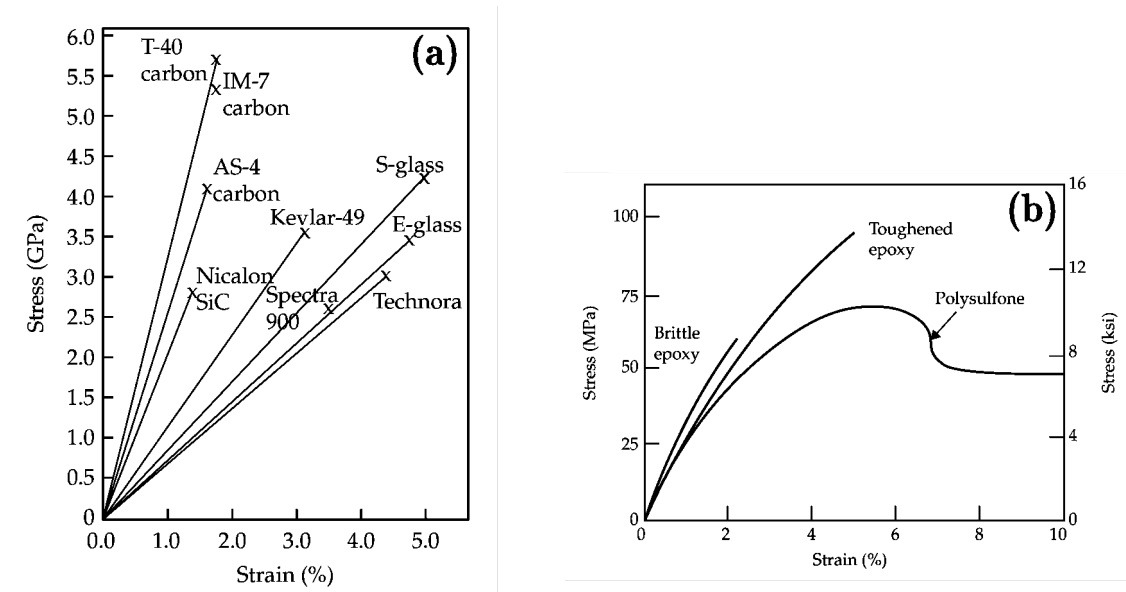
Figure 1.4 – Stress – strain curve for advanced composite constituents: (a) fiber and (b) polymeric matrix [10].

strength of the fibrous reinforcement is significantly higher (typically 50 to 100 times) than that of the matrix bulk material, whose contribution to the composite material in-plane strength is thus negligible. The high tensile strength of the fibers is mainly attributed to their filamentary form. In fact, owing to the fiber dimensions, the flaws within the material are statistically lower than within the matrix. Analogous to other brittle materials, the tensile strength of the high-performance fibrous reinforcement shows a wide statistical spread. The tensile failure stress is highly affected by the presence of weak points (e.g., flaws, voids, and defects), which might accidentally arise from fiber bundling and handling as well as fiber sliding. Since failure always occurs at the weakest point, the ultimate strength mainly depends on the largest flaw. Moreover, because both the flaw size and location randomly vary along the fiber length, the tensile strength might significantly differ from one fiber to another, with long fibers having a greater chance of breaking than shorter ones.

1.2.2 Mesoscale level: unidirectional lamina

At a mesoscopic level, a fiber-reinforced composite structure mainly consists of several laminae (also termed plies) made up of fibers embedded within an otherwise

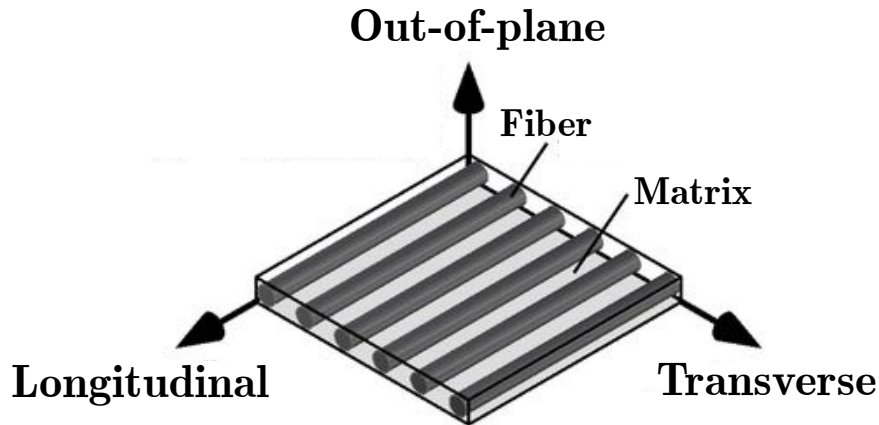**Figure 1.5 –** Unidirectional composite lamina: directions of orthotropy.

homogeneous matrix and aligned with the primary loading direction to achieve the required mechanical properties. Therefore, each ply can be regarded as a quasi-homogeneous orthotropic layer (figure 1.5) whose failure behavior relies upon several different mechanisms.

- **Longitudinal failure in tension**

    Under longitudinal tensile load, the behavior of a unidirectional composite is controlled by the ultimate strain of the fibers. In this context, the most likely damage scenario provides a fiber break leading to the establishment of an ineffective length, in which the load previously carried by the broken fiber is redistributed to the adjacent fibers [11]. Further increasing the load amplitude does not increase the size of the first failure site but triggers the onset of other localized fractures throughout the composite, whose structural integrity is gradually undermined. Nonetheless, ultimate failure occurs only when the damage sites spread over the composite volume providing a low-resistance path for fracture propagation. Depending on the fiber volume fraction, the lamina failure might result from the emergence of three damage mechanisms. In fact, while plies with low fiber-volume ratio ($v_f < 0.4$) exhibit brittle fracture, plies with intermediate filament volume fraction ($0.4 < v_f < 0.65$) undergoes a brittle fracture accompanied by filament pullout (figure 1.6). Moreover, if its fiber content is high ($v_f > 0.65$), the composite ply experiences a complex
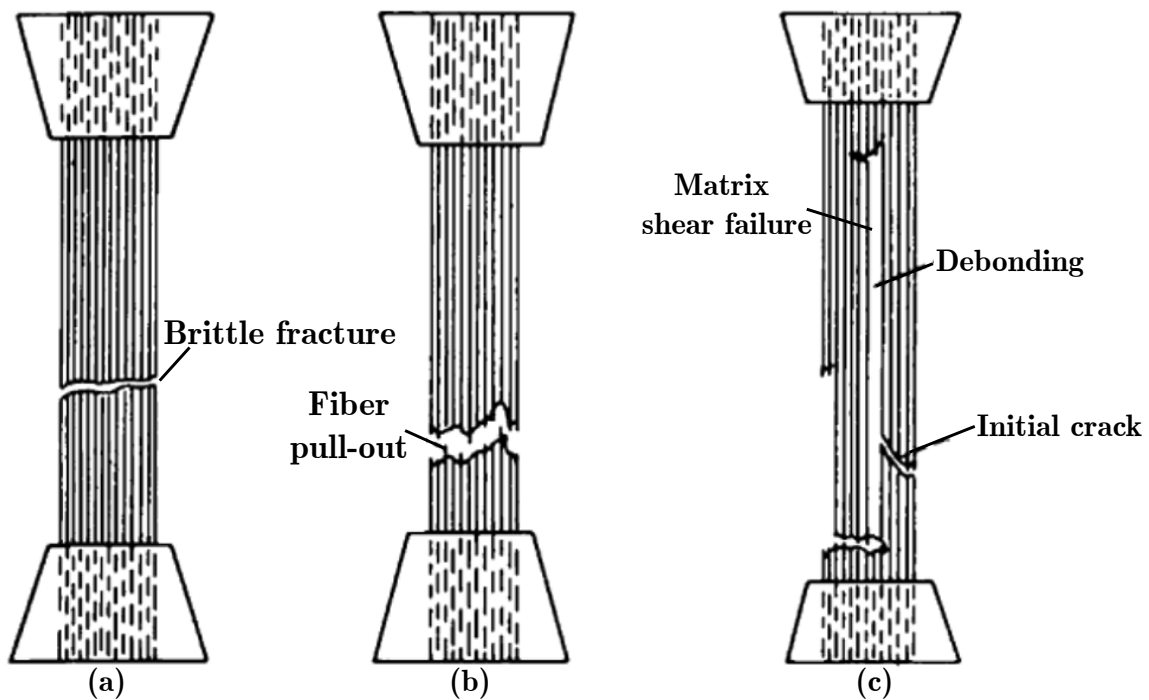
Figure 1.6 – Longitudinal failure mechanisms under tensile loads: (a) brittle facture, (b) fiber pull-out, and (c) debonding and matrix shear failure [12].

failure process, in which a brittle fracture goes together with fiber pullout, constituent debonding, or matrix shear [12] (figure 1.6).

- **Longitudinal failure in compression**

  Despite their high performance under tensile load, fatigue, and corrosion, aerospace composite materials manifest a compressive strength ranging between 50-60% of their tensile strength. Moreover, their ability to withstand compressive loads is severely affected by both stiffness and strength of the polymeric matrix and the fiber alignment. Therefore, since the early 60s, great research effort has been devoted to characterizing the failure of composite unidirectional laminate under compressive loads. Under these loading conditions, the plie failure mainly relies upon a fiber micro-buckling mechanism (also referred to as kinking), owing to which the fibers embedded within the matrix behave as elastic beams on an
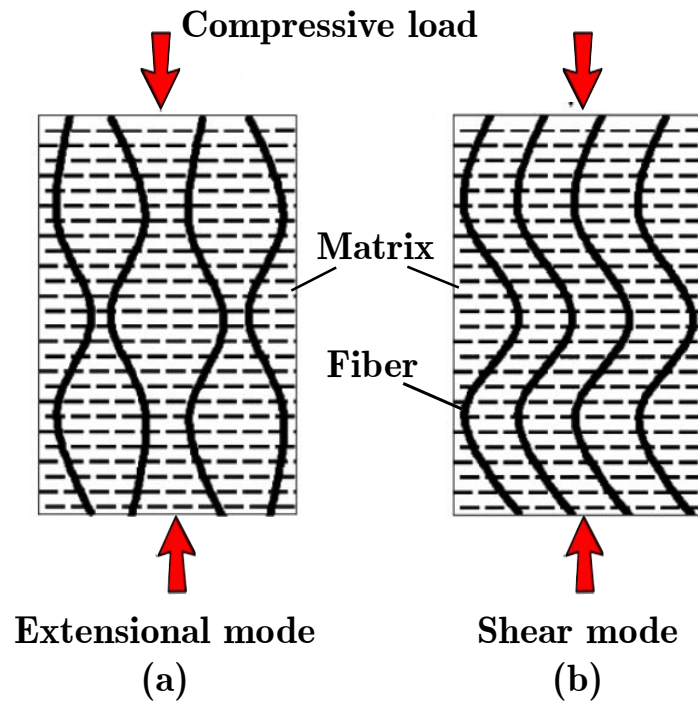
Figure 1.7 – Longitudinal failure mechanisms under compressive loads: (a) extensional micro-buckling mode and (b) shear micro-buckling mode. Adapted from [17].

elastic foundation [13]. Although affected by several factors (i.e., fiber size and shape, fiber volume fraction, fiber and matrix stiffness, fiber waviness, fiber-matrix bonding [14]), the instability at the scale of a few fibers might occur in two modes depending on the relative motion of adjacent fibers [15] [16]. In this context, when fibers buckle out of phase (figure1.7a), the points between them are no longer aligned with the fiber length but arranged in sinusoidal patterns, whose amplitude varies from zero at the midpoint between two adjacent fibers to a maximum at the fiber location. Hence, the matrix extends or contracts transversely to the fiber length undergoing a transverse or extensional buckling mode. Conversely, if the fibers buckle in phase (figure 1.7b), the matrix oscillates with the fibers. By translating perpendicularly to the fiber direction, the matrix experiences shear deformation and, thus, a shear mode occurs.

(a)   (b)
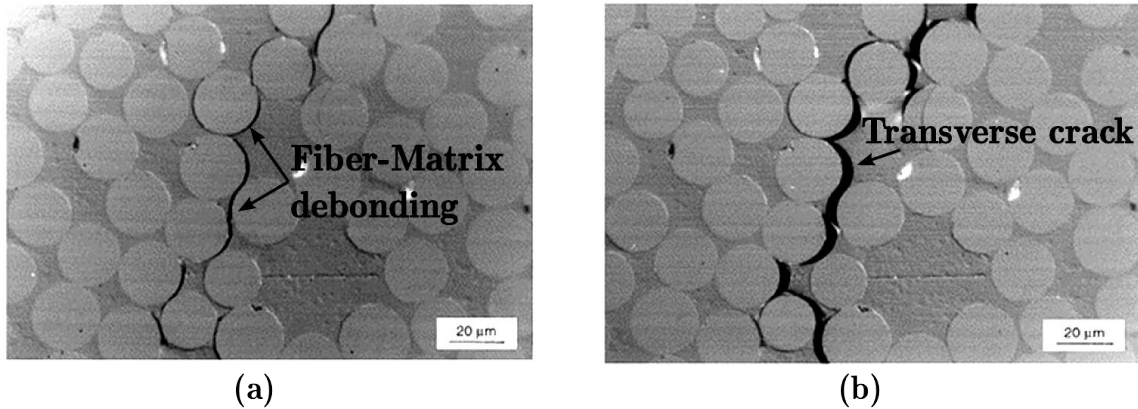
Figure 1.8 – Transverse failure under tensile loads: (a) occurrence of fiber-matrix debonding and (b) coalescence into a transverse macro-crack. Adapted from [18].

- **Transverse failure in tension**

  Under transverse tensile loads, stress related to the applied loads superimpose to those associated with matrix shrinkage during cure, hygrothermal stresses related to temperature variations, and moisture concentration within the material, inducing severe stress concentration occurring at the interface between matrix and fibrous reinforcement. Although primary local failures involve matrix cracking, interface debonding, and fiber longitudinal splitting, the damage progresses analogously to longitudinal tensile failure. In fact, after the first isolated interfacial microcracks have occurred, increases in the load intensity induced the onset of other flaws, whose coalescence into macrocracks might lead to catastrophic failure (figure 1.8).

- **Transverse failure in compression**

  In unidirectional composites, transverse compression might trigger the emergence of several failure mechanisms, including matrix compression failure, matrix shear failure, fiber/matrix interface shear failure, or fiber crushing. Compressive failure occurs in the matrix when the maximum compressive strain exceeds the ultimate compressive strain.
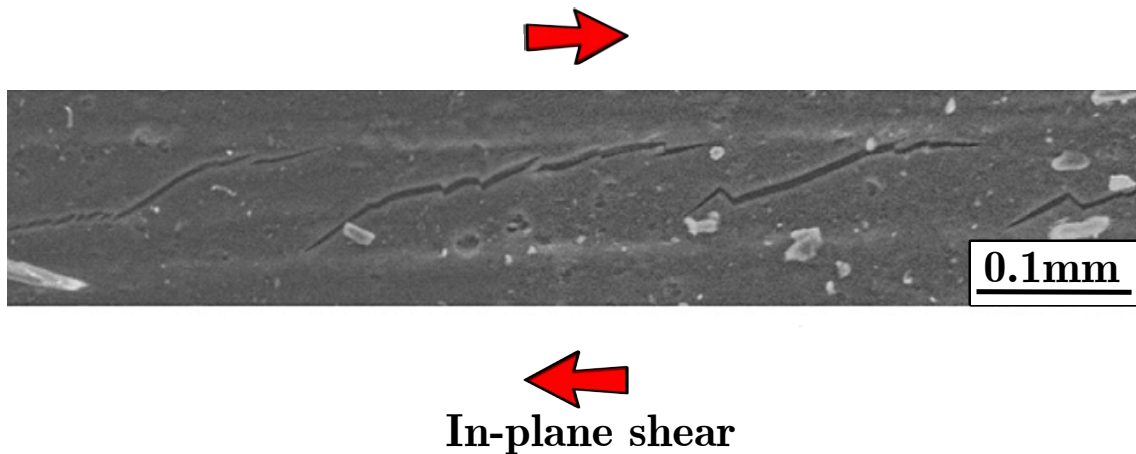
Figure 1.9 – Failure under in-plane shear: formation of an array of matrix cracks. Adapted from [22].

- **Failure through in-plane shear**

  Under in-plane shear stresses, unidirectional composites behavior is mainly governed by the strength of the matrix and that of the fiber-matrix interface. Intralaminar shear stresses result in the onset of an array of matrix cracks with a roughly sigmoidal shape that may coalesce, leading to catastrophic failure [19]. More in detail, matrix micro-cracks nucleating in a plane whose orientation to the fibers depends on the acting stress components propagate under increasing shear strains [20]. However, once the crack tips reach the fibers, the direction of propagation turns parallel to the fibers axis, leading the cracks to assume a sigmoidal shape (figure 1.9). At the fiber-matrix interface, neighboring cracks coalesce, causing the failure surface to be aligned with the fiber direction [21].

1.2.3 Macroscopic level: composite laminates

At a macroscopic level, a composite structure is made up of a homogeneous anisotropic material consisting of several plies with different orientations stacked to achieve the desired mechanical properties. Owing to the material anisotropy, the stress distribution through the component thickness varies from ply to ply. Thus, since the projection of the stress components onto the lamina orthotropy directions

varies proportionally to the load intensity, the ply failure conditions may be met, reducing both the stiffness and the strength of the laminate, but without necessarily leading to its failure. Therefore, the evolution of internal damage in a composite material is a multiscale process, whose underlying mechanisms depend on the constituent phase properties, lamination geometry, stacking sequence, discontinuities (i.e., flaws and voids), loading and environmental conditions. Nonetheless, the damage mechanisms involved in the damage of composite laminates are mainly three: (1) matrix cracking, (2) delamination, and (3) fiber breakage.

- **Matrix cracking**

  Since cracks tend to propagate along the lowest-strength path, the material anisotropy allows certain crack orientations to be preferred. In fact, due to the low load-carrying capacity of the matrix, the damage usually initiates as matrix cracks propagating parallel to the fibrous reinforcement, which might act as a crack arrester. *Matrix cracking* (also referred to as *transverse cracking*) is an intralaminar damage mechanism occurring long before the laminate fails. Nonetheless, once the matrix failure condition is met, the number of nucleating cracks increases until the matrix reaches a saturation state. Although not significantly affecting the laminate structural integrity, matrix cracking was shown to progressively reduce the stiffness and strength of the laminate [23] and change its coefficients of thermal expansion [24], moisture absorption [25], its damping [26] and the natural frequency [27]. Moreover, matrix cracking might trigger the emergence of other damage mechanisms that might significantly compromise the ability of the structure to fulfill its function, such as localized clusters of fiber fractures and delamination. In fact, stress concentration near the crack tip at the ply interface may cause either delamination [28] [29] or matrix cracking in the adjacent ply.

- **Delamination**

  Composite laminates consist of bundles of fibers that, lying in the laminate plane, do not provide any reinforcement in the thickness direction. Thus,

the laminate ability to carry loads through its thickness almost relies on the matrix. In this context, the low strength of the matrix and the high interlaminar stresses caused by the differences between the elastic properties of adjacent plies equally trigger the emergence of interlaminar damage mechanisms, especially delamination.

Activated by geometrical perturbations (e.g., complex shapes) and discontinuities (e.g., matrix cracks and free edges), *delamination* consists of a crack that, propagating within the inter-ply matrix, leads bonded plies to peel. Besides the chance to induce through-thickness failure, delamination enables transverse matrix cracks to coalesce and, thus, give rise to a wide fracture surface. Nonetheless, delamination is more harmful when impact damage is involved. Impact events might result in the onset of wide delaminations, which significantly affect the material ability to withstand in-service loads despite the absence of clear indications of damage on the composite structure surface. The growth and the extension of impact-induced delaminations rely upon two mechanisms, namely interlaminar shear, which results from contact forces, and transverse tensile cracks, whose relevance depends on the laminate thickness [30]. In fact, while interlaminar shear stress governs the damage behavior of thick composite laminates, transverse cracks become the primary damage mechanism for thin composites whose response is dominated by bending. Nevertheless, since these two mechanisms simultaneously occur, multiple delaminations occurring through the thickness join up via transverse cracks, resulting in a spiral staircase pattern of delaminations [30].

- **Fiber breakage**

  Multidirectional composites consist of bundles of fibers whose failure strain is not necessarily the same. Owing to the defect induced during the fiber fabrication process (i.e., flaws and voids) and the laminate manufacturing (e.g., accidental scratches on the fiber surface), the ultimate strength of fibers belonging to a nominally identical bundle varies accordingly to a Weibull distribution. In these conditions, fibers

progressively fail according to their place in the statistical distribution. At high strain and, especially, when other damage mechanisms emerge, the resulting isolated fiber fractures may lead to localized stress concentrations, due to which cluster of fractured fibers form compromising the laminate structural integrity.

In practical laminate configurations, none of these damage mechanisms occur in isolated modes. Engagement of various damage modes usually leads to further energy absorption during a progressive damage growth. In composite structures and components, damage usually initiates at the microscale level as matrix cracking, typically accompanied by small-scale delamination at the layer interfaces. Further increases in the load intensity result in the sequential accumulation of various types of intra- and interlaminar damage. So, matrix cracks grow to mesoscale cracks and delaminations, which eventually leads to macroscale cracks and fiber breakage.

Chapter 2

Structural Health Monitoring for composite materials

Conventionally damage is used to indicate any change introduced into the material structure or the component geometry, including variations in the boundary conditions and structural connectivity, which impair the system's ability to bear operational loads. The damage onset always occurs at the microscopic scale. Under in-service operations, micro-defects and flaws, which are present to some extent in all materials, grow and coalesce at different rates leading to macroscopic-level of damage. The damage severity increases until the system is no longer able to perform its function. Then, failure occurs.

The need to prevent catastrophic failure and human losses highlights the inspection and maintenance of existing structures as primary concerns. To both detect the presence of damage and assure the desired level of safety, a wide variety of Non-Destructive Testing and Evaluation (NDT/E) approaches has been proposed. However, the efficacy and the reliability of the available NDT techniques, whose application leads to costly and time-consuming experimental investigations, are strictly dependent on the operator skills. Furthermore, their application requires a priori knowledge of the damage location and that the portion of the structure to be inspected is readily accessible for testing. Moreover, NDT/E inspections, generally performed according to a predefined timetable, are often not sufficient to capture the evolution of the damage process. To overcome these limitations, Structural Health Monitoring approaches have been developed.

2.1 Structural Health Monitoring

Structural Health Monitoring (SHM) is an emerging interdisciplinary field that aims to design and implement a strategy for real-time continuous damage detection and characterization [31] [32]. To this purpose, SHM gathers several disciplines, such as structural dynamics, signal processing, electronics, and microelectronics, which provide essential know-how for monitoring the structure and giving at any moment both a diagnosis of the structure health and a prognosis about its remaining life. Through embedding data processing and communication systems and transducers for both sensing and actuation, SHM aims to create smart structures making nondestructive testing an integral part of the structure itself. As stated in Farrar et al. [32], Structural Health Monitoring involves observing a component during its working life, sensing its response through periodically spaced measurements, identifying, and extracting specific damage-sensitive features to assess the current state of the structure health. Therefore, in a long-term perspective, SHM leads to a periodically up-date of the information on the system behavior, i.e., assessing its ability to perform its intended function by considering structural aging, fatigue, corrosion, and degradation due to environmental conditions. Provided that the information delivered is reliable, SHM should prevent catastrophic failures and unanticipated machine downtimes, enabling to estimate the component residual life or, at least, the period between two subsequent maintenance events. Moreover, the recent development of the automation science allows to automate and repeat as often as possible the inspections and limit, at the same time, the influence of operator skills on the results interpretation.

Damage indicates any change in the material structure or the component geometry that adversely affects the system's ability to fulfill its function. However, a more precise damage definition arises from considering the structure as a system whose response depends on the applied inputs. In this context, the damage represents an additional input that induces both flow and transformation energy [33]. Consequently, damage detection is, at one time, an inverse problem, and an identification problem, in which measurable outputs have to be analyzed to identify specific damage-related features and material parameters to assess the presence of damage. Similar to classical NDT/E techniques, SHM's primary purpose is damage
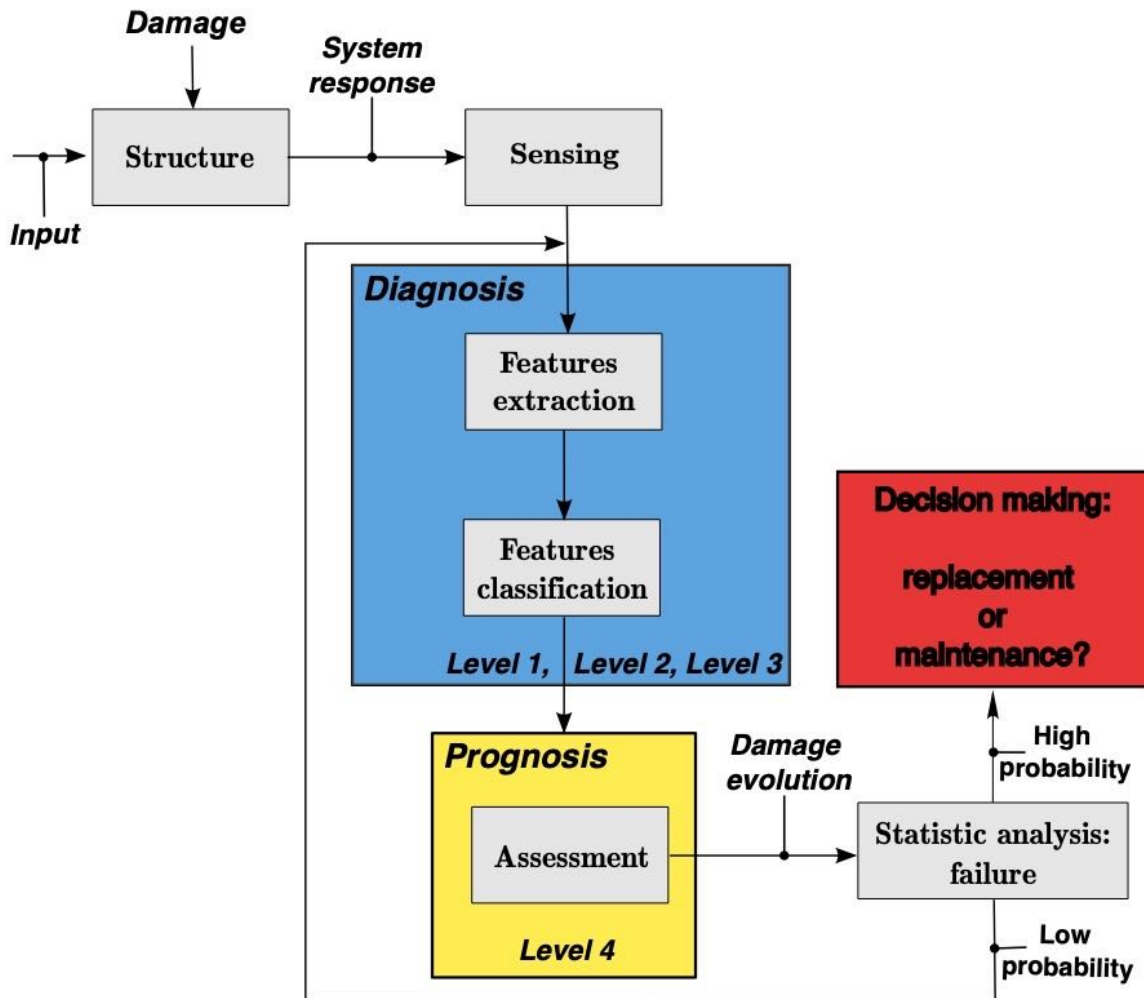
Figure 2.1 - Structural Health Monitoring process.

detection. However, SHM goes further. As reported by Farrar et al. [31], the structural health monitoring process is a four-step statistical pattern recognition paradigm, i.e., a data (pattern) classification algorithm based on either a priori knowledge or information extracted from previous patterns (e.g., groups of measurements or observations), that includes (figure 2.1):

- **Level 1. Operational evaluation**

  Operational evaluation (problem definition phase) tries to answer questions regarding the design and the implementation of a viable damage identification system, such as in-service and environmental conditions,

mode failure, and sources of possible limitation for the acquiring data system arising from the operational environment.

- **Level 2. Data acquisition**

  This second step aims to design the data acquisition system by accounting for the variables that have to be acquired and the frequency of the measurements. Therefore, it is necessary to select the excitation mode, type, number, and relative positioning of the sensing transducers as well as the acquisition and storage hardware to be used.

- **Level 3. Feature selection and extraction**

  Feature extraction deals with the identification of the damage-sensitive parameters that allow distinguishing between undamaged and damaged structures. Among the several damage features, which might exist in frequency, modal, or time domain, the best ones are application-specific. However, the SHM process generates a large amount of data making the information condensation of primary concern, especially when many measurements over the structure working life have to be compared.

- **Level 4. Statistical model definition**

  This fourth step aims to implement statistical algorithms (i.e., neural network) that operate on the extracted features to discriminate between undamaged and damaged structures and quantify the extent of the damage. Moreover, when coupled with analytical models, statistical methods may offer a better understanding of damage type and its severity as well as reduce false damage indication.

Being dedicated to the identification of the impact-induced damage in composite structure and components, this thesis only deals with the first level of the Structural Health Monitoring capability, i.e., damage detection. Thus, the following paragraphs provide a general classification of SHM strategies and a review of those commonly applied to composite materials.

2.2 Structural Health Monitoring strategies: classification

According to Doebling et al. [34], a robust damage identification scheme should preform several tasks:

- detect early-stage damage.

- identify the damage location within the used sensor resolution.

- provide information on the damage severity.

- evaluate the remaining useful life of the structure.

In addition, the method should be well-suited for automation to be independent from the operator skills and judgement. Structural Health Monitoring embraced these requirements, regardless of the underlying physical principles and the application field. The innumerable SHM approaches proposed in the last few decades may be classified in several ways.

- **Passive and active methods**

  Structural Health Monitoring methodology may fall into two categories: active and passive SHM [7], depending on whether actuators are used or not. Passive SHM mainly consists of measuring a set of operational parameters (i.e., critical loads, vibration level, stress, and acoustic emission) to infer the state of structural health. Therefore, passive SHM, which listens to the structures without interacting with them, does not directly investigate whether damage occurred or not. Conversely, active SHM attempts to address the state of structural health. To this purpose, the inspected structures are firstly excited through actuators in prescribed manners and, subsequently, interrogated by analyzing the received structural responses.

- **Local and global methods**

  This second classification relies upon the dimensional ratios between the size of the inspected area and the length of the wave or the vibration

pattern with respect to the overall dimensions of the structure. Based on this criterion, SHM methods may be divided into global SHM and local SHM [33] [35]. Global SHM is mainly concerned with monitoring the whole structure by exciting low-frequency vibrations, whose wavelength is approximately equal to the structure's overall dimension. Thus, global SHM sensitivity to early-stage damage is relatively low. Nevertheless, only limited knowledge about the critical location is sufficient to retrieve a rough estimation of the damage location through a coarse network of sensors that do not necessarily have to be located close to damage. Conversely, local SHM focuses on a small portion of the structure surrounding the sensors. In this context, excitation wavelengths smaller or in the same range of the defect size are generally needed to provide high sensitivity to early-stage damage. Moreover, local SHM requires a dense sensor network or sophisticated phased-array sensors that have to be placed close to the damaged area (i.e., the hot spot), whose location has to be known a priori knowledge.

- **Baseline and non-baseline methods**
  As stated in [36], assessing the damage presence requires a comparison between two system states, one of which is assumed to represent the system response in pristine conditions. Hence, depending on whether a reference state is considered or not, SHM methods may be divided into baseline and non-baseline approaches. Conventional structural health monitoring methods rely upon schemes where baseline signals are measured, and any retrieved change from the reference is detected and related to the onset of structural damage. Thus, a baseline measurement allows distinguishing between damaged and undamaged states. Nonetheless, if defects occur long after the reference measurement, operational and environmental conditions may induce significant changes in the system responses, potentially masking signal changes due to the initiation of structure defects [37]. To tackle this limitation non-baseline SHM (i.e., reference-free) methods have been proposed [38] [39] [40]. In this case, the baseline is no longer a system response, but an adopted

normal behavior (e.g., linear elastic model) so that any deviation from the norm allows distinguishing between damaged ad undamaged responses.

2.3 Structural Health Monitoring for damage detection in composite materials

As proof of the extensive and ever-raising interest in Structural Health Monitoring, approximately 19000 research papers have been published in the last decade. Structural Health Monitoring includes applications in several branches, such as the aeronautic and chemical industry, automotive, and civil engineering. Thus, many different approaches have been proposed to assess the state of a structure. In the following, a description of the methods commonly applied to inspect composite materials is presented.

2.3.1 Acoustic emission

Acoustic Emission (AE) is a passive Structural Health Monitoring approach that relies upon transient elastic waves generated by a sudden release of localized strain energy produced by changes in the structural integrity of material [41]. More specifically, acoustic emissions are pressure impulses caused by the deformation energy released during dynamic processes. So, when load application induces the onset of internal damage or the propagation of a pre-existing crack, the associated deformation energy propagates as vibrations. Therefore, AE consists of listening to these vibrations (figure 2.2), which may provide information on the internal deformation process, allowing real-time monitoring and making the method promising for SHM applications [42].

Even though the method was pioneered in 1950 by Kaiser, who first used electronic instrumentation to acquire the acoustic emission of metallic samples under tensile stress [43], the first applications for nondestructive testing, i.e., the inspection of a Polaris rocket motor, the analysis of the fracture behavior of single edge notched and unnotched metallic specimen [44], and pressure vessels [45], date back to the
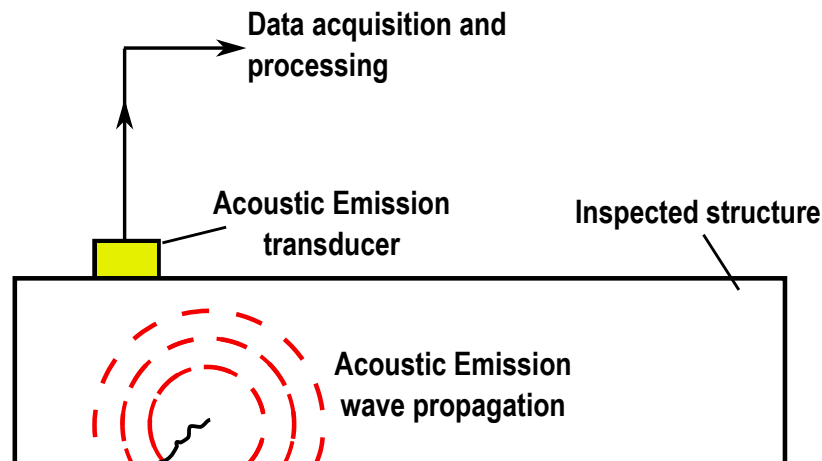
Figure 2.2 – Basic principle of Acoustic Emission method.

1960s. Later in the 1970s, research on the reliability of the acoustic emission as a viable NDT technique for fiber-reinforced polymers (FRP) started [46].

To date, applications of the acoustic emission technique to laminated composite materials include initiation and early-stage damage detection [47] [48], crack propagation under quasi-static [49] [50] [51], and dynamic loads [50] [51]. Moreover, the need to investigate and characterize the damage process of fiber-reinforced polymers led to an extensive research effort [52]. These studies highlighted the existence of four main damage mechanisms, namely matrix cracking, delamination/interfacial debonding, fiber fracture, and fiber pull-out, which may be distinguished through their acoustic signature (i.e., acoustic emission) [53] [54] [55] [56]. Approaches used to discriminate these mechanisms include energy [48] [50] [57], amplitude and frequency distribution [49] [54], wavelet analysis [49] [58], and pattern recognition [55] [56].

2.3.2 Electro – Mechanical impedance method

The electro-mechanical impedance (EMI) method is an active sensing Structural Health Monitoring approach that exploits energy transferred between the transducer and the host structure to assess its integrity. Due to the converse
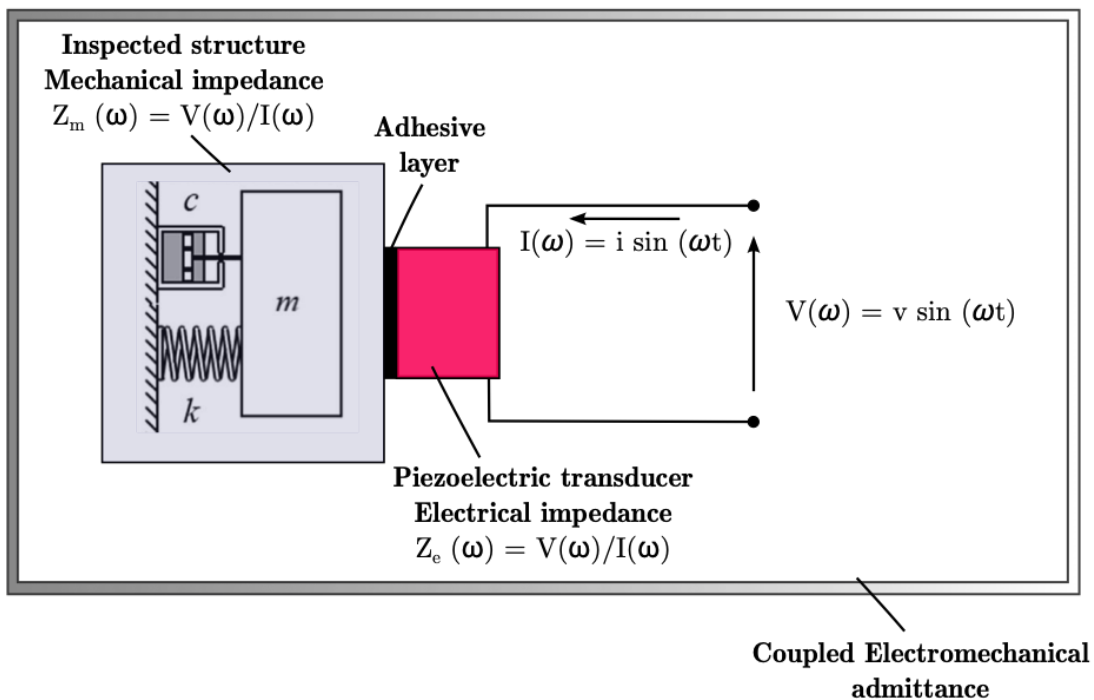
Figure 2.3 - Basic principle of Electro – Mechanical Impedance method.

piezoelectric effect, applying a harmonic voltage to a piezo-transducer results in a mechanical strain, subsequently transmitted to the bonded component. Therefore, the coupling between the sensor and the host structure allows to relate the electro-mechanical impedance, i.e., the ratio between the applied voltage and the current measured at the transducer terminals, to the mechanical impedance of the structure (figure 2.3). Since the mechanical impedance depends on material properties, boundary conditions, and structural configuration, the EMI signatures extracted from PZT sensors or wafers are affected by the presence of structural damage.

The energy transfer underlying the EMI techniques was first described by Liang et al., who presented a coupled electro-mechanical approach to investigate the energy transfer and the consumption of an active system represented as a one-degree-of-freedom PZT actuator [59]. Zhou et al. further developed this model to include a two-dimensional PZT patch actuator-driven system behavior [60]. Nonetheless, the model did not consider the influence of dynamic parameters, such as damping and inertia. Later in 2002, Giurgiutiu and Zagrai [61] developed an EMI expression that

takes into account the effect of both sensor and structural dynamics, even though the analysis was carried out only for one-dimensional structures.

In the field of Structural Health monitoring, the electro-mechanical impedance method was pioneered by Sun et al. [62], while the first application to composite materials dates back to 1995 when Chaudhry et al. investigate the local-area health monitoring of the aircraft junction between tail and fuselage [63]. In the past few decades, the EMI technique has been widely used to assess the presence of damage in both composite laminates and sandwich components [61] [64] [65] [66]. A comprehensive review of the electro-mechanical impedance technique may be found in [67] [68].

2.3.3 Vibration – based methods

Vibration-based methods are a global Structural Health Monitoring approach that exploit the structure vibration pattern to provide information on structural integrity. [69] [70] [71] [72] offer a comprehensive literature review on these methods, which received great interest due to the chance of on-line inspecting the whole structure through several types of sensors and data acquisition systems.

The underlying principle of vibration-based methods is that the presence of damage affects the structural properties, such as stiffness, mass, and damping, leading to changes in the dynamic parameters of the structure (i.e., natural frequencies, mode shapes, and modal damping) [32]. According to the type of the employed model, vibration-based techniques may fall into two classes: model-based and data-based (i.e., response) methods [72] [73]. While approaches belonging to the former class require a detailed model of the considered structure that should offer a complete description of the system dynamics, response-based methods rely upon a model describing only the part of the dynamics that can be assessed through experimentally obtained signals.

Nonetheless, a classification based on the features extracted from the vibration signal to assess the presence of damage is also possible. In this context, vibration-based methods may be divided into:

- **Natural frequencies – based methods**

  Natural frequencies are an attractive feature for damage detection and identification. In fact, the measurement of the resonance frequencies require access at few points of the system surface and is highly accurate repeatable, and not affected by experimental noise. The firsts attempt to use vibration-based methods to identify both the location and the size of the damage date back to 1978 when Adams et al. [74] exploited the natural frequencies of a one-dimensional component to detect the presence of damage. One year later, Cawley and Adams [75] presented an approach for damage localization based on the ratio between the measured frequency shifts of a couple of modes and those obtained from the finite element models of aluminum and carbon fiber-reinforced composite (CFRP) plate. Tracy and Pardoen [76] analyzed the influence of a midplane delamination length on the frequency shift of the first modes of a graphite-epoxy laminated beam. Subsequently, modal-sensitivity equations were used to detect and locate damage associated with transverse cracking in composite beams [77]. [78] [79] report and discuss other applications of vibration-based methods in composite beams and plates. However, these approaches are not exempt from limitations. Only severe levels of damage induce significant frequency shifts, making these techniques less sensitive than other SHM methods. Furthermore, defects of similar severity located in symmetric locations within a structure may produce similar effects on the system resonance frequency. In the same way, the presence of damage at different locations may equally influence the modal parameters of the structure. Therefore, the damage detection and location issue do not have a unique solution, especially when multiple cracks occur.

- **Mode shape – based methods**

  According to Doebling et al. [34], mode shape-based methods have been used to assess the presence of damage and its location since 1984 [80], when West et al. first applied the Modal Assurance Criteria (MAC) to

determine the level of correlation between modes of a space shuttle orbiter body flap, measured before and after the application of acoustic loading. Mode shape-based methods exploit the change in the structural vibration patterns (e.g., mode shapes) induced by damage to retrieve information on the structural integrity. Since the onset and the growth of damage affect how a structure vibrates, changes in mode shapes may be related to the damage severity or location. Hence, these approaches require baseline data, i.e., structural monitoring relies upon the analysis of different datasets: the mode shapes of the intact structure (i.e., baseline data) and those measured after the damage occurred. Unlike global approaches (e.g., natural frequencies-based methods), mode shapes-based techniques allow to gather information on the integrity of specific points or small portions of the structure, which results in higher sensitivity to local damage. Even though this high sensitivity may lead to detect and identify multiple defects, the analysis of the mode shape changes without any further signal processing or pattern recognition technique makes impossible a precise localization of defects and flaws. Moreover, the measurement of the mode shapes, which requires several sensors or a network of sensors, is more sensitive to noise effects than natural frequencies.

- **Mode shape curvature – based methods**
  In order to enhance both the sensitivity and the efficiency of the mode shape-based methods, the mode shape curvature has been investigated as a feature for damage detection since the early nineties. In 1991, Pandey et al. [81] applied a central difference approximation to calculate the mode shape curvature, i.e., the second derivative of mode shapes, suggesting that the difference of curvature mode shapes of the intact and the damaged structure may be a highly sensitive indicator for damage detection and localization. A few years later, Salawu and Williams [82] considered two procedures for locating damage and made a comparative study. To this purpose, the performance of the mode shape curvature-based approach proposed in [73] was evaluated and compared to that of the mode shape changes-based method presented in [83], in which the

damage position is identified through a graphical comparison of displacement mode shapes. The study proved the ability of the mode shape curvature-based approach to locate damage, but it also pointed out the necessity to select the proper mode shape. Later on, Wahab and De Roeck, who investigated the use of the central difference approximation, suggested that the modal curvature of the lower modes provides more reliable information on damage than that of the higher ones [84]. In the same years, Ho and Ewins investigated the ability of five methods (i.e., flexibility index, mode shape curvature, mode shape curvature square, mode shape slope, and mode shape amplitude comparison) to locate the damage, revealing that higher derivatives are more promising for damage identification [85]. However, false damage indications may arise at boundaries, nodal points, or where the quality of the measurements is relatively poor. Hanagud et al. [86] derived a mathematical relationship that relates the natural frequency changes and the modes of an undamaged and a damaged beam, allowing the identification of the location and the extent of the damage by using only the first modes of the damaged structure.

From the early 2000s, the mode shapes curvature-based methods have been applied for damage detection of composite structures. Hamey et al. [87] evaluated several damage detection algorithms in carbon/epoxy composite beams with different damage configurations using directly measured curvature mode shape (strain mode shape), showing that modal curvature measured through piezoelectric sensors may be a viable tool for damage detection. Lestari and Qiao [88] used the curvature mode shapes to detect and locate debonding and core crushing in composite honeycomb sandwich beams, while Qiao et al. [89] and Lestari et al. [90] employed this approach to detect and characterize the presence of delamination in composite laminate beams, managing to identify the existence, location, and size of delamination. More recently, He et al. [91] carried out modal analysis on undamaged and damaged composite beams with single and multiple damages of different severity. The evaluation of the curvature mode shapes differences, which were found to increase with the number

(figure 2.4) and the extent of delamination, allowed to identify damage and its severity (figure 2.5). Besides the above-mentioned methods, complex signal processing approaches, such as a two-dimensional (2D) wavelet transform, have also been applied to detect damage in composite structures [92] [93] [94] [95].
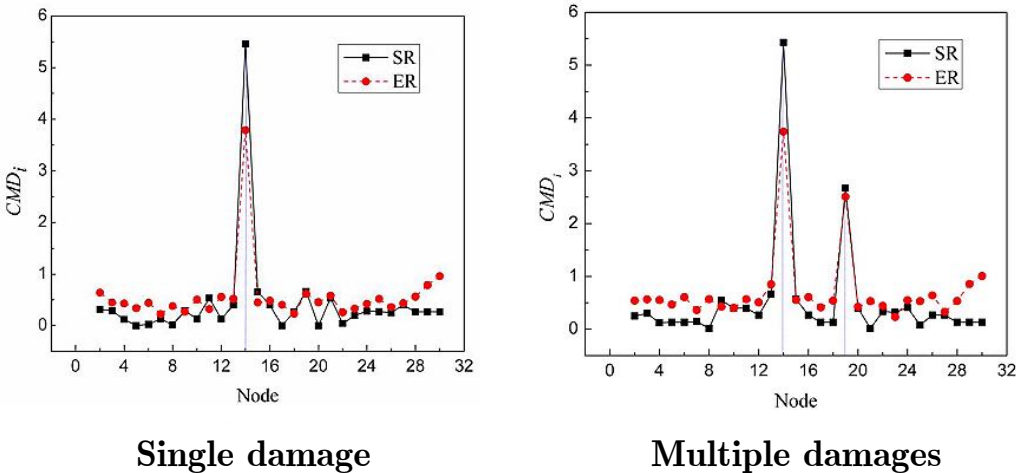
Single damage   **Multiple damages**

Figure 2.4 - The Curvature Mode Difference on composite beam with single and multiple damages: comparison between experimental (ER) and simulation (SR) results [91].
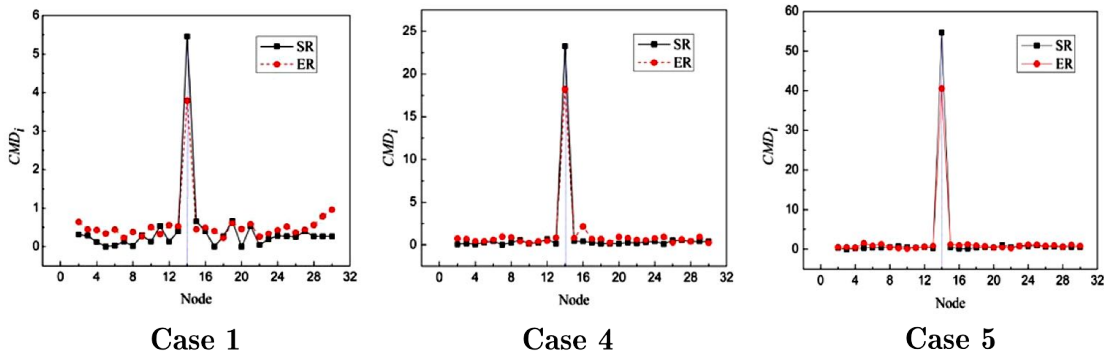
Case 1   **Case 4**   **Case 5**

Figure 2.5 - The Curvature Mode Difference on composite beam with different level of damage severity: Case 1, Case 4, and Case 5 refer to samples with one, two and three delaminations, respectively. A comparison between experimental (ER) and simulation (SR) results [91].

2.3.4 Elastic waves – based methods

Elastic wave propagation originates from the forces associated with the volume (i.e., tension and compression) and the shape (shear) deformation of a medium, whose behavior varies according to Hooke's law. The presence of material discontinuities (e.g., inclusions, flaws, crack, and delaminations) might perturbate the wave propagation pattern, leading to wave scattering, reflection, absorption, and diffraction. Non-destructive testing and evaluation methods have widely exploited these phenomena. However, since Structural Health Monitoring aims to inspect large surfaces, great attention has been devoted to waves propagating through the structure thickness, such as Rayleigh and Lamb waves.

First described by Lord Rayleigh in 1885 [96], Rayleigh waves propagate on the surface of solids components, combining a longitudinal and transverse motion to create an elliptic orbit motion. The amplitude of Rayleigh waves decays with the depth below the surface, becoming ignorable at a depth of few wavelengths. Hence, the disturbance induced by these waves is limited to a thin surface layer of the solid, whose thickness depends on the wave frequency. Nevertheless, when the thickness of this layer is smaller than one wavelength of the Rayleigh wave, Lamb waves occur. Named after Horace Lamb, who first described them in 1917 in homogeneous isotropic materials [97], Lamb waves are elastic waves existing in plate-like thin components with free edges that can propagate across large areas parallel to the direction of propagation and perpendicular to the plane of the plate at once. The resulting complex motion can be symmetrical or anti-symmetrical with respect to the plate's neutral axis (figure 2.6). Although Lamb succeeded in proving the existence of such waves, it was only in the early 1950s that Firestone and Ling managed to generate Lamb waves in plates. Nowadays, several approaches have been proposed to address the issue of Lamb waves excitation and sensing. Piezoelectric transducers imposing perturbations to the structure surface are among the most common solutions. However, the use of glued/bonded sensors, such as PZT transducer or PZT arrays, makes both the location and the arrangement of sensors crucial due to their ability to affect the sensitivity of the damage detection process. Moreover, when linear arrays are used to interrogate the region of interest, mirrored images might be produced, leading to ambiguities in damage localization [98]. Thus, aiming at further
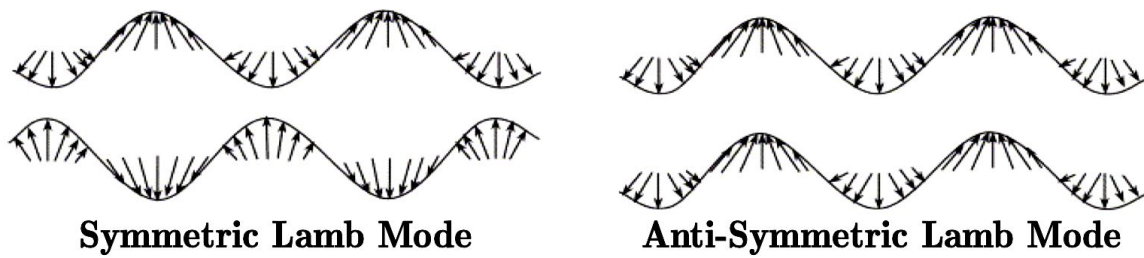
Figure 2.6 – Symmetric and anti-symmetric Lamb wave modes. Adapted from [103].

investigating these effects, various configurations, i.e., square [99], circular [100] [101], and star [102] shaped arrays, have been considered. Furthermore, good acoustic coupling between the inspected structure and sensors is of the uttermost importance to ensure the mechanical energy transfer from the transducer to the test component and vice versa. Since the acoustic impedance difference between the air and engineering materials, reflections and poor signal transmission occur at the solid/air interfaces. Even if immersing the specimen in a water bath may assure an almost perfect coupling, it turns out to be unfeasible for large structures or field inspection.

Hence, non-contact techniques for the excitation of Lamb waves have been developed. Among them, the Scanning Laser Doppler Vibrometry (SLDV) has been widely applied for wave-field analysis and visualization [98] and damage detection, i.e., debonding and delamination in composite materials [104] [105] and fatigue crack detection [106] [107]. In recent years, the ever-raising interest in intelligent and self-sensing structures, which necessitate small transducers permanently integrated into the component itself, drives the attention to Interdigital transducers (ITDs) that convert electric signals to surface acoustic/ultrasonic waves and back through the piezoelectric effect. IDTs, consisting of two interlocking comb-shaped arrays of metallic electrodes wired alternately to two electrodes and deposited on a piezoelectric substrate, meet the size requirement and result in good quality coupling at once.

The ability of Lamb waves to travel over a long distance with low energy dispersion, even in materials with a high attenuation ratio, such as carbon fiber-reinforced composites (CFRP), allows the quick inspection of broad structures and

components, as well as their elevated susceptibility to interference on the propagation path, e.g., damage or boundaries, makes them a promising and high-sensitive feature for damage detection.

The first theoretical studies on Lamb waves date back to the early 1950s when Mindlin and Onoe managed to calculate the real and the complex branches of Lamb modes in a traction-free plate [108] [109]. A few years later, Viktorov's monography (1967, [110]) focused on the physical acoustics of Rayleigh and Lamb waves isotropic elastic media, besides suggesting possible applications of both waves to materials testing. However, it was probably Worlton who pioneered the use of Lamb waves as a means of damage detection [111]. Later on, Alleyne and Cawley investigated the interaction of Lamb waves with different kinds of defects [112] and discussed the selection of appropriate Lamb modes to ease the interpretation of acquired data [113], In the same years, Lamb waves were applied to detect damage in composite materials and structures. Thus, Saravanos et al. [114] used Lamb Waves and embedded piezoelectric sensors to detect the presence of delamination in composite beams, Seale et al. [115] exploited Lamb waves capability to detect fatigue and thermal damage on laminated composite coupons, while Toyama et al. [116] investigated the sensitivity of Lamb waves to transverse cracking in glass and carbon fiber-reinforced laminates. Kessler et al. [117] explored the optimization of Lamb waves-based approaches for damage detection in composite materials, addressing the issue of determining the appropriate driving parameter (i.e., actuating frequency, pulse shape, and sensor geometry) for testing. The authors concluded that due to their high sensitivity to local effects generated by structural discontinuities, these Lamb waves-based methods might provide more information about damage detection and location than previously proposed methods, such as those based on FRFs. However, the need for an external active driving element and the complex propagation pattern, which makes data interpretation complicated, were identified as the main disadvantages of Lamb waves approaches. In the early 2000s, Su et al. [118] studied the interaction between the fundamental Lamb wave modes and delamination in carbon-fiber-reinforced laminates instrumented through piezoelectric wafers for both sensing and actuating. In the meanwhile, Sohn et al. [119] developed a wavelet-based signal processing combined with an active sensing system to produce a near real-time online monitoring system for composite structures. [71] [103] [120] present a

comprehensive review on the Lamb wave application for damage detection in composite materials and structures, while more recently published works on Lamb waves application for structural health monitoring include [121] [122] [123] [124] [125] [126].

Chapter 3

Nonlinear acoustics

3.1   Nonlinear acoustics: introduction

Conventional non-destructive testing and evaluation (NDT/E) techniques focus on the linear interaction of ultrasonic waves with inherent discontinuities, such as flaws, cracks, voids, and defects, to provide information on the presence of damage through measurements of transmission, reflection, sound velocity, and absorption of acoustic energy. The presence of discontinuities within the material micro-structure perturbate the way an impinging wave propagates through the medium, inducing several effects (i.e., variation in the phase and the amplitude of the structure response), whose magnitudes depend on the vibration amplitude.

Under the hypothesis of small vibration amplitude, an elastic continuum subjected to a pure-tone harmonic excitation follows a simple harmonic motion at the sole frequency excitation. According to Hooke's Law, the perturbation of a preexisting equilibrium state results in the onset of restoring forces, whose amplitude is proportional to the displacement entity [127]. Linear acoustics exploits the vibrations associated with the propagation of transmitted and reflected waves through the medium, enabling to relate the changes that occurred in wave scattering pattern and wave attenuation to the crack geometry. Nonetheless, the application of linear approaches allows to detect only severe damage, i.e., large delaminations, gross defects or open cracks, which represent an effective barrier to wave transmission. Hence, the sensitivity of these methods is limited to those discontinuities whose characteristic length is of the same order (or higher) of the wavelength and, thus, that can significantly change the acoustic impedance and the linear elastic properties

of the medium. However, early-stage defects (e.g., evenly distributed micro-cracks) may not perceptibly affect the response of the inspected system and consequently may not be detected. In addition, the anisotropy of composite materials, due to their laminar or multi-material nature, may lead to more complex wave pattern propagation, in which variations associated with a low level of damage are difficult to recognize and detect. In light of these challenges, nonlinear acoustic methods have been proposed and further investigated. Linear acoustics relies upon the validity of Hooke's Law, but as the amplitude vibration increases, its underlying assumption (i.e., small displacement or vibration amplitudes) is no longer valid, and the restoring forces cannot keep up with the displacement. Thus, nonlinear vibration occurs.

A wave propagating through a material may encounter micro-structure regions containing anharmonicity, i.e., imperfections of atomic lattices and/or nonsymmetric thermoelastic behavior of interfaces, which may cause the onset of nonlinear vibrations. However, all materials have some extent of inherent nonlinearity. Although inherent nonlinearities are generally small, distortion of the propagating wave may arise. Therefore, nonlinear ultrasonic methods infer information on the presence of damage and its severity by measuring the amount of nonlinearity in the material response and establish whether the observed increments exceed the level of inherent material nonlinearity. To this purpose, nonlinear ultrasonic techniques should make it possible to distinguish the damage-related nonlinearity from the inherent one. Even though the implementation of viable and reliable engineering tools requires a good understanding of the physics behind nonlinear phenomena, the mechanisms involved are still not fully understood. The reasons are mainly two: (1) different mechanisms may produce similar nonlinear effects, and vice versa, and (2) nonlinear mechanisms are intrinsically interconnected, making it almost impossible to discern them all. Moreover, nonlinearities may also arise from non-damage related factors, such as overloads, boundary conditions, connections between transducers and monitored surfaces, and instrumentation. Nonetheless, nonlinear acoustics remains a promising option for damage detection and characterization.

3.2   Nonlinear Acoustic in solids

In 2013, Klepka [33] provided a comprehensive review of the theoretical background of nonlinear acoustics, focusing on nonlinear mechanisms related to cracks in solids and that can be exploited for damage detection and characterization. In the following, nonlinear acoustic phenomena induced in solids, i.e., contact acoustic nonlinearity, higher harmonic generation, resonance frequency shift, and frequency mixing, are discussed.

3.2.1 Contact Acoustic Nonlinearity

The presence of gaps (e.g., closed cracks) into the material micro-structure perturbs the propagation of an imping acoustic wave. Moreover, the interaction between the gap surfaces, which manifests itself as repeated collisions between the gap surfaces due to propagating acoustic waves, leads to the emergence of the contact acoustic nonlinearity (CAN), namely a nonlinear phenomenon that has recently gained increasing attention for the detection and characterization of closed defects or imperfect bond interfaces. The mechanisms involved in contact acoustic nonlinearity are mainly two: clapping and friction.

Clapping (also termed *kissing*) manifests as a mechanical diode effect and results from the asymmetry of the material constitutive equation, i.e., the material exhibits a stiffer response to compression than to tensile stress [33]. In fact, if compression stress helps to bring and keep two free surfaces into contact, tensile stress may induce a weakening, and even the rupture, of the contact between interfaces and closed defects surfaces. Therefore, when an incident wave reaches the border of an imperfect contact interface, only its compressional part can travel across it, while the tensile component cannot penetrate it (figure 3.1). Thus, the propagation of an acoustic wave through a rough interface leads to a cyclic local opening - closure motion. As reported in [128] [129] , the *clapping* mechanism can be expressed as:

$$\sigma = E_0 \left[1 - H(\varepsilon) \, \frac{\Delta E}{E} \right] \varepsilon \qquad (3.1)$$
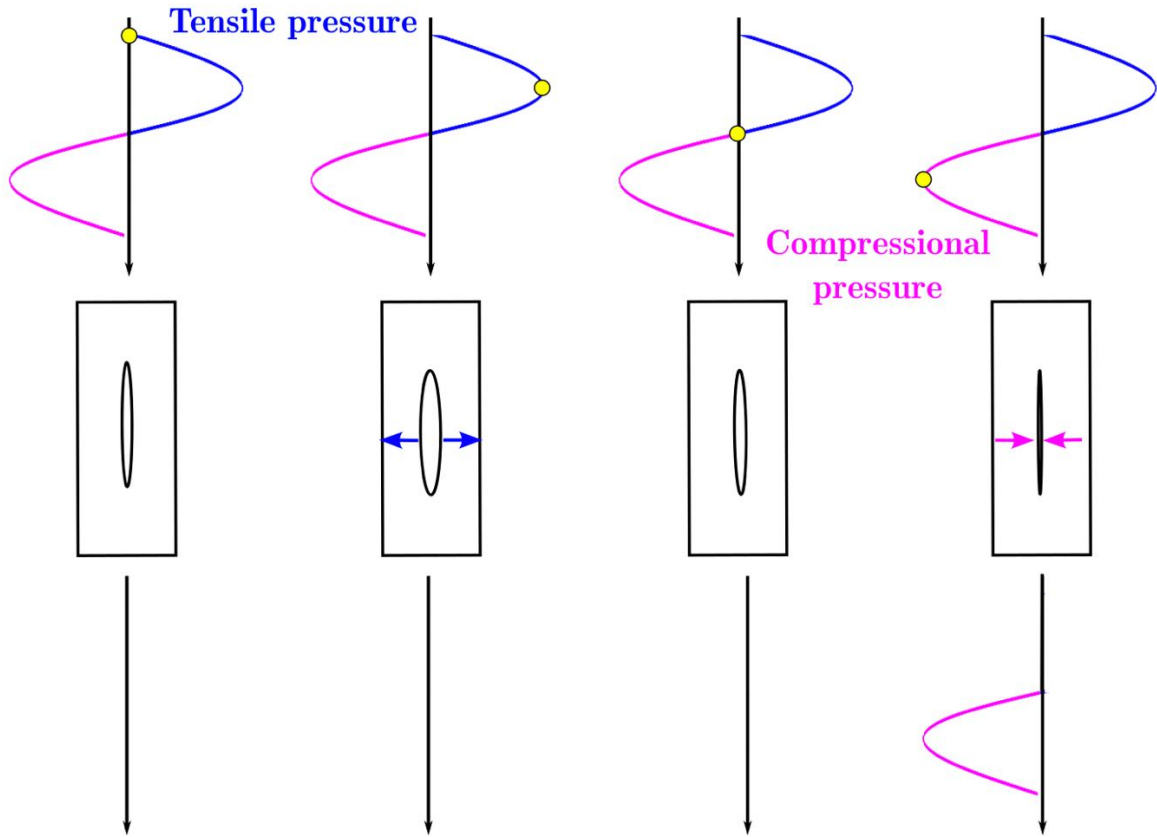
Figure 3.1 – Contact Acoustic Nonlinearity: interaction between an acoustic wave and an imperfect contact interface.

$$\Delta E = E_0 - \left(\frac{d\sigma}{d\varepsilon}\right) \ \ if \ \varepsilon > 0 \tag{3.2}$$

where $H(\varepsilon)$ indicates the Heaviside function, E represents the linear elastic modulus, ε the strain and σ the stress. The wave deformation associated with this bimodular contact formulation results in the onset of both even and odd higher harmonics of the fundamental frequency.

The second nonlinear mechanism involved in *Contact Acoustic Nonlinearity* is friction. Thus, the interaction between the damage interfaces and a propagating shear wave relies upon friction forces. Therefore, the intensity of the wave deformation depends on the wave amplitude, meaning that the amplitude of the relative displacement between the interacting surfaces is governed by friction forces. So, when shear wave amplitude is low, the damage interfaces are displaced in micro-
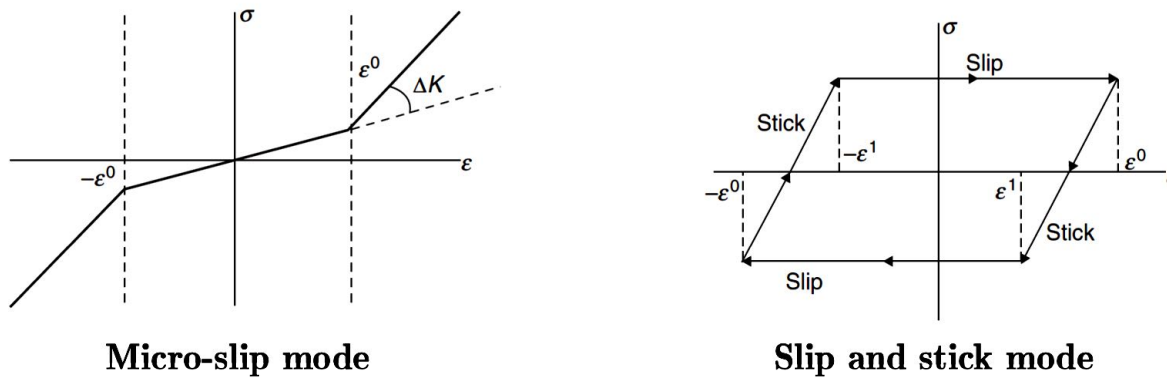
Micro-slip mode   **Slip and stick mode**

Figure 3.2 – Stress–strain characteristics for micro-slip mode and stick and slip mode [33].

slip mode between the neighboring roughness areas [33], inducing a double variation in the stress-strain relationship (figure 3.2). However, if the amplitude of the acoustic wave exceeds a characteristic threshold level, the intensity of static friction forces is not sufficient to preserve the contact between the interfaces. Thus, the crack surfaces start sliding in stick and slip mode, characterized by a cyclic alternation of static and kinematic friction, leading to a hysteretic stress-strain characteristic [129].

3.2.2 Higher Harmonics

A mono-harmonic acoustic wave that propagates in an elastic continuum does not undergo changes in the driving frequency, even though its amplitude is reduced owing to absorption and dissipation. In 1896, Lord Rayleigh was the first to point out that nonlinear terms in the wave equation induce the generation of new frequency components (i.e., new waves) corresponding to multiples of the excitation frequency. Therefore, this phenomenon, generally referred to as *Higher Harmonic generation*, relies upon the distortion an impinging wave undergoes due to the nonlinear elastic response of the medium (figure 3.3). The mechanisms underlying the emergence of higher harmonics are mainly two: (1) nonlinear elasticity and (2) contact acoustics nonlinearity.

In order to illustrate the generation of higher harmonics, a one-dimensional nonlinear system consisting of a circular rod subjected to pure-tone harmonic
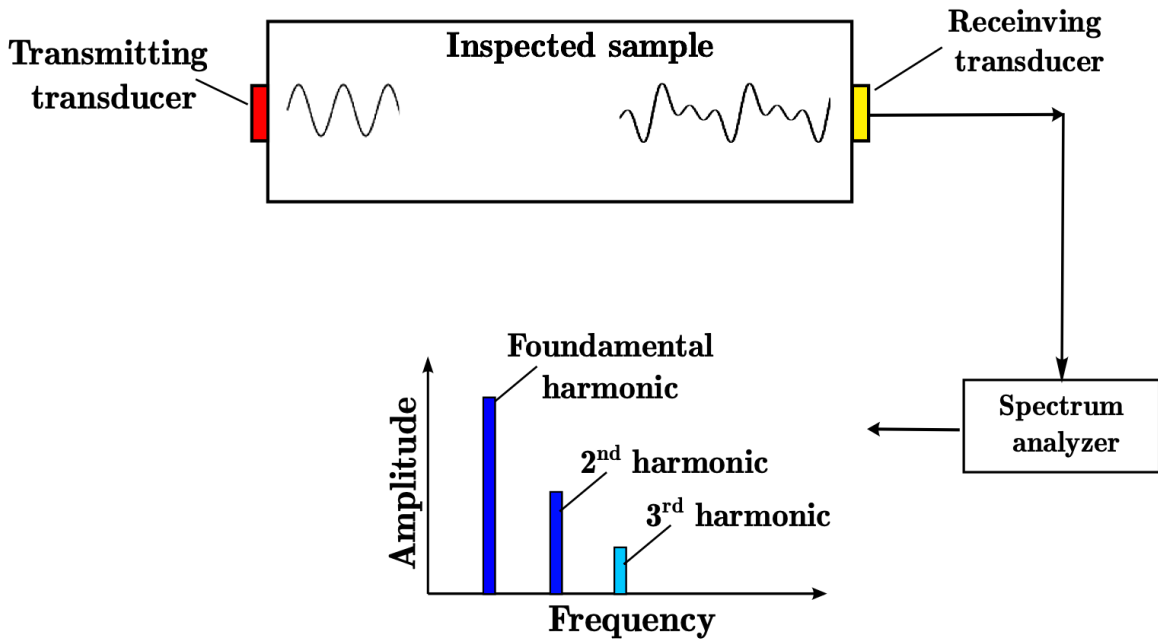
Figure 3.3 – Distortion induced by material nonlinearity and higher harmonics generation.

excitation needs to be considered. The propagation of an acoustic longitudinal wave follows by the equation:

$$\rho \frac{\partial^2 u}{\partial^2 t} = \frac{\partial \sigma}{\partial x} \tag{3.3}$$

where ρ represents the medium density, u the displacement field, and σ the stress. The analytical description of higher harmonics generation for the nonlinear response of the material makes it necessary to assume the material behavior governed by a nonlinear stress-strain relationship (figure 3.4), which might be expressed through a polynomial expansion as,

$$\sigma = E_0 \, \varepsilon \, (1 + \beta \varepsilon^2 + \delta \varepsilon^3 + \cdots) \tag{3.4}$$

where E_0 is the linear elastic modulus, β and δ are higher-order elastic coefficients. Therefore, by combining equations 3.3 and 3.4, the equation that describes the wave motion can be written as:
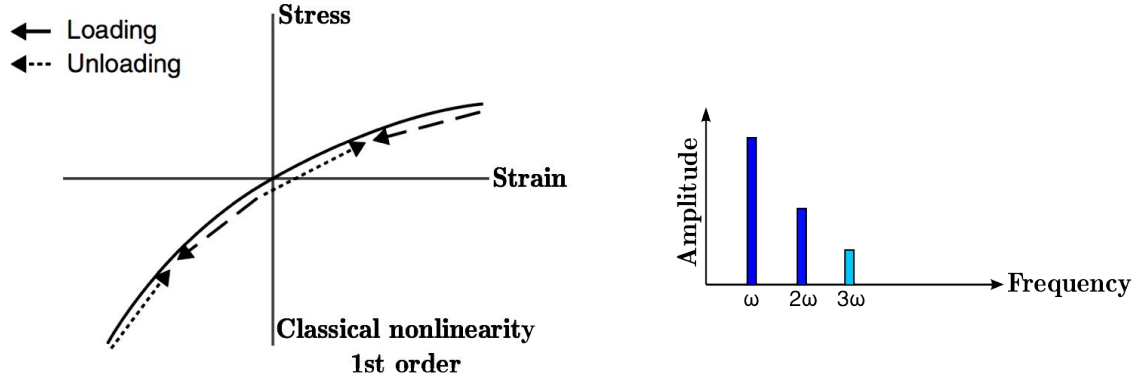
Figure 3.4 - Stress-strain relations and frequency spectra for 1st order classical nonlinearity. Adapted from [33].

$$\rho \; \frac{\partial^2 u}{\partial^2 t} = E_0 \; \frac{\partial^2 u}{\partial^2 x} + 2 \, E_0 \, \beta \; \frac{\partial u}{\partial x} \frac{\partial^2 u}{\partial^2 x} + 3 \, E_0 \left(\frac{\partial u}{\partial x}\right)^2 \frac{\partial^2 u}{\partial^2 x} \qquad (3.5)$$

The solution of the wave motion equation, i.e., the displacement field, is generally found by applying a perturbation theory, where the zero-order solutions are assumed to be of the form of a single frequency wave:

$$u = A_1 \cos(kx - \omega t) \qquad (3.6)$$

Thus, when only the first term of the Hooke's Law is considered, the displacement field results:

$$u = A_1 \cos(kx - \omega t) - A_2 \sin(2kx - 2\omega t) \qquad (3.7)$$

where A_2, which indicates the amplitude of the first-order perturbation solution, may be expressed as

$$A_2 = \frac{1}{8} \, \beta \, A_1^2 \, k^2 \, x \qquad (3.8)$$

being k the wavenumber and x the propagation distance travelled by the excitation signal. Since both the wavenumber and the propagation distance do not change during a set of experimental tests, both the analysis and the comparison of the

nonlinear parameter between different damage levels reduce to depend only on the relative amplitudes of the fundamental frequency and its second harmonic. Therefore, the first-order perturbation solution (namely the second term in equation 3.7) predicts the generation of the second higher harmonic, i.e., a spectral component at twice the frequency of the original longitudinal wave. Although the sole first nonlinear term closely approximates the response of several materials, extending the perturbation analysis to include higher-order nonlinear parameters allows describing more complex nonlinear responses, and hence, the emergence of higher-order harmonics. Moreover, since the amplitude of vibrations associated with these additional spectral components depends on the nonlinear parameters (i.e., β and δ), monitoring the increase in the harmonic amplitude might provide information on the degradation of the material properties.

Among the material degradation mechanisms investigated through higher harmonics, fatigue damage is probably one of the most common. To date, great research effort has been devoted to assessing fatigue damage detection in different materials. Cantrell and Yost [130] carried out some ultrasonic measurements on aluminum $AA2024$-$T4$ dog-bone samples showing that the material nonlinearity monotonically increases as the number of fatigue cycles raises (figure 3.5). Similarly, substantial increases in the nonlinear parameter β were also observed in fatigued
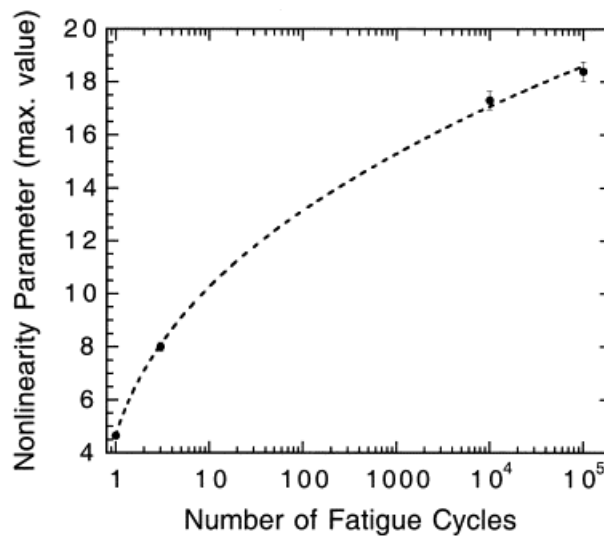

Figure 3.5 – Nonlinearity parameter as function of number of fatigue cycles for aluminum alloy 2024-T4 [130].

titanium *Ti-6Al-4V* alloys [131], stainless steel *410Cb* specimens [132], and quenched steels with different carbon contents [133]. Moreover, in the late 1990s, Nagy utilized both linear (e.g., static modulus, sound velocity, and attenuation) and nonlinear parameters to detect the onset of fatigue damage in plastic materials (i.e., PVC, ABS, nylon, and polycarbonate) [134]. The obtained results showed that: (1) shortly before failure, the nonlinear content in the material response rapidly increases, assuming values one order of magnitude higher than the intrinsic nonlinearity of the pristine material, (2) nonlinear parameters might provide robust and earlier indications on the onset of fatigue damage earlier over their linear counterparts (figure 3.6). Nevertheless, few studies report attempts to apply higher harmonic
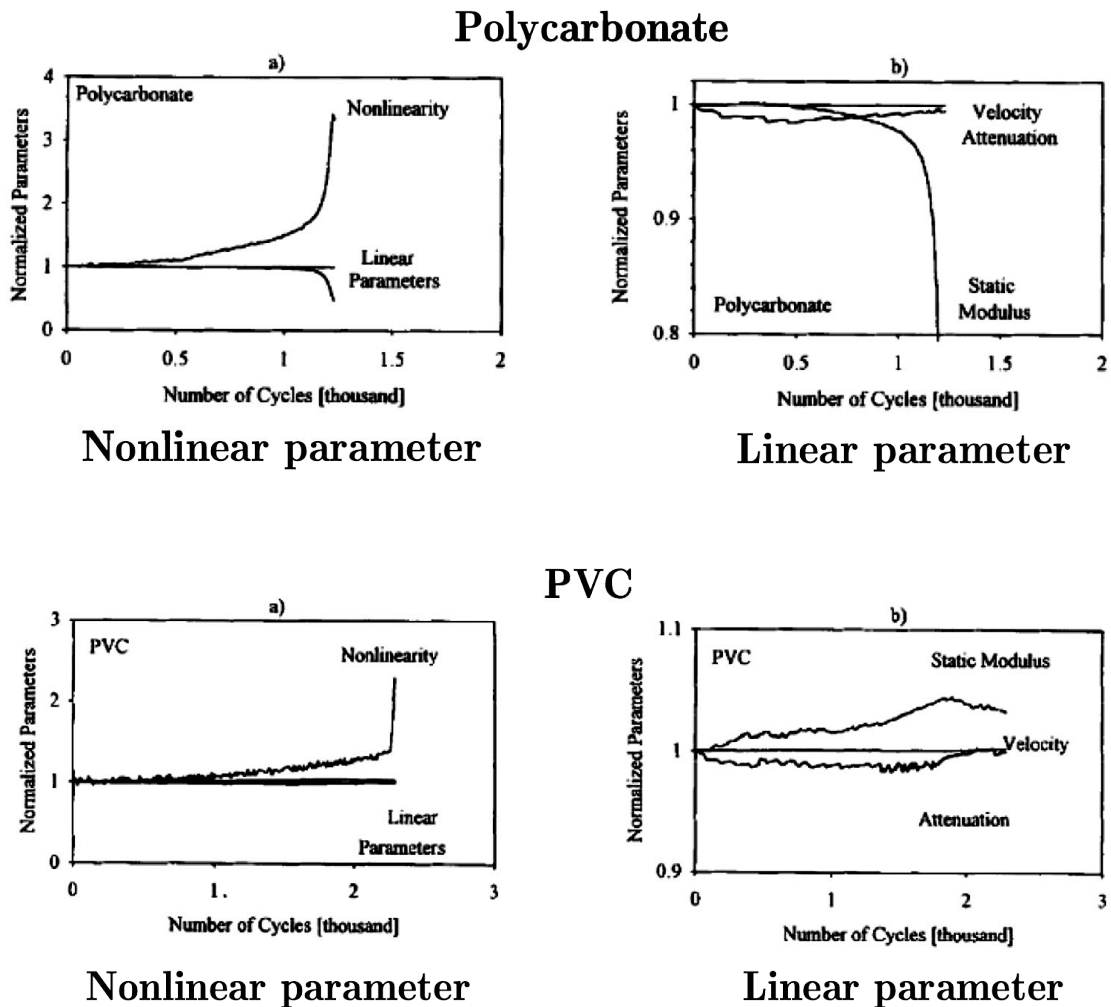
Polycarbonate

Nonlinear parameter   Linear parameter

PVC

Nonlinear parameter   Linear parameter

Figure 3.6 – Variation of both linear and nonlinear parameters with fatigue cycles for polycarbonate and PVC samples [134].
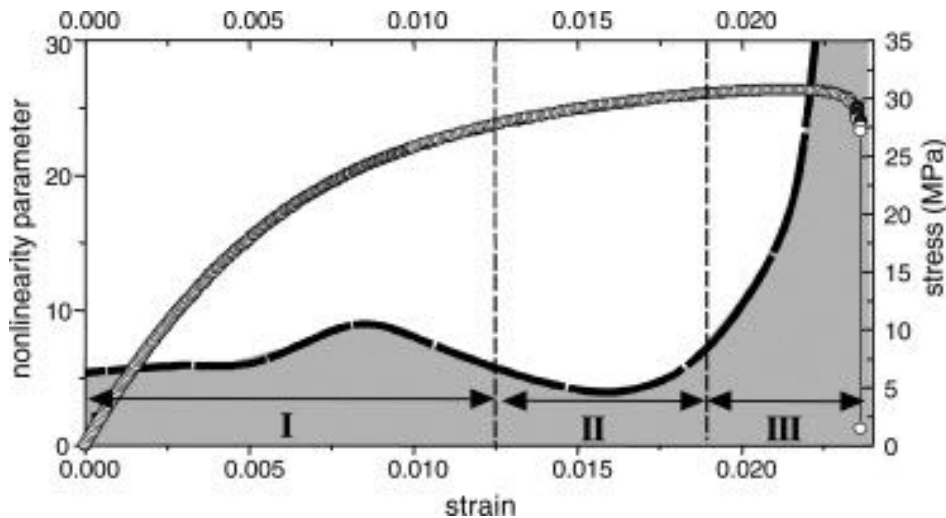
Figure 3.7 – Stress – strain curve (hashed line) and nonlinear parameter β – strain curve (black line with grey shaded area) for longitudinal load in 30% GFRPP specimen [135].

generation for damage detection in fiber-reinforced composite materials. In 2004, Solodov et al. [135] characterized the nonlinear behavior of polypropylene (PP) and glass fiber-reinforced polypropylene (GFRPP) specimens during tensile testing through measurements of wave velocity. By focusing on the way the nonlinear parameter varies with strain (figure 3.7), the authors identified the presence of three different regimes:

- *Regime I*, in which strain is low, and the nonlinear term remains mostly constant.

- *Regime II*, where the nonlinear parameter slightly decreases due to the occurrence of plastic deformation.

- *Regime III*, in which the nonlinear parameter dramatically increases before the material failure.

Therefore, within strain regimes I and II, the nonlinear parameter assumes positive and almost constant values indicating a slow material weakening. As a result, the occurring micro-cracks, which develop between longitudinal fibers, are bridged by fiber tension and gradual pull-out. Further increase in the strain level leads to a sharp rise in the nonlinear parameter preceding the occurrence of fiber fracture and the following unstable growth of cracks, which results in material failure.
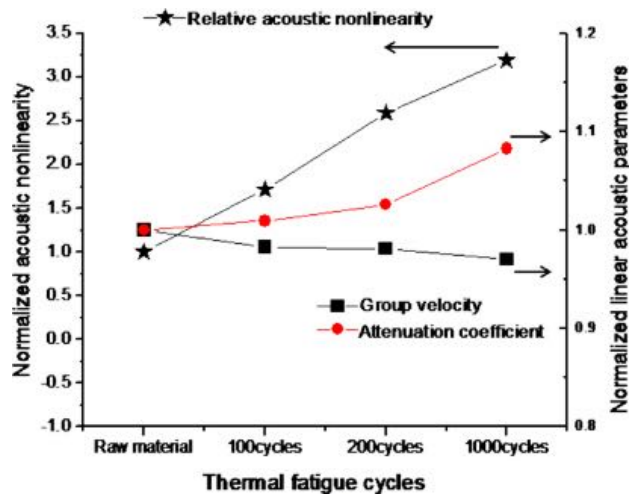
Figure 3.8 – Comparison of the sensitivity of acoustic nonlinearity and linear parameters (i.e., group velocity, attenuation coefficient) to thermal fatigue damage in carbon/epoxy composites [123].

More recently, Li et al. [123] exploited the second higher harmonic to evaluate the effect of thermal fatigue on carbon/epoxy composite laminates, showing that the nonlinear ultrasonic parameter might allow a significant improvement of the sensitivity to early-stage detection of thermal fatigue damage over linear parameters, such as group velocity or attenuation (figure 3.8). Similar conclusions were reported by Rauter and Lammering [136], who applied the cumulative second harmonic modes to investigate impact damages in carbon/epoxy composite laminates.

3.2.3 Resonance frequency shift

Resonant ultrasound spectroscopy (RUS) is a linear ultrasonic or acoustical approach relying on the principle that solids components and structures have specific natural frequencies depending on their elastic constants, size, and shape.

In the late 1990s, Guyer and Johnson [137] proposed an extension of the RUS, termed *Nonlinear Resonant Ultrasound Spectroscopy* (NRUS), that looks at the nonlinear response of a continuum to investigate the relationship between resonance frequencies and strain magnitude based on the amplitude of the vibration. Therefore,
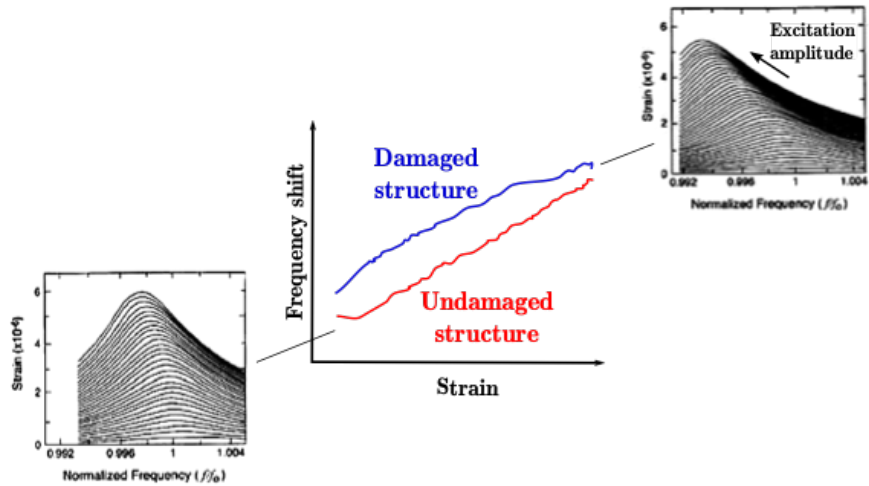
Figure 3.9 – Nonlinear Resonant Ultrasound Spectrometry: resonance frequency shift for undamaged and damaged sample[1].

NRUS provides insight into the degradation of the microstructural properties of a medium by exploiting the changes in the resonance frequencies and the attenuation of the vibration amplitude due to excitation level variations. Increasing the excitation level was found to result in a downward resonance peak shift (figure 3.9) and a decrease of quality factor (i.e., the inverse of attenuation) [10].

In 1989, Zarembo et al. [138] showed that third-order elastic parameter (δ, equation 3.4), which may provide information on the ultimate stress in brittle materials (e.g., concrete) and the yield stress for ductile materials in both compression and tension, is strictly related to the resonance frequency shift through the equation:

$$\frac{f_i - f_0}{f_0} \approx \frac{\delta}{2} \, \varepsilon^2 \tag{3.9}$$

where ε indicates the strain amplitude, f_i is the frequency peak value retrieved at the i-th excitation amplitude level, and f_0 represents the resonance frequency
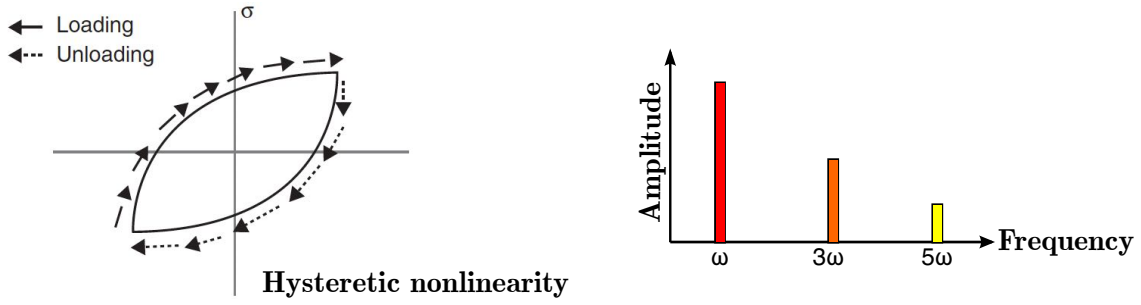
Figure 3.10 - Stress-strain relations and frequency spectra for hysteretic nonlinear behavior. Adapted from [33].

measured in the linear strain range, i.e., the resonance frequency retrieved at the lowest excitation level. Nevertheless, several studies focused on polycrystalline solids and rocks showed that resonance frequency and attenuation amplitude arise along with other nonlinear effects (e.g., the emergence of higher harmonics) [10]. Since this evidence does not comply with the classical nonlinear theory, which relies on a polynomial expansion of the elastic modulus as a function of strain (equation 3.4), but with a hysteretic behavior (figure 3.10), a different constitutive equation has to be defined. Thus, Hooke's Law can be written as:

$$\sigma = \varepsilon \left\{ E_0 \left[1 + \beta\varepsilon + \delta\varepsilon^2 + \alpha(\Delta\varepsilon + \varepsilon(t)\ sign(\dot{\varepsilon}) + \dots) \right] \right\} \qquad (3.10)$$

where E_0 is the linear elastic modulus, β and δ are the second and the third order elastic coefficients, α accounts for the material stress history through the sign of the strain rate ($\dot{\varepsilon}$). Under the assumption that hysteresis dominates the structure response, the frequency shift depends on both the average strain amplitude ($\Delta\varepsilon$) and the hysteresis parameter (α), according to the expression [139]:

$$\alpha\ \Delta\varepsilon = \frac{\Delta f}{f_0} \qquad (3.11)$$

To date, NRUS has been applied to detect the presence of early-stage damage in heterogeneous materials and to characterize the nonlinear behavior of different materials, such as geo-materials [137], metals [140], composites materials [139] [140]. In this context, the studies performed on fiber-reinforced composites focus on the degradation due to exposure to chemical treatments on pultruded E-glass [141],

imaging microcracks caused by thermal degradation [142], and the characterization impact fatigue damage [143].

3.2.4 Frequency mixing

Analogous to higher harmonic generation, *frequency mixing*-based techniques exploit the emergence of additional spectral components to quantify the material nonlinearity and provide information on the degradation of the material properties or the presence of the damage and its extent. In particular, frequency mixing relies upon the simultaneous application of two waves with distinct frequencies and amplitudes that propagate within the medium and interact with each other. If the material behaves linearly, the spectrum of the system response exhibits only the two frequency components associated with the excitation signals. Conversely, the presence of cracks, damage, or discontinuities in the material perturbates the wave propagation, leading to the onset of multiple new frequency components.

Among the frequency mixing-based approaches, the so-called pump-probe techniques have been widely investigated for structural damage detection [144] [145] [10]. These methods reside in exciting the inspected component through a high-frequency, low-amplitude wave (i.e., probe wave) and a low-frequency, high-amplitude vibration wave (namely, pump wave) at once. Therefore, the dynamic fields associated with the two input signals intermingle and wave modulation arises. Belonging to this category, the *Nonlinear Vibro-Acoustic Modulation* (VAM), also referred to as *Nonlinear Wave Modulation Spectrometry* (NWMS) [146], *Nonlinear Ultrasonic Wave Modulation* [147] or *Nonlinear Acoustic Modulation* (NAM), consists in concurrently using a pump wave corresponding to a given resonance mode of the considered structure to induce stresses within the sample, and a probe wave that senses the variation of modulus produced by the pump vibration. Under the hypothesis of perfect linear material behavior, the stresses induced by the pump wave excitation do not affect the propagation of the probe wave. Instead, the presence of cracks, defects, or discontinuities triggers the probe wave amplitude- or frequency-modulation by the pump wave excitation (figure 3.11). In this context, the wave propagation through a medium that behaves according to the modified Hooke's Law
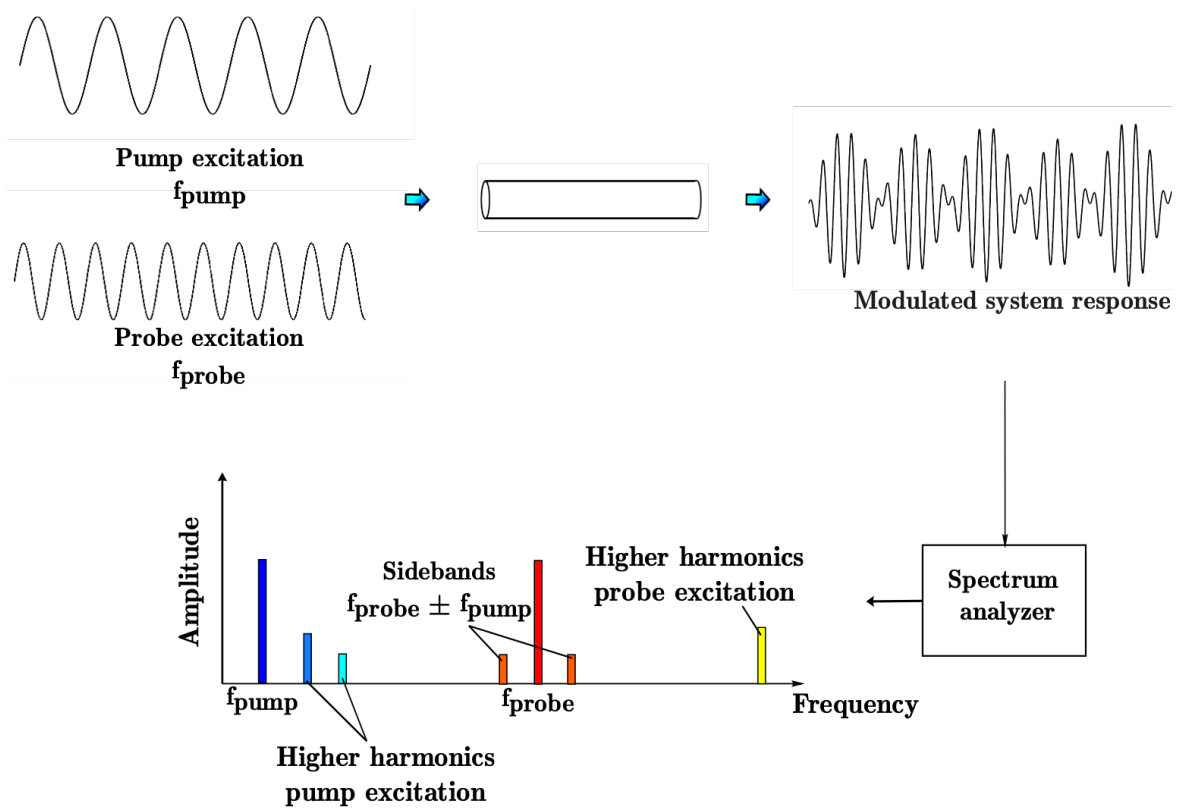
Nonlinear acoustics

Figure 3.11 – Frequency mixing: solution of the wave propagation equation for first-order nonlinear material in both time- and frequency-domain.

(equation 3.4) can be described through equation 3.5. The solution of this second-order differential equation makes it necessary to apply the perturbation theory with a displacement field defined as the linear combination of two sine waves, i.e.,

$$u\,(t) = \, A_1\,\sin(2\pi f_1 t) + \, A_2\,sin(2\pi f_2 t) \qquad (3.12)$$

where A_1 and A_2 are the amplitudes of the two excitation signals, and f_1 and f_2 indicate their frequency. In this context, the time-domain solution of equation 3.5 consists of a wave of frequency f_2 modulated by the lower frequency excitation signal, whereas its spectrum highlights the presence of several terms (figure 3.11):

- The original inputs terms at frequencies f_1 and f_2.

- Higher harmonics, whose emergence is a frequency mixing limiting case assuming the introduction of a pure-tone harmonic signal [33].

- Multiple mixed frequency components, generally referred to as sidebands, occurring at specific frequencies values corresponding to both the sum and the difference of the frequencies of the original excitation terms (namely, the probe and pump frequencies).

Nonlinear Vibro-Acoustic Modulation methods address the problem of both detection and localization of damage (i.e., cracks, defect, and flaws) in structure and components [148] [149]. In fact, since the early works, their application allowed to efficiently detect small cracks in both metal [150] and non-metallic structures (i.e., plexiglass and sandstone) [146], fatigue damage in steel pipes welds [149], graphite electrodes [151], and aluminum plates [152]. More recently, pump-probe techniques have been further investigated to identify the presence of matrix cracking [153] and low-velocity impact damage in fiber-reinforced composite laminates [139] [154] [155] and composite sandwich panels [156] [157].

Apart from the Nonlinear Vibro-Acoustic Modulation technique, described in more detail in Chapter 5, different modulation effects might occur and be exploited for damage detection. Among them, *cross-modulation* relies on the application of a pump wave that is itself amplitude-modulated (figure 3.12). The cross-modulation is a nonlinear acoustic technique based on the *Luxembourg-Gorky* (L-G) effect, which arises from a transfer modulation mechanism. In 1933, the electrical engineer and professor Bernard Tellegen noticed that while listening to the transmission of a swiss
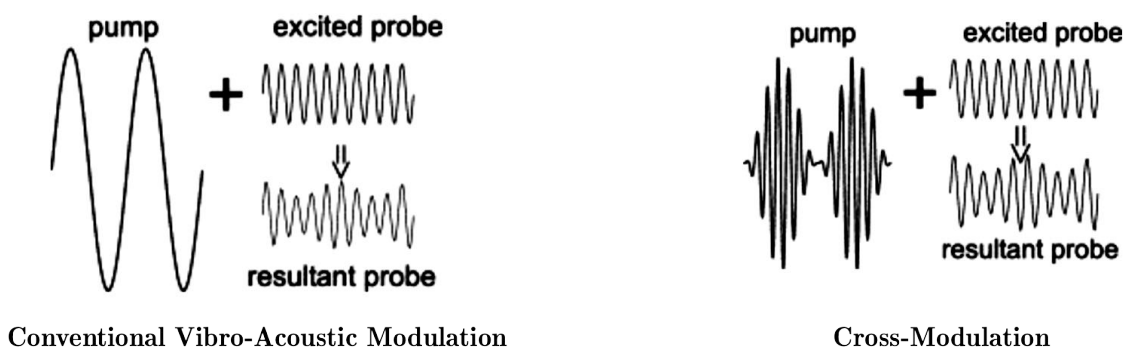

Conventional Vibro-Acoustic Modulation   Cross-Modulation

Figure 3.12 – Schematical representation of pump and probe excitation signals and their associated resultant in the case of conventional nonlinear vibro-acoustic modulation and Luxemburg-Gorky type cross-modulation. Adapted from [158].

radio, the broadcast of Radio Luxembourg was audible in the background [159]. Later on, the same phenomenon was observed in the city of Gorky, where the transmissions of powerful Moscow radio stations superimposed on those of radio stations located to the west of Moscow. Therefore, the Luxembourg-Gorky effect manifests in the modulation of a weak wave due to the propagation of an amplitude-modulated strong wave (namely a pump wave). The transfer modulation between the two waves is assumed to depend on the ability of the pump wave to perturbate the absorption properties of the propagation medium (i.e., the ionosphere). In the early 2000s, Zaitsev et al. [158] and Zaitsev et al. [160] observed that transfer modulation effects also occur in damaged solids and granular media. Despite the several applications to damage detection, the underlying principle of the modulation transfer is not fully understood. However, some studies show that the Luxembourg-Gorky effect is related to non-classical nonlinear mechanisms. More in detail, the modulation transfer was shown to depend on the thermo-elastic properties of a crack, due to which the interaction between an imping acoustic wave and the defect surfaces leads to the onset of thermal gradients [160] [161].

In the past few decades, frequency mixing-based approaches have gained increasing attention over other nonlinear acoustic techniques, such as higher harmonic generation. The reasons are mainly two [162]: (1) higher harmonic components attenuate quickly, making their measurement almost impossible at large distances, and (2) the intrinsic nonlinearity of the measurement chain.

In general, providing information on the material properties degradation exploiting frequency mixing phenomena allow to measure the system response at frequencies close to the probing frequency. Conversely, methods based on higher harmonics generation require sensing the structure response at twice, trice (or even more) the excitation frequency. Nevertheless, every measurement equipment, such as piezo-electric transducers, actuators, signal digitizers, and data acquisition units, works properly in a limited range of frequencies, which could prevent the identification of high-frequency spectral terms. Instead, monitoring spectral components close to the probe frequency (i.e., sidebands) does not need instrumentation different from that used to excite the system at that specific frequency. Moreover, the intrinsic nonlinearity of the measurement chain leads to

distortions in electrical circuits and vibroacoustic actuators and sensors, which might mask the emergence of damage-related nonlinear effects. In particular, the phenomenon through which a signal acquires overtones of its frequency (i.e., higher harmonics) when passing through a nonlinear device is a nonlinear effect overlapping with the spectral components associated with the material nonlinearity. Therefore, this harmonic distortion limits the practical implementation of damage detection approaches based on the generation of higher harmonics and the analysis of their magnitude, making it necessary to resort to expensive high performance (i.e., low nonlinearity) instrumentation.

In the end, although several structural health monitoring techniques based on nonlinear acoustic phenomena have recently been proposed, numerous critical issues still must be faced. In this perspective, the following chapters illustrate applications of two nonlinear acoustic techniques, i.e., the Scaling Subtraction Method (Chapter 4) and the Nonlinear Vibro-Acoustic Modulation (Chapter 5), aimed at further investigating both their efficacy and sensitivity in detecting and characterizing the emergence of impact damage in laminated composite beams.

Chapter 4

Scaling Subtraction Method

The need to identify and estimate the nonlinear features in the response of a system to external input and, hence, retrieve information on both the presence of damage and its severity has led to the development of various Structural Health Monitoring approaches. Among them, those based on nonlinear acoustic phenomena have gained increasing attention. However, the evaluation of the material integrity and its ability to withstand critical loads arise from the analysis of specific components of the nonlinear signature of the system, such as higher- and sub-harmonics [123] [130] [163] [164], sidebands [156] or wave modulation [154] [165] [166]. Since the amplitude of these additional contributions is orders of magnitudes smaller than that of the recorded signal, they may not be easily distinguished from the background noise, especially when early-stage damage is involved. In order to overcome this limitation and, at once, account for the total nonlinear content of the structural response, Scalerandi et al. [167] recently proposed the Scaling Subtraction Method.

4.1   Scaling Subtraction Method: theory

The *Scaling Subtraction Method* (SSM) is a nonlinear acoustic approach aimed to draw out the entire nonlinear content of an acquired signal and, thus, provide information on the effects that the emergence and evolution of nonlinear mechanisms may produce on the global response of the inspected structure or component.

Scaling Subtraction Method

The SSM relies upon the principle that the nonlinear effects tend to be negligible as long as the amplitude of the driving signal is sufficiently low. In fact, the presence of discontinuities within the material microstructure (e.g., voids, cracks, and defects) affects the system response by inducing the occurrence of nonlinear contributions only when the amount of energy that an impinging wave can transfer to a propagating material exceeds a threshold level. Therefore, beyond this limit, sources of nonlinear phenomena, such as crack, defects, and discontinuities, are activated and, nonlinear mechanisms emerge. Conversely, if the activation threshold is not met, material inherent nonlinearities cannot be triggered. Hence, a damaged structure acted through low amplitude excitations is expected to behave linearly.

Under the hypothesis of perfect linearity, the system response varies proportionally to the excitation signal. Thus, proven the linearity of the measurement chain, deviations from the otherwise proportional relation between input and output might be related to the presence of nonlinear terms in the material constitutive law (i.e., its stress-strain relationship) or to the occurrence of internal damage. Due to these contributions, the stationary response of a damaged specimen to a mono-harmonic excitation should be expressed as a sum of harmonic terms (namely a Fourier expansion) [168]:

$$v_A(t) = \sum_{n=1}^{\infty} B_n(A) \cos[n\omega_0 t + \varphi_n(A)] \qquad (4.1)$$

where $B_n(A)$ and $\varphi_n(A)$ represent the amplitude and the phase of each harmonic contribution, respectively. Nevertheless, in the limit of a small excitation amplitude, nonlinear terms in the Fourier expansion, i.e., those associated with values of the index n higher than 1, do not significantly contribute to the system response and can be disregarded. Subsequently, the stationary response of a damaged structure driven through a small amplitude pure-tone harmonic excitation should not contain any additional spectral components except the fundamental one. Thus, it might be written as:

$$v_{low}(t) = B(A_{low}) \cos(\omega_0 t + \varphi_0) \qquad (4.2)$$

where $B(A_{low})$ is the amplitude of the system response to a driving signal whose amplitude falls below the threshold for the activation of the material nonlinearities.

As long as the input signal does not inject a consistent amount of energy into the system, the system behaves almost linearly, and the superposition principle holds. In these conditions, if the amplitude of the excitation signal amplitude varies by a scaling factor k:

$$A_{high} = k\, A_{low} \tag{4.3}$$

the system response is expected to be

$$v_{ref}\,(t) = k\, v_{low}\,(t) \tag{4.4}$$

and, thus,

$$v_{ref}\,(t) = k\, B(A_{low})\cos(\omega_0 t + \varphi_0) \tag{4.5}$$

Owing to these general assumptions, the recorded signal at low excitation amplitude, i.e., low enough to not activate the nonlinear source, allows the definition of a *linear reference signal*, which represents the linear response associated with an equivalent linear undamaged system (equation 4.5).

The Scaling Subtraction Method detects the onset of the internal damage and monitors its evolution by exploiting the loss of the scaling properties of the system response. As stated in [167] [168], the mechanisms involved in the break of proportionality between the system response and the excitation are mainly three:

- *Phase distortion*, which arises from the dependence of the wave velocity on its amplitude. Due to this correlation, different portions of a longitudinal or a shear wave traveling across a damaged area do not propagate at the same speed. Thus, wave distortion occurs, and the signal acquired at the receiver stands out for a phase shift that depends on the presence and the characteristics of the encountered damaged zone (especially its extent).

- *Nonlinear attenuation mechanisms*, due to which the amplitude of the system response might decrease or increase according to the width and shift of the resonance curve.

- *Nonlinear coupling* in the wave equation, i.e., the presence of nonlinear terms in the stress-strain relationship (equation 3.4), results in the appearance of additional spectral components at multiples or fractions of the excitation frequency (e.g., higher-order harmonics, sidebands, or sub-harmonics). Consequently, the elastic energy associated with the fundamental frequency component decreases, while, at once, that of the generated additional spectral lines increases. Thus, the energy loss at the driving frequency goes along with a redistribution of the signal energy among the spectral lines whose emergence derives from the intrinsic material nonlinearity.

In practice, the application of the Scaling Subtraction Method resides in driving the specimen through a small amplitude excitation (A_{low}) and recording the corresponding response signal ($v_{low}(t)$) at the sensor locations. Then the amplitude of the excitation signal is scaled according to equation 4.3, and the correspondent response ($v_{high}(t)$)) is recorded, enabling the evaluation of the so-called *scaled subtracted signal*, which has been defined as the difference between the actual response ($v_{high}(t)$) and the linearly reference signal ($v_{ref}(t)$):

$$w(t) = v_{high}(t) - v_{ref}(t) = v_{high}(t) - k\,v_{low}(t) \qquad (4.6)$$

Except for noise effects, the subtracted signal $w(t)$ should vanish for non-damaged specimens (i.e., approximating a perfectly linear behavior). Conversely, since the scaled subtracted signal should contain the global nonlinear signature of the inspected structure [167] [168], including the effects associated with both the amplitude reduction or the phase shift (figure 4.1), its amplitude is expected to augment as the damage severity increases.

In the end, the Scaling Subtraction Method provides information on the material integrity by simply comparing the system response acquired at a specific excitation level and the corresponding linearly rescaled signal. Therefore, over more conventional techniques, such as FFT analysis and filtering procedures, the Scaling Subtraction Method has the advantage of deriving the nonlinear signature through a simple subtraction without requiring the introduction of any mathematical parameters (e.g., time window length).
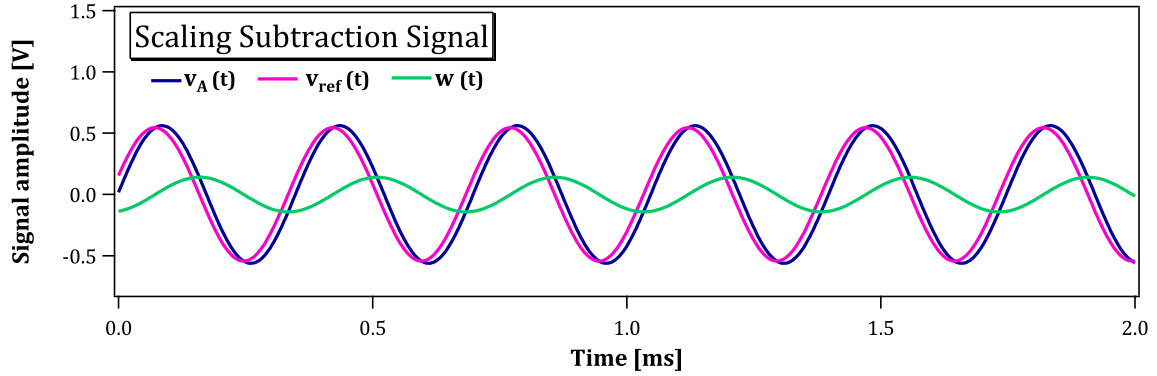
Figure 4.1 – An instance of the system response corresponding to a generic amplitude ($v_A(t)$), the linearly rescaled signal ($v_{ref}(t)$) and scaled subtracted signal ($w(t)$).

The need to quantify the nonlinear contributions in the response of a system to an impinging wave led to the introduction of two damage indicators [167]:

$$\beta = \sqrt{\sum_{i=1}^{n} w_i^2} \tag{4.7}$$

$$\alpha = \max[w_i(t)] \tag{4.8}$$

where n and w_i indicate the numbers of sampled points and the amplitude of the scaled subtracted signal at the i-th point, respectively. Therefore, while the damage indicator β is calculated as the root-mean-square of the scaled subtracted signal and denotes the energy of the same signal, the index α provides information on the amplitude of the scaled subtracted signal.

4.2   Scaling Subtraction Method: applications

In 2008, Scalerandi et al. [167] proposed and firstly applied the Scaling Subtraction Method to characterize the nonlinear behavior of a set of five samples of different materials (i.e., steel, damaged Teflon, mortar, intact and damaged concrete)

through the definition of two quantitative parameters (equations 4.7 and 4.8). In more detail, the authors described the response of a concrete bar subjected to increasing amplitude loads and, thus, at different damage severity levels, showing that the amplitude of the subtracted signal significantly increases when the load intensity reaches a value between 30% and 50% of its rupture stress (figure 4.2). Since the FFT-based approach, applied to validate the obtained results, cannot provide reliable information on the material integrity for load amplitude lower than 60% of the critical load, the authors concluded that the proposed approach was more sensitive to variations in the nonlinearity of the specimen. In fact, the emergence of the nonlinear mechanisms involved in the loss of proportionality between the driving signal and system response, i.e., nonlinear attenuation, nonlinear frequency shift, and phase distortion, produce stronger effects on the fundamental frequency component than on the higher-order harmonic terms. A year later, Bruno et al. [168] further investigated the SSM capabilities managing to separate and individually evaluate the contribution of these mechanisms to the nonlinear signature of the inspected structure. For this purpose, the scaled subtracted signal was decomposed into the sum of three terms, individually accounting for one of the considered nonlinear effects. Moreover, the necessity to estimate the nonlinear contribution each of these mechanisms gives to the nonlinear response of the tested structure led to the definition of three indicators.
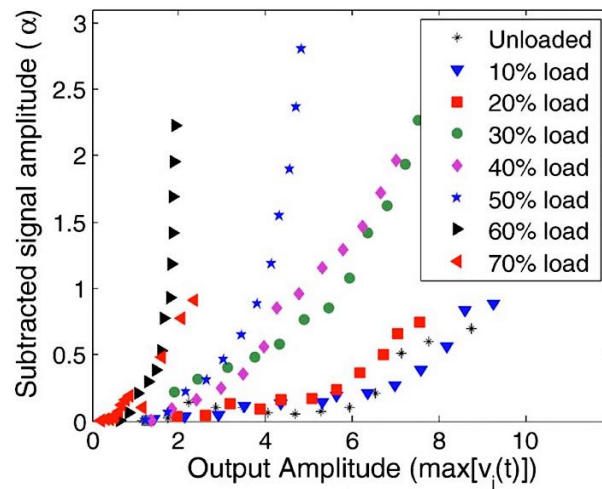

Figure 4.2 – Nonlinear index α (equation 4.8) for a concrete sample tested in different damage states [167].

Scaling Subtraction Method

For what concerns the contribution of the phase shift of the fundamental component, a quantitative index might be defined as:

$$\theta_1 = 2 \, k^2 \, [B \, (A_{low})]^2 \, \cos^2 \left(\frac{\varphi(A_i) - \varphi_0}{2} \right) \tag{4.9}$$

where $\varphi(A_i)$ and φ_0 indicate the phase of the system response corresponding to an input signal with a generic amplitude A_i and A_{low}, respectively. Under the hypothesis of a non-dispersive medium, the phase of the scaled subtracted signal depends only on the wave velocity, which is related to both the bulk modulus and the density of the propagating medium. Therefore, the phase index provides information on the changes in medium stiffness occurring when the magnitude of the driving input varies from A_i to A_{low}.

The second contribution accounts for the phenomenon of nonlinear attenuation, whose emergence relies upon several factors, such as spectral broadening (i.e., the energy transferred to higher harmonics) and resonance frequency shift. The correspondent quantitative index depends on the amplitude of both the linear reference signal and the actual system response to a driving input of amplitude A_i, according to the equation:

$$\theta_2 = \frac{1}{2} \, (B \, (A_i) - k \, B \, (A_{low}))^2 \tag{4.10}$$

Since nonlinear attenuation increases with amplitude, the magnitude of the scaled linear signal should be slightly higher than that of the signal recorded at the corresponding excitation level, except for effects related to the shift of the resonance curve of the specimen. Therefore, the nonlinear attenuation index that reflects the variations of the material attenuation properties on the excitation amplitude is expected to increase with the driving magnitude when evaluated for damaged structures. Conversely, it should have a negligible effect on the behavior of pristine components.

In the end, the first two contributions to the scaled subtracted signal affect the sole fundamental harmonic, while the third accounts for the generation of additional spectral components. Therefore, assessing the material integrity by

analyzing specific features of the nonlinear signature of the inspected structure without considering the effects associated with the fundamental frequency corresponds to neglecting the most meaningful nonlinear effects. This approach was validated by analyzing the damage progression in masonry samples under compressive quasi-static loading [168]. The results showed good agreement with previous studies on similar specimens, confirming both the sensitivity and the effectiveness of the Scaling Subtraction Method in retrieving information on the damage evolution over more traditional approaches (e.g., FFT-based techniques, higher harmonic measurements).

To date, the Scaling Subtraction Method has been applied to characterize the nonlinear behavior of several materials, i.e., steel [167], damaged Teflon [146], and consolidated granular media (e.g., mortar and concrete) under compressive load [168] [169] [170] and thermal load [171]. However, very few attempts have been made to apply the Scaling Subtraction Method to detect impact damage in composite materials.

In 2017, Porcu et al. [172] were among the first to assess the capability of the Scaling Subtraction Methods to detect both the onset and the progression of the impact damage in laminate composites plates. More in detail, the authors investigated the influence of several parameters (e.g., laminate size, input-output scenario, damage severity, and location, both the excitation frequency and amplitude) on the SSM capability to provide clear indications on the occurrence of damage and its growth. The investigation showed that this method was generally able to identify the presence of impact damage, even though its sensitivity was found to depend on both the excitation amplitude and the input-output scenario, i.e., the relative positioning between sensor location and actuation point. Furthermore, the results highlighted a strong dependency of the effectiveness on the excitation frequency, which has to be chosen in advance. Therefore, preliminary tests are required to identify the resonance frequencies of the inspected structure. In addition, there is still no robust algorithm to select the natural frequencies of the considered specimen with the highest sensitivity for the SSM. In light of these limitations, which make the procedure time-consuming, and to further explore the potential of the Scaling Subtraction Method approach, an attempt was made to apply this technique

for impact damage detection in composite material by using a broadband impulsive excitation. Both the experimental procedure and the obtained results are described in detail in the following sessions.

4.3   Experimental procedure

4.3.1 Sample manufacturing and description

Experimental tests were conducted on a laminated composite beam measuring 563 mm × 28 mm × 2 mm. The sample was manufactured from *Seal Texipreg®* *HS160/REM* carbon/epoxy unidirectional pre-preg. Pre-preg plies generally come as rolled-up fibrous reinforcement absorbed in a partially cured polymer matrix (e.g., epoxy or phenolic resin), which bonds the fibers together by keeping them aligned in a single direction and protects them from the outside environment (figure 4.3).

Figure 4.3 – Pre-preg plies (carbon - epoxy).

Since the thermosetting resin has not yet completed its curing cycle, cold storage is required to avoid slowly curing at ambient conditions. Therefore, before handling, pre-preg plies have to be taken out from the freezer and kept at room temperature for thawing. During this time interval, the polymer matrix gets soft and regains a part of its adhesive properties. Thus, good cleanliness of the work surface is of the uttermost importance to prevent dust particles from sticking to the plies surfaces and, hence, being embedded within the laminate. For the same reason, being human skin greasy and gross, latex gloves have to be worn for the whole process. In fact, the presence of heterogeneous inclusions adversely affects the mechanical properties of the laminate by reducing its strength or triggering the onset of nonlinear effects.

Once these preliminary operations have been completed, the pre-preg plies were cut employing a cutter, a steel template, i.e., a steel frame, whose dimensions are equal to those desired for the laminate, and a pair of setsquares, which allows to define the cutting line and, thus, ensures to align the reinforcement of each ply in a specific direction (figure 4.4).

Figure 4.4 – Tools employed during the lamination process.

After cutting, the plies were stacked to obtain a quasi-isotropic $[0/+45/-45/90]_{2s}$ stacking sequence. During this step, generally referred to as *lamination*, each ply was overlapped to the previous one by carefully removing the protective layers. Because air pockets might be entrapped between layers, and the side effects associated with their presence are comparable to those of other inclusions, employing a roll (figure 4.4) allows to press the layers together and, at once, remove air pockets might be helpful.

Prior to completing the curing process in autoclave, the laminate was sealed in a vacuum bag, i.e., a bag made of a thin layer of an airproof film (e.g., polyamide), which allows the use of a vacuum pump to extract the air out of the bag by applying an even negative pressure over the laminate. As shown in figure 4.5, a vacuum bag is composed of several layers of which the airtight film is only the outermost component. Thus, starting from the bottom, there are:

- A steel frame that supports the laminate and whose surface was treated through one or more applications of a releasing agent (i.e., *Zyvax*) to prevent the resin that might sprout out from the curing laminate to stick on it.

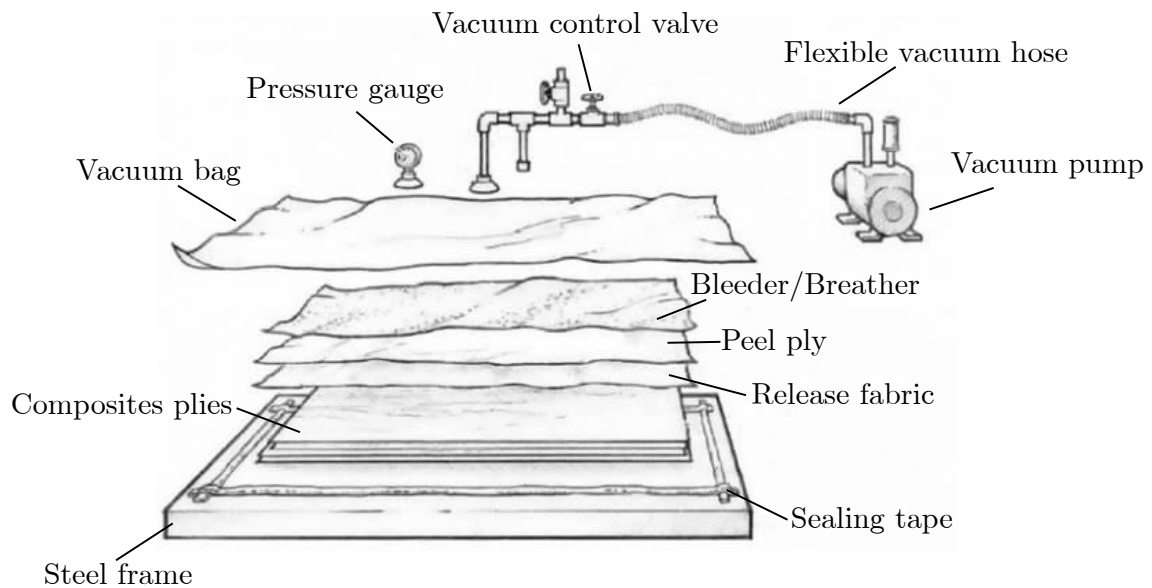**Figure 4.5 –** Vacuum bag for composite component manufacturing (adapted from
https://www.epoxyworks.com/index.php/tag/vacuum-bagging)

- A realising film made of Teflon.

- The composite laminate, after removing the protective layers from both the top and the bottom surface.

- A second layer of Teflon.

- A second steel plate that, together with the second Teflon sheet, allows to obtain a smooth and clean surface.

- The bleeder/breather, i.e., a porous fabric that accomplishes a dual function: (1) absorbing the excess resin caused by the layers compaction, and (2) ensuring the proper air circulation, and, thus, helping to air entrapped between layers to be evacuated.

- An airproof layer that was pierced outside the laminate edges to insert the vacuum valve (figure 4.6).
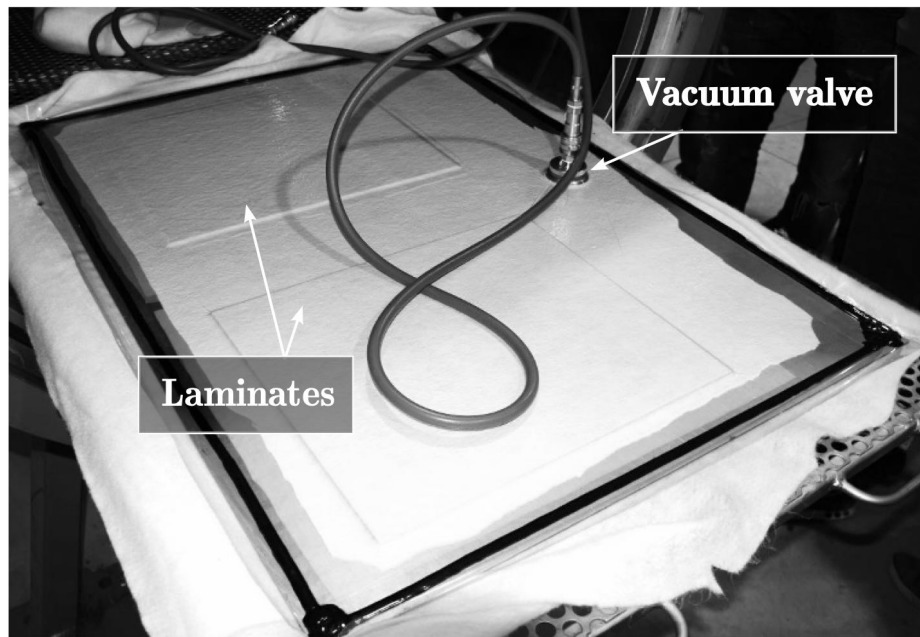
Figure 4.6 – Insertion of the vacuum valve outside the laminate edges to prevent the valve from leaving a print on the surface of the composite laminates.

Finally, the vacuum bag was closed with sealant tape, and its leaknessproof assessed. For this purpose, the valve on the bag was connected to the autoclave vacuum pump, and the internal pressure of the vacuum bag sharply decreased. Then, the valve was closed and, the vacuum bag internal pressure monitored. In these conditions, if the value on the display of the pressure gauge associated with the vacuum pump does not vary, there are no undesired air pathways. Conversely, air leaks would have induced a significant increase in the bag pressure, making it necessary to add sealant tape to get rid of them.

Completed the lamination process, the autoclave, whose technical specifications are given in table 1, was booted, and the consolidation stage started. According to the characteristics of the matrix, the curing cycle consists of five steps (figure 4.7):

Autoclave *Maroso*	
Internal volume [l]	2250
Maximum temperature [°C]	200
Maximum pressure [bar]	10

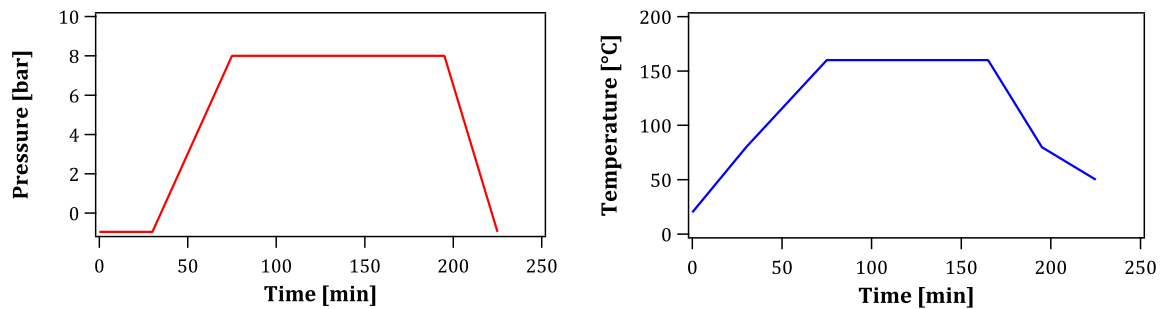**Table 3.1 –** Technical characteristics of the *Maroso* autoclave.

Figure 4.7 – Cure cycle associated with *Seal Texipreg® HS160/REM* carbon/epoxy pre-preg: pressure and temperature.

- *Step* 1: in 20 minutes, the temperature is raised from the environment value up to 50°, while the laminate is kept under vacuum.

- *Step 2*: in 45 minutes, the temperature is raised up to 160°C and the pressure up to 8 bar.

- *Step 3*: for 90 minutes, both the pressure and the temperature are held constant, allowing the epoxy matrix to cure.

- *Step 4*: in 30 minutes, the temperature is reduced to 80°C at 8 bar.

- *Step 5*: the pressure applied through the autoclave is removed, while the temperature is further reduced to 50°C.

At the end of the cycle, the composite laminate was extracted from the vacuum bag and cut in the shape of a rectangular beam (dimensions 563 mm × 28 mm × 2 mm) through a diamond wheel. Even though vacuum bagging results in uniform distribution of matrix and good adhesion between layers, and, thus, high-quality laminates, the beam was examined before SSM testing through ultrasonic C-scanning to exclude the presence of pre-existing manufacturing defects.

4.3.2 Impact damage

Assessing the effectiveness of the Scaling Subtraction Method to detect the onset of internal damage in composite materials as well as to monitor its growth requires considering multiple levels of damage severity that were produced by applying impact loads through a drop-weight impact testing tower.

As shown in figure 4.8, the impact testing machine, used for this purpose, consists of three main components:

- A *heavy metal basement* (i.e., an anvil with 350 kg of mass), provided with a clamping system to fix the sample.

- An *impactor* (also referred to as *hammer*) that has to be rigid enough to transfer the impact energy to the specimen without undergoing excessive elastic deformation or vibrations, which might result in both energy absorption and dissipation

- Two *vertical rod guides* on which the impactor runs through two roller bearings.

- A *pneumatic braking system* that catches the dropping mass after the first impact preventing it from rebounding on the specimen surface.

Since changes in the hammer mass and its dropping height result in variations of both the velocity and the energy associated with the impact, the design of an impact testing machine should consider the user need for adjusting the total weight of the impactor, and, thus, allowing to achieve the desired energy. Because of this,

the testing apparatus is provided with two interchangeable impactors of different mass: a light one (2.2 kg), actually used to induce the onset of internal damage on the inspected composite sample, and a heavy one (4.6 kg). In both cases, adding extra masses allows to increase the falling mass up to 7kg.
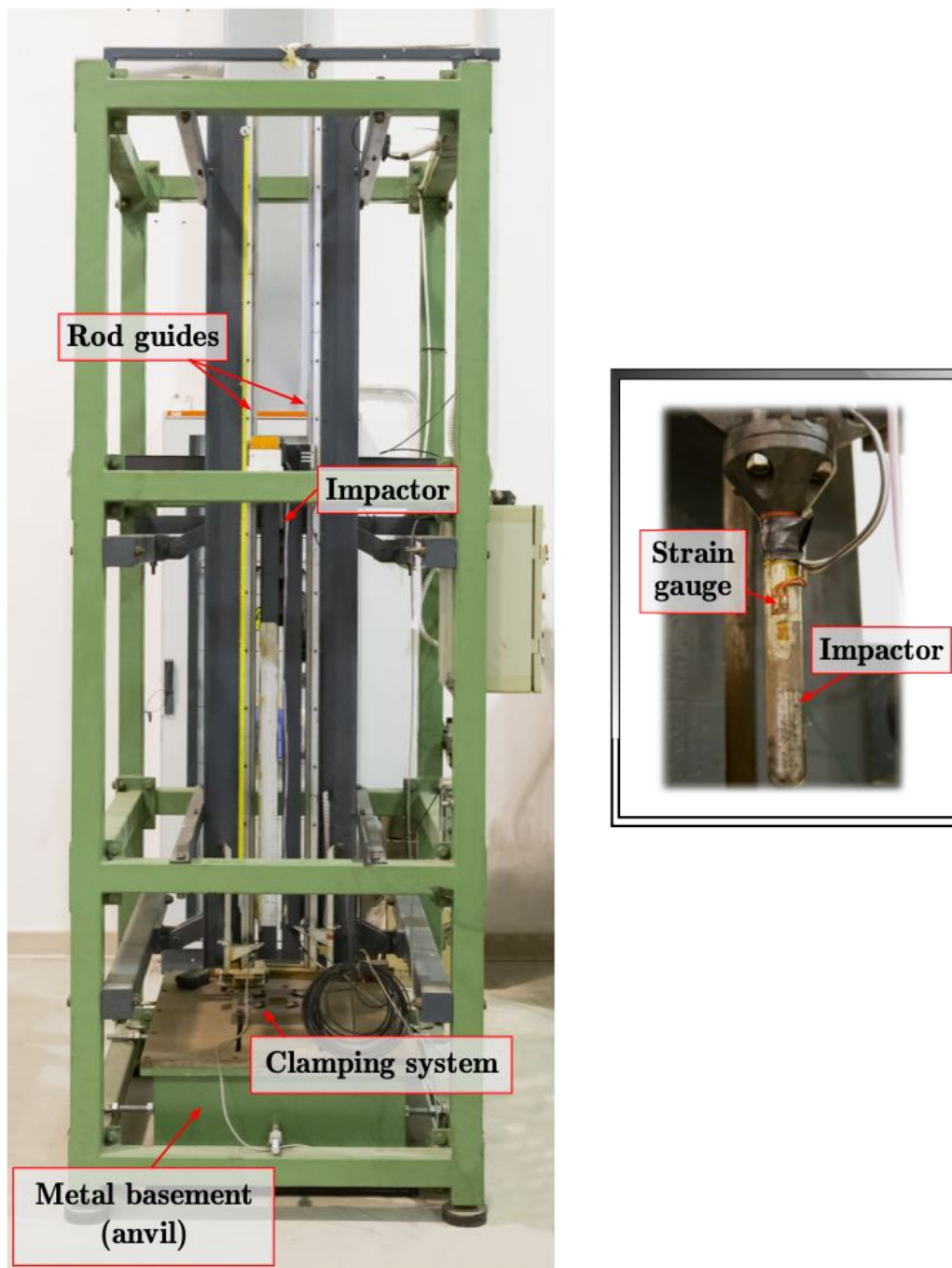

Figure 4.8 – Drop-weight impact testing machine.

Scaling Subtraction Method

Even though the complete characterization of an impact event makes it necessary to measure several variables (e.g., load on the anvil, impactor speed, and specimen deflection), only two parameters have been monitored during testing: the before-impact velocity and the contact force. In fact, both the energy absorbed by the sample and its deflection might be obtained from the two selected variables.

For what concerns the impact velocity, the employed metering system comprises two main elements: (1) an infrared emitting diode and (2) a photo-transistor. When the former illuminates a reflecting surface, the latter, which acts as sensing element, generates an output voltage. Thus, three parallel white stripes were arranged at a fixed distance on a black background and, subsequently, placed on the lateral surface of one of the bearings. When the hammer drops, the sensor sees the stripes, starting or stopping a clock. Hence, under the general hypothesis of constant acceleration, knowing the distance between these white stripes allows the evaluation of both the first impact and rebound velocities. However, neglecting the effects of the friction by assuming the impactor acceleration to be constant might result in high measurement errors. As a matter of principle, this assumption can be regarded as acceptable only if the distance between stripes is small.

In addition, *Kuwai KSP-1-350-E4* semi-conductor strain gauges, which have been glued to the impactor and then connected in a full-bridge Wheatstone circuit, were used to measure the contact force. Sensitivity and accuracy in measuring the contact force are of the uttermost importance. In fact, both the specimen deflection and the energy absorption are derived by integrating the load-time curve. In this context, even low error levels in the contact force estimation might result in wrong energy evaluation. Moreover, unerring load-time curves may provide information about the onset and evolution of the induced internal damage.

In order to assess the effectiveness of the Scaling Subtraction Method to detect the damage initiation and monitor its progression, the hammer, provided with a flat face indenter of 5 mm diameter, was dropped from different heights to vary the impact energy. Thus, the laminated composite sample, simply supported on a steel frame with a central hole of 20 mm diameter, was hit at 1.7, 5.5, and 9.0 J. The damage associated with each impact (termed Damage 1, Damage 2, and Damage 3) was characterized through non-destructive penetrant-enhanced X-radiographies

through an *HP Faxitron* cabinet. As shown in figure 4.9, impact damage is mainly a combination of delamination, matrix cracks, and fiber fracture occurring at the interfaces between layers with different orientations. Moreover, the length of the broken fiber path significantly increases with the impact energy as the extent of the delaminated area (table 3.2 and figure 4.9).

Damage severity	Impact energy	Delamination	Length of the broken fibers path
	[J]	[mm^2]	[mm]
Damage 1	1.7	67	11
Damage 2	5.5	202	18
Damage 3	9.0	402	28

Table 3.2 – Damage characterization: main features of the impact damage at each of the three considered damage severities [173].

Damage 1
Impact energy = 1.7J

Damage 2
Impact energy = 5.5J

Damage 3
Impact energy = 9.J
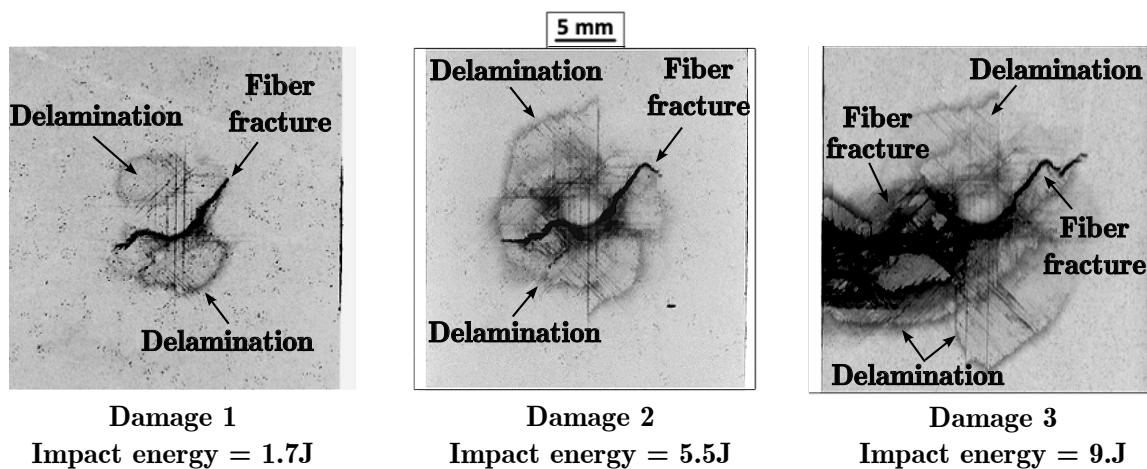
Figure 4.9 – X-ray images of the three considered level of impact damage.

4.3.3 Experimental tests

During the Scaling Subtraction Method tests, the laminated composite was instrumented with a *PI PL055.31* stack actuator to drive the system and two *PI Ceramic PIC 151* low-profile piezoceramic transducers (10 mm diameter, 1 mm thickness) that sense the system response at location S1 and S2 of figure 4.10. The three piezoelectric transducers were glued on the top surface of the composite beam by applying a thin layer of a two-component epoxy adhesive and then wired through bonded connectors. Coupling between transducers and the employed instrumentation are highlighted in figure 4.10, in which a schematic representation of the setup adopted for the experimental tests is given.
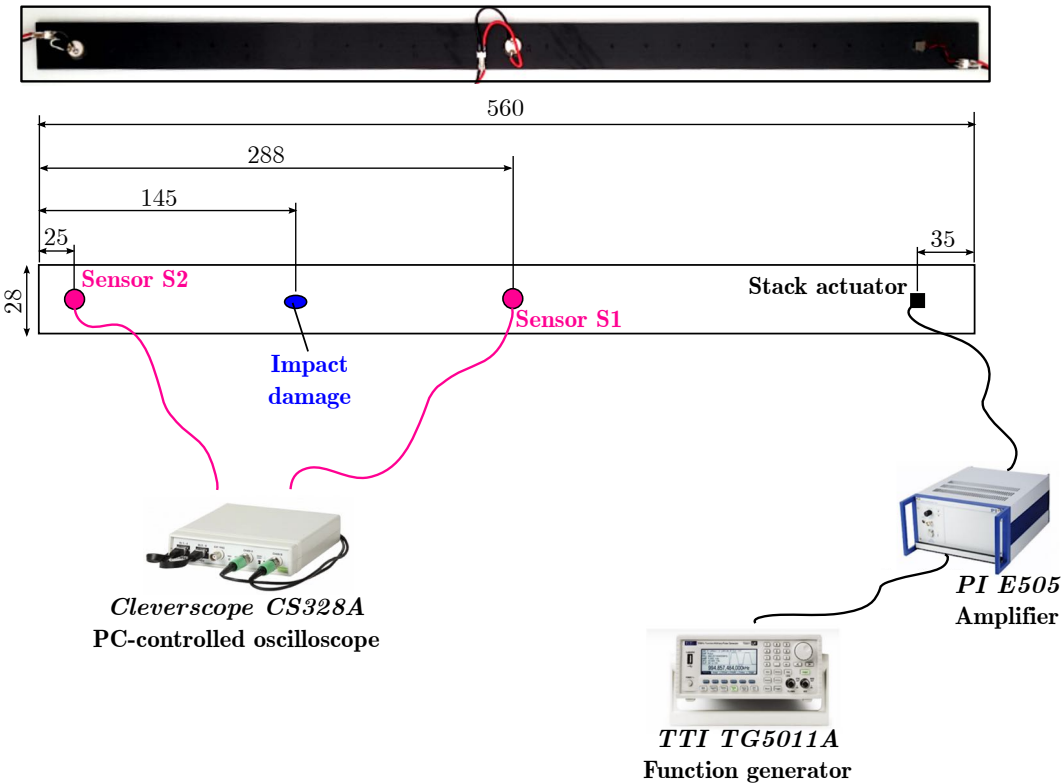
Figure 4.10 – Composite sample and scheme of the experimental set-up adopted for the SSM tests.

The composite sample was freely suspended through thin nylon cords to prevent the structural boundaries nonlinearity from triggering the emergence of

nonlinear effects, which might overlap those due to damage initiation and evolution, leading to an erroneous interpretation of the experimental data.

In order to demonstrate the feasibility of a pulse-based extension of the Scaling Subtraction Method, two series of independent experimental tests were required. In fact, if the first measurements were performed by exciting the samples through a broadband impulsive excitation, the second ones, which were aimed to validate the proposed approach, required the laminated composite beam to be driven with a stationary mono-harmonic signal. Nevertheless, applying the Scaling Subtraction Method with harmonic excitation makes it necessary to characterize the modal response of the samples. Since the SSM excitation frequencies are generally selected among the natural frequencies of the inspected structure, performing a preliminary experimental analysis is needed. To this purpose, the stack actuator was fed with a pulse generated by a *TTI TG5011A* function generator and then amplified by a factor of 10 through a *PI E505.00* high-voltage linear amplifier. Both the response of the laminated composite beam and the driving input were monitored and acquired through a 14 bit, 100 MHz PC-controlled oscilloscope (*Cleverscope CS328A*). Then, the forty data sets acquired at each sensor location were post-processed in *Matlab* to calculate the average Frequency Fourier Transform (FFT) and, thus, improving the signal to noise ratio. By analyzing the magnitude of the mean FFT, three natural frequencies, namely, 1580 Hz, 2860 Hz, and 3915 Hz, were selected for the following SSM tests. As shown in figure 4.11, these frequency values were associated with clearly detectable resonance peaks in the spectra of both sensors.

During the SSM tests with harmonic excitation, a pure-tone harmonic signal produced by a *TTI TG5011A* function generator was fed into the stack actuator. Simultaneously, the stationary response of the system at both sensor locations (i.e., S1 and S2) was acquired employing the *Cleverscope CS328A* data acquisition unit with a sampling rate of 267 kSamples/s and a time window of 2 s. The composite beam was first tested in pristine conditions at any of the three selected frequencies and by ranging the excitation amplitude between 1 and 6 V_{pp} in 1 V steps. Subsequently, the measurements were repeated after each impact, i.e., for each considered stage of the damage evolution process.
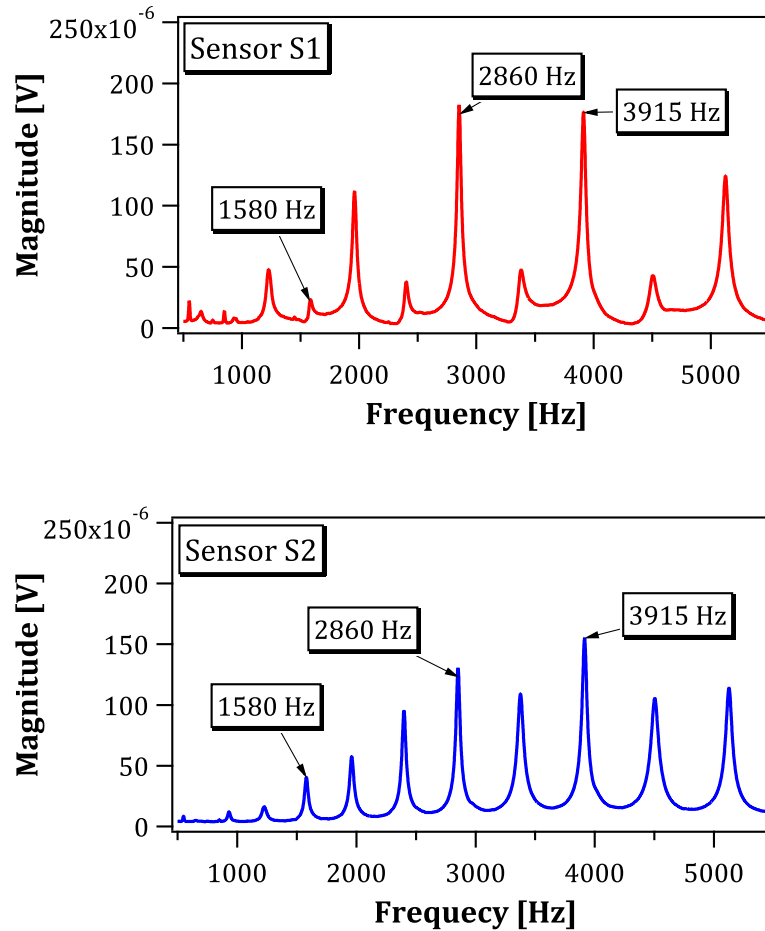
Figure 4.11 – Averaged power spectrum of the inspected composite sample at sensor locations S1 (red line) and S2 (blue line).

Concerning the pulse-based approach, the adopted experimental procedure was analogous to the one used for the SSM harmonic tests. The stack actuator was again piloted by the *TTI TG5011A* function generator, even though the driving signal consisted of only one cycle of a square wave with 40 μs width and coupled rise and fall time of 40 ns (figure 4.12). The input signal amplitude was raised from 1 V_{pp} up to 6 V_{pp} in 1 V increments. The corresponding responses at sensors S1 and S2 were recorded at the sampling frequency of 267 kSamples/s in both pristine and damaged conditions. Moreover, 40 datasets were acquired to improve the signal-to-noise ratio and evaluate the averaged spectra of the system response.
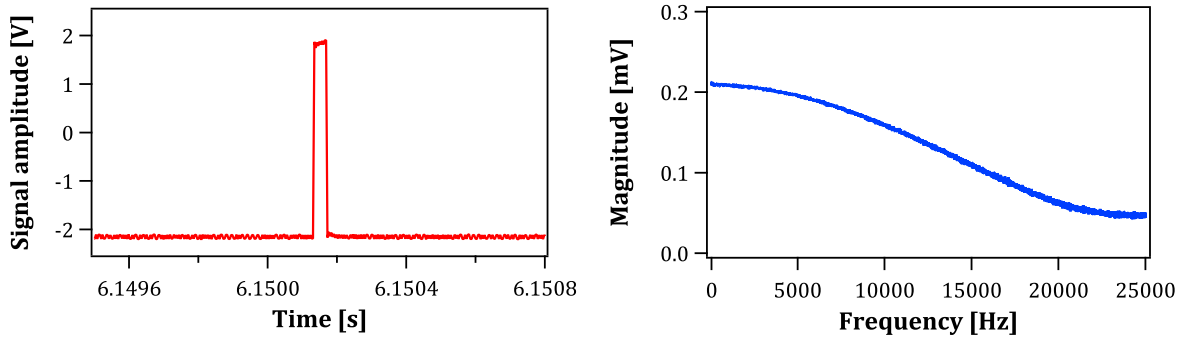
Figure 4.12 – Pulse signal: time history (red line) and frequency spectrum (blue line).

4.4   Data analysis

As stated in [172], the effectiveness of the Scaling Subtraction Method in detecting the occurrence of impact damage in composite materials depends on the interrogating frequency. Since the frequency selection requires the preliminary characterization of the modal response of the inspected structure, the use of an impulsive broadband excitation allows to bypass this limitation and, at once, reduce the risk of picking natural frequencies whose sensitivity to damage detection could be low.

To date, the first attempt to apply rectangular pulse excitation to characterize the nonlinear behavior of a structure employing the Scaling Subtraction Method was reported by Ouarabi et al. [174] in 2017. The analysis, which was aimed to investigate the acoustic response of a cracked cementitious mortar interacting with a sodium silicate solution, was performed in the time domain according to the procedure described in [167] [168]. Therefore, the damage indicators adopted to quantify the nonlinear content of the acquired signals were those defined by equations 4.7 and 4.8.

Nevertheless, since an impulsive input excites a wide range of frequencies, it is possible to estimate the contribution that a specific spectral component gives to the nonlinear signature of the inspected sample by carrying out the damage detection

analysis in the frequency domain. Thus, in analogy to the time-domain approach proposed by Scalerandi et al. [167], the information on the material integrity was provided by comparing the spectral magnitude of the considered frequency component of both the actual system response and the linear reference signal. In fact, calculating the difference between the amplitude of the selected spectral components of the system response and that of the linear reference signal permits the identification of any deviations from the theoretical linearity and, hence, both the detection and the monitoring of internal damage. The need to evaluate both the applicability and the sensitivity of the Scaling Subtraction Method and, at once, quantify the nonlinear content of the system response resulted in the definition of two novel damage indexes based on the analysis of the magnitude of the spectral components associated with the considered frequencies. The first damage index, which estimates the deviation of system response from the expected linearity at the highest excitation level, can be expressed as:

$$DI = \frac{B\left(A_{high}\right) - k\, B(A_{low})}{k_{high}\, B(A_{low})} \tag{4.11}$$

where $B\left(A_{high}\right)$ refers to the amplitude of the system response acquired at the highest excitation level, and $B(A_{low})$ represents the system response amplitude corresponding to the minimum (A_{low}) excitation level, which was also used for defining the linear reference signal, and k_{high} is the scaling factor associated with the highest excitation level.

Instead, since the second damage index aims to quantify the cumulative effects of the nonlinear contributions associated with the considered excitation levels, it has been defined as

$$DI_{\Sigma} = \sum_{i=1} \frac{B(A_i) - k\, B(A_{low})}{k\, B(A_{low})} \tag{4.12}$$

where $B(A_i)$ is the amplitude of the output signal recorded at a generic excitation level $(A_i = k\, A_{low})$. Thus, this second damage parameter allows to aggregate the nonlinear effects related to the applied excitation levels by calculating how far experimental data deviate from the theoretical linearity. Therefore, in order to both evaluate and analyze the two proposed damage indexes (i.e., DI and DI_{Σ}), the system

responses to an impulsive broadband excitation were post-processed in *Matlab* to calculate the averaged Fast Fourier Transform (FFT) and extract the magnitude corresponding to the considered frequency components. Conversely, the signals acquired in response to the pure-tone harmonic excitations were loaded in *Matlab* and analyzed to determine their peak-to-peak amplitudes. As an example, figure 4.13 shows the amplitude of the system response acquired, for both the undamaged and the damaged specimen impacted at 1.7 and 5.5 J (i.e., Damage 1 and Damage 2), at the sensor location S1 as a function of the amplitude of the driving harmonic input at 3915 Hz. These trends make it possible to notice that even if the undamaged beam behaves almost linearly within the whole range of excitation amplitudes, the curve associated with the first level of damage severity starts to deviate from the theoretical linearity at an excitation of about 4 V_{pp}.
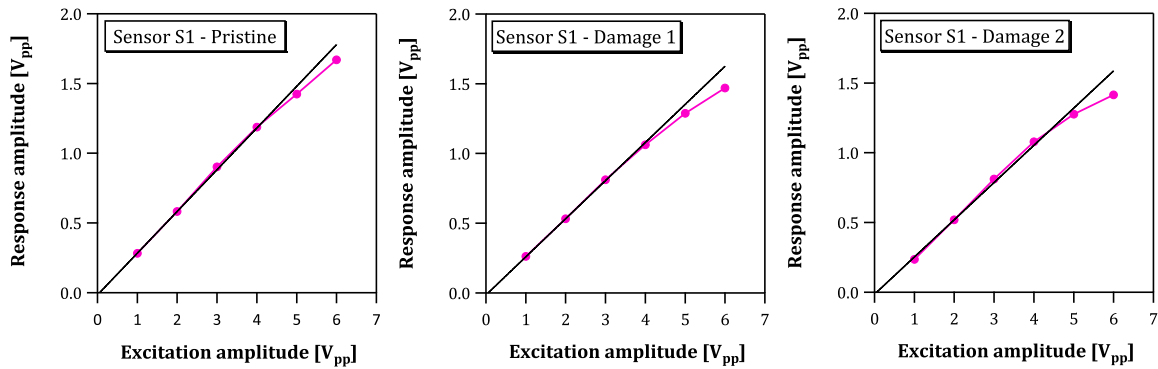
Figure 4.13 – System response amplitude *vs.* excitation amplitude for the (a) undamaged pristine, (b) Damage 1 and (c) Damage 2 conditions. Signals were recorded at sensor S1 for the excitation frequency of 3915 Hz.

4.5   Results

The damage index *DI* quantifies the distance between the amplitude actually measured at the maximum excitation (i.e., 6 V_{pp}) and the amplitude that would have been recorded if the hypothesis of perfect linearity were to be confirmed. By

independently analyzing the response acquired at both sensor locations (i.e., S1 and S2 in figure 4.10) and for the three considered harmonic excitations (i.e., 1580, 2860, and 3915 Hz), the damage index DI was evaluated through equation 4.11. Plotting the obtained values against the damage severity (figure 4.14) allows noticing that contrary to what was expected, the damage indicator DI does not vanish for the undamaged beam (namely, pristine case in the diagrams of figure 4.14). Previous studies that aimed to characterize the nonlinear response of laminated composite samples to acoustic or ultrasonic waves [175] [172] have already reported the emergence of this evidence, indicating as possible causes the intrinsic nonlinearity of the instrumentation and non-damage-related inherent nonlinear sources. The latter mainly consists of manufacturing defects whose size falls below the detection threshold of ultrasonic C-scanning. Moreover, it is worth remarking that the damage indicator DI sharply increases with the damage severity, whatever the interrogating frequency and the examined sensor location. In particular, even though the two sensors were located on the opposite sides of the damaged area (figure 4.10), no significant difference might be observed between the corresponding DI values. This evidence appears to suggest the chance to detect internal damage even when the path between the excitation and the sensing location does not cross the impacted region. Furthermore, although the damage index DI provides a clear indication of the presence of impact damage in correspondence of all the selected frequencies, the sensitivity of the Scaling Subtraction Method seems to be affected by the excitation frequency. In this context, it may be observed that at the lowest damage severity (i.e., Damage 1), the damage index values associated with the excitation frequencies of 1580 and 2860 Hz more than doubled relative to the pristine condition. However, when the excitation frequency of 3915 Hz was applied to drive the system, the damage index evaluated at the undamaged condition differs from that obtained for the early damaged level (Damage 1) only by about 60%. Similar considerations also apply to the analysis of damage index DI_Σ trend (figure 4.15). In fact, by accounting for the cumulative effect of the nonlinear contributions evaluated overall excitation amplitudes applied in the experiments, this second index (equation 4.12) seems to ensure enhanced sensitivity to damage for the tests that employ 1580 and 2860 Hz excitations. However, no significant improvement was observed in the efficiency with which the considered approach identifies the onset of the lowest damage severity at

the 3915 Hz excitation. Therefore, these results highlight the dependence of the damage detection capabilities of the Scaling Subtraction Method on the excitation frequency, confirming the findings reported in [172].
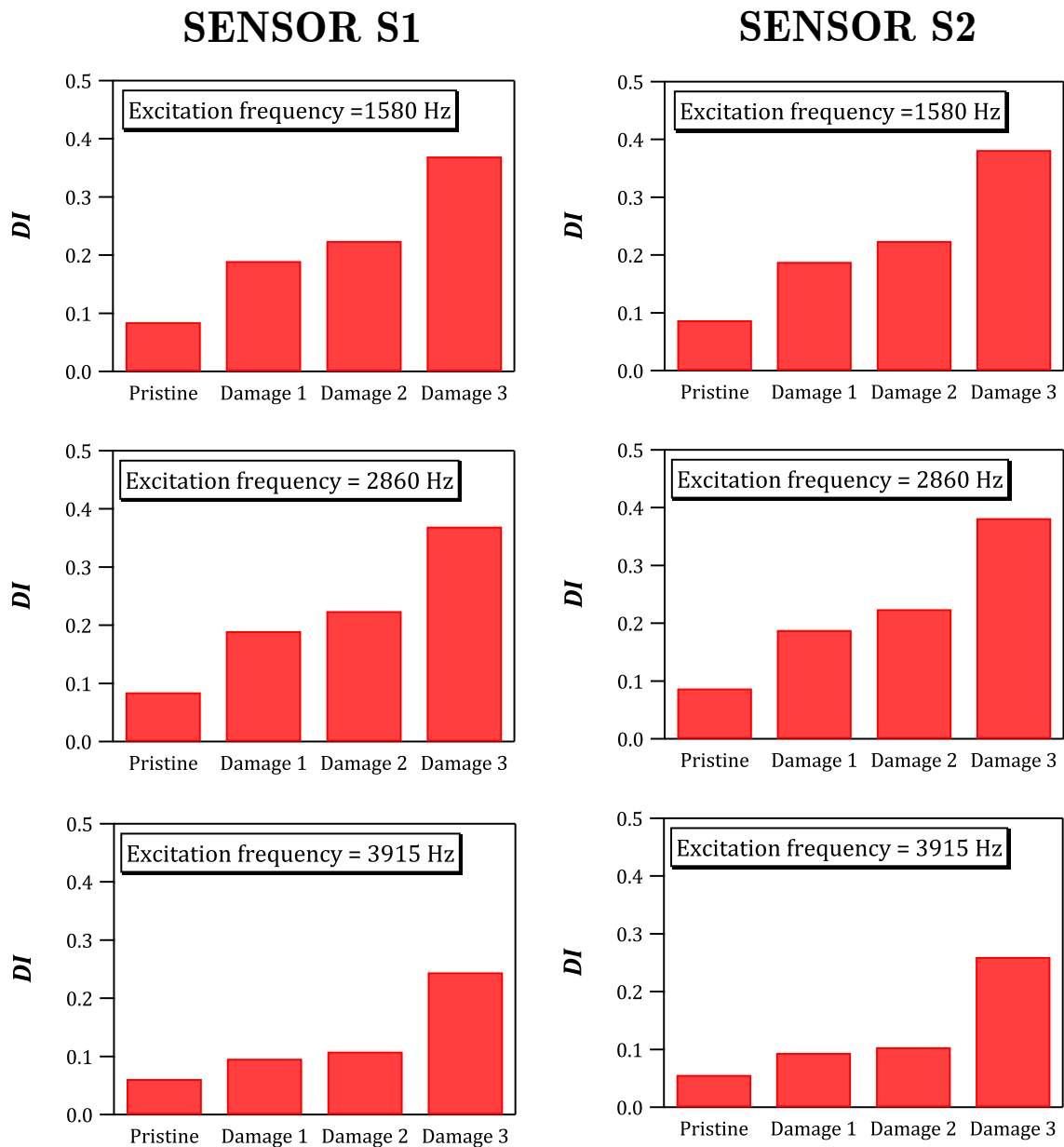

Figure 4.14 – Harmonic excitation: damage index *DI* evaluated for the three excitation frequencies vs. increasing damage severities.
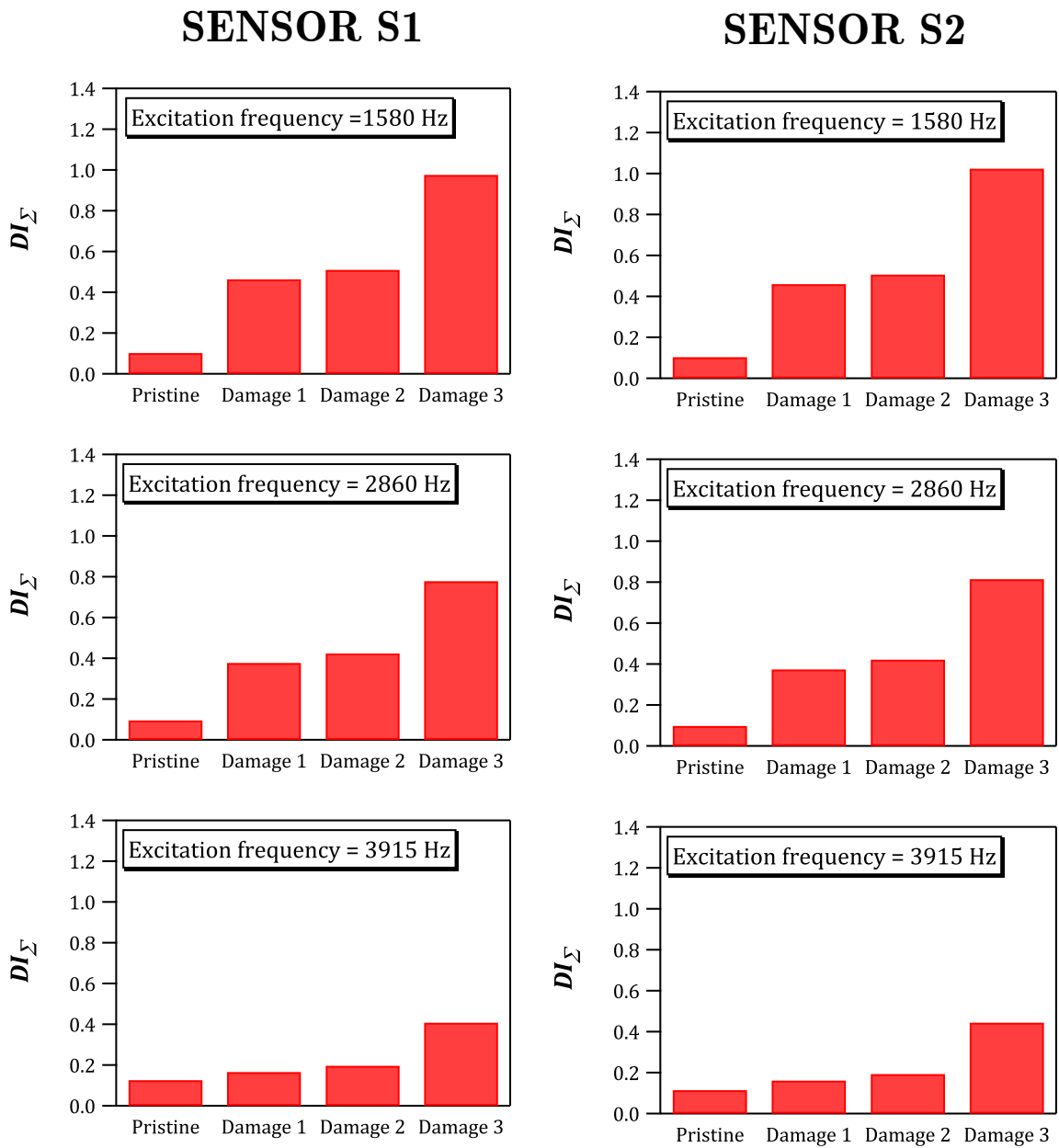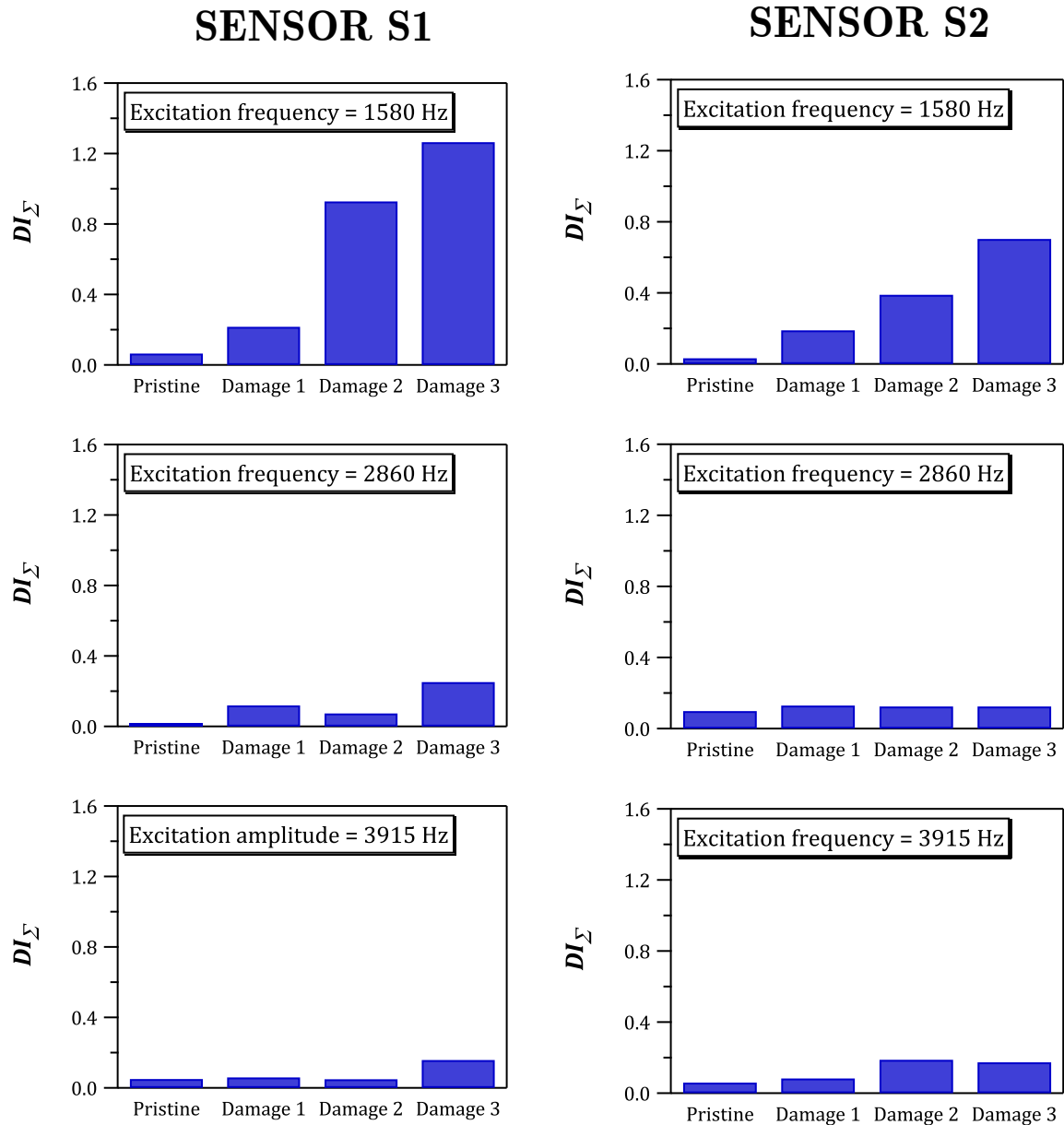
SENSOR S1

SENSOR S2

Figure 4.15 – Harmonic excitation: damage index DI_{Σ} evaluated for the three excitation frequencies vs. increasing damage severities.

Since the damage index DI_{Σ} was able to provide reliable indications on the onset and the growth of internal damage when a pure-tone harmonic excitation was applied, it was also employed to characterize the efficiency and the sensitivity of the proposed pulse-based SSM approach. For this purpose, the magnitudes of the spectral lines that correspond to the three frequencies applied for the harmonic excitation

tests (i.e., 1580, 2860, and 3915 Hz) were extracted from the averaged spectra of the signals acquired in response to an impulsive broadband excitation and then used to calculate the damage index DI_Σ. The obtained results corresponding to the two sensor locations (i.e., S1 and S2) and the three interrogating frequencies were plotted as a function of the damage severity and then reported in figure 4.16.

Figure 4.16 – Impulsive excitation: damage index DI_Σ evaluated for the three excitation frequencies vs. increasing damage severities.

These graphics indicate that the damage index DI_{Σ} associated with the spectral frequency of 1580 Hz provides clear information on the presence of impact damage at both sensor locations and, at one, manages to monitor the damage evolution process by ranking the damage levels in order of increasing severity. However, it is worth remarking that at the sensor location S1, the damage index assumes values significantly higher than those measured through the other sensor (i.e., sensor S2). This evidence appears to suggest that also the sensor position might affect the performance of this approach. In this context, an explanation is to be sought in the relative positioning of the two sensors. In fact, sensor S2 is positioned at a longer distance from the actuator than sensor S1 (see figure 4.10). However, a further explanation arises from considering that in contrast to the stationary nature of a pure-tone harmonic wave, the propagation of an impulsive signal in a continuum is a transient phenomenon. Conversely, the results relative to the interrogating frequencies of 2860 and 3915 Hz do not provide any reliable indication of the presence of impact damage or its severity. Therefore, as for the harmonic excitation case, the effectiveness of the Scaling Subtraction Method was found to be significantly affected by the selected excitation frequency. It is also worth remarking that with respect to the frequency of 1580Hz, the damage index DI_{Σ} assumes values considerably higher than those relative to the other two considered frequencies (namely, 2860 Hz and 3915 Hz), indicating a good level of sensitivity to the damage detection. Hence, in order to further improve both the efficiency and robustness of the proposed SSM
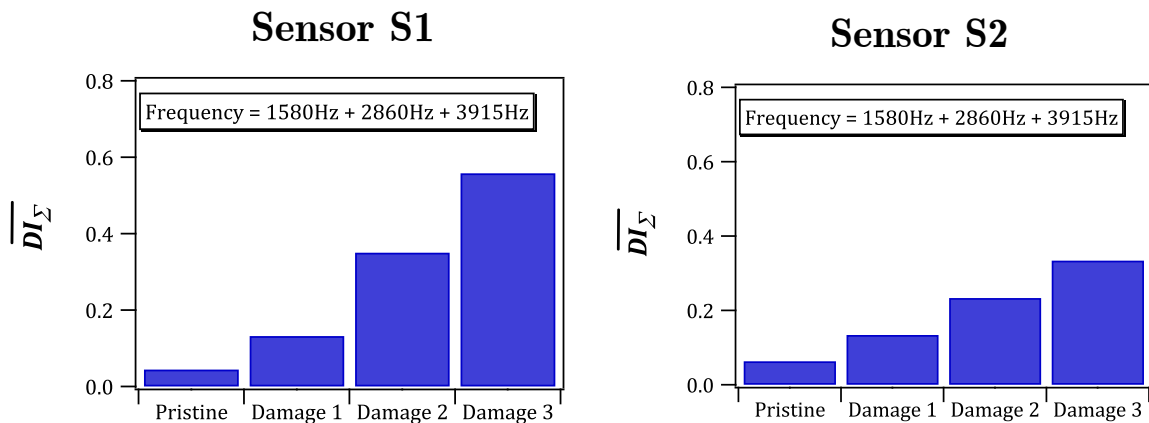

Figure 4.17 – Impulsive excitation: damage index DI_{Σ} evaluated for the three excitation frequencies vs. increasing damage severities.

pulse-based approach, a third index was introduced. Defined as the average values of the damage indexes DI_Σ associated with each of the considered testing frequencies, this index provides a global estimation of the nonlinear content of the system response. As shown in figure 4.17, averaging the damage index corresponding to all the interrogating frequencies (i.e., 1580, 2860, and 3915 Hz) leads to an improvement of the effectiveness of the proposed pulse-based SSM approach in both detecting the damage occurrence and monitoring its evolution.

4.6   Conclusions

Since its first applications, the Scaling Subtraction Method has been used to characterize the nonlinear response of an inspected system driven through a pure-tone harmonic excitation at a frequency chosen among the system natural frequencies. Thus, these investigations highlighted the two main drawbacks of the Scaling Subtraction Method: (1) the need for preliminary characterization of the modal response of the sample and (2) its sensitivity to the interrogating frequency. Since both these limitations might be overcome by driving the system through a broadband excitation, the above-described experimental investigation aimed to assess the effectiveness of SSM-based methodology in which a transient impulsive excitation is applied to excite the structure. Moreover, to both verify the feasibility of a pulse-based SSM approach and validate the obtained results, two series of experimental tests in which the composite sample was excited in turn through a monoharmonic input and an impulsive signal were performed.

The results relative to the tests carried out under harmonic excitation confirm the influence of interrogating frequency on the Scaling Subtraction Method sensitivity. Moreover, no significant difference has been observed in the results associated with the two considered sensor locations, suggesting the chance of detecting the presence of impact damage and monitoring its progression regardless of the sensor position.

Given the reliable indications provided in the harmonic excitation case, the damage index DI_Σ was chosen for testing and characterizing both the feasibility and

the performance of the pulse-based SSM approach. In fact, by summing up the nonlinear contributions associated with all the considered excitation levels at each of the interrogating frequencies, this damage indicator managed to retrieve a consistent and reliable indication of the damage occurrence. Furthermore, its application allowed to monitor the damage evolution by properly grading the damage severity, at least in correspondence to the 1580 Hz excitation frequency. In fact, the values assumed by the damage index for the driving frequencies of 2860 and 3915 Hz do not regularly vary with the damage severity, not providing any clear evidence of the presence and the extent of the internal damage. Therefore, in analogy to the results obtained for the harmonic excitation case, the sensitivity of the proposed pulse-based SSM approach was found to depend on the frequency chosen for the analysis. In order to address this issue, the mean of the damage index DI_{Σ} values relative to all the interrogating frequencies was assumed as a global damage indicator to improve both effectiveness and the robustness of the described pulse-based approach.

In the end, the obtained results reveal this approach as a rather promising option for both detecting and characterizing the nonlinearities arising from the onset of impact damage in composite materials. Nevertheless, further investigations are needed to investigate the effects of factors as the sample geometry, the stacking sequence, the operating and environmental conditions on the performance of the pulse-based SSM approach.

Chapter 5

Nonlinear Vibroacoustic Modulation

Among the so-called pump-probe techniques (section 3.2.4), which rely upon simultaneously exciting the inspected structure through two impinging waves (namely, a probe and a pump signal), the Nonlinear Vibro-Acoustic Modulation has gained increasing attention. In fact, in the past few decades, the VAM approach has been widely applied to retrieve information on the onset and the growth of internal damage in metallic and composite structures. Nonetheless, the physics behind the interaction of the dynamic fields associated with the two input signals and the nonlinear mechanisms involved in the arising wave modulation are still not fully understood.

5.1   Nonlinear Vibro-Acoustic Modulation: theory

The *Nonlinear Vibro-Acoustic Modulation* (VAM), also referred to as *Nonlinear Wave Modulation Spectrometry* (NWMS) [146], *Nonlinear Ultrasonic Wave Modulation* [147] or Nonlinear Acoustic Modulation (NAM), was proposed in [148] as a viable tool for crack detection in solid materials. By investigating the interaction of a probe acoustic wave and a powerful pump pulse signal, the authors theoretically demonstrated the feasibility of the suggested approach to identify the emergence of the nonlinear effects related to the intrinsic nonlinearity of closed cracks. These findings were confirmed by experimental investigations aimed to characterize the nonlinear response of cracks and discontinuity-like inhomogeneities in solids.
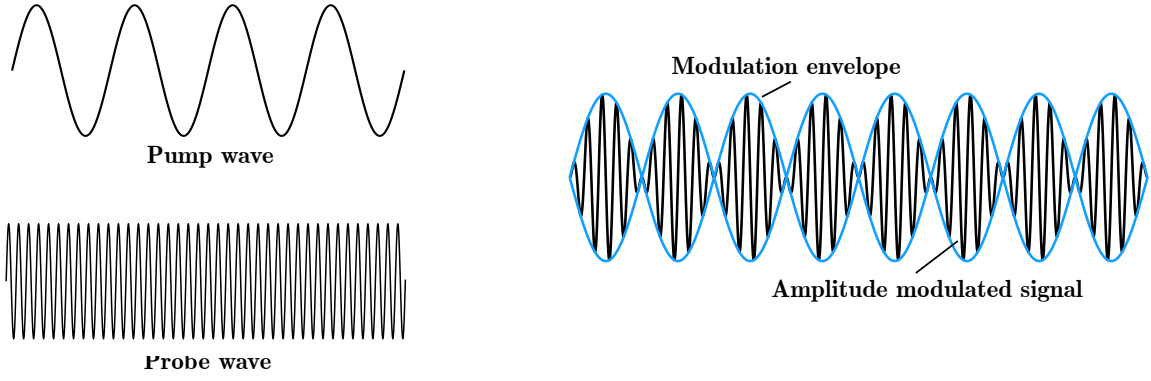
Figure 5.1 – Amplitude modulation signal: modulation index lower than 1 (undermodulation).

In more general terms, the Nonlinear Vibro-Acoustic Modulation consists in concurrently exciting the considered structure through a pump wave corresponding to one of its resonance frequencies to induce a stress field within the specimen and, at once, perturb the enclosed sources of nonlinearities, and a probe wave (also referred to as carrier wave) that senses the stiffness variation caused by the pump vibration. In fact, the presence of internal damage and discontinuities results in the emergence of modulation effects, due to which the pump wave modulates the probe wave. In this context, given the pump and the probe signals:

$$v_{pump}(t) = V_{pump} \cos(2\pi f_{pump} t + \varphi_{pump}) \qquad (5.1)$$

$$v_{probe}(t) = V_{probe} \cos(2\pi f_{probe} t) \qquad (5.2)$$

the amplitude modulated signal (figure 5.1) can be expressed according to the equation:

$$v_{mod}(t) = V_{probe} [1 + v_{pump}(t)] \cos(2\pi f_{probe} t) \qquad (5.3)$$

and, thus,

$$v_{mod}(t) = v_{probe}(t) + \frac{V_{probe} V_{pump}}{2} \cos[2\pi (f_{pump} + f_{probe}) t + \varphi_{pump}] +$$
$$\frac{V_{probe} V_{pump}}{2} \cos[2\pi (f_{probe} - f_{pump}) t + \varphi_{pump}] \qquad (5.4)$$
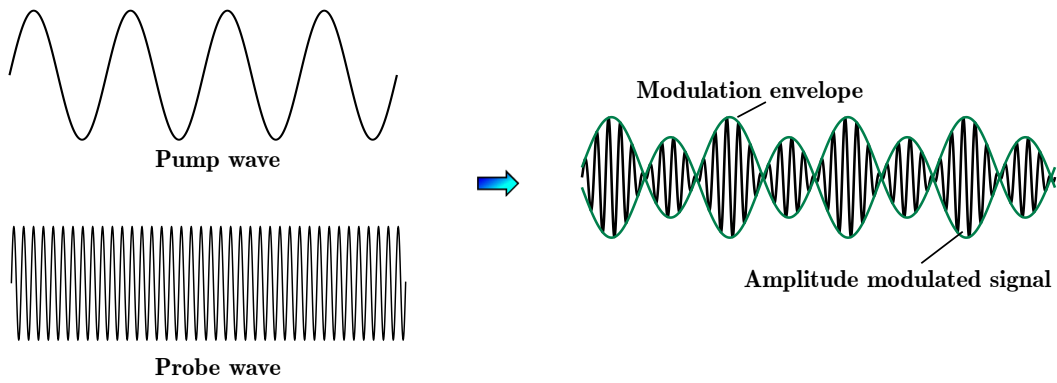
Figure 5.2 – Amplitude modulation signal: modulation index greater than 1 (overmodulation).

where V_{pump} and f_{pump} represent the amplitude and the frequency of the pump excitation signal and V_{probe} and f_{probe} those of the probe wave. The modulation intensity the carrier wave undergoes can be expressed as the ratio between the amplitude of the two excitation waves (i.e., pump and probe wave). This parameter, generally referred to as *modulation depth* or *modulation index*, assumes values minor to 1. In fact, an increase in the modulation index corresponds to a 180° phase reversal of the carrier wave, which causes the occurrence of additional spurious components. Thus, when the modulation index becomes higher than 1, the system response becomes overmodulated (figure 5.2), and hence, the wave gets distorted, making it impossible to retrieve the information on the material integrity or the damage presence.

Under the hypothesis of perfect linearity, the material response varies in proportion to the input signal, and the superposition principle holds. Therefore, if the displacement field applied to excite the inspected structure consists of the linear combination of two sine waves (namely, the pump and the probe wave), the spectrum of the signal response of a linear undamaged material exhibits only the two frequency components corresponding to the carrier and the pump excitation signals (figure 5.3). Conversely, the presence of internal damage (i.e., cracks, delaminations, voids, and discontinuities) within the sample triggers the occurrence of nonlinear mechanisms, due to which the material behavior deviates from the theoretical linearity. Thus, in order to account for the emerged nonlinearities, Hooke's Law has to be expanded
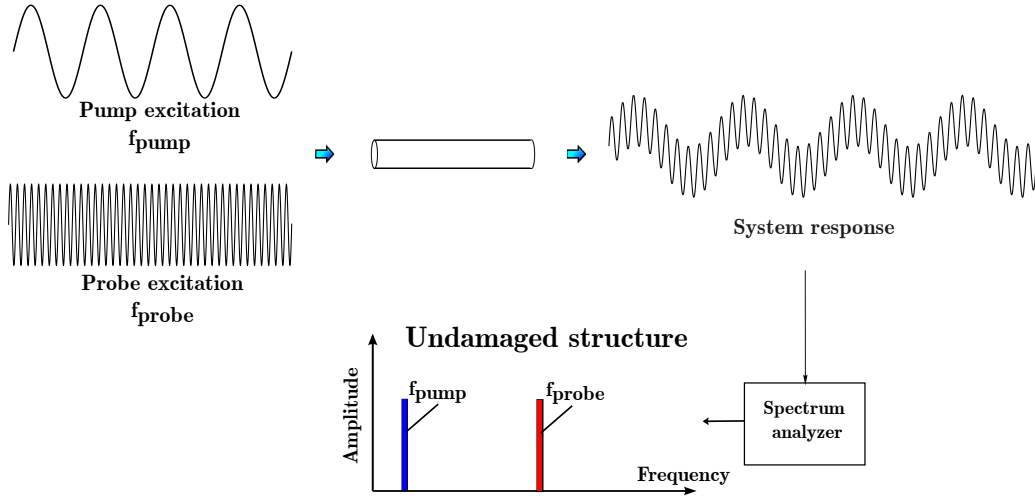
Nonlinear Vibroacoustic Modulation

Figure 5.3 – Schematic representation of the Nonlinear Vibro-Acoustic Modulation (VAM): response of a linear undamaged structure.

accordingly to equation 3.4. In this context, the solution of the wave propagation equation (equations 3.1 and 3.5), i.e., the displacement field arising from the interaction of the two excitation waves can be determined by applying the perturbation theory. Therefore, if the zero-order solutions are assumed to be of the form of a pure-tone harmonic wave, the global displacement field resulting from the sum of the displacement fields associated with the two waves (i.e., the pump and the probe excitation) might be expressed as: [10]:

$$u\,(x,t) = \; u_{pump}\,(x,t) + \; u_{probe}\,(x,t)$$

$$u\,(x,t) = A_1 \sin\left(2\pi f_{pump}\,t\right) + B_1 \cos\left(2\pi f_{pump}\,t\right) + A_2 \sin\left(2\pi f_{probe}\,t\right) + B_2 \cos\left(2\pi f_{probe}\,t\right) \tag{5.5}$$

where A_i and B_i are amplitude coefficients that are a function of the direction of the wave propagation. Consequently, the stress field associated with the two excitation waves can be expressed are [10]:

$$\sigma\,(x,t) = E_0\,\varepsilon\,(x,t) + \; E_0\beta\,\varepsilon^2(x,t) \tag{5.6}$$

and, thus [10]:

$$
\begin{aligned}
\sigma\left(x, t\right) = \ & E_0 \left[A_1' \sin\left(\omega_{pump} t\right) + B_1' \cos\left(\omega_{pump} t\right) + A_2' \sin\left(\omega_{probe} t\right) + \right. \\
& \left. B_2' \cos\left(\omega_{probe} t\right)\right] + E_0 \beta \left[N_1 \cos\left(2\omega_{probe} t\right) + N_2 \cos\left(2\omega_{pump} t\right)\left(\omega_{probe} t\right) + \right. \\
& N_3 \cos[\left(\omega_{probe} + \omega_{pump}\right) t] + N_4 \cos[\left(\omega_{probe} - \omega_{pump}\right) t] + \\
& N_5 \sin\left(2\omega_{probe} t\right) + N_6 \sin\left(2\omega_{pump} t\right)\left(\omega_{probe} t\right) + \\
& N_7 \sin[\left(\omega_{probe} + \omega_{pump}\right) t] + N_8 \sin[\left(\omega_{probe} - \omega_{pump}\right) t]
\end{aligned} \tag{5.7}
$$

where E_0 represents the linear elastic modulus, β is the first-order elastic coefficients, ω_{pump} and ω_{probe} indicate the angular frequencies of the pump and the probe wave, respectively, A_i' and B_i' denotes derivative of A_i and B_i (equation 5.5), and N_i is multiply factors that depend on the amplitude coefficients A_i and B_i of equation 5.5. It is worth noticing that when applied to the wave propagation equation (equation 3.1), the perturbation theory allows to predict the emergence of several spectral lines. In fact, if the first term of Hooke's law expansion (i.e., the linear term associated with E_0) is responsible for the frequency components corresponding to the input frequencies, the first-order nonlinear term (namely, the contribution related to the nonlinear parameter β) leads to the occurrence of spectral lines at frequency values that are multiples of the fundamental ones, i.e., higher harmonics of both the pump and probe waves, as well as the modulation components. Therefore, the occurrence and the progression of internal damage perturbate the propagation of the two input waves, leading to the emergence of additional frequency components (sidebands) around the probing carrier frequency (figure 5.4). These modulation sidebands typically occur in pairs (i.e., left and right sidebands) at frequency values corresponding to the sum and the difference of the frequencies of the excitation signals:

$$
f_{SB_n} = f_{probe} \pm n \, f_{pump} \tag{5.8}
$$

where f_{probe} and f_{pump} are the frequency of the pump and probe waves, respectively, and n is a positive integer number.

Since the earlier applications of the Nonlinear Vibro-Acoustic Modulation, several authors highlighted the dependence of the onset and the magnitude of the modulation sidebands on the presence of internal damaged and its severity. In this context, the need to quantify the nonlinear content of the structural response and, at once,
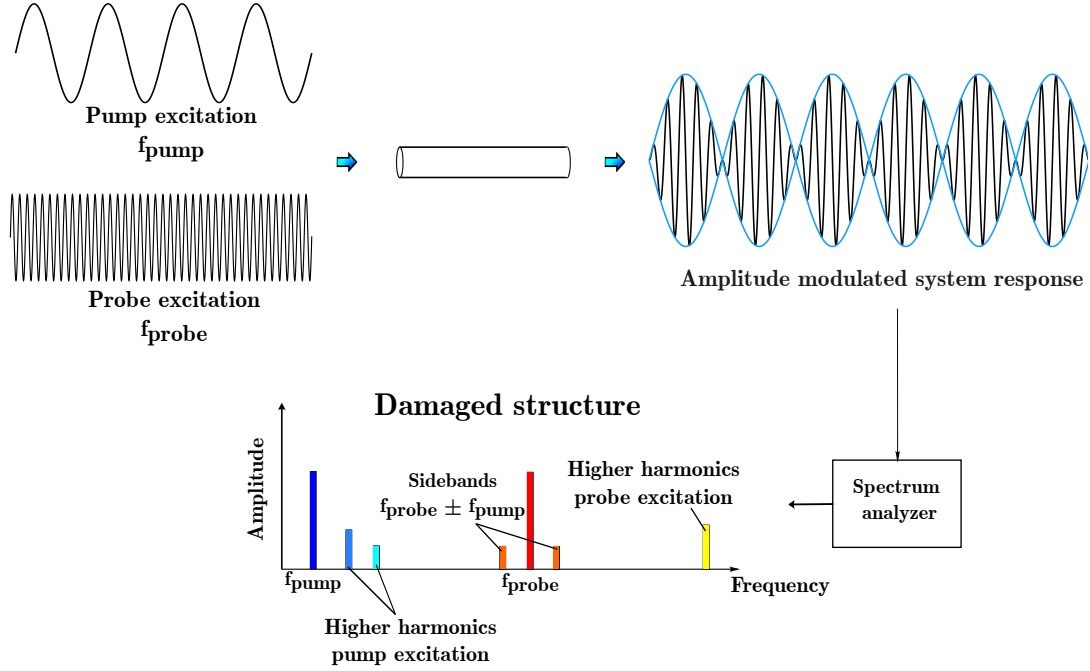
Figure 5.4 – Schematic representation of the Nonlinear Vibro-Acoustic Modulation (VAM): response of a nonlinear damaged structure.

monitor the degradation of the material properties resulted in the definition of various damage indicators. Therefore, besides the amplitude of the first pair of modulation sidebands, the most commonly adopted damage parameter is the ratio between the sum of the amplitudes of the *i-th* pair of sidebands ($A_{SB,left}^i$ and $A_{SB,right}^i$) and the amplitude of the probe frequency spectral component (A_{probe}) [157] [166] [175]:

$$R = \frac{\sum_{i=1}^{k} A_{SB,left}^i + A_{SB,right}^i}{A_{probe}} \qquad (5.8)$$

More recently, many advanced signal processing techniques have been proposed and applied to further explore the effectiveness of the modulation sidebands as a damage detection tool. In this regard, in 2010, Yoder and Adams [176] developed an approach to investigate the influence of the probe frequency and, at once, improve the robustness of the VAM method for Structural Health Monitoring applications. To this purpose, the system response to a sweep sine probe excitation was acquired in the time domain and, subsequently, post-processed to extract the modulation

envelope through a Hilbert transform-based algorithm. The analysis of the short-time Fourier transform of the extracted envelope allows quantifying the modulation level of the recorded signals. Later on, Sohn et al. [147] [177] proposed a signal processing approach to isolate the first pair of modulation sidebands, relying upon the idea of separately exciting the inspected structure through a pure-tone harmonic pump excitation and linear chirp probe excitation before the actual VAM test. Subsequently, the Linear Response Subtraction (LRS) algorithm was applied in the time domain to calculate the difference between the system response recorded under a simultaneous dual excitation (i.e., VAM measurement) and the signals acquired when the two driving signals are applied independently from each other. Then, the subtracted signal was demodulated to extract the spectral components corresponding to the first pair of modulation sidebands. In this context, comparing the amplitudes of the sidebands measured in intact and damaged conditions allows to retrieve information on both the occurrence and the evolution of internal damage. Similar to the above-mentioned LRS-SD algorithm, the signal processing scheme presented in [178] [179], aims to attain a frequency-amplitude representation of the modulation sidebands. To this purpose, the acquired structural response are post-processed through a wavelet transform-based algorithm to extract the signal envelope and calculate its Fourier transform. Moreover, the need to quantify the extent of internal damage and locate it led to the development of approaches based on the bispectral analysis [180], the time-reversal algorithm [181] [182] [183], and the cointegration analysis [184].

5.2 Nonlinear Vibro-Acoustics Modulation: applications to impact damage in composite materials

Since its development, the Nonlinear Vibro-Acoustic Modulation method has been widely applied to detect the onset and the progression of structural damage in metallic materials. To date, VAM applications include the detection of fatigue crack detection in steel [185] [186] [176] and aluminum [187] [177] [183], aluminum and steel pipes [188], aircraft fuselage panels [189]. Nevertheless, applications to

composite materials are fewer and mostly concern the detection of barely visible impact damage in laminated composites and composite sandwich panels.

Among the first to explore the feasibility of applying the VAM method to composite materials, Meo and Zumpano [156] presented an experimental investigation on a sandwich panel cut from the firewall of a helicopter and impacted through a sharp indenter to produce a visible hole of 1 mm diameter and 5 mm depth. By comparing the spectra corresponding to the pristine and damaged conditions, the authors observed that the emergence of the modulation sideband followed the impact event. Therefore, they concluded that the spectra alone might provide a clear indication of the internal damage, which was said to be a combination of fiber breakage, matrix cracking, and core crushing. A few years later, Meo et al. [139] applied this technique to detect the presence of barely visible impact damage in unidirectional composite laminates with increasing damage severity. The results obtained through the Nonlinear Vibro-Acoustic Modulation testing highlighted the presence of a clear pattern of modulation sidebands in the response spectrum of the plate with the severest structural internal damage. Despite the details of the applied experimental procedure, such as the excitation frequencies of both the pump and the probe wave, the acquisition parameters, and the extent of the projected delaminated areas, are missing, the VAM method provided indications on the material integrity in good agreement with those obtained through the Nonlinear Resonant Ultrasound Spectroscopy (NRUS, section 3.2.3), demonstrating its damage detection capabilities.

Later on, in 2010, Aymerich and Staszewski [154] further explored the applicability of Nonlinear Vibro-Ultrasonics to detect impact damage in a carbon-epoxy composite laminate. The sample, which was impacted twice by a drop-weight testing machine to induce progressive damage, was simultaneously excited by means of a pump and a probe excitation in both intact and damaged conditions. In order to investigate the emergence and the growth of modulation sidebands and, at once, explore the dependence of their amplitude on both the damage severity and the frequency values selected for the excitation, multiple VAM tests were carried out by varying the pump and the probe frequency. In this regard, the averaged increase in the amplitude of the modulation sidebands was found to increase with the extent of the delaminated area (figure 5.5), even though the recorded increases were different
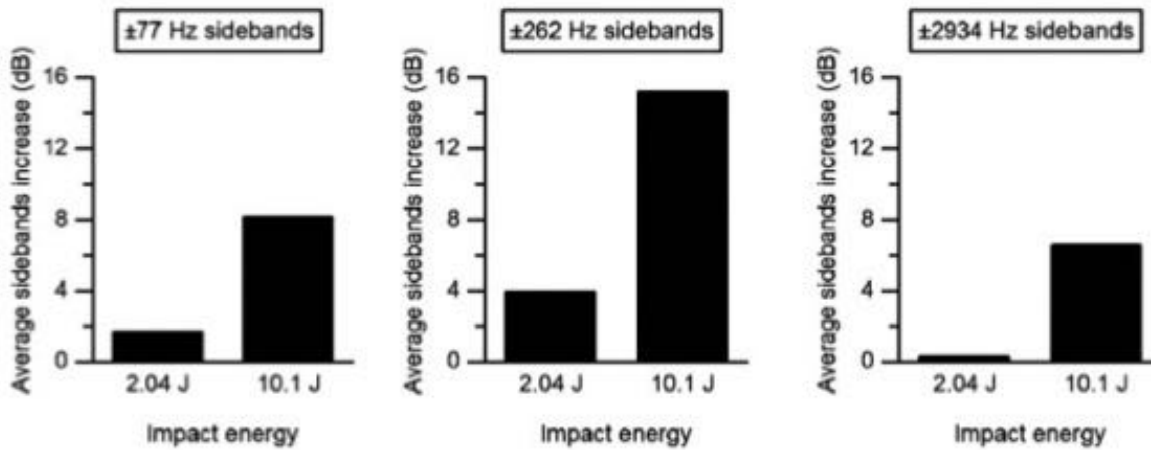
Figure 5.5 – Average increase in the amplitude of the modulation sidebands in impact-induced damaged composite plates [154].

for each of the considered pump-probe frequency combinations. Moreover, the presence of sidebands in the spectrum of the undamaged structure (figure 5.6) led the authors to suggest that the clamping force applied to the sample with a servo-hydraulic testing machine might result in additional nonlinear contributions. Therefore, the effects the nonlinearities associated with the boundary conditions (i.e., the clamping force) may produce on the effectiveness of the VAM technique were further investigated, showing that an increase in the clamping force corresponds to a decrease in the amplitude of the modulation sidebands (figure 5.7). This experimental evidence, i.e., reduced nonlinearity for increased clamping force, might be attributed to contact at the clamp-specimen interface. In fact, since raising the clamping force reduces the relative motion at the contact interface, the energy dissipation due to friction lessens. In the same year, the authors performed a second experimental investigation to explore the applicability of the cross-modulation technique [190], whose details are given in section 3.2.4. As the Nonlinear Vibro-Acoustic Modulation, the considered method exploits the occurrence of the modulation sideband to provide information on the material integrity. Thus, the amplitude of both the spectral lines associated with the probe excitation and the sidebands were used to define two damage indices [190]:

$$DI_1 \, [dB] = \left| A_{probe} - A_{SB} \right|_{undamaged} - \left| A_{probe} - A_{SB} \right|_{damaged} \qquad (5.9)$$
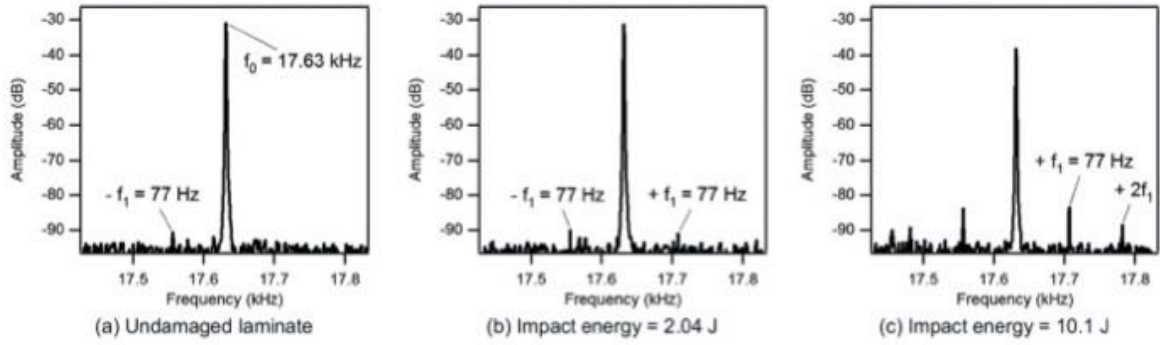
Figure 5.6 – Power spectra of the acoustic response of a laminated composite plate in both pristine and damaged conditions [154].
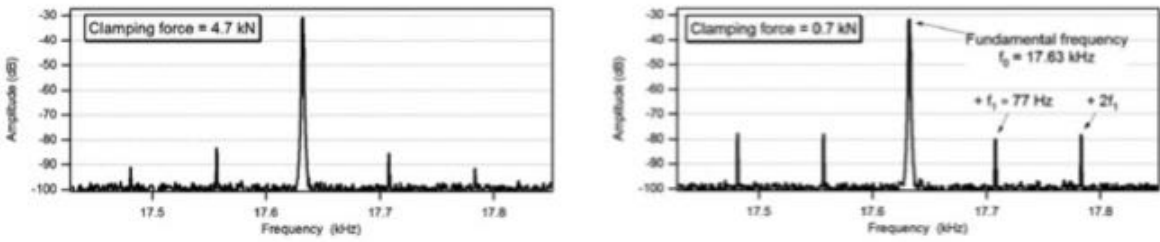
Figure 5.7 – Spectral magnitude of the acoustic response of a laminated composite plate for different clamping forces [154].

$$DI_2 \; = \; \frac{\left(V_{SB} / V_{probe}\right)_{damaged}}{\left(V_{SB} / V_{probe}\right)_{undamged}} - 1 \tag{5.10}$$

where A_{probe} and V_{probe} indicate the amplitude of the probe frequency spectral component measured in dB and volts, respectively, and A_{SB} and V_{SB} are the average amplitude of the first pair of sidebands expressed in dB and volts. Their variation with respect to the impact energy and the extent of the delaminated area reveal the sensitivity of both indexes to the onset of impact-induced damage in laminated composite samples.
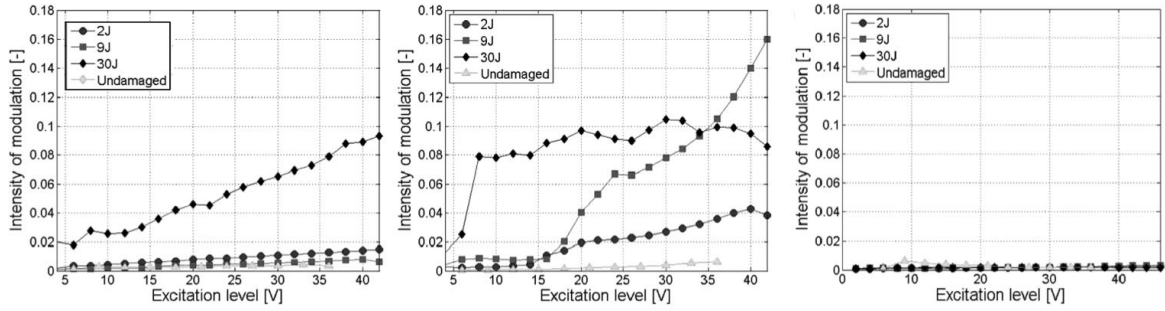
Figure 5.8 – Modulation intensity as a function of the pump excitation amplitude for different pumping frequencies [157].

More recently, a great research effort has been devoted to investigating the influence of the excitation frequency selection on the efficacy of the VAM and its capability to provide a clear indication of the presence of structural damage. In 2013, Klepka et al. [157] applied the Nonlinear Vibro-Acoustic Modulation to detect both the onset and the progression of impact damage in a chiral-core composite sandwich and, at once, analyzed the influence of the pump frequency selection on the VAM performance. To this purpose, the authors selected the frequency values associated with a global torsional mode shape, a pure flexural mode, and a combined torsional-flexural mode shape. Therefore, for each of the considered excitation scenarios, the modulation index was calculated accordingly with equation 5.4 and, subsequently, plotted against the excitation level (figure 5.8). The obtained results showed that the considered index varied almost monotonically with the driving amplitude for two out of the three selected pumping frequencies. Later on, Klepka et al. [178] attempted to investigate the effect of both the pump and the probe frequency selection on the Nonlinear Vibro-Acoustic Modulation performance. In this context, the authors picked out two ultrasonic probe frequencies and the frequency values of the 5th and the 7th mode shape of the inspected composite plate. Based on the evidence that changing either the pump or the probe wave might result in significant variation of the nonlinear content of the system response, it was observed that higher intensities of modulation derive from selecting pump frequencies that excite the delaminated interfaces with predominant out-of-plane motion and ultrasonic probe frequencies that match the natural resonances of the damage itself.

To conclude, the state of the art on the Nonlinear Vibro-Acoustic Modulation demonstrates the applicability and the effectiveness of this approach to provide information on the occurrence and the progression of internal damage in composite materials, and, at once, assuring a higher sensitivity than the traditional linear approaches. Nevertheless, the experimental studies conducted so far highlight that the method performance might be considerably affected by several parameters, i.e., the selection of excitation frequencies, the nonlinearities arising from boundaries and instrumentation. In particular, the boundary conditions might prevent the clear identification and characterization of the internal damage. In fact, boundary conditions are susceptible to introducing nonlinear effects that overlap with those strictly related to the material nonlinearity and, thus, mask the effects associated with the onset of internal damage. Similarly, since electronic devices and components have inherent nonlinearities, the measurement chain might influence the response of the inspected system and reduce the chance to detect the presence of damage by triggering the emergence of additional nonlinear effects. In addition, the lack of a robust algorithm to select the proper excitation frequencies, i.e., those with the highest sensitivity to internal damage, might result in low analysis effectiveness and, thus, the inability to provide clear indications of both the damage presence and severity. Moreover, since the frequencies of the two excitation signals (i.e., pump and probe signals) are commonly picked out among the natural frequencies of the inspected structure, preliminary modal analysis is required, making the procedure cumbersome and time-consuming. The need to further assessing whether the selection of these parameters (i.e., boundary conditions, excitation frequency, and actuation-sensing configuration) may affect the performance of the Nonlinear Vibro-Acoustic Modulation resulted in the development of the experimental campaign described in the following section.

5.3 Experimental investigations

Nonlinear Vibro-Acoustic Modulation tests have been conducted on three identical composite beams (also referred to as B1, B2, and B3 in the following sections) manufactured from *Seal Texipreg ®HS160/REM* carbon/epoxy prepreg

plies accordingly with the procedure described in detail in section 4.3.1. The composite samples were cut from a laminate with a $[0/90]_{3s}$ stacking sequence, which was cured in autoclave at a pressure of 8 bar and a maximum temperature of 160 °C in the shape of a 530 mm x 59 mm beam with a thickness of 2 mm. Before being tested under different boundary conditions and through different actuation-sensing scenarios (table 5.1), the composite beams were ultrasonically C-scanned to exclude the presence of manufacturing defects.
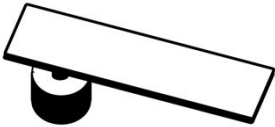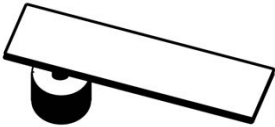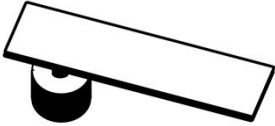
	Boundary conditions	Pump actuator	Probe actuator	Sensor
Sample B1	Supported at one end	Shaker	PZT	Accelorometer
Sample B2	Free-Free	Stack actuator	PZT	PZT
Sample B3	Supported at one end	Shaker	PZT	PZT - Accelerometer
Sample B3	Supported at one end	Stack actuator	PZT	PZT - Accelerometer

Table 5.1 – Test scenarios considered for the three inspected composite samples.

5.3.1 Sample B1

The composite sample B1 was instrumented with two transducers: a *PI Ceramic PIC 151* low-profile piezoelectric transducer (10 mm diameter and 1 mm thickness) glued to the beam top surface through a two-component epoxy adhesive and wired through welded connectors (figure 5.9), and a *DYTRAN 3224A1* micro-accelerometer attached to the beam top surface through a thin wax layer.
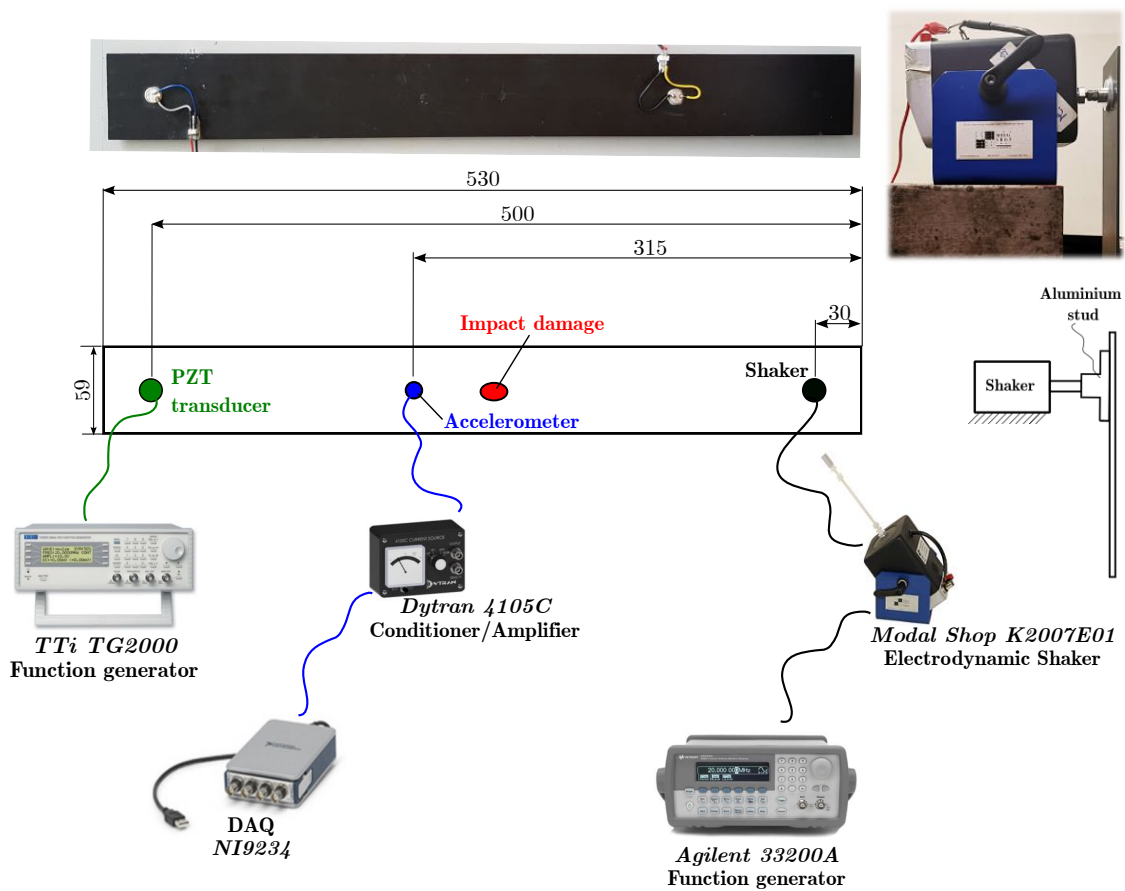

Figure 5.9 – Composite sample B1 and scheme of the experimental set-up adopted for the Nonlinear Vibro-Acoustic Modulation tests.

Aiming at introducing damage in the sample, the drop-weight testing machine described in section 4.3.2 was equipped with a hemispherical indenter (10 mm diameter) and employed to hit the composite specimen with an impact energy of 1.8 J and 2.4 J. The penetrant-enhanced X-radiography taken to characterize the extent
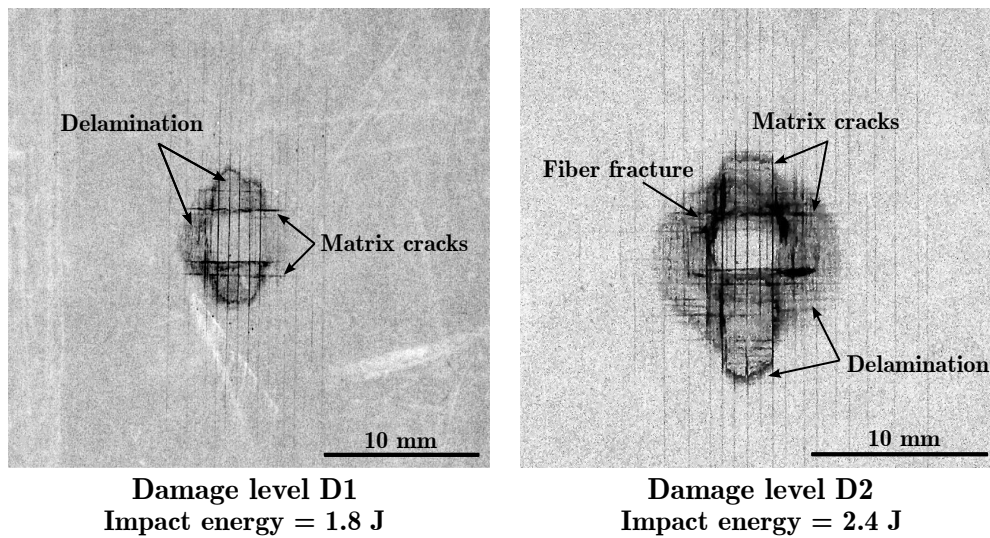
Damage level D1
Impact energy = 1.8 J

Damage level D2
Impact energy = 2.4 J

Figure 5.10 – X-ray images of the damaged areas corresponding to the tow considered impact severities.

and the nature of the internal damage resulting from the two impact events (also referred to as D1 and D2 in the following sections) revealed that the induced impact damage is mainly a combination of matrix cracks and delaminations at various interfaces of the laminated beam (figure 5.10). Nonetheless, some minor fiber breakage occurred at the indentation area after the 2.4 J impact. Moreover, the projected delamination areas corresponding to the two damage levels are 31.5 mm^2 and 92 mm^2, respectively.

5.3.1.1 Modal analysis

Since the selection of the pump frequency requires preliminary experimental modal analyses, the laminated composite beam was excited through a linear sweep sine starting from 1 Hz and crossing 1000 Hz in 15 s. The input signal was generated by an *Agilent 33200A* function generator driving a *Modal Shop K2007E01* electrodynamic shaker (figure 5.9). The connection between sample and shaker consists of a threaded aluminum stud, whose right end was glued to the bottom surface of the laminated beam by a two-component epoxy adhesive, and the left one connected to the threaded hole of the shaker (figure 5.9). The response of the
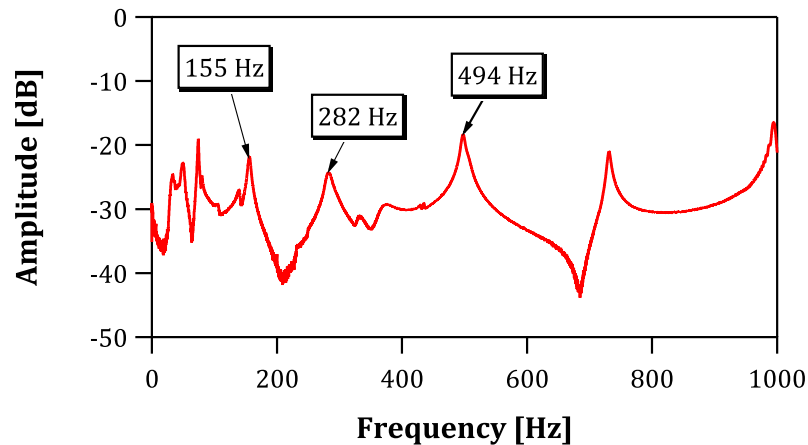
Figure 5.11 – Power spectrum of the system response acquired at the accelerometer location in the low-frequency range.

inspected sample monitored with the miniature accelerometer *DYTRAN 3224A1* mounted on the axis of the beam was subsequently fed into a *DYTRAN 4105C* conditioner set to amplify its input signal by a factor of 100. Then, a *National Instrument NI9234* PC-controlled data acquisition unit was used for recording ten data sets, allowing the calculation of the average Fast Fourier Transform (FFT) of the beam response and, thus, improving the signal-to-noise ratio. Three frequencies, namely 155 Hz, 282 Hz, and 494 Hz, were selected for the pump excitation in the VAM experiments (figure 5.11). In order to evaluate the mode shapes associated with these three frequencies, a 3D finite element model of the inspected structure, i.e., the set of the aluminum stud and the composite beam, was developed in *Abaqus*. The results obtained discretizing the aluminum stud with 10-nodes solid tetrahedral elements and the sample with 8-nodes brick element highlighted that the mode shapes corresponding to the selected frequencies are mainly characterized by out-of-plane bending (figure 5.12).

As regarding the carrier frequency selection, a procedure analogous to that described above was applied. In fact, a broadband a line sweep sine wave s starting from 1 kHz and reaching 7.5 kHz in 15 s was generated through an *Agilent 33200A* function generator and fed into the electrodynamic shaker. The composite beam response was sensed and acquired at the miniature accelerometer location. Ten data sets were recorded and post-processed in *Matlab* to calculate the magnitude of the
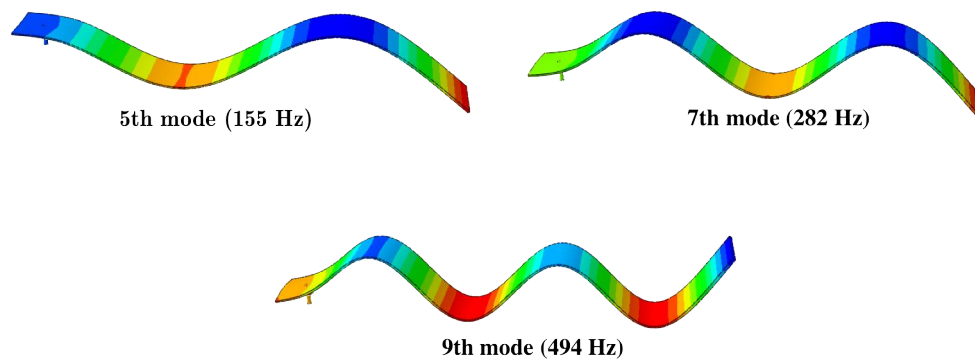
5th mode (155 Hz)   **7th mode (282 Hz)**

9th mode (494 Hz)

Figure 5.12 – Numerically predicted mode shapes relative to the selected pump frequencies.
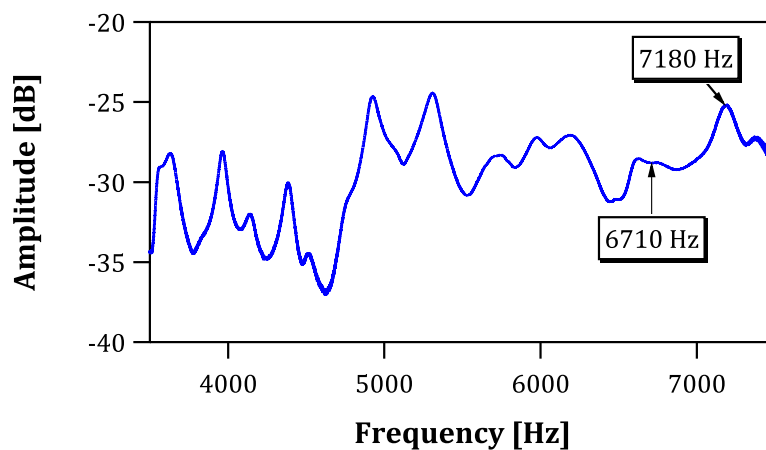

Figure 5.13 – Power spectrum of the system response acquired at the accelerometer location in the high-frequency range.

average power spectrum. Aiming to assess whether selecting a resonance as the probing frequency might affect the effectiveness of the Nonlinear Vibro-Acoustic Modulation, a resonance frequency, namely 7180 Hz, and a generic frequency value, i.e., 6710 Hz, were selected for the subsequent VAM test (figure 5.13).

In the end, the need to investigate the role of the two excitation frequencies on both the sensitivity and the efficacy of the Nonlinear Vibro-Acoustic Modulation method led to select three pump and two probe frequency values. Moreover, assessing

Probe frequency	Pump frequency	Pump amplitude		
	152 Hz	$0.5 V_{pp}$	$1.0\ V_{pp}$	$2.0\ V_{pp}$
6710 Hz	282 Hz	$2.0\ V_{pp}$	$4.0\ V_{pp}$	$6.0\ V_{pp}$
	494 Hz	$1.0\ V_{pp}$	$2.0\ V_{pp}$	$3.0\ V_{pp}$
	152 Hz	$0.2\ V_{pp}$	$0.5\ V_{pp}$	$1.0\ V_{pp}$
7180 Hz	282 Hz	$2.0\ V_{pp}$	$4.0\ V_{pp}$	$6.0\ V_{pp}$
	494 Hz	$1.0\ V_{pp}$	$2.0\ V_{pp}$	$3.0\ V_{pp}$

Table 5.2 – Damage characterization: main features of the impact damage at each of the three considered damage severities

the influence of the pump excitation level on the VAM ability to provide clear indications of the occurrence of internal damage make it necessary to consider three amplitude levels for each pump frequency. Thus, the Nonlinear Vibro-Acoustic Modulation tests were carried out on a total of eighteen different scenarios (table 5.2).

5.3.1.2 Nonlinear Vibro-Acoustic Modulation tests

The Nonlinear Vibro-Acoustic Modulation tests were conducted by driving the piezoelectric transducer (PZT) with a high-frequency monoharmonic sinusoidal signal (namely, probe excitation wave) and simultaneously exciting the selected low-frequency mode shape through the electrodynamic shaker (figure 5.9). Concerning the excitation level, while the magnitude of the probe signal was set to 20 V_{pp} and kept unchanged for the entire duration of the measurement campaign, the amplitude of the pump signal was varied in the considered range accordingly to the experimental plan of table 5.2. The system response to the two concurrent impinging waves has

been sensed at the miniature accelerometer location and recorded with a National Instrument *NI9234* digitizer at a 51.2 kSa/s sampling rate. In this context, for any of the considered excitation scenarios, thirty data sets consisting of 256 kpoints have been acquired and post-processed in *Matlab* to determine their averaged Fast Fourier Transform and, subsequently, extract the average amplitude of the first pair modulation sideband.

5.3.1.3 Results

In order to retrieve information on both the emergence and the growth of modulation sidebands, the power spectra of the response of the laminated composite beam were zoomed on a window centered on the probe frequency. Purely by way of example, figures 5.14 and 5.15 show the magnitude of the specimen response spectra acquired both before (i.e., pristine condition) and after the two low-velocity impacts (i.e., damaged conditions) in correspondence of a pump excitation of 4 V_{pp} at a frequency of 282 Hz together with a simultaneous probe excitation of 20 V_{pp} at a frequency of 6710 Hz and 7180 Hz, respectively. In particular, focusing on the graphs of figure 5.14 makes it possible to observe that when the probe frequency value was set to 6710 Hz, the Nonlinear Vibro-Acoustics Modulation provided clear indications on both the onset of internal damage and its progression. In fact, as the spectral response of the undamaged beam did not exhibit spectral lines besides those associated with the two excitation signals (namely, the pump and the probe excitations), the emergence of the additional spectral components corresponding to the first pair of modulation sidebands might be observed only after the first impact. Moreover, increasing the damage severity through a second impact event induced an increase in the amplitude of both the left and right sidebands. More in detail, when advancing from damage level D1 to damage level D2, the average amplitude of the first pair of the modulation sidebands was observed to almost double. Conversely, the spectra acquired at a probe excitation frequency of 7180 Hz and a pump frequency of 282 Hz (figure 5.15) reveal that after the first impact (i.e., damage level D1), a modulation sideband emerged on the left side of the carrier frequency and then disappeared when the damage severity was increased to level D2. According to these results, it might be concluded that given a certain level of the pump excitation
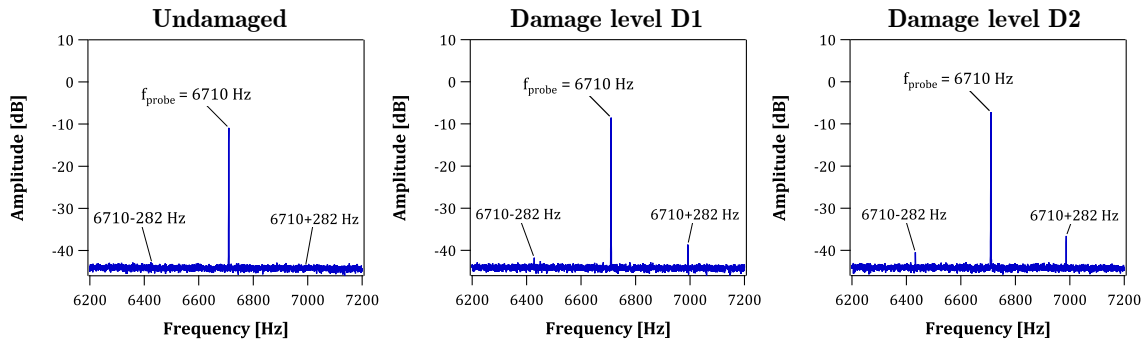
Figure 5.14 – Power spectrum of the system response acquired at the accelerometer location in both pristine and damaged conditions: probe frequency 6710 Hz and pump frequency 282 Hz (4 V_{pp} amplitude).
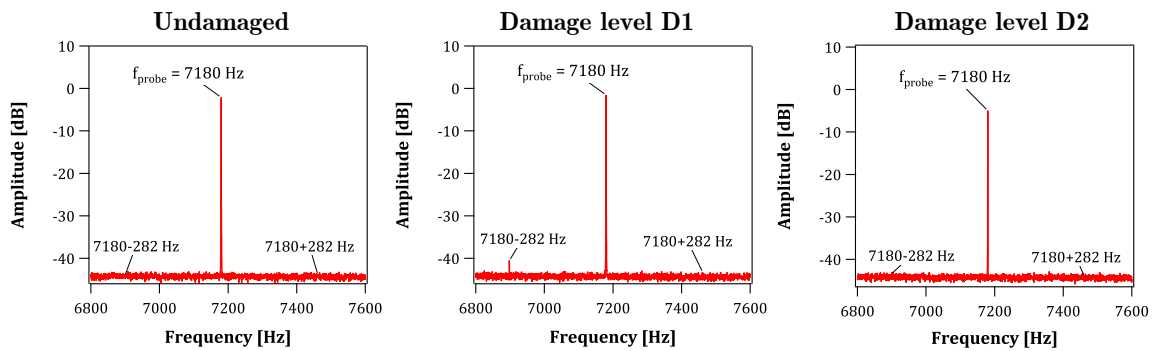
Figure 5.15 – Power spectrum of the system response acquired at the accelerometer location in both pristine and damaged conditions: probe frequency 7180 Hz and pump frequency 282 Hz (4 V_{pp} amplitude).

amplitude, the capabilities of the VAM to detect the presence of internal damage may depend on the choice of both the excitation frequencies.

Aiming to assess the ability of the Nonlinear Vibro-Acoustics Modulation to provide information on the evolution of the damage process, the average amplitude of the first pair of modulation sidebands has been assumed as a damage indicator. Moreover, to further investigate the role of both the amplitude of the pump wave and the selection of the excitation frequency on the method efficacy, the amplitude of the modulation sidebands was extracted from the response spectra associated with

each of the considered pump-probe frequency combinations (table 5.2) and, then, plotted as a function of the pump excitation amplitude. The graphs of figures 5.16 and 5.17, which correspond to a probe frequency of 6710 Hz and 7180 Hz, respectively, highlight the overall ability of the nonlinear VAM technique to identify the occurrence of the damage induced by the two low-velocity impacts, even though their comparison reveals that picking out the probe frequency among the system high-frequency resonances does not necessarily enhance the VAM detection performances. Therefore, as mentioned above, the selection of both the pump and the probe frequency might significantly affect the effectiveness of the nonlinear vibro-acoustic approach.

The experimental data show that increases in the pump excitation level or the damage severity mostly led to an increase in the amplitude of the sidebands (figures 5.16 and 5.17). More in detail, the results obtained at the maximum pump excitation levels point out that the amplitude of the modulation sidebands extracted from the response of the damaged sample tends to be higher than those measured in pristine conditions. Nevertheless, in some cases (see figures 5.17a and 5.17c) the sideband amplitude relative to the undamaged specimen is comparable to that measured for the damaged beam. These results indicate that at low pump excitation levels, the nonlinear VAM sensitivity decays due to the difficulty in measuring low-level signals, whose amplitude is close to the background noise floor, or the need of attaining minimum excitation energy to trigger the nonlinear mechanisms underlying the interaction between the two impinging waves.

In addition, it can be noted that for some of the considered pump-probe frequency combinations (figure 5.16c and 5.17b), the amplitude of the sidebands observed at the most severe damage (namely, D2) is lower than that recorded after the introduction of the first damage level (i.e., D1). This evidence might be attributed to two main reasons: (1) the small extent of the damaged regions and (2) the similarities between the two considered damage severities. In fact, since the two impact-induced damage levels mostly consist of delamination and matrix cracking, the nonlinear wave perturbation mechanisms occurring at the two damage states are not supposed to be significantly different.
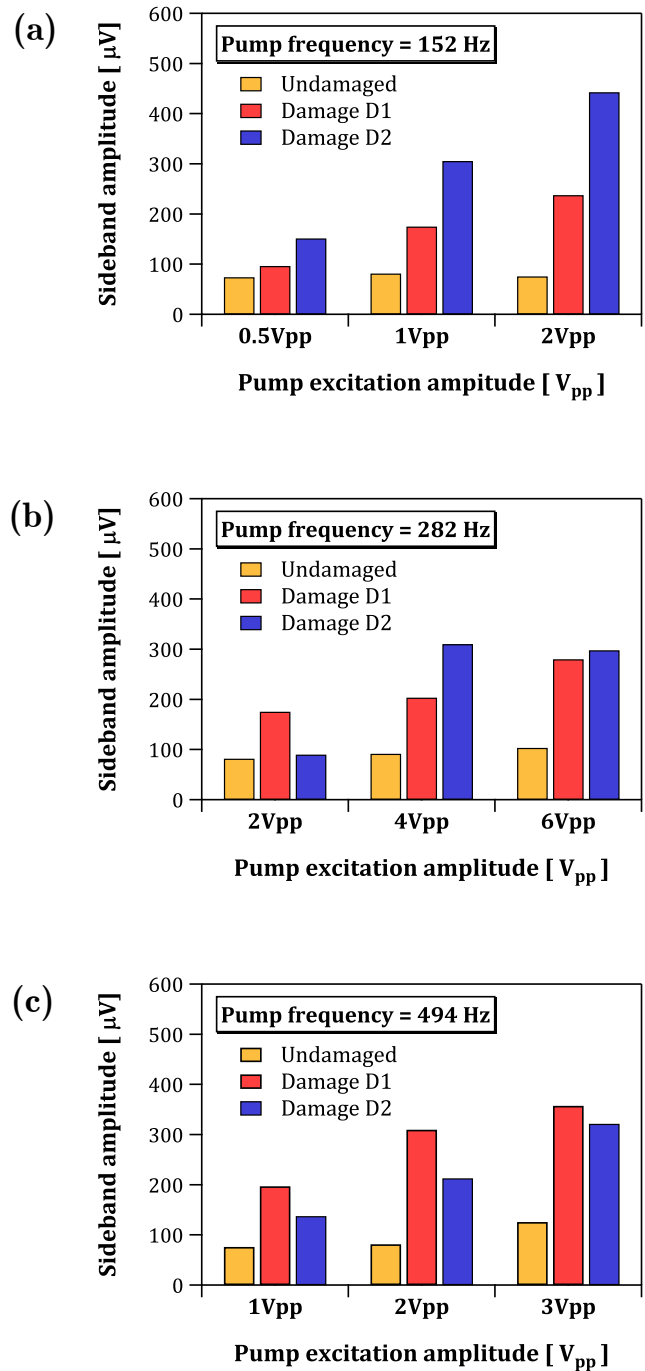
PROBE FREQUENCY = 6710 Hz

Figure 5.16 – Average amplitudes of the first pair of modulation sidebands measured for the different damage conditions at increasing pump excitation levels. The data plotted in the graphs correspond to a probe frequency of 6710 Hz and pump frequencies of 152 Hz (a), 282 Hz (b) and 494 Hz (c), respectively.
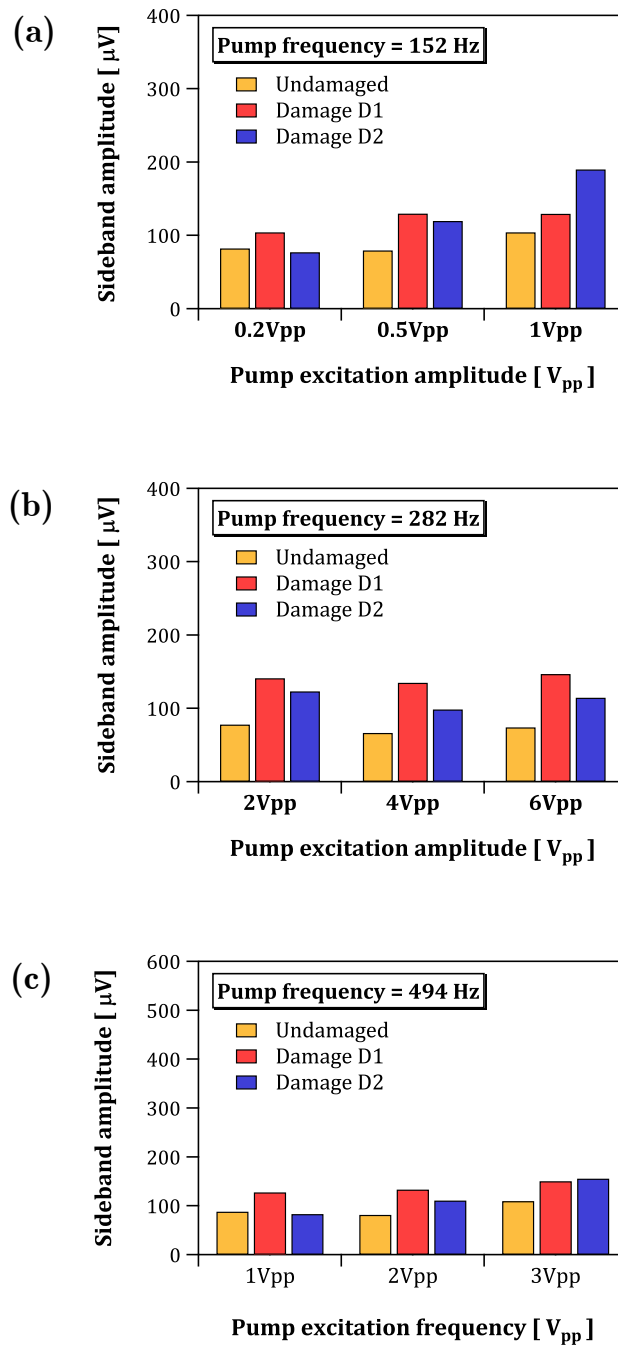
PROBE FREQUENCY = 7180 Hz

Figure 5.17 – Average amplitudes of the first pair of modulation sidebands measured for the different damage conditions at increasing pump excitation levels. The data plotted in the graphs correspond to a probe frequency of 7180 Hz and pump frequencies of 152 Hz (a), 282 Hz (b) and 494 Hz (c), respectively.

5.3.2 Samples B2

Aiming to explore the influence of the sensor positioning on the effectiveness of the Nonlinear Vibro-Acoustic Modulation, a second beam, referred to as sample B2, was simply supported on a thin layer of foam and instrumented with four piezoelectric transducers, which were glued on the sample top surface through a thin layer of a two-component epoxy adhesive and, subsequently, wired through welded connectors. More in detail, the two *PI Ceramic PIC 151* low-profile piezoceramic transducers (10 mm diameter, 1 mm thickness) at locations S1 and S2 (figure 5.18) were employed to sense the system response, while the *PI PL055.31* stack actuator and the third piezoceramic transducer (at location A1 in figure 5.18) were used to drive the sample.
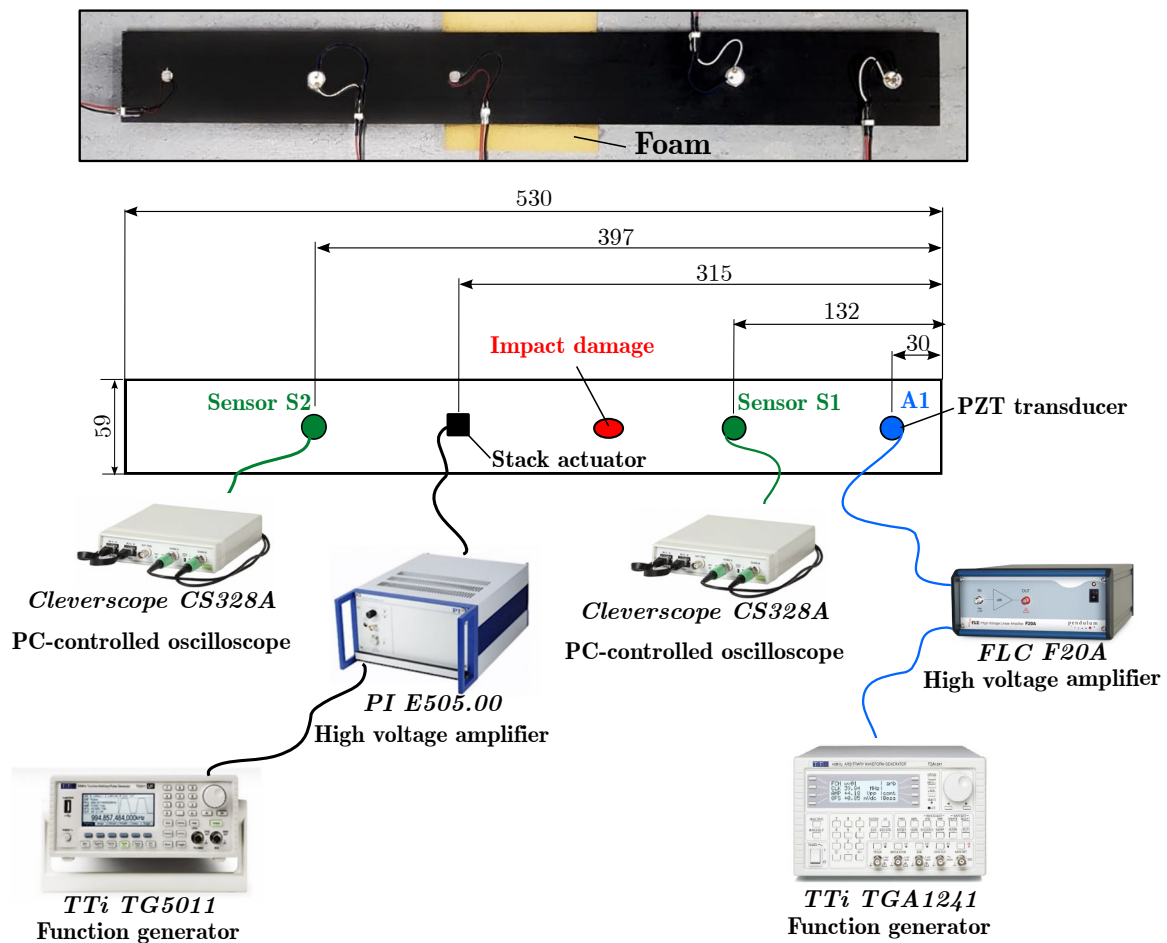

Figure 5.18 – Composite sample B2 and scheme of the experimental set-up adopted for the Nonlinear Vibro-Acoustic Modulation tests.

Damage level D1
Impact energy = 1.9 J

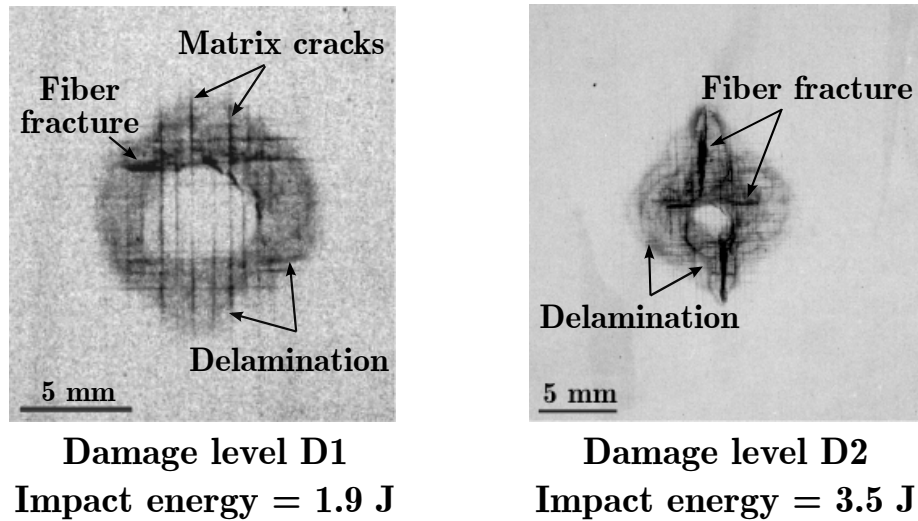**Damage level D2**
Impact energy = 3.5 J

Figure 5.19 – X-ray images of the damaged areas corresponding to the tow considered impact severities.

In order to induce the emergence of different damage severities, the composite sample was impacted by means of a hemispherical indenter of 10 mm diameter that, mounted on the impactor of the drop-weight testing machine described in section 4.3.2, was dropped from different heights to achieve increasing impact energy levels. Characterized by taking penetrant-enhanced X-radiographies through an *HP Faxitron* cabinet, the internal damage resulting from two consecutive impact loads at 1.9 J and 3.5 J mainly consists of a combination of matrix cracks and delaminations at various interfaces of the laminated beam, even though some minor fiber breakage occurred at the indentation area after the first impact (figure 5.19). The extent of the projected delamination areas corresponding to the two damage levels, referred to as D1 and D2 in the following sections, is 36 mm^2 and 160 mm^2, respectively.

5.3.2.1 Modal analysis

Identifying the frequency for both the pump and the probe excitation requires carrying out preliminary experimental modal analyses. To this purpose, the composite sample was excited through a series of linear sine sweeps that, individually
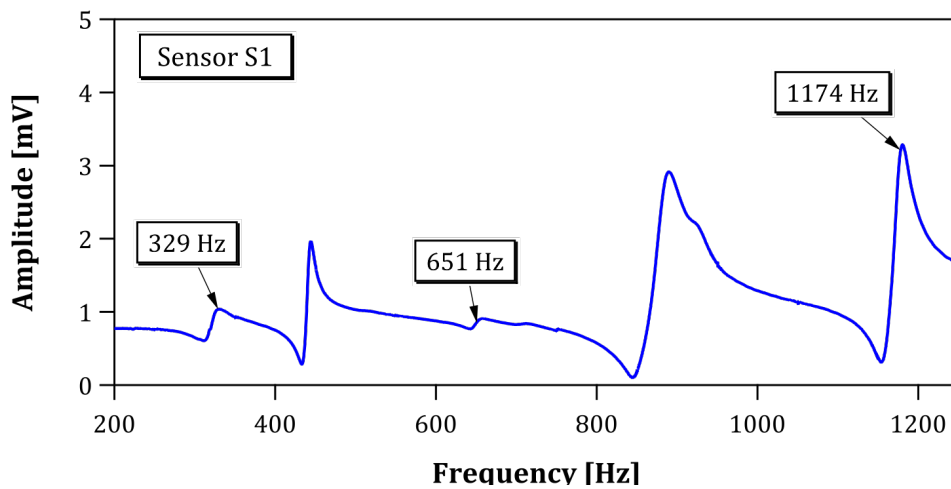
Figure 5.20 – Power spectrum of the system response acquired at the sensor location S1 in the low-frequency range.

covering a range of 200 Hz in 4s, allowed the piecewise determination of the beam spectrum over the whole range between 1 and 1300 Hz. The excitation signals were generated by means of a *TTI-TGA1241* function generator and amplified by a factor of 10 through a *PI E505.00* high-voltage linear amplifier, whose output was fed into the *PI PL055.31* stack actuator (figure 5.18). Instead, the system response was monitored and recorded at the sensor locations S1 and S2 through the *Cleverscope CS328A* acquisition unit. Moreover, the need to increase the signal-to-noise ratio results in acquiring ten data sets, which were post-processed in *Matlab* to calculate the average Fast Fourier Transform (FFT) and, thus, facilitate the identification of the system resonance frequencies. Three natural frequencies of the laminated composite beam, namely 329 Hz, 651 Hz, and 1174 Hz (evidenced in figure 5.20), were selected for the pump/modal excitation in the subsequent VAM experiments.

Concerning the selection of the probe excitation, an analogous procedure is applied. In this case, the piezo-transducer at location A1 (figure 5.17) was used to excite the sample by means of a series of linear sweep sine signals generated by a *TTi-TG5011* function generator to cover 5 kHz in 10 s and, then, amplified through an *FLC F20A* amplifier by a factor of 20. The system response was acquired at the two sensor locations S1 and S2 through the *Cleverscope CS328A* acquisition unit at a 4 MSa/s sampling rate. Then, ten data sets were recorded and used to calculate
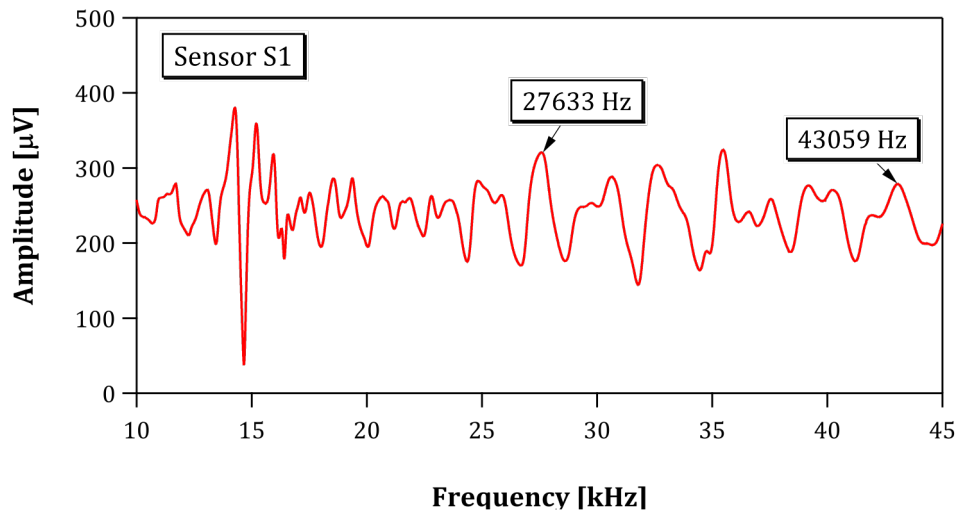
Figure 5.21 – Power spectrum of the system response acquired at the sensor location S1 in the high-frequency range.

the average spectrum (figure 5.21). In order to assess whether the selection of probing frequency might affect the effectiveness of the Nonlinear Vibro-Acoustic Modulation, two resonance frequencies, namely 27633 Hz and 43059 Hz, were selected for the VAM tests.

5.3.2.2 Nonlinear Vibro-Acoustic Modulation tests

During the Nonlinear Vibro-Acoustic Modulation tests, a high-frequency monoharmonic sinusoidal signal (namely, probe excitation wave) was fed into the composite sample through the piezoelectric transducer at location A1 of figure 5.18 The amplitude of the probe signal, generated by a *TTi-TG5011* function and amplified 20 times with an *FLC F20A* amplifier, was set to 2 V_{pp}. This amplitude value, which was kept unchanged for all the considered testing scenarios, refers to the output of the employed function generator. Simultaneously, a low-frequency pure-tone harmonic signal, whose amplitude was ranged between 1 V_{pp} and 5 V_{pp} in 1 V_{pp} steps (values at function generator output), was applied through the stack actuator to excite the selected low-frequency mode shape. The system response to the two concurrent impinging waves was sensed at the two sensor locations, i.e., S1 and S2, and recorded with *Cleverscope CS328A* acquisition unit at a 2 MSa/s

sampling rate. In this context, for any of the six considered excitation scenarios, twenty data sets consisting of 2 Mpoints each have been acquired and post-processed in *Matlab* to determine their averaged Fast Fourier Transform and, subsequently, extract the average amplitude of the first pair modulation sideband.

5.3.2.3 Results

Detecting the occurrence of modulation sidebands and monitoring their evolution require zooming the sample power spectra around the spectral line corresponding to the probe frequency. Hence, purely by way of example, figures 5.22 and 5.23 show the spectral magnitude of the signals acquired at the two considered sensor locations (namely, S2 and S1) when the inspected sample was driven through a pump excitation of 2 V_{pp} at a frequency of 329 Hz together with a probe excitation of 2 V_{pp} at a frequency of 27633 Hz. In particular, focusing on the spectra corresponding to the signal recorded at the sensor location S2 (figure 5.22) makes it possible to observe that the response of the pristine sample did not exhibit any additional spectral components besides those associated with the two excitation waves. In fact, the emergence of the first pair of modulation sidebands, whose amplitude was found to slightly increase when advancing from damage severity D1 to damage level D2, was triggered by the impact at 1.9 J. Therefore, even though the probe and pump frequencies invariably dominated the response of the composite sample, the Nonlinear Vibro-Acoustic Modulation managed to both identify the onset of internal damage and monitor its progression.

Similar considerations may apply to the spectra acquired at sensor location S1 (figure 5.23), in which increasing impact energy led to an increase in the amplitude of the modulation sidebands. Nonetheless, it is worth noticing that a clear pattern of modulation sidebands is already visible in the spectrum of the pristine sample response. Besides pointing out the existence of no damage-related nonlinearities (i.e., contact and friction effects) that might arise from the interaction between the inspected structure and the boundary, this evidence reveals the effectiveness of the Nonlinear Vibro-Acoustic Modulation to be affected by the sensor positioning relative to the excitation points and thus, on the relative path through which the impinging
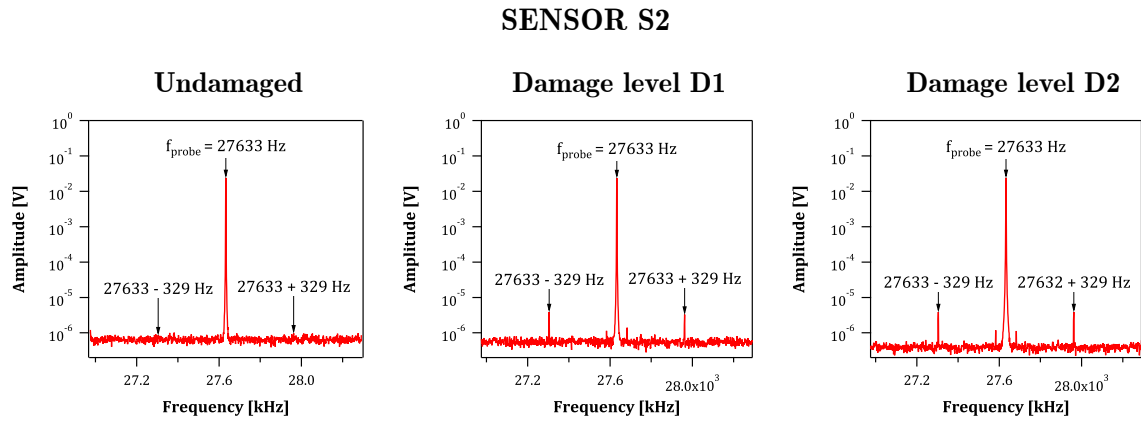
SENSOR S2

Undamaged	Damage level D1	Damage level D2

Figure 5.22 – Power spectrum of the system response acquired at the sensor location S2 in both pristine and damaged conditions: probe frequency 27633 Hz and pump frequency 329 Hz (2 V_{pp} amplitude).

SENSOR S1

Undamaged	Damage level D1	Damage level D2

Figure 5.23 – Power spectrum of the system response acquired at the sensor location S1 in both pristine and damaged conditions: probe frequency 27633 Hz and pump frequency 329 Hz (2 V_{pp} amplitude).

waves propagate. In addition, the power spectra acquired at sensor location S1 for a probe excitation of 43059 Hz at 2 V_{pp} and a pump frequency of 329 Hz at 2 V_{pp} (figure 5.24) reveal similar features. In fact, although already detectable in the response of the pristine sample, the modulation sidebands monotonically increase
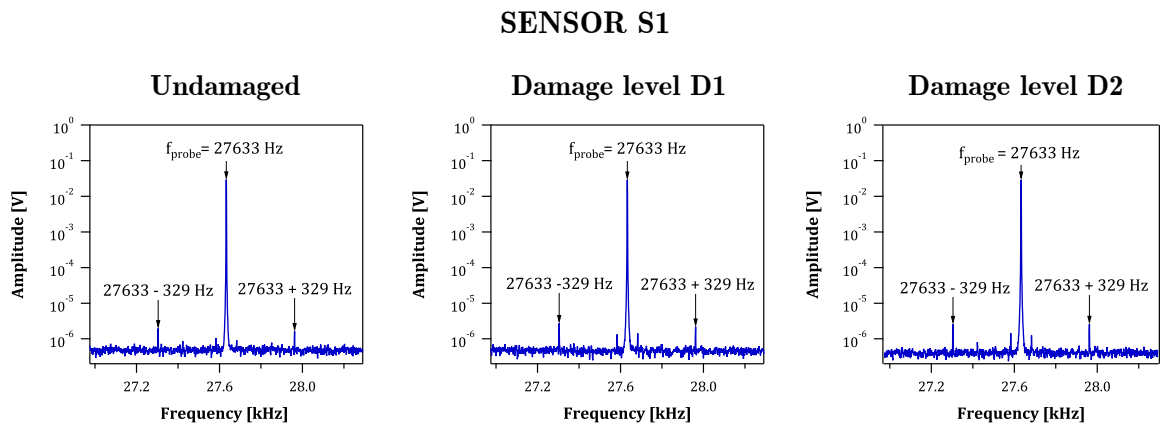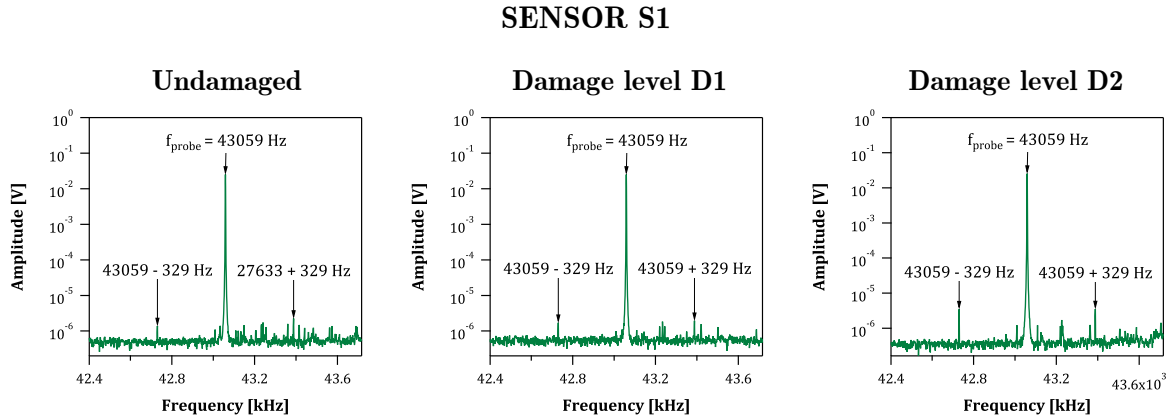
SENSOR S1

Figure 5.24 – Power spectrum of the system response acquired at the sensor location S1 in both pristine and damaged conditions: probe frequency 43059 Hz and pump frequency 329 Hz (2 V_{pp} amplitude).

with the damage severity. However, after the 3.5 J impact (i.e., damage level D2), the average increase in their amplitude was found to be significantly higher than that measured when a probe frequency of 27633 Hz was applied to drive the composite sample. Thus, under a specific testing scenario, the VAM capability to detect the presence of internal damage appears to depend on the choice of the probe excitation frequency.

Aiming to assess the effectiveness of the Nonlinear Vibro-Acoustics Modulation in detecting the presence of barely visible impact damage in composite materials, the average amplitude of the first pair of modulation sidebands was assumed as a damage indicator. Thus, the amplitude values were extracted from the power spectra of the acquired system response for each of the considered pump-probe frequency combinations and, subsequently, plotted as a function of the pump excitation amplitude. In this context, figures 5.25 and 5.26 show the results obtained at a probe excitation of 27633 Hz at the sensor locations S1 and S2, respectively. Analogously, figures 5.27 and 5.28 refer to the beam response at sensor locations S1 and S2 under a probe frequency of 43059 Hz.

The data reassumed in the graphs highlight the overall ability of the nonlinear Vibro-Acoustic Modulation technique to identify the onset of impact damage and monitor its evolution. In this context, it is worth noticing that for two of the

considered pump frequencies, namely 329 Hz and 651 Hz, the method retrieved the presence of significant differences between the amplitude of the sidebands measured in pristine and damaged conditions (see for example 5.25a, 5.25b, 5.27a, and 5.27b) and, thus, provided clear indications of the damage occurred after the two impacts. Conversely, vibrating the sample at a pump frequency of 1174 Hz (figures 5.25c, 5.26c, 5.27c, and 5.28c) did not result in a monotonic increase in the amplitude of the sidebands with the damage severity, inferring the dependence of the VAM effectiveness on the frequency selected for the pump excitation. Similarly, the performance of the Nonlinear Vibro-Acoustic technique was found to be affected by probe excitation frequency. In this perspective, focusing on the data acquired at a pump frequency of 651 Hz at the two considered probe frequencies highlights differences in the indications provided by the method. As shown in figure 5.26b, setting the probe frequency to 27633 Hz led the amplitude of the first pair of modulation sidebands to monotonically increase with the damage severity, enabling the detection of both the damage onset and its progression. Conversely, when the 43059 Hz probe frequency was used (figure 5.28b), the sideband amplitudes measured at damage level D2 were significantly lower than those attained both in pristine conditions and after the 1.9 J impact (i.e., damage level D1). These findings confirm the results of previous studies [186] [187] [191], which showed the damage detection capabilities of nonlinear vibroacoustic approaches to be affected by the frequencies selected for both the pump and the probe wave.

It has to be noticed that with the only exceptions of figure 5.26c, the amplitude of the sidebands proportionally increased with the amplitude of the pump excitation. Therefore, even though for some of the considered testing scenarios (figures 5.25a, 5.26a, 5.26b, and 5.28b), the level of the sidebands recorded for the severest damage severity (i.e., damage level D2) is lower than or close to that recorded after the 1.9 J impact (i.e., damage level D1), the data acquired at the maximum pump excitation level reveal that the amplitude of the modulation sidebands is generally higher than that measured on the undamaged beam. Due to the small size of the damaged areas and the similarities in the features of the two impact-induced damage levels, which mainly consist of matrix cracking and delamination damage modes (figure 5.19), the nonlinear mechanisms involved in the wave perturbation did not lead to significant differences in the induced modulation process.

PROBE FREQUENCY = 27633 Hz
SENSOR S1

(a)

(b)

(c)

Figure 5.25 – Average amplitudes of the first pair of modulation sidebands measured at sensor location S1. The data plotted in the graphs correspond to a probe frequency of 27633 Hz and pump frequencies of 329 Hz (a), 651 Hz (b) and 1174 Hz (c).
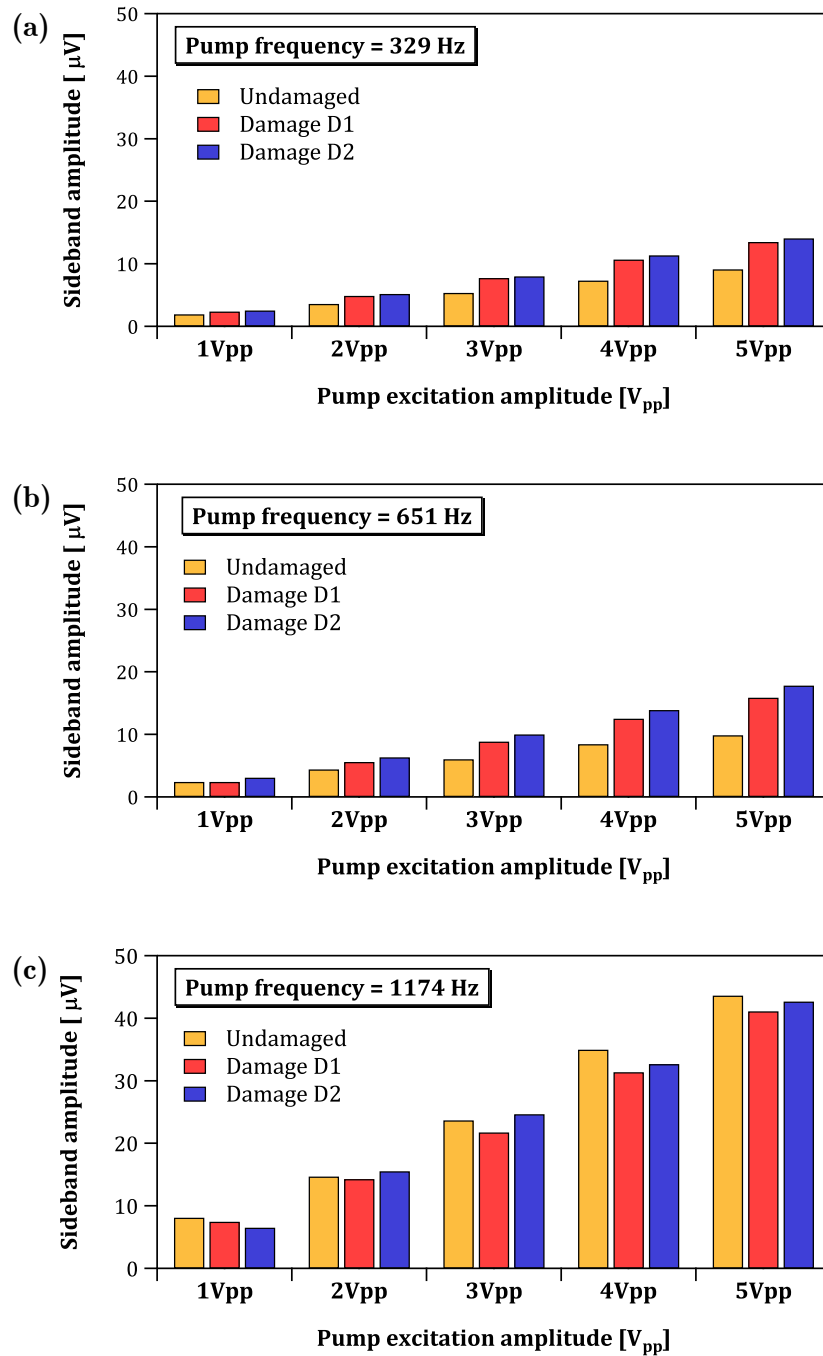
PROBE FREQUENCY = 27633 Hz
SENSOR S2

Figure 5.26 – Average amplitudes of the first pair of modulation sidebands measured at sensor location S2. The data plotted in the graphs correspond to a probe frequency of 27633 Hz and pump frequencies of 329 Hz (a), 651 Hz (b) and 1174 Hz (c).

PROBE FREQUENCY = 43059 Hz

SENSOR S1

Figure 5.27 – Average amplitudes of the first pair of modulation sidebands measured at sensor location S1. The data plotted in the graphs correspond to a probe frequency of 43059 Hz and pump frequencies of 329 Hz (a), 651 Hz (b) and 1174 Hz (c).

PROBE FREQUENCY = 43059 Hz
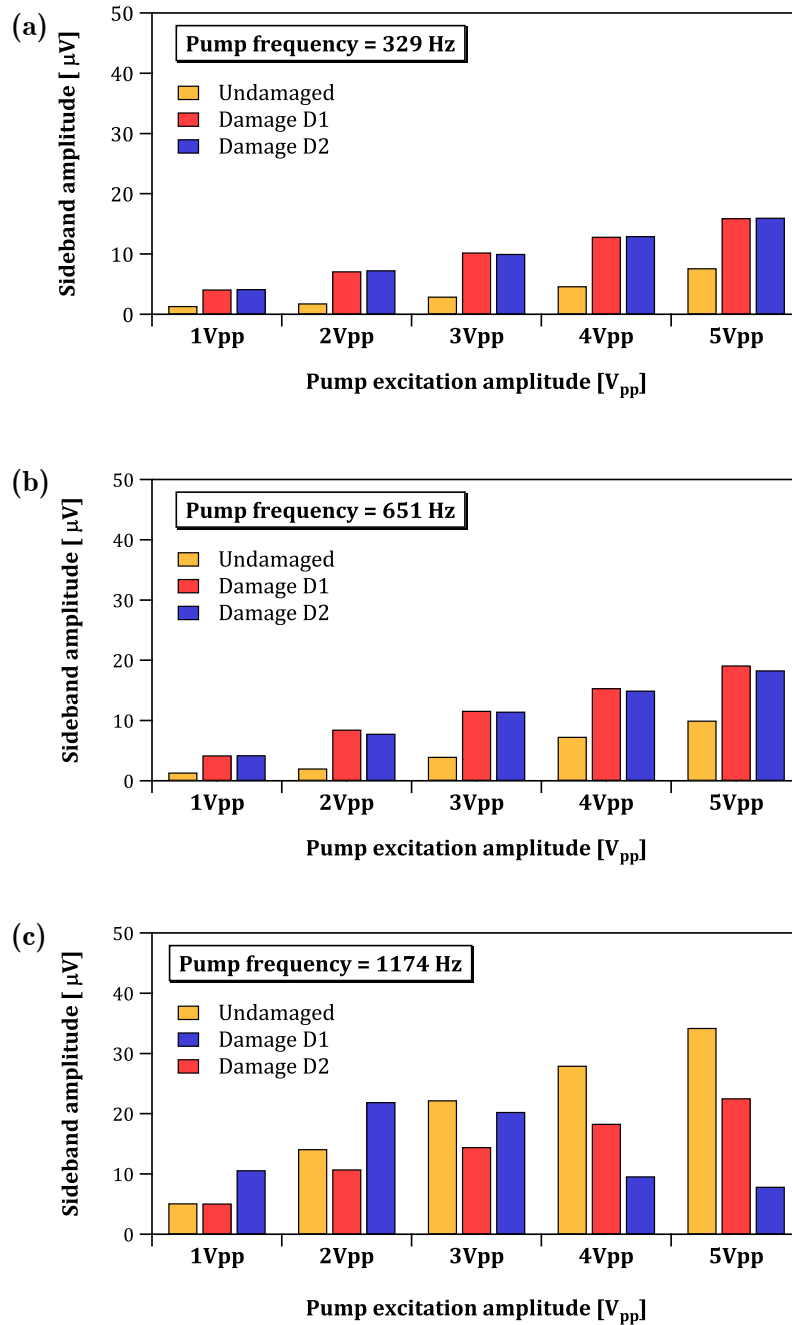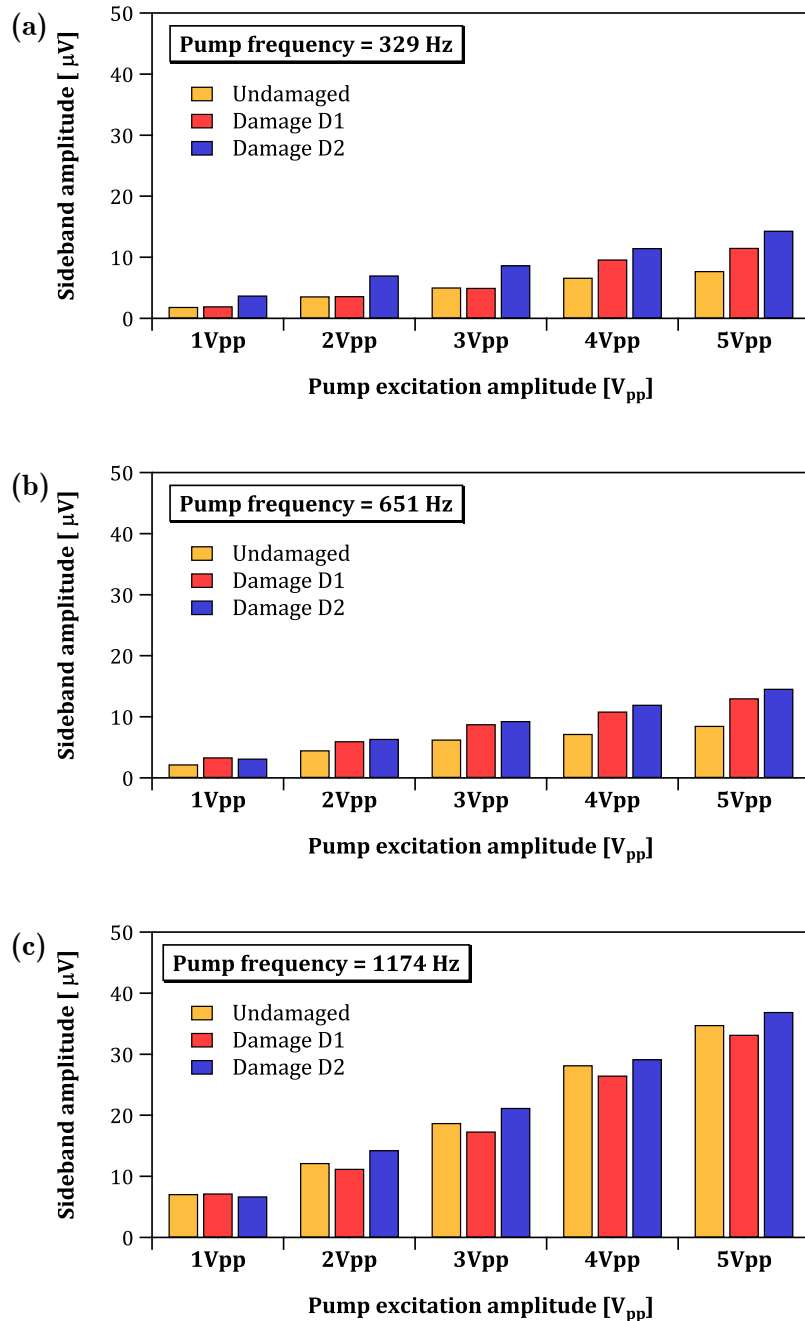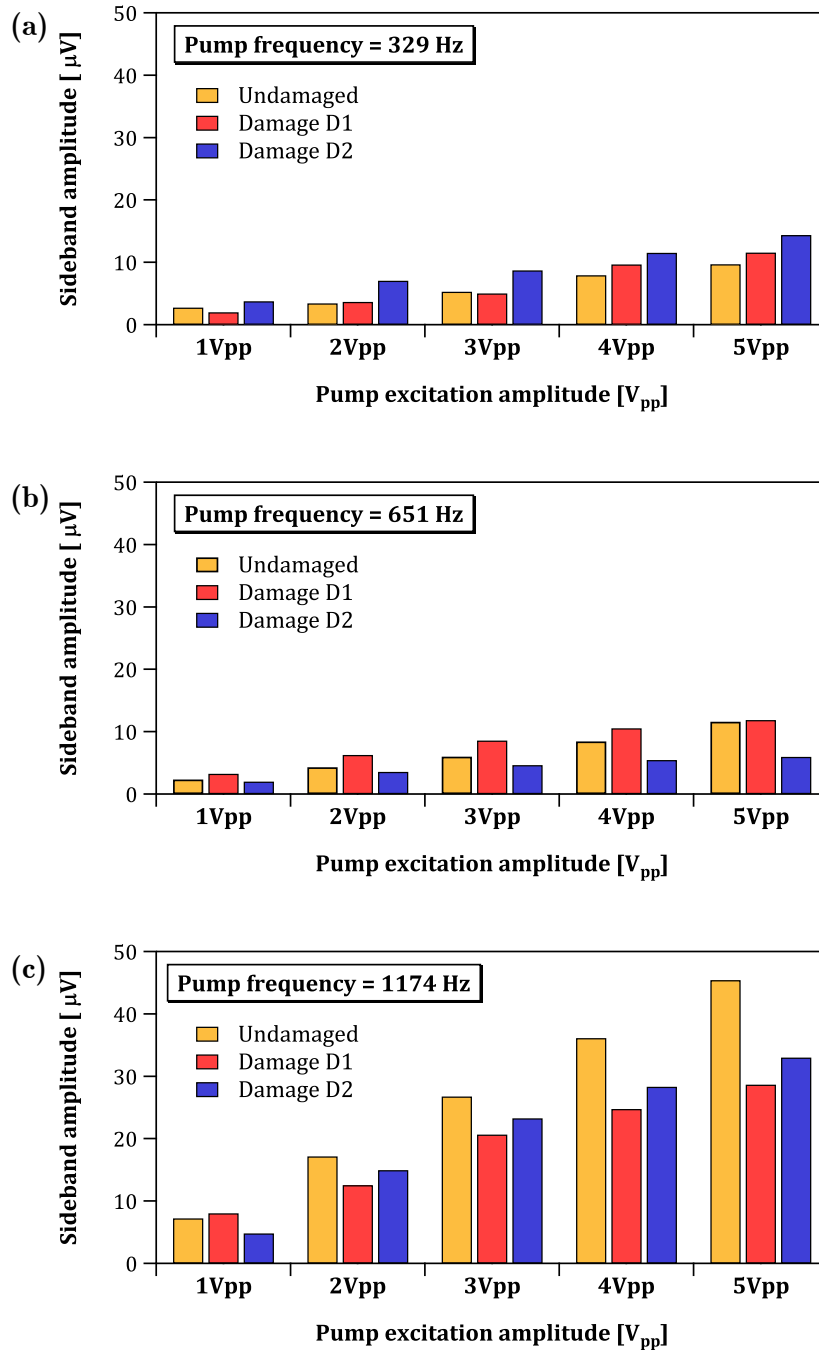
SENSOR S2

Figure 5.28 – Average amplitudes of the first pair of modulation sidebands measured at sensor location S2. The data plotted in the graphs correspond to a probe frequency of 43059 Hz and pump frequencies of 329 Hz (a), 651 Hz (b) and 1174 Hz (c).

Furthermore, the Nonlinear Vibro-Acoustic Modulation sensitivity to damage of the method also appears to decay when the amplitude of the pump vibration decreases. In fact, at the low pump excitation level (i.e., 1 V_{pp}), the average sideband amplitude recorded for the undamaged beam is broadly comparable or even higher than that measured for the D1 or D2 damaged beam (figure 5.27b and 5.28b). Aside from the difficulty in measuring low-level signals close to or below the background noise floor, this loss of sensitivity at low excitation levels may be due to the need to provide a minimum amount of energy to trigger the nonlinear mechanisms underlying the interaction between the two impinging waves. Nonetheless, it is worth remarking that some of the considered pump-probe frequency combinations induced the emergence of a clear pattern of modulation sidebands in the response of the undamaged sample. Especially at the lowest pump excitation levels, the amplitude of these spectral components is comparable to that measured at damage level D1 (see, for example, figures 5.25a, 5.27a, and 5.28a). As already mentioned when analyzing the power spectra of figure 5.23 and 5.24, this evidence may be linked to the emergence of no damage-related mechanisms that mostly rely upon inherent material nonlinearities (i.e., fiber/matrix internal friction and flaws) and nonlinear contact effects occurring at boundaries. In this perspective, besides damping the beam vibrations, the interaction between the inspected sample and the thin foam layer acting as support might trigger the emergence of nonlinear mechanisms whose effects may overlap with those associated with the material damage.

Finally, purely by way of example, figures 5.29 and 5.30 represent the averaged increase in the amplitude of the sidebands measured at the sensor location S1 and S2 when a pump frequency of 329 Hz was applied together with a probe frequency of 27633 Hz and 43059 Hz, respectively. In this context, given a pump-probe frequency combination, comparing the graphs referring to the two sensor locations allows noticing that the averaged sidebands amplitude increments measured at sensor location S1 monotonically vary both with respect to the damage severity than to the pump excitation amplitude. Therefore, sensing the response of the composite beam at location S1 allows retrieving more accurate information on the progression of internal damage than that provided by sensor S2. Thus, the Nonlinear Vibro-Acoustic Modulation performance (i.e., efficacy and the sensitivity) appears to

depend on the sensor positioning relative to both the excitation sources and the supports and, thus, the path through which the excitation waves propagate.
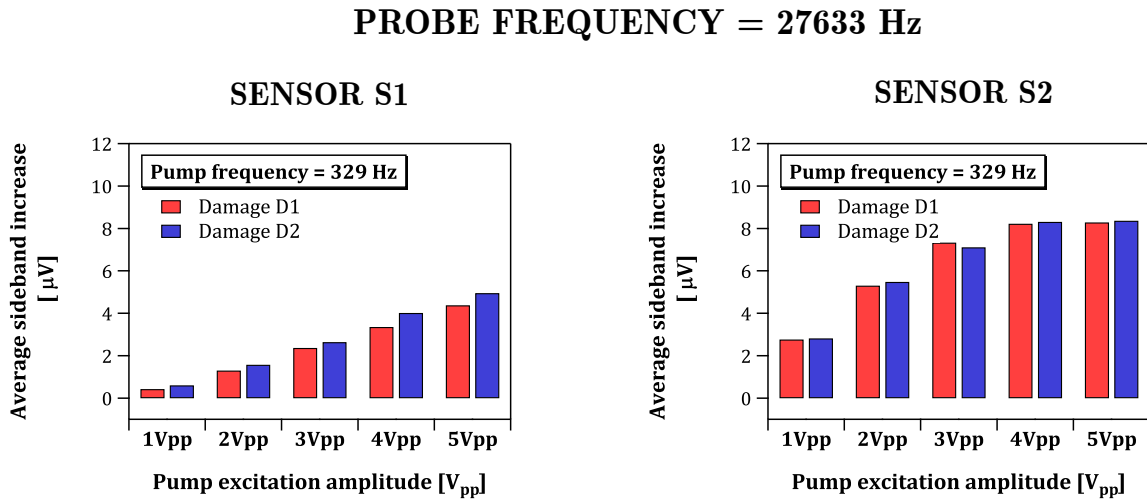
PROBE FREQUENCY = 27633 Hz

Figure 5.29 – Average increase in the amplitude of the modulation sidebands measured at a probe frequency of 27633 Hz and pump frequencies of 329 Hz.

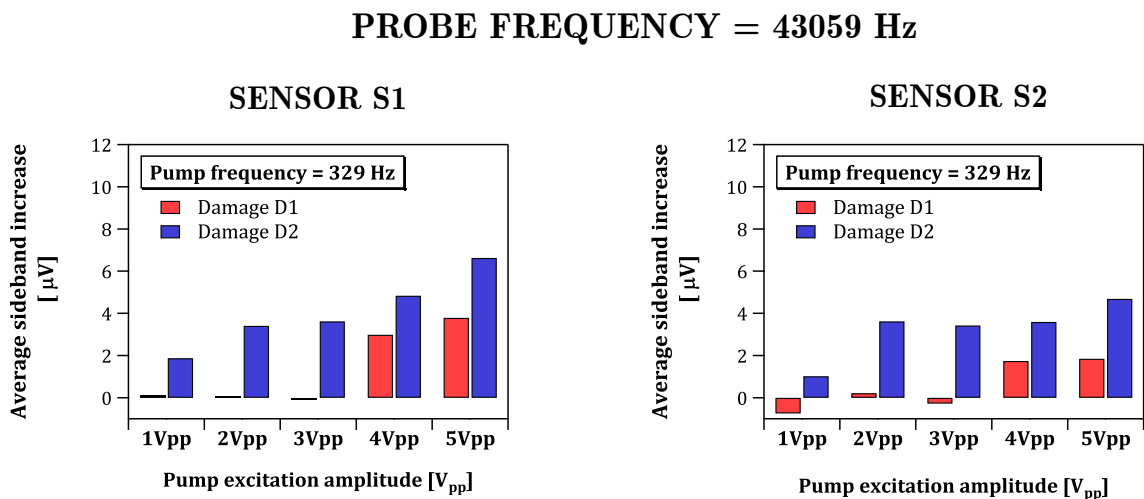**PROBE FREQUENCY = 43059 Hz**

Figure 5.30 – Average increase in the amplitude of the modulation sidebands measured at a probe frequency of 43059 Hz and pump frequencies of 329 Hz.

5.3.3 Sample B3

The need to explore the effects of the actuation source on the effectiveness of the Nonlinear Vibro-Acoustics Modulation led to instrument the third laminated composite beam, referred to as sample B3 (figure 5.31), with a *PI PL055.31* stack actuator and concurrently mount it on a *Bruel & Kjaer 4809* electrodynamic shaker by means of a threaded aluminum stud, which was glued to the beam by a two-component epoxy adhesive on one end and connected to the threaded hole of the shaker on the other end. At the same time, to further investigate the role of the positioning and the type of the employed sensors on both the efficacy and the sensitivity of the Nonlinear Vibro-Acoustics Modulation, a sensing apparatus consisting of two *PI Ceramic PIC 151* low-profile piezoceramic transducers of 10 mm diameter and 1 mm thickness and two accelerometers, namely a *Brüel & Kjær 4375* and a *Brüel & Kjær 4385* piezoelectric charge accelerometers, was mounted on the beam top surface. More in detail, while the piezoelectric transducers were glued at locations S2 and S3 (figure 5.31) through a thin layer of a two-component epoxy adhesive and, subsequently, wired through welded connectors, the two accelerometers were bonded through a thin wax layer at locations S4 and S5 (figure 5.31).
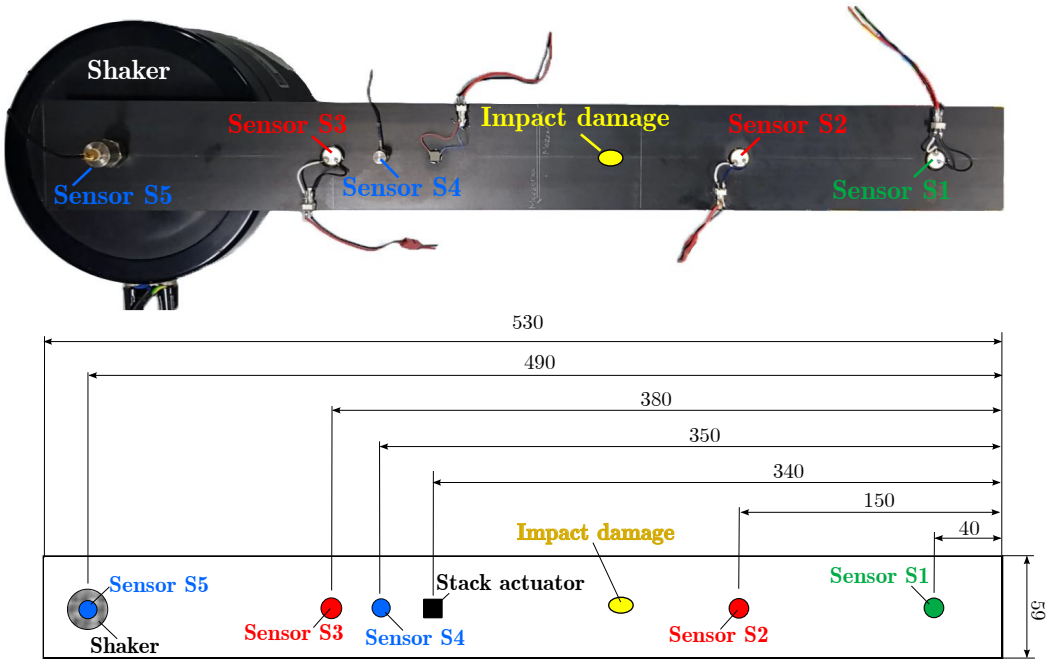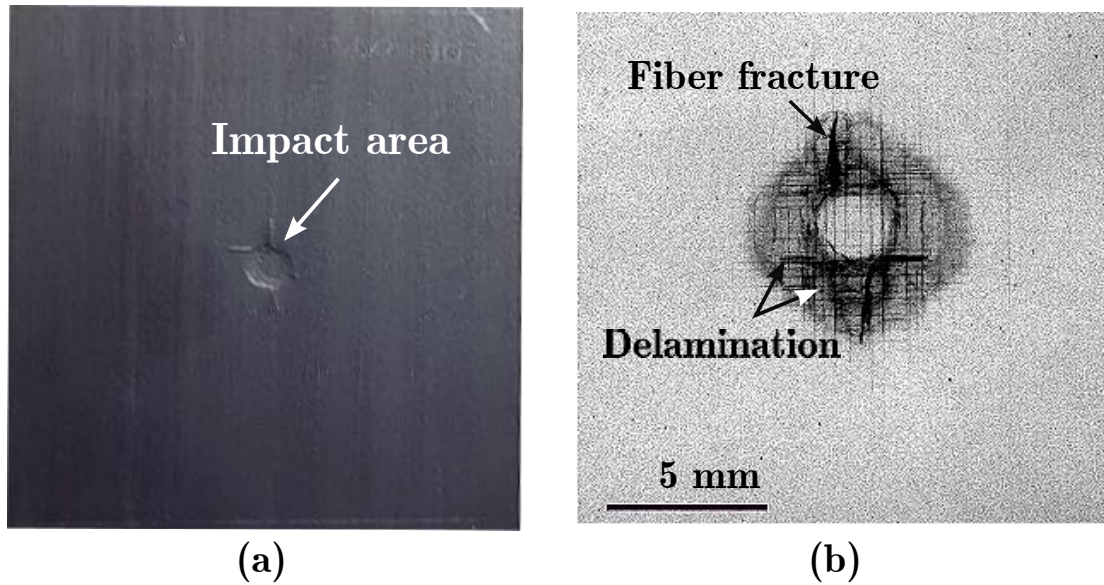

Figure 5.31 – Schematic diagram of the composite sample B3.

(a)   **(b)**

Damage level D1 - Impact energy 1.9 J

Figure 5.32 – Impacted region (a) and X-ray image of the internal damage induced through a low-velocity transverse impact load at 1.9 J.

The laminated composite beam was tested in pristine (i.e., undamaged) conditions and after an impact of 1.9 J energy. Applied through a drop-weight testing machine (see section 4.3.2) provided with a hemispheric indenter of 10 mm diameter, the low-velocity transverse impact load triggered the onset of a typical barely visible impact damage (BVID). The penetrant-enhanced X-radiography taken through an *HP Faxitron cabinet* to characterize the resulting internal damage (figure 5.32) highlighted the presence of both matrix cracks and delaminations whose projected area was 40 mm^2.

5.3.3.1 Modal analysis

Identifying the frequency for both the pump and the probe excitation requires carrying out preliminary experimental modal analyses. According to the procedure applied to determine the test frequencies for the sample B2 (see paragraph 6.3.3), the composite sample was excited through a series of linear sine sweeps that,
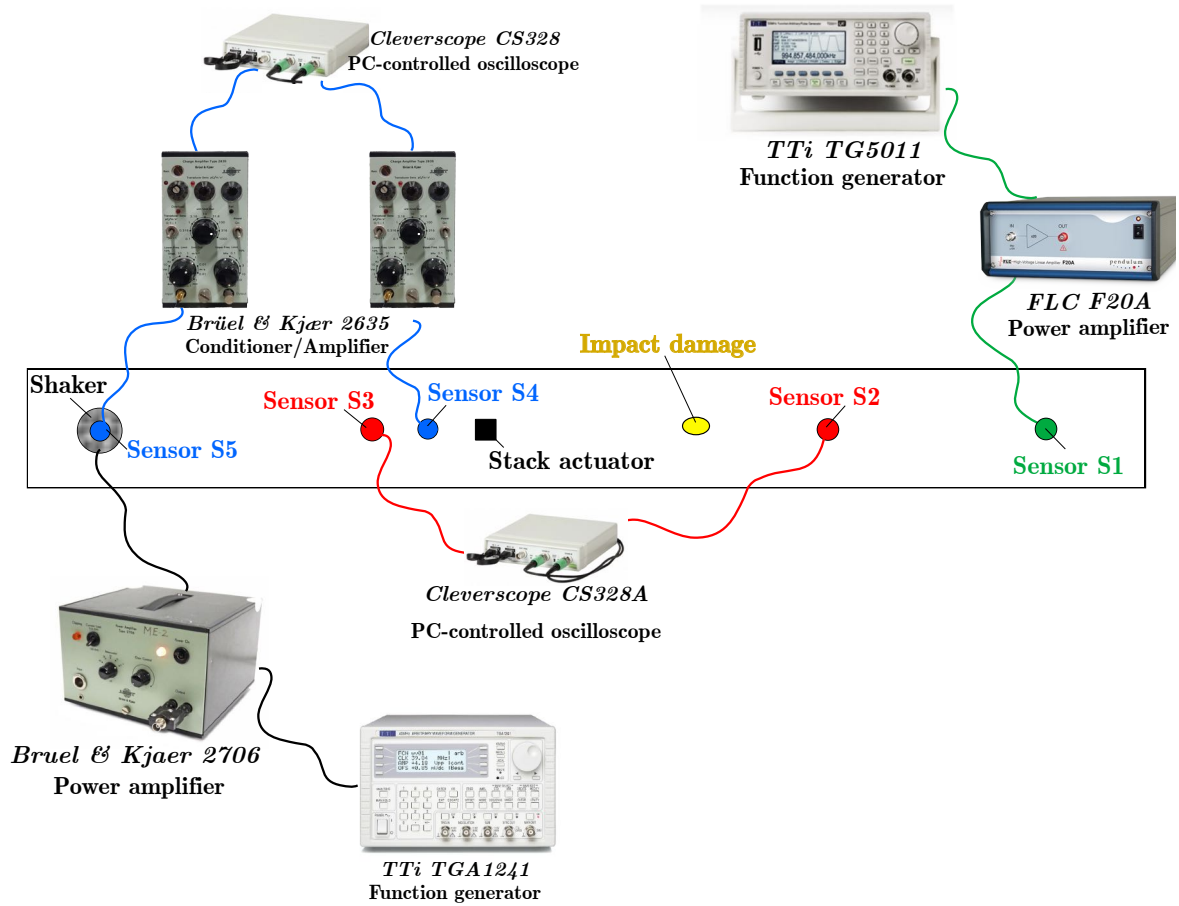
Figure 5.33 – Composite sample B3: scheme of the experimental set-up adopted for the modal analysis and the second series of Nonlinear VAM tests.

individually covering a range of 200 Hz in 4 s, allowed the piecewise determination of the beam spectrum over the whole range between 1 and 1200 Hz. The excitation signals were generated by means of a *TTI-TGA1241* function generator and amplified through a *Bruel & Kjaer 2706* power amplifier, whose output was fed into the *Bruel & Kjaer 4809* electrodynamic shaker (figure 5.33). The system response was monitored and recorded at the three sensor locations (i.e., S2, S3, and S4) with two 14 bit, 100MSa/s PC-controlled oscilloscopes, namely a *Cleverscope CS328A* and a *Cleverscope CS328* (figure 5.33). Connecting the two acquisition units through a link cable allows synchronizing their triggers and, thus, simultaneously acquiring the composite sample response at the piezoceramic transducer locations (i.e., S2 and S3) and the accelerometer position (namely, S4) at a 2 MSa/s sampling rate. In order to

increase the signal-to-noise ratio, ten data sets were recorded and post-processed in *Matlab* to calculate the average power spectrum and, at once, facilitate the identification of the resonance frequencies of the inspected sample. Three natural frequencies of the laminated composite beam, i.e., 145 Hz, 316 Hz, 510 Hz, and 760 Hz (figures 5.34, 5.35, and 5.36), were picked for the pump/modal excitation in the subsequent VAM tests.
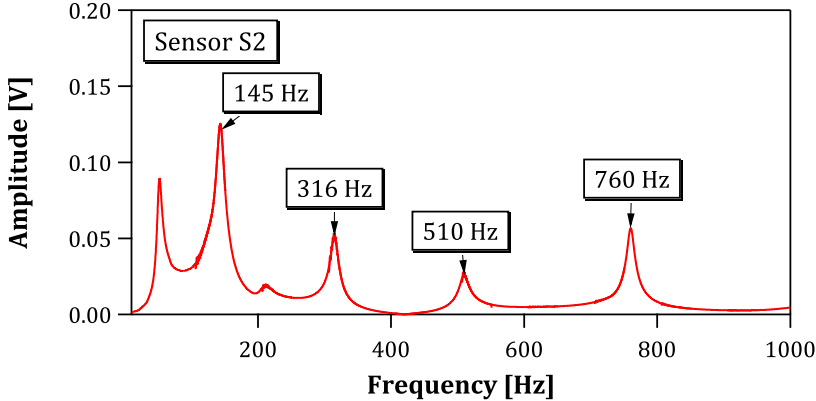

Figure 5.34 – Power spectrum of the system response acquired through a piezoceramic transducer at the sensor location S2 in the low-frequency range.
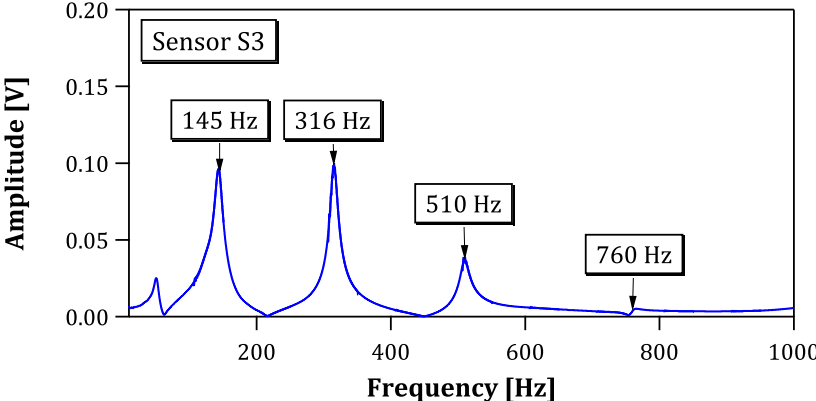
Figure 5.35 – Power spectrum of the system response acquired through a piezoceramic transducer at the sensor location S3 in the low-frequency range.
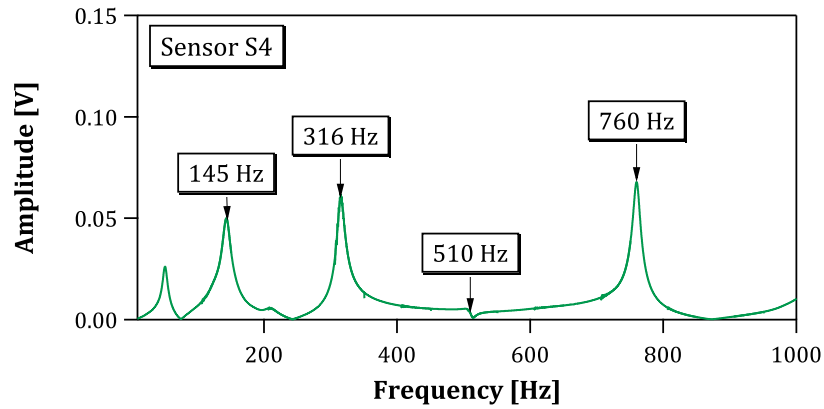
Figure 5.36 – Power spectrum of the system response acquired through a charge accelerometer at the sensor location S4 in the low-frequency range.
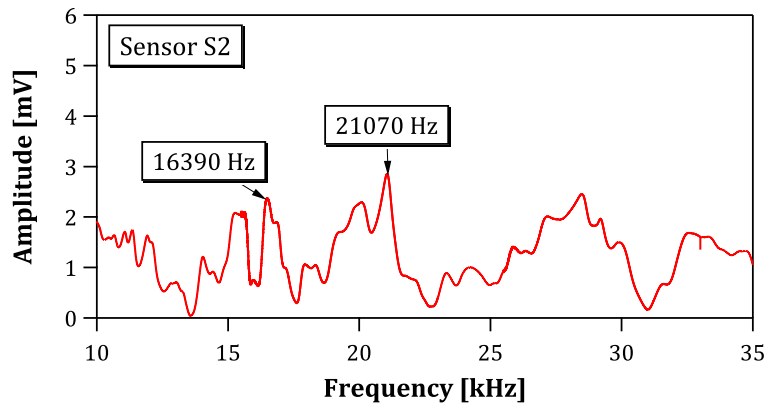
Figure 5.37 – Power spectrum of the system response acquired in the high-frequency range at sensor location S2.

Concerning the selection of the probe frequency values, a similar procedure was applied. To this purpose, the sample was driven through the piezoceramic transducer at location S1, which has been fed with a series of linear sweep sine signals generated by a *TTi-TG5011* function generator to cover 5 kHz in 10 s and subsequently amplified by a factor of 20 through an *FLC F20A* amplifier. The system response was acquired at the four sensor locations through the *Cleverscope* acquisition units at a 2 MSa/s sampling rate. Then, ten data sets were recorded and used to calculate the average Fast Fourier Transform in the range between 5 kHz and 30 kHz (figures 5.37, 5.38, and 5.39). In order to assess whether picking the
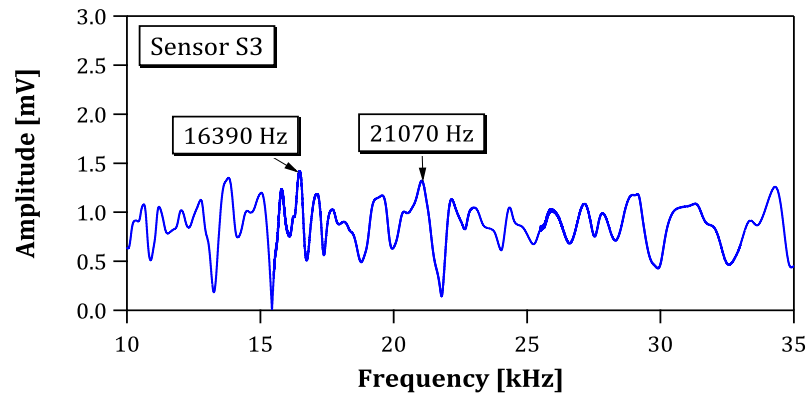
Figure 5.38 – Power spectrum of the system response acquired in the high-frequency range at sensor location S3.
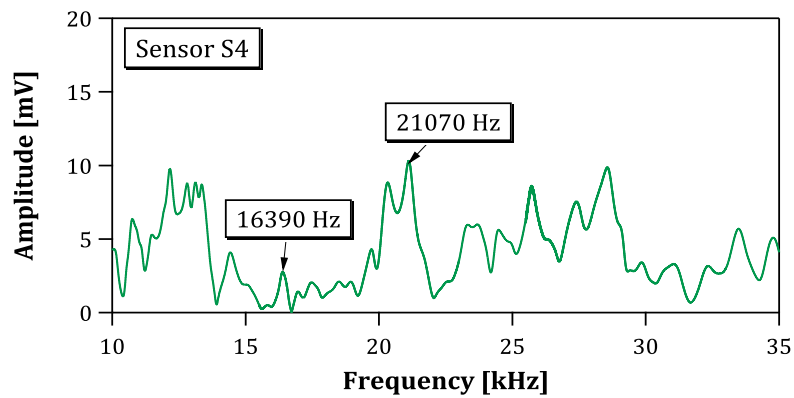
Figure 5.39 – Power spectrum of the system response acquired in the high-frequency range at sensor location S4.

probe frequency in the ultrasonic range rather than in the acoustic one may affect the ability of the Nonlinear Vibro-Acoustic Modulation to provide clear indications on the material integrity, two resonance frequencies, namely 21070 Hz and 16390 Hz, were selected for the VAM tests.

5.3.3.2 Nonlinear Vibro-Acoustic Modulation tests

Aiming to investigate the effects the actuation system may produce on both the efficacy and the sensitivity of the Nonlinear Vibro-Acoustics Modulation, two

series of experimental tests, differing in the kind of actuator used to excite the selected low-frequency mode shape (i.e., the pump excitation), were conducted. In the first set of measurements, the piezoceramic transducer at location S1 (figure 5.40) was driven through a high-frequency pure-tone harmonic signal (i.e., probe excitation wave) generated by a *TTi-TG5011* function generator and, subsequently, amplified 20 times with an *FLC F20A* power amplifier. Concurrently, a pump excitation signal, generated by a *TTI-TGA1241* function generator and amplified through a *PI E501.00* high voltage linear amplifier, was fed into the *PI PL055.31* stack actuator to vibrate the laminated composite beam (figure 5.40). By referring to the value set

Figure 5.40 – Composite sample B3: scheme of the experimental set-up adopted to carry out the first series of Nonlinear Vibro-Acoustics Modulation tests.

on the displays of the function generators, the amplitude of the carrier wave was fixed to 125 mV_{pp} and kept unchanged for all the considered testing scenarios. Howev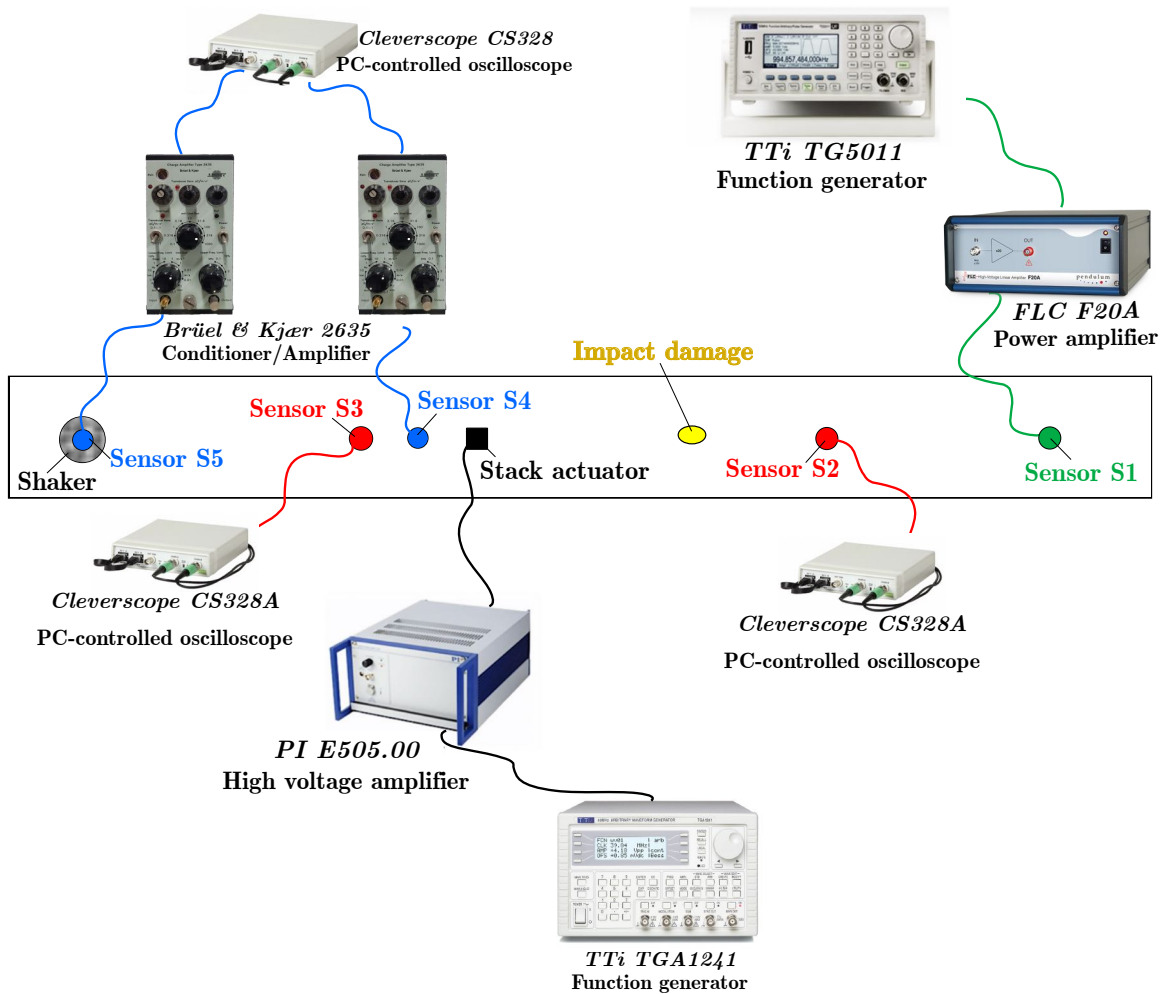er, the need to explore the role of the pump excitation level on the VAM performance resulted in considering four different amplitude levels for the pump frequency (namely, 0.5 V_{pp}, 1 V_{pp}, 2 V_{pp}, and 4 V_{pp}). Conversely, in the second series of VAM measurements, the selected low-frequency resonance was excited employing a *Bruel & Kjaer 4809* electrodynamic shaker (figure 5.32) fed with a low-frequency monoharmonic signal generated via a *TTI-TGA1241* function generator. Simultaneously, a high-frequency pure-tone harmonic sine wave at 125 mV_{pp} was introduced to the low-profile piezoceramic transducer at location S1 (figure 5.33). According to the first set of measurements, in which a piezoceramic stack actuator was used to provide the excite the selected low-frequency mode, four pump excitation levels ranging between 125 mV_{pp} and 1 V_{pp} were considered for testing.

During the two series of tests, the system response to the two concurrent impinging waves was sensed at the three sensor locations (i.e., S2, S3, and S4) and recorded at a 2 MSa/s sampling rate with the *Cleverscope CS328*A and the *Cleverscope CS328* acquisition units, which were linked together to simultaneously trigger the acquisition of the beam response from the considered sensors. Hence, the experimental tests were carried out for six pump-probe frequency combinations at various amplitudes of the pump excitation and two different actuation scenarios, resulting in a total of thirty-six different testing configurations. In correspondence of each of these test configurations, twenty data sets consisting of 2 Mpoints each have been acquired and post-processed in *Matlab* to determine their averaged Fast Fourier Transform and, subsequently, extract the average amplitude of the first pair modulation sideband.

5.3.3.3 Results

Detecting the emergence of modulation sidebands requires zooming the sample power spectra around the spectral line corresponding to the probe frequency. Hence, purely by way of example, figures 5.41, 5.42, and 5.43 show the spectral magnitude of the signals acquired in correspondence of a testing scenario in which the 21070 Hz

signal generated by a low-profile piezoceramic transducer was combined with the low-frequency signal provided by means of a stack actuator at a frequency of 145 Hz and 2 V_{pp}. More in detail, while figures 5.41 and 5.42 refer to the signals acquired at the sensor locations S2 and S3 through piezoelectric transducers, figure 5.43 corresponds to the responses recorded at location S4 using a charge accelerometer. In this perspective, focusing on the spectra corresponding to the signal recorded at the sensor location S2 (figure 5.41) allows detecting the presence of a clear pattern of modulation sidebands in the power spectrum of the pristine sample response. Nonetheless, although the probe frequency dominated the sample response in both pristine and damaged conditions, the amplitude of these additional spectral components, which corresponds to the multiple of the selected modal frequency (i.e., 145 Hz), was found to increase after the 1.9 J impact. Similar considerations apply to the spectra acquired at sensor location S4 (figure 5.43). In fact, although a 145 Hz sideband was clearly visible on the right side of the ultrasonic carrier frequency component (figure 5.43) in the spectrum of the undamaged sample, the internal damage induced by the 1.9 J impact led to an increase in the amplitude of the modulation sidebands. Conversely, the spectra associated with the signal recorded at the sensor location S3 (figure 5.42) make it possible to observe that the response of both the pristine and the damaged sample did not exhibit any additional spectral

Figure 5.41 – Power spectrum of the system response acquired at the sensor location S2 in both pristine and damaged conditions: probe frequency 21070 Hz and pump frequency 145 Hz (2 V_{pp} amplitude).

SENSOR S3

Undamaged **Damage D1**

Figure 5.42 – Power spectrum of the system response acquired at the sensor location S3 in both pristine and damaged conditions: probe frequency 21070 Hz and pump frequency 145 Hz (2 V_{pp} amplitude).

SENSOR S4

Undamaged **Damage D1**

Figure 5.43 – Power spectrum of the system response acquired at the sensor location S4 in both pristine and damaged conditions: probe frequency 21070 Hz and pump frequency 145 Hz (2 V_{pp} amplitude).

components besides those associated with the two excitation waves. Thus, the Nonlinear Vibro-Acoustic Modulation correctly identified the onset of the induced barely visible impact damage, even though its effectiveness seems to rely upon the sensor position relative to both the excitation sources and the impacted area. In addition, comparing the response spectra recorded at sensor location S4 in correspondence of a pump frequency of 145 Hz and a probe frequency of 16390 Hz

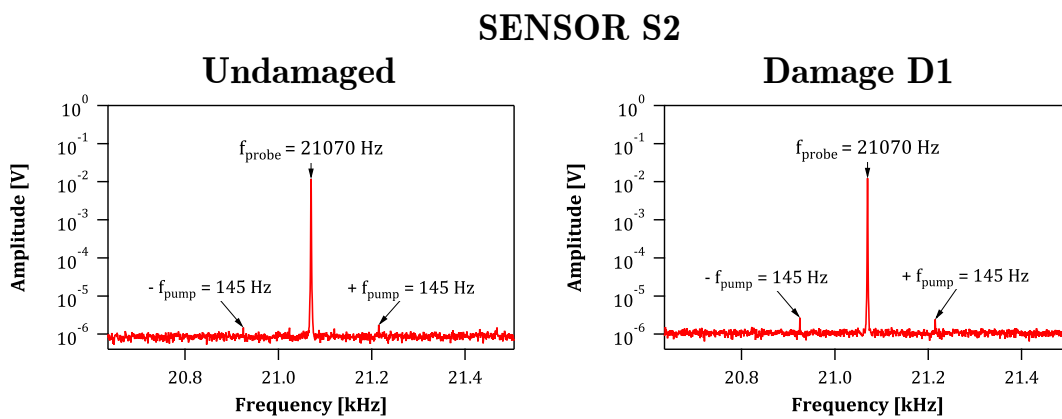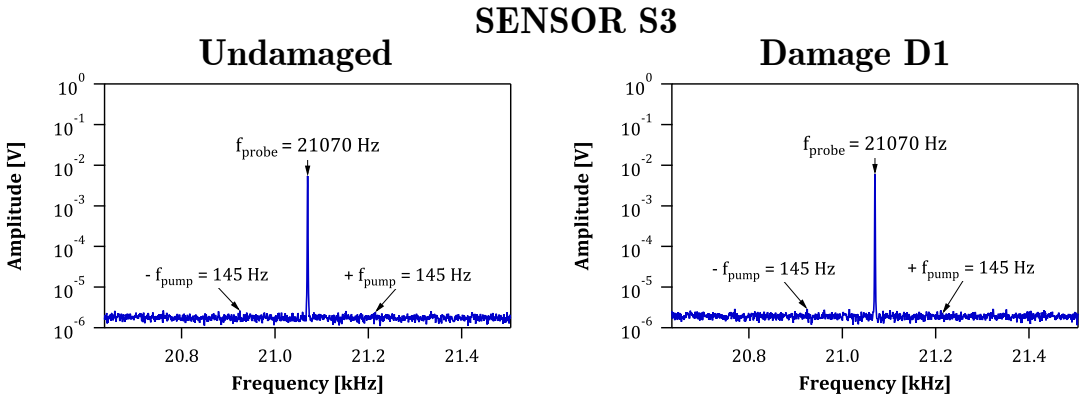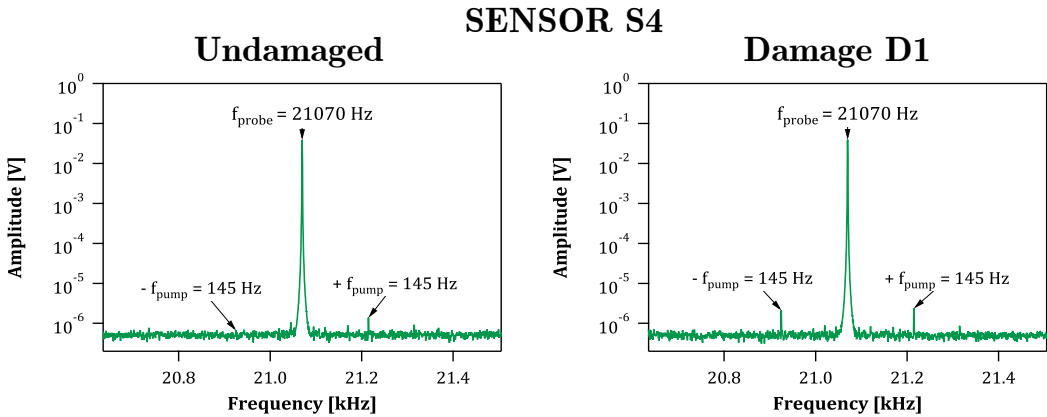**SENSOR S4**

Undamaged   **Damage D1**
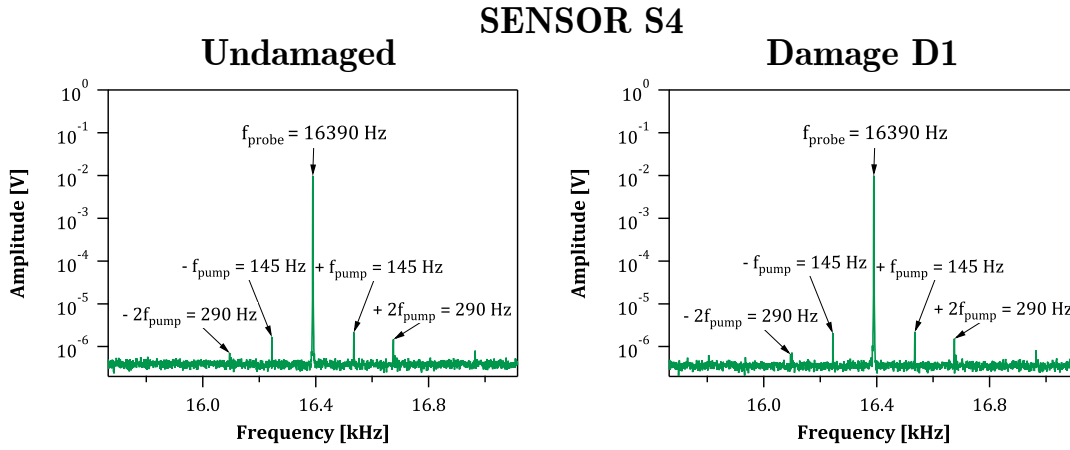
Figure 5.44 – Power spectrum of the system response acquired at the sensor location S4 in both pristine and damaged conditions: probe frequency 16390 Hz and pump frequency 145 Hz (2 V_{pp} amplitude).

(figure 5.44) with those recorded by the selfsame sensor for a pump frequency of 145 Hz and a carrier frequency of 21070 Hz probe frequency (figure 5.43) allows noticing that the applied low-velocity impact triggered an increase in the amplitude of the first pair of modulation sidebands and, at once, the emergence of the second pair of modulation, suggesting a dependence of the selected pump frequency on the VAM sensitivity.

The graphs of figures 5.45 - 5.50, which compare the average amplitude of the first pair of modulation sidebands measured in correspondence of all testing scenarios in both pristine and damaged conditions, resume the data obtained by simultaneously using a low-profile piezoceramic disk to vibrate the laminated composite beam at the considered carrier frequency and a stack actuator to excite the selected low-frequency vibration mode. Chosen as an indicator of the occurrence of internal damage, the amplitude of the first pair of modulation sidebands was plotted as a function of the pump excitation amplitude. In particular, figures 5.45, 5.46, and 5.47 show the results obtained for a probe excitation of 21070 Hz at the sensor locations S2, S3, and S4, respectively. Analogously, figures 5.48, 5.49, and 5.50 refer to the signals acquired at sensor locations S2, S3, and S4 under a probe frequency of 16390 Hz. Therefore, the obtained results highlight the overall ability of the Nonlinear Vibro-Acoustic Modulation to detect the emergence of internal damage. In fact, with only a few

exceptions (see figures 5.45b, 5.46a, and 5.46b), the applied transverse impact load led to a general increase in the amplitude of the sidebands. However, as already pointed out by the spectra analysis, the method efficacy appears to depend on the choice of both the probe and the pump frequency. Purely by way of example, comparing the graphs of figures 5.46c and 5.49c, which refer to the signal acquired at the sensor location S3 and a 510 Hz pump frequency, enables noticing that picking the probe frequency among the ultrasonic or the acoustic resonances of the inspected sample may significantly affect both the sensitivity and the efficacy of the applied method. In fact, while setting the probe frequency to 21070 Hz did not provide any clear indication of the material degradation (figure 5.46c), driving the sample with a 16390 Hz carrier signal allows observing the average amplitude of the first pair of modulation sidebands to increase after the 1.9 J low-velocity impact and, thus, detecting the occurrence of the impact-induced damage (figure 5.49c). Analogously, the analysis of the spectra associated with the system responses to a 21070 Hz probe frequency and a pump frequency at 145 Hz (figure 5.45a) and 316 Hz (figure 5.45b) reveals that vibrating the inspected sample at 145 Hz resulted in the emergence of a clear pattern of sidebands whose amplitude increased after the introduction of impact damage. Conversely, exciting the low-frequency mode at 316 Hz did not induce noticeable changes in the amplitude of the emerged sidebands, inferring the dependence of the selected pump frequency on the VAM performance. In addition, it is worth noticing that the data corresponding to the signal recorded at sensor location S3 (figures 5.46 and 5.49) highlight that the method invariably failed in detecting the onset of the impact-induced damage, calling for an influence of the wave propagation path on the VAM sensitivity. Moreover, an overall analysis of the results obtained at a given pump-probe frequency in the whole range of considered pump excitation levels points out that reducing the magnitude of the pump wave led to a proportional decrease in the amplitude of the first pair of modulation sidebands. Therefore, since the Nonlinear Vibro-Acoustic Modulation appeared to decay at low pump vibration amplitudes, unique indications on the occurrence of impact damage were attained only at the highest excitation levels. In fact, with a few exceptions (e.g., figures 5.42b, 5.43a, and 5.45b), the amplitude of the first pair modulation sidebands measured in correspondence of a pump magnitude of 4 V_{pp} was invariably higher at damage level D1 than in pristine conditions. The reduced sensitivity at low

PROBE FREQUENCY = 21070 Hz

SENSOR S2

Figure 5.45 – Average amplitudes of the first pair of modulation sidebands measured at sensor location S2 at a probe frequency of 21070 Hz and pump frequencies of 145 Hz (a), 316 Hz (b), 510 Hz (c), and 760 Hz (d).

PROBE FREQUENCY = 21070 Hz

Figure 5.46 – Average amplitudes of the first pair of modulation sidebands measured at sensor location S3 at a probe frequency of 21070 Hz and pump frequencies of 145 Hz (a), 316 Hz (b), 510 Hz (c), and 760 Hz (d).

PROBE FREQUENCY = 21070 Hz

SENSOR S4

Figure 5.47 – Average amplitudes of the first pair of modulation sidebands measured at sensor location S4 at a probe frequency of 21070 Hz and pump frequencies of 145 Hz (a), 316 Hz (b), 510 Hz (c), and 760 Hz (d)

PROBE FREQUENCY = 16390 Hz

Figure 5.48 – Average amplitudes of the first pair of modulation sidebands measured at sensor location S2 at a probe frequency of 16390 Hz and pump frequencies of 145 Hz (a), 316 Hz (b), 510 Hz (c), and 760 Hz (d).

PROBE FREQUENCY = 16390 Hz

SENSOR S3

Figure 5.49 – Average amplitudes of the first pair of modulation sidebands measured at sensor location S3 at a probe frequency of 16390 Hz and pump frequencies of 145 Hz (a), 316 Hz (b), 510 Hz (c), and 760 Hz (d).

PROBE FREQUENCY = 16390 Hz
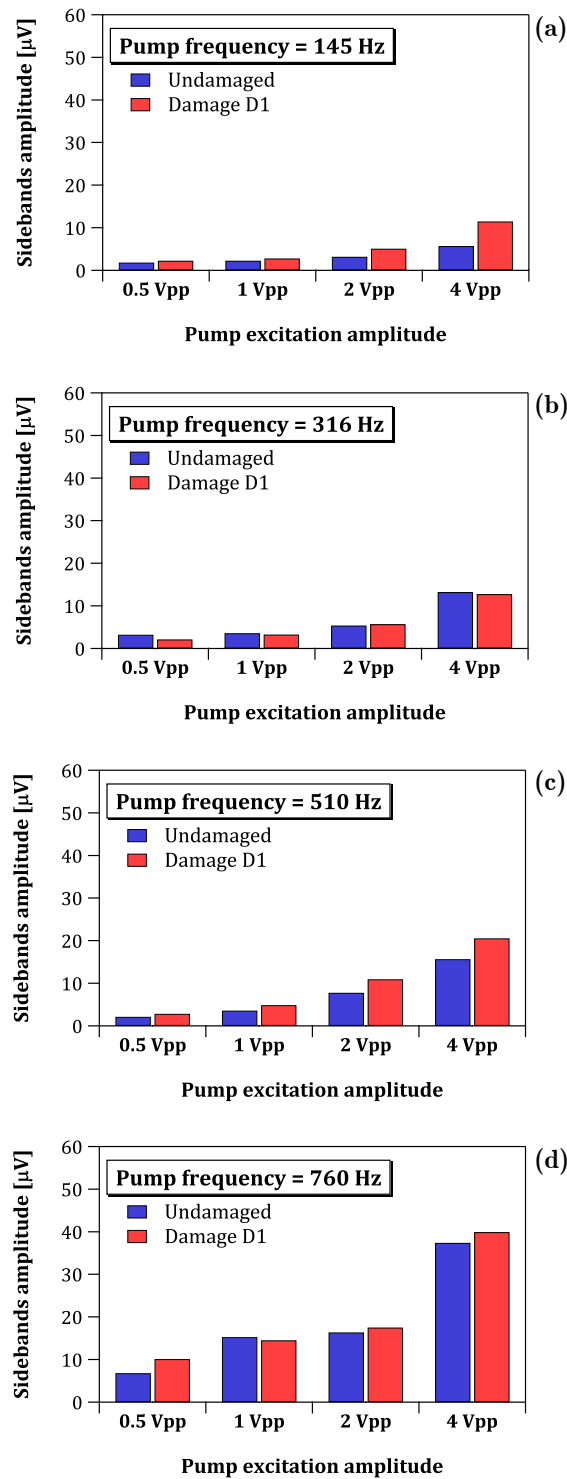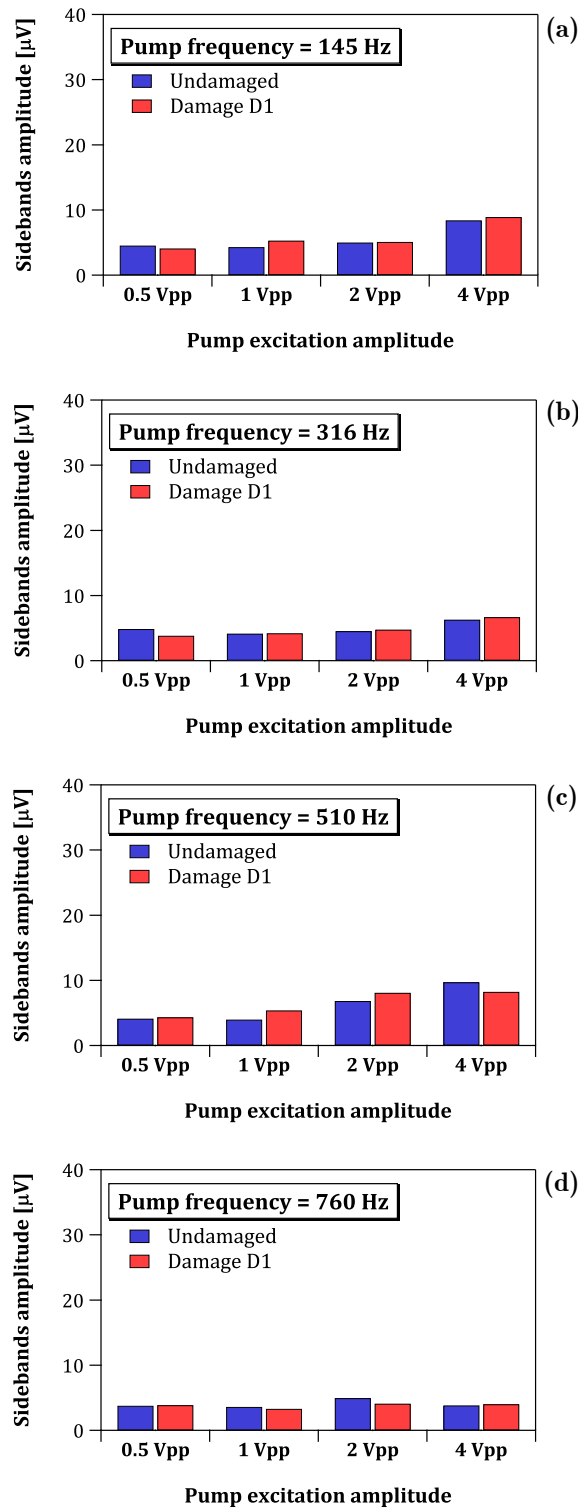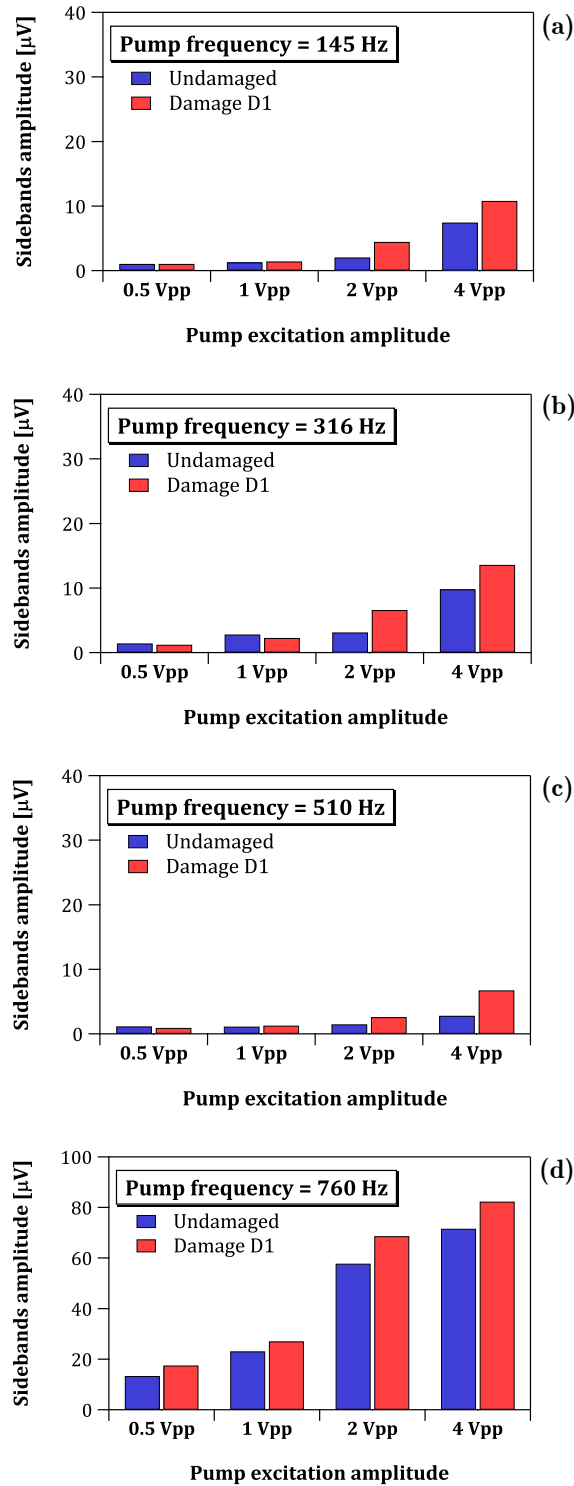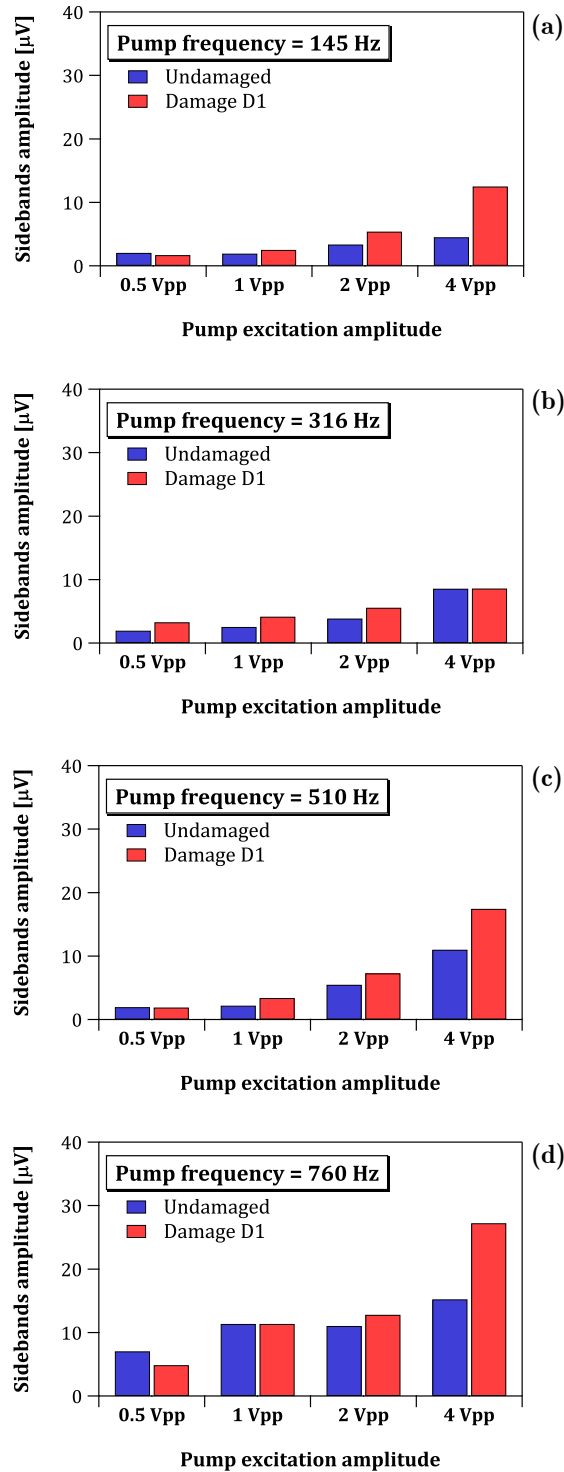
SENSOR S4

Figure 5.50 – Average amplitudes of the first pair of modulation sidebands measured at sensor location S4 at a probe frequency of 16390 Hz and pump frequencies of 145 Hz (a), 316 Hz (b), 510 Hz (c), and 760 Hz (d).

excitation levels may be related to the difficulty in measuring a signal whose amplitude falls close to the background noise floor or the need to provide the minimum amount of energy required to activate the damage-related nonlinearities. In this perspective, it is worth noticing that a stack actuator generally provides less energy than other driving systems. Thus, aiming to investigate the role of the adopted driving system, a second set of experimental measurements, in which an electrodynamic shaker was employed to vibrate the inspected sample at the selected low-frequency resonance, was carried out.

Purely by way of illustration, the graphs of figures 5.51, 5.52 represent the spectra of the system response acquired at the sensor locations S2 and S4 when the laminated composite sample B3 was simultaneously driven by the low-profile piezoceramic transducer S1 (figure 5.33), which provided a probe excitation at 21070 Hz, and an electrodynamic shaker (figure 5.33) that vibrate the sample at a 145 Hz pump frequency. Either way, a clear pattern of additional spectral components that correspond to multiples of the examined resonance frequency can be clearly detected in the response spectra of both the pristine and the damaged sample. Although their amplitude increased after the 1.9 J low-velocity impact, the presence of two (figure 5.51) or three (figure 5.52) pairs of modulation sidebands in the response of the undamaged beam reveals the emergence of non-damage-related nonlinear
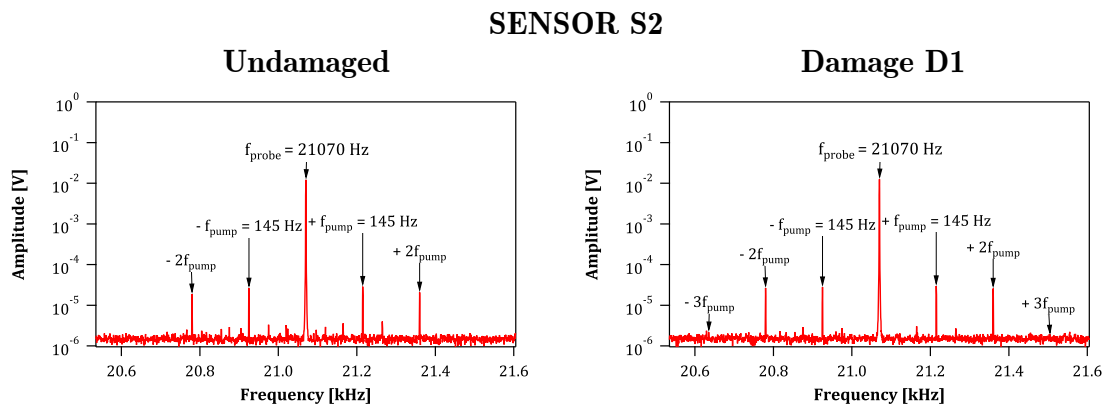
SENSOR S2

Figure 5.51 – Power spectrum of the system response acquired at the sensor location S2 in both pristine and damaged conditions: probe frequency 21070 Hz and pump frequency 145 Hz (125 mV$_{pp}$ amplitude).

SENSOR S4

Undamaged
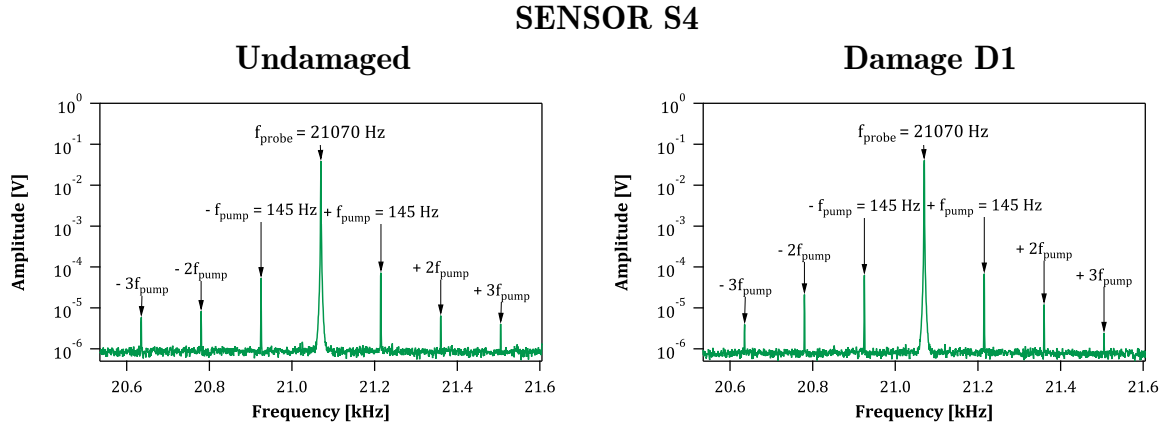
Damage D1

Figure 5.52 – Power spectrum of the system response acquired at the sensor location S4 in both pristine and damaged conditions: probe frequency 21070 Hz and pump frequency 145 Hz (125 mV$_{pp}$ amplitude).

mechanisms, such as those related to the contact effects occurring at the interfaces between the monitored structure and external bodies, material deformation (e.g., fiber/matrix internal friction), and inherent nonlinearities of the employed measurement chain.

In order to reliably detect the occurrence of impact-induced damage in the monitored composite sample, the average amplitude of the nonlinear modulation sidebands, which was assumed as a damage indicator to investigate the applicability of the VAM approach, was extracted from the spectra associated with each of the examined pump-probe frequency combinations and, subsequently, plotted as a function of the pump excitation amplitude (figures 5.53 - 5.58). In this context, while figures 5.53 - 5.55 correspond to the signals acquired at 21070 Hz probe frequency at the three considered sensor locations (namely S2, S3, and S4), those in figures 5.56 - 5.58 refer to the signals recorded at locations S2, S3, and S4 for a probe frequency of 16390 Hz. With a few exceptions (see figures 5.53d, 5.56a, and 5.56d), the data reveal that the applied impact load led to a general increase in the amplitude of the modulation sidebands, demonstrating the overall ability of the Nonlinear Vibro-Acoustic Modulation to identify the emergence of internal damage. In this perspective, it is worth stressing the low severity of the detected damage. In fact,
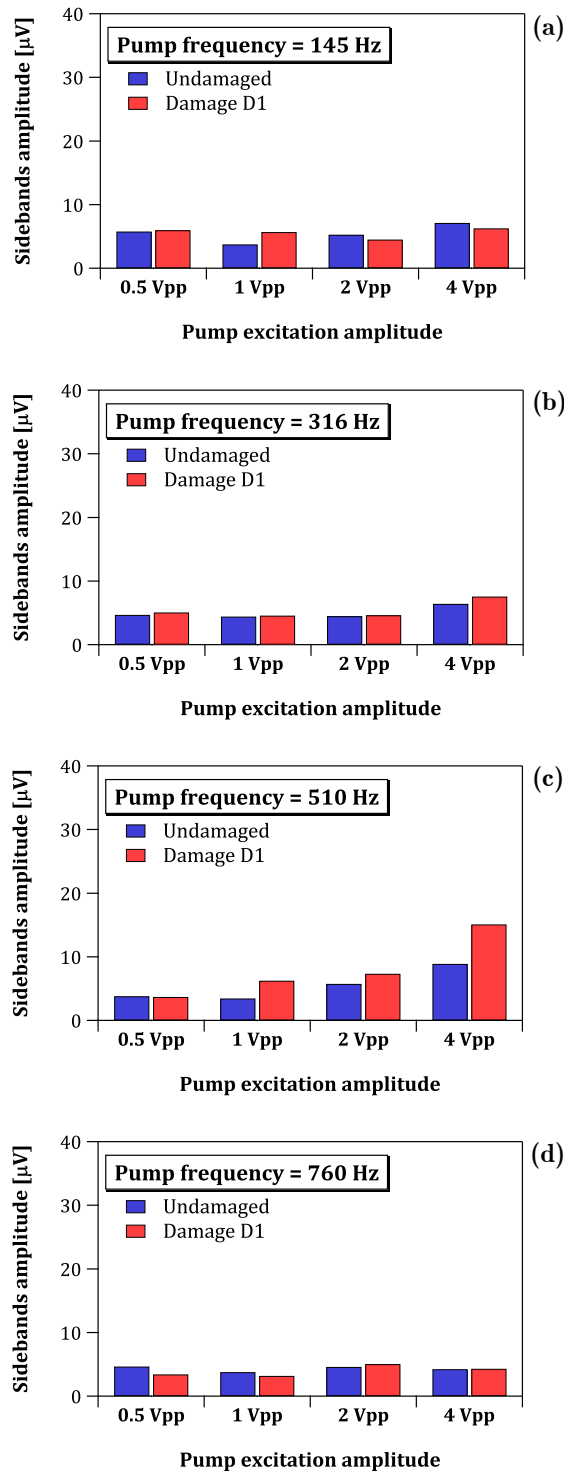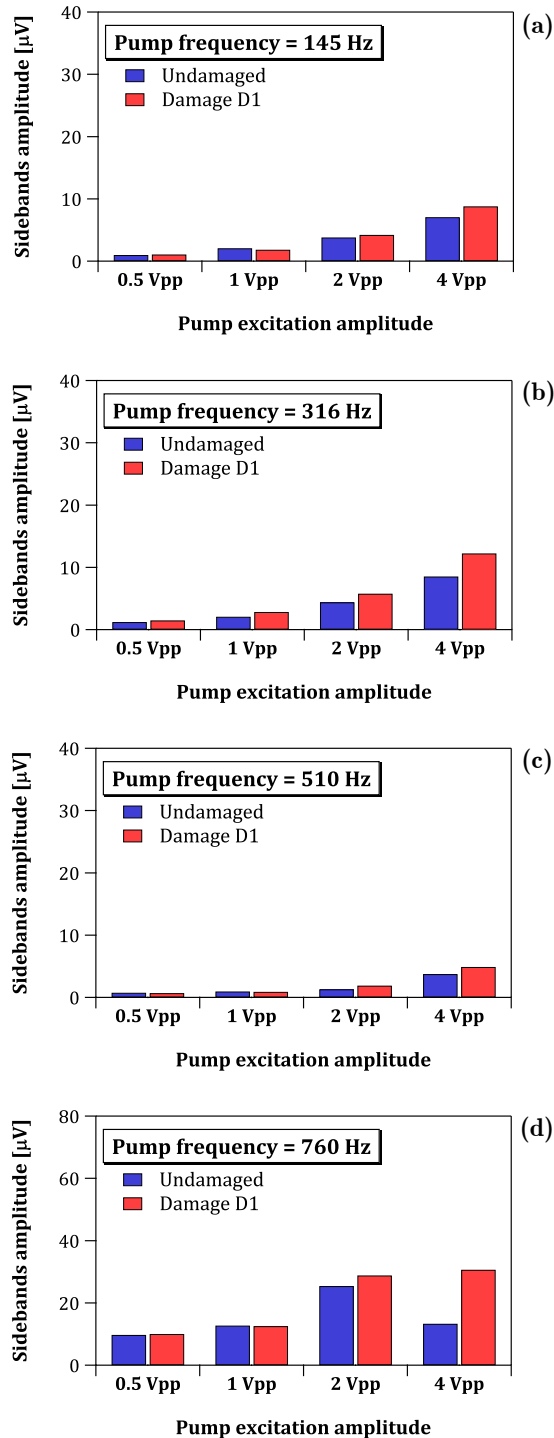
Figure 5.53 – Average amplitudes of the first pair of modulation sidebands measured at sensor location S2 at a probe frequency of 21070 Hz and pump frequencies of 145 Hz (a), 316 Hz (b), 510 Hz (c), and 760 Hz (d).

PROBE FREQUENCY = 21070 Hz

SENSOR S3

Figure 5.54 – Average amplitudes of the first pair of modulation sidebands measured at sensor location S3 at a probe frequency of 21070 Hz and pump frequencies of 145 Hz (a), 316 Hz (b), 510 Hz (c), and 760 Hz (d).

PROBE FREQUENCY = 21070 Hz

Figure 5.55 – Average amplitudes of the first pair of modulation sidebands measured at sensor location S4 at a probe frequency of 21070 Hz and pump frequencies of 145 Hz (a), 316 Hz (b), 510 Hz (c), and 760 Hz (d).

PROBE FREQUENCY = 16390 Hz

SENSOR S2

Figure 5.56 – Average amplitudes of the first pair of modulation sidebands measured at sensor location S2 at a probe frequency of 16390 Hz and pump frequencies of 145 Hz (a), 316 Hz (b), 510 Hz (c), and 760 Hz (d).

PROBE FREQUENCY = 16390 Hz

SENSOR S3

Figure 5.57 – Average amplitudes of the first pair of modulation sidebands measured at sensor location S3 at a probe frequency of 16390 Hz and pump frequencies of 145 Hz (a), 316 Hz (b), 510 Hz (c), and 760 Hz (d)

PROBE FREQUENCY = 16390 Hz
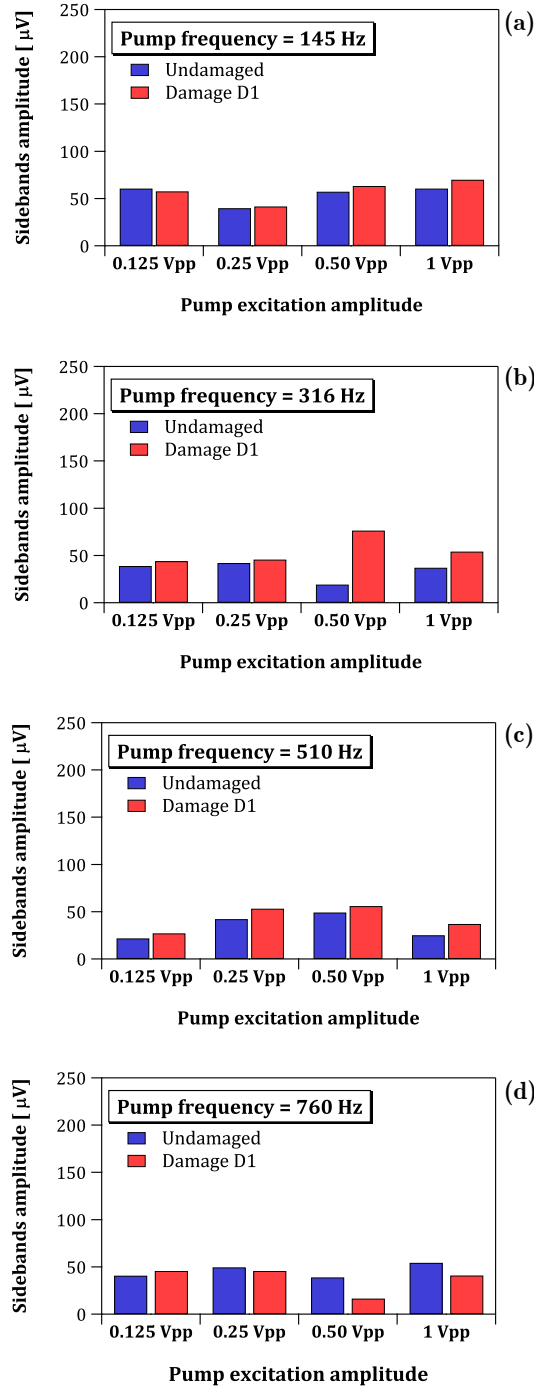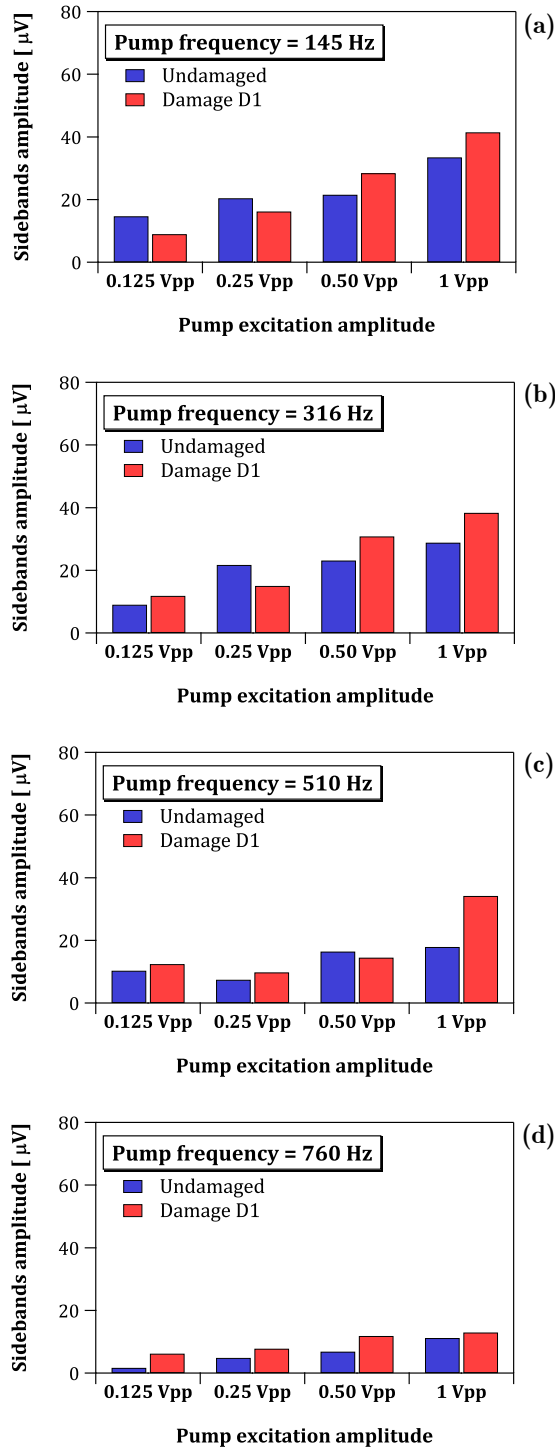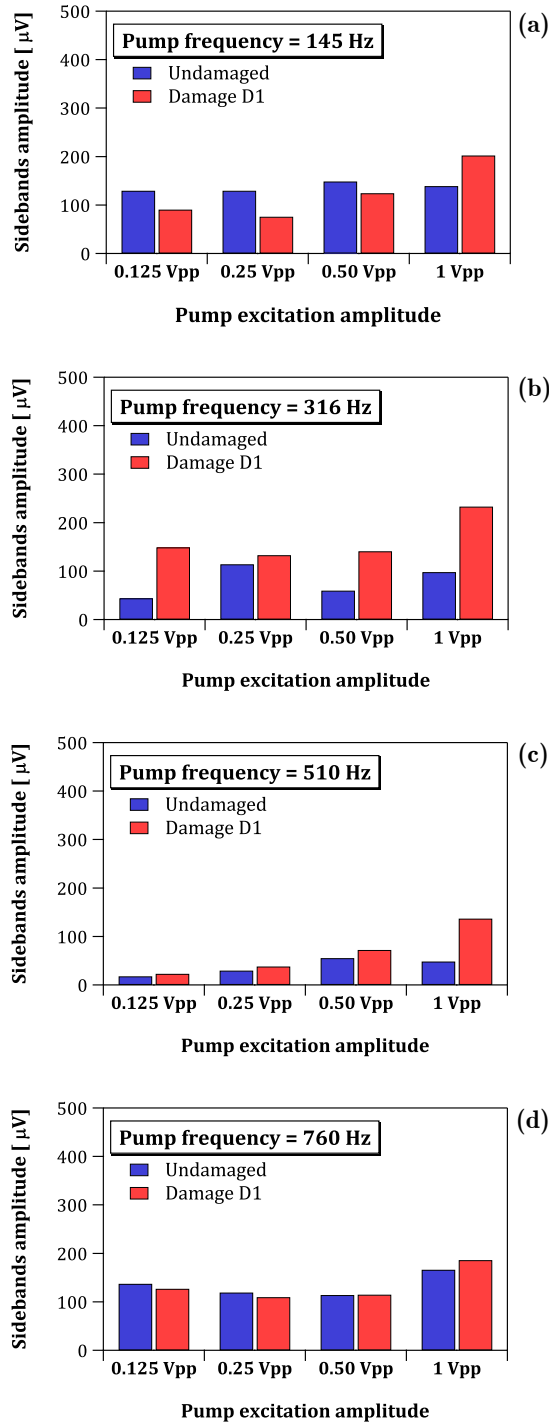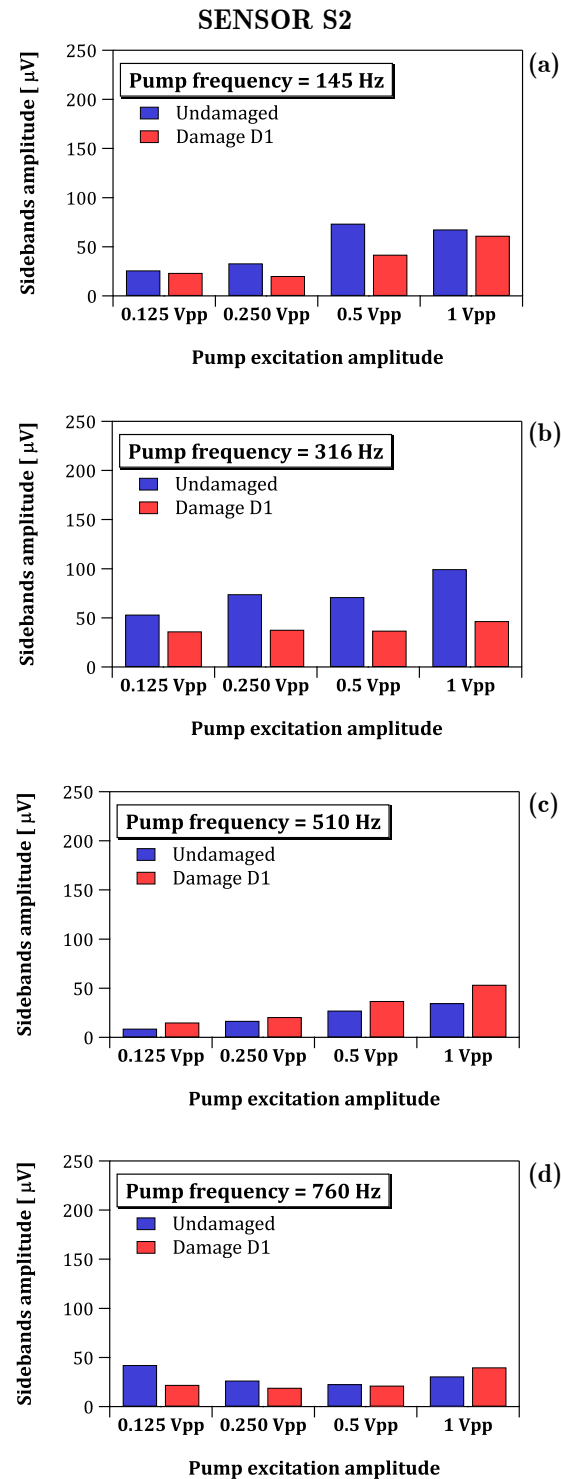
SENSOR S4

Figure 5.58 – Average amplitudes of the first pair of modulation sidebands measured at sensor location S3 at a probe frequency of 16390 Hz and pump frequencies of 145 Hz (a), 316 Hz (b), 510 Hz (c), and 760 Hz (d)

although almost impossible to be perceived by a visual inspection, the internal damage resulting from the applied low-velocity impact, which mainly consists of a small, delaminated area with some minor fiber breakage at the indentation area, might not significantly perturbate the propagation of the two impinging excitation signals. Nonetheless, similar to the findings relative to the analysis conducted on samples B1 and B2, the obtained results point out some inherent limitations of the VAM approach, especially the influence of the sensor positioning and the selected probe and pump frequency. As an illustration, the graphs of figures 5.55b and 5.58b show that a 16390 Hz probe frequency did not allow to retrieve a clear indication of the occurred damage. Instead, vibrating the sample with a 21070 Hz carrier signal allows observing an average increase in the amplitude of the first pair of modulation sidebands after the 1.9 J low-velocity impact, demonstrating the selection of the probe frequency might significantly affect both the sensitivity and the efficacy of the VAM technique. Analogously, the analysis of the graphs corresponding to the system responses acquired at sensor location S2 under a 21070 Hz probe frequency and a pump frequency of 760 Hz (figure 5.53d) and 316 Hz (figure 5.53b) reveal that driving the specimen through a pump wave at 316 Hz resulted in the emergence of a clear pattern of sidebands whose amplitude approximately increased by 17 μV after the introduction of impact damage. Conversely, exciting the low-frequency mode at 760 Hz (figure 5.53d) did not induce noticeable changes in the amplitude of the emerged sidebands, inferring the dependence of the selected pump frequency on the VAM performance.

Concerning the role of the sensor positioning, the data indicate that the quality of the indications provided depends on the sensor positioning relative to the source of excitation, the damaged region, and the sample support. In this context, comparing the figures 5.56b and 5.57b, which refer to the signals acquired in correspondence of a 316 Hz pump frequency and a 16390 Hz probe, allows noticing that the signal acquired at sensor location S3 (figure 5.57b) provided unique information on the occurred damage. In fact, contrary to the values retrieved in S2 (figure 5.56b), the amplitude of the first pair of modulation sidebands significantly increased after applied impact load. Similarly, the graph in figures 5.53d and 5.54d, which concern the system response to a 760 Hz pump frequency combined with a 21070 Hz probe frequency, point out that the amplitude measured in damaged

condition at sensor location S3 was invariably higher than that acquired at sensor location S2 across the whole range of the examined pump excitation levels.

Since the averaged spectra (figures 5.51 and 5.52) acquired by vibrating the sample through the electrodynamic shaker revealed the emergence of the second pairs of modulation sidebands, summing the amplitude of all the emerged components might improve the reliability of the considered method. Hence, to further investigate both the efficiency and sensitivity of the VAM approach, the sum of the average amplitude of the first three pairs of modulation sidebands was assumed as a second damage indicator, whose values were plotted as a function of the pump excitation amplitude. Thus, while figures 5.59 - 5.61 refer to a probe frequency of 21070, figures 5.62 - 5.64 correspond to the acoustic probe frequency of 16390 Hz. Besides confirming the overall ability of the Nonlinear Vibro-Acoustic Modulation to retrieve information on the induced damage, the data point out that accounting for all the emerged modulation sidebands allows detecting the damage resulting from the applied transverse impact load even for pump-probe frequency combinations at which the sole first sidebands was not effective. As an illustration, the graph of figure 5.56d, which refers to a probe frequency of 16390 Hz and a pump frequency of 760 Hz, shows that the amplitude of the first pair of sidebands in pristine conditions was invariably higher than that measured at damage level D1 (figure 5.56d). Conversely, summing the contribution of the three pairs of modulation sidebands allows retrieving an increase after the damage introduction (figures 5.59d).

In addition, investigating the role of the pump excitation amplitude, which represents a measure of the level of strain in the material, on the method's performance, the amplitude of the modulation sidebands was shown to increase with the pump excitation level (see, for example, figures 5.60a, 5.60b, and 5.62a). However, it is worth noticing that, by contrast with the observations made in relation to the loss of sensitivity occurred at low pump excitation amplitude when the sample was driven with a stack actuator, the Nonlinear Vibro-Acoustic Modulation managed to identify the occurrence of internal damage even at the minimum excitation level (i.e., 125 mV_{pp}).

PROBE FREQUENCY = 21070 Hz

SENSOR S2

Figure 5.59 – Sum of the amplitudes of the first three pair of modulation sidebands measured at sensor location S2 at a probe frequency of 21070 Hz and pump frequencies of 145 Hz (a), 316 Hz (b), 510 Hz (c), and 760 Hz (d).
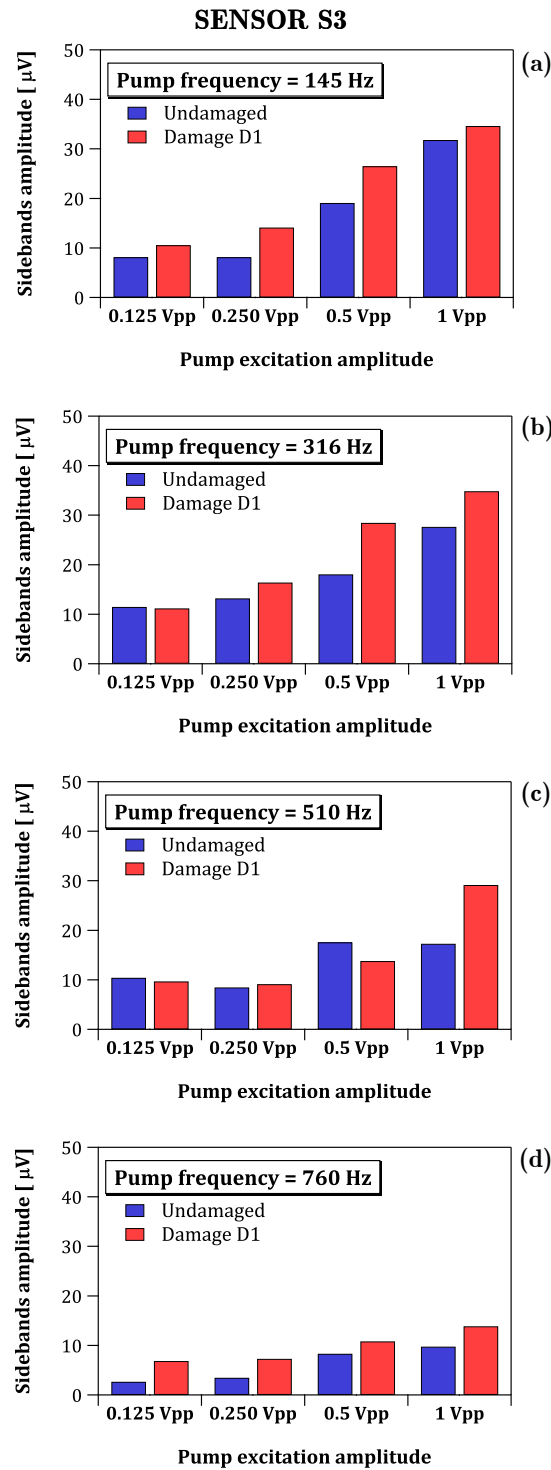
PROBE FREQUENCY = 21070 Hz

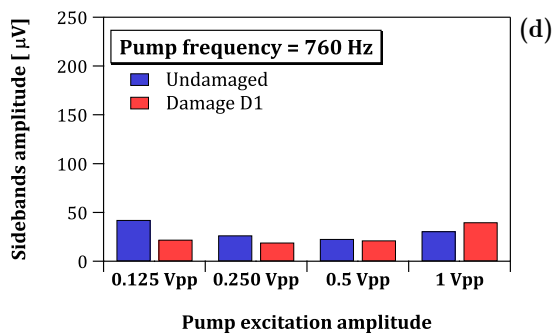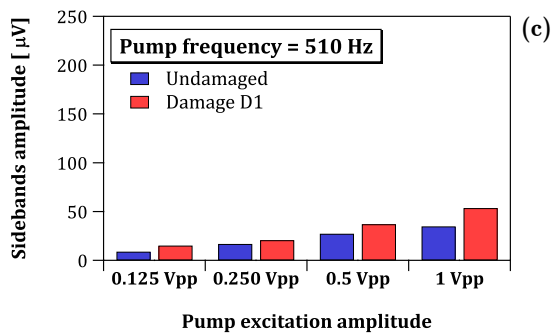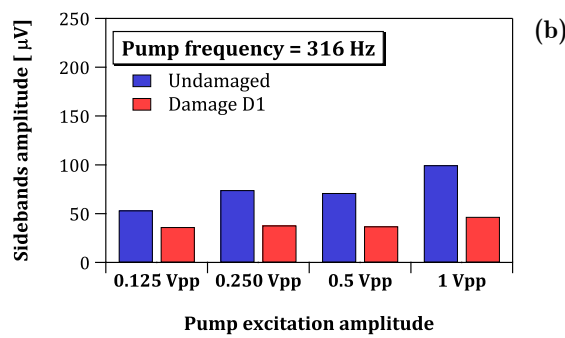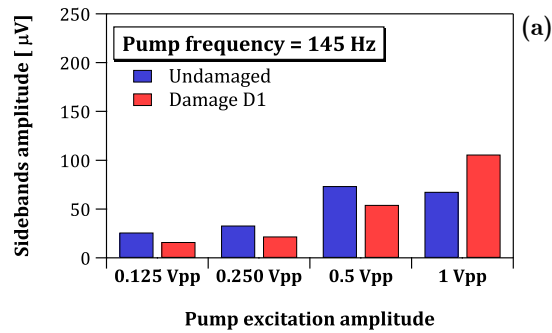**Figure 5.60 –** Sum of the amplitudes of the first three pair of modulation sidebands measured at sensor location S3 at a probe frequency of 21070 Hz and pump frequencies of 145 Hz (a), 316 Hz (b), 510 Hz (c), and 760 Hz (d).

PROBE FREQUENCY = 21070 Hz
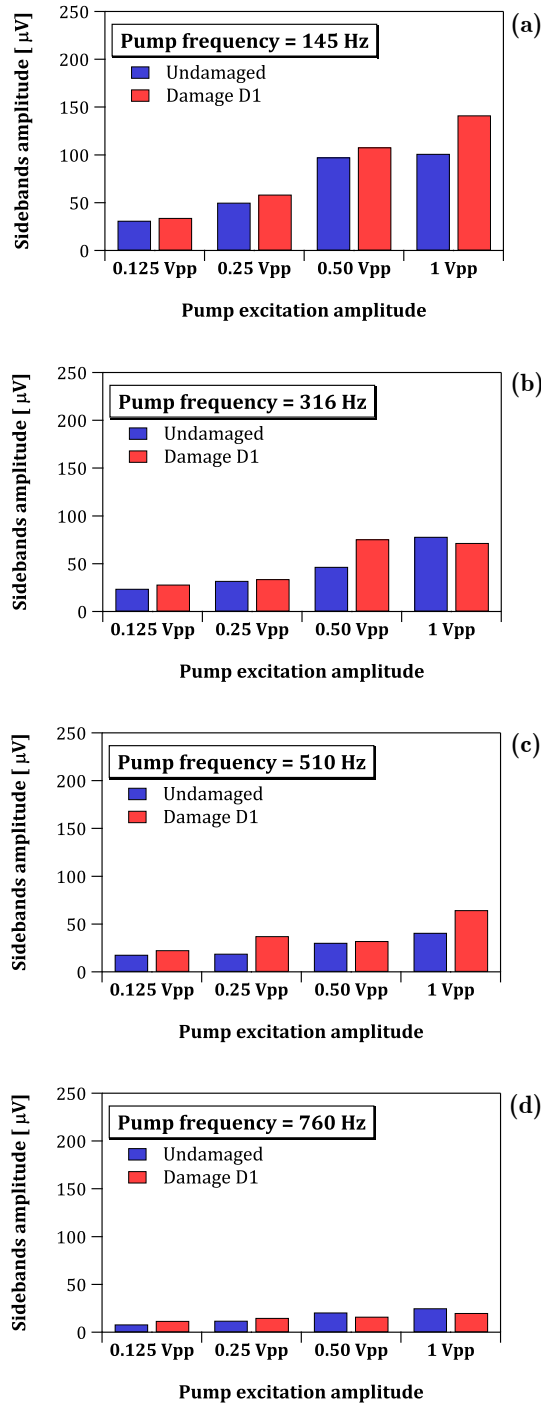
SENSOR S4

Figure 5.61 – Sum of the amplitudes of the first three pair of modulation sidebands measured at sensor location S4 at a probe frequency of 21070 Hz and pump frequencies of 145 Hz (a), 316 Hz (b), 510 Hz (c), and 760 Hz (d).

PROBE FREQUENCY = 16390 Hz
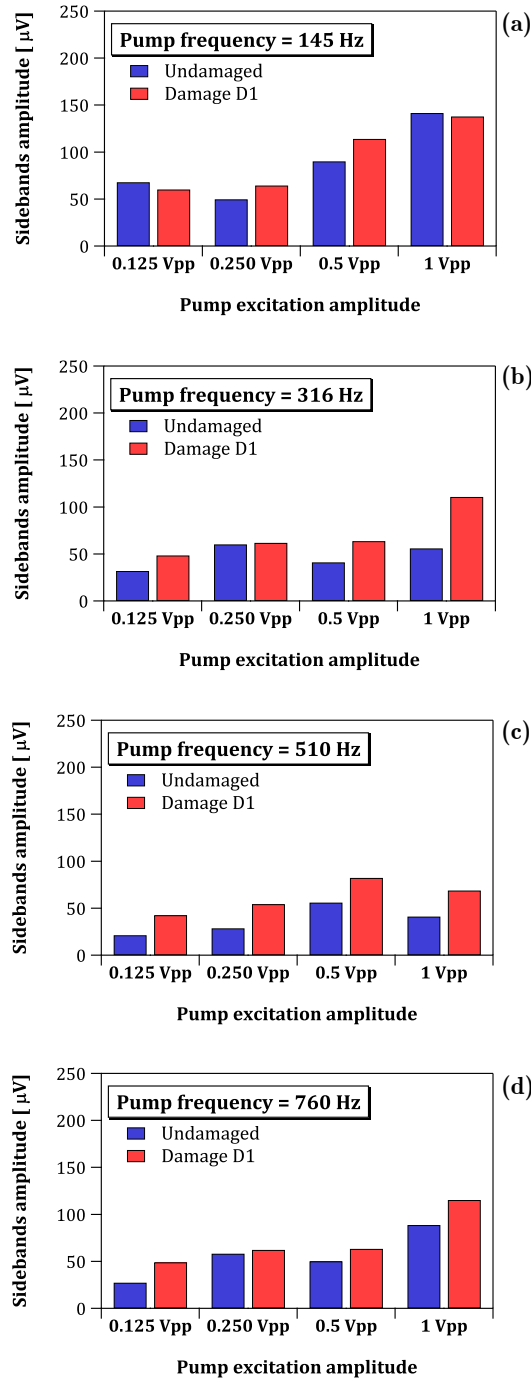
Figure 5.62 – Sum of the amplitudes of the first three pair of modulation sidebands measured at sensor location S2 at a probe frequency of 16390 Hz and pump frequencies of 145 Hz (a), 316 Hz (b), 510 Hz (c), and 760 Hz (d).

PROBE FREQUENCY = 16390 Hz
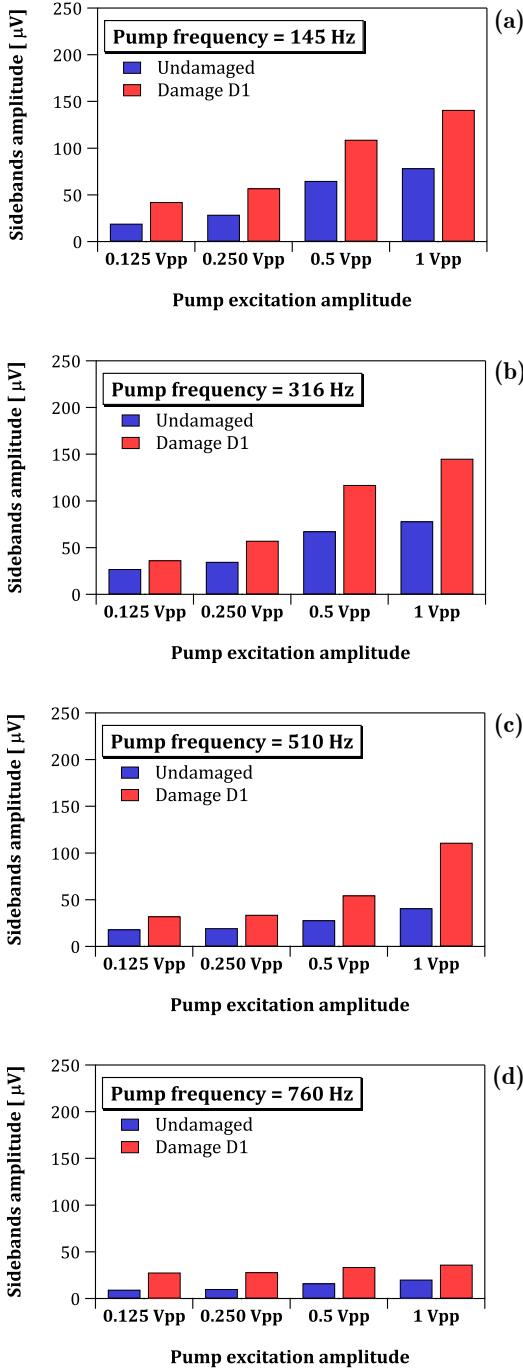
SENSOR S3

Figure 5.63 – Sum of the amplitudes of the first three pair of modulation sidebands measured at sensor location S3 at a probe frequency of 16390 Hz and pump frequencies of 145 Hz (a), 316 Hz (b), 510 Hz (c), and 760 Hz (d).
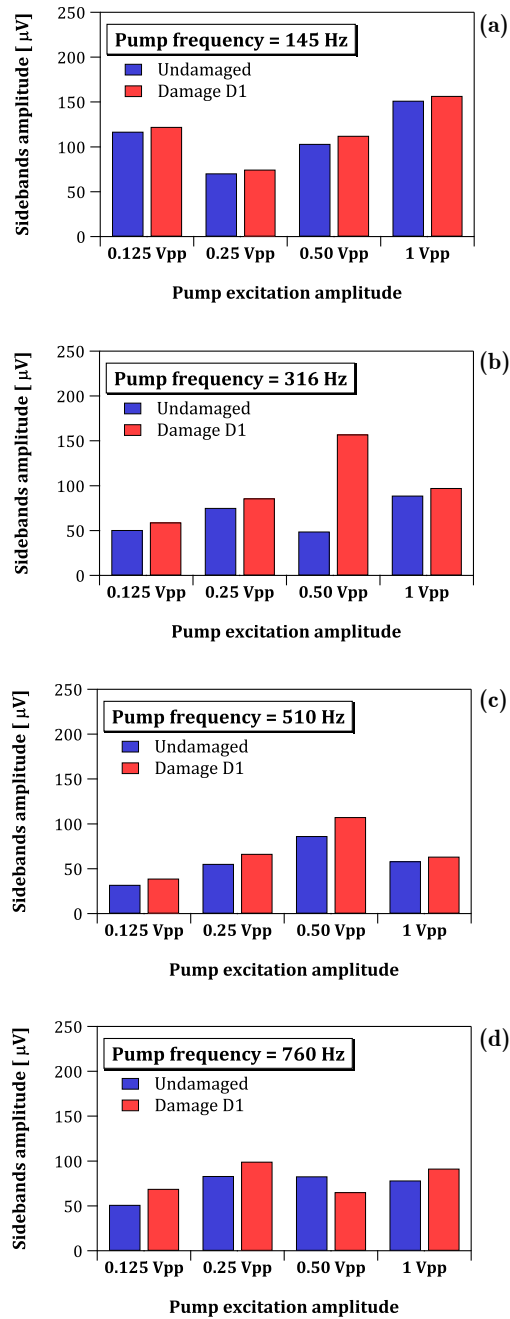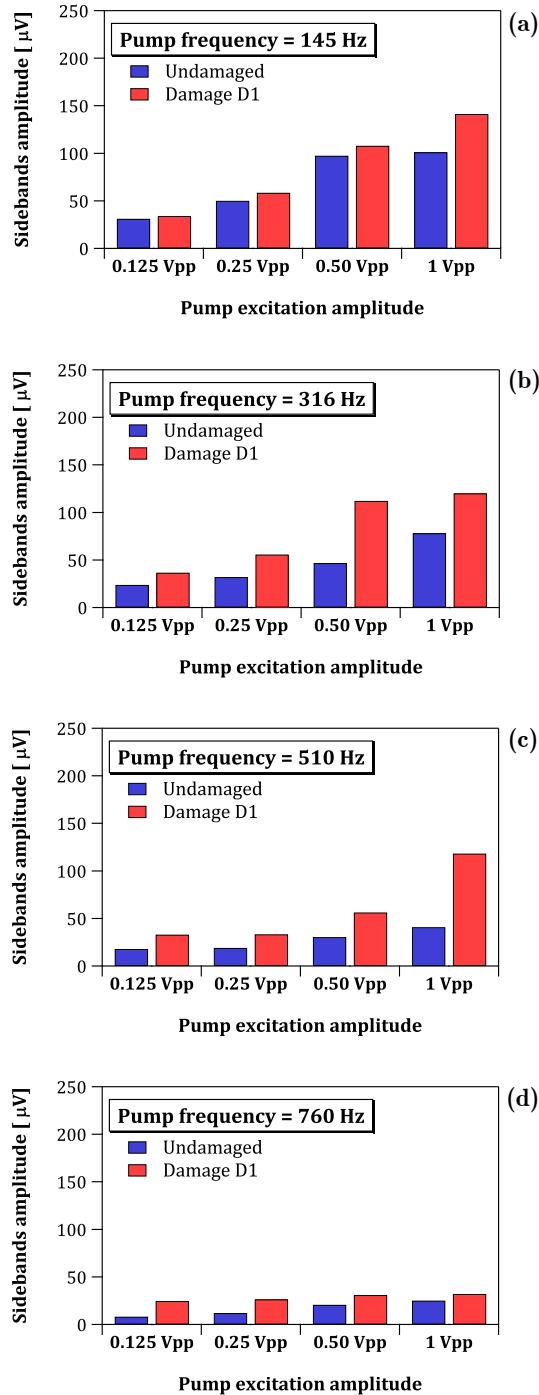
PROBE FREQUENCY = 16390 Hz
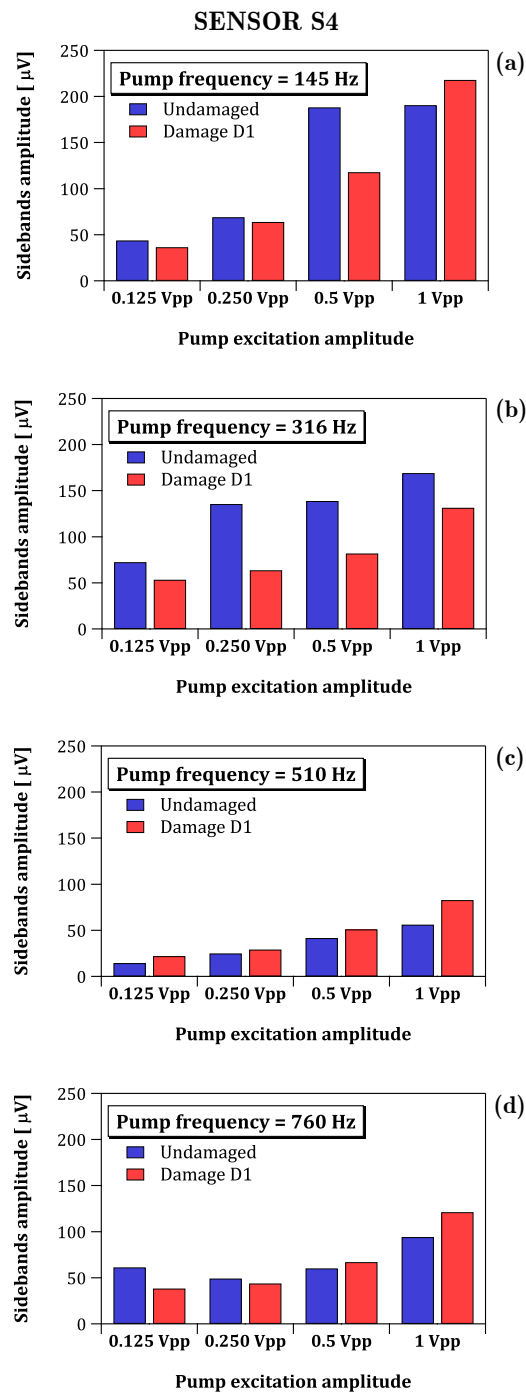
SENSOR S4

Figure 5.64 – Sum of the amplitudes of the first three pair of modulation sidebands measured at sensor location S4 at a probe frequency of 16390 Hz and pump frequencies of 145 Hz (a), 316 Hz (b), 510 Hz (c), and 760 Hz (d).

5.4   Conclusions

Among the non-destructive testing technique relying on the frequency-mixing phenomena, the Nonlinear Vibro-Acoustic Modulation relies upon the simultaneous application of two excitation signals with distinct frequencies and amplitudes that propagate within the medium and interact with each other. The presence of cracks, flaws, or discontinuities along the wave propagation path triggers the emergence of several nonlinear mechanisms, i.e., frequency mixing, higher and sub-harmonics. In particular, the nonlinear VAM exploits the occurrence of additional spectral components to characterize the nonlinear signature of the inspected sample and, thus, provides information on the presence of the damage, its localization, and its extent. With the advantage of not requiring complex setups, the Nonlinear Vibro-Acoustic Modulation was shown to efficiently detect the presence of small cracks in both metal and non-metallic structures. However, to make it a viable and effective non-destructive testing technique in real applications, the nonlinear VAM efficacy has to be improved by further investigating the method critical issues, e.g., the selection of both the frequency and amplitude of the pump and probe excitation waves, the characteristic of the testing setup, the actuators, and sensors. As a contribution to addressing this matter, this chapter aimed to present the results obtained by applying the Nonlinear Vibro-Acoustic Modulation to detect the presence of impact-induced damage in laminated composite beams. Subjected to a couple of low-velocity transverse impact loads, the three inspected samples underwent increasing damage severity. Although barely detectable at a visual inspection, the impact-induced damage, which mainly consisted of a combination of delaminations and matrix cracking, was found to cause the onset of a clear pattern of modulation sidebands around the spectral line corresponding to the probe frequency.

The need to address whether the type of the employed actuators and sensors affect the VAM efficacy led to consider different actuation-sensing scenarios, showing the overall method ability to provide clear indications on both the damage occurrence. In this perspective, the quality of the information the method retrieved did not significantly vary with the employed sensing apparatus, which consisted of accelerometers (sample B1), piezoceramic transducer (sample B2), or a combination of the two (sample B3). Moreover, the VAM performance (i.e., efficacy and

sensitivity) appeared to depend on the sensor positioning relative to the excitation sources and the impact area, suggesting the influence of the path through which the excitation waves propagate. Analogously, the VAM capability to detect the damage did not rely upon the adopted actuation scenarios, which alternatively combined the piezoceramic disk that provided the probe excitation with an electrodynamic shaker (samples B1 and B3) or a stack actuator (sample B2) for exciting the pump excitation. Nonetheless, although the amplitude of the emerged modulation sidebands generally increased with both the severity of damage and the amplitude of the pump wave, the selection of both the probe and pump frequencies was found to affect the method's performance. In this context, conducting an experimental campaign in which several pump-probe frequencies combinations were considered allowed noticing that the choice of the probe frequency may significantly impact the sensitivity of the Nonlinear Vibro-Acoustic Modulation, even though picking it among the inspected structure resonance frequencies did not necessarily improve the damage detection efficacy. In the same way, the results highlighted that some of the considered pump frequencies were more effective in retrieving the presence of the induced-impact damage and ranking its severity. Hence, the lack of robustness and, thus, the lack of an algorithm to select the frequency values (i.e., both pump and probe frequency excitation) with the highest sensitivity for the Nonlinear Vibro-Acoustic Modulation reduces the analysis effectiveness and, at once, prevents the method from being widely employed in practical non-destructive testing applications.

In addition, since the amplitude of the modulation sidebands predominantly increased with the pump excitation level, the indications provided were generally more unique at the highest pump excitation level. In fact, when the selected low-frequency vibration modes (i.e., pump excitation) were excited at the highest excitation level, the Nonlinear Vibro-Acoustic Modulation was generally able to detect the internal damage and, at once, correctly rank its severity. The loss of sensitivity observed at lower pump excitation amplitudes may be attributed to the difficulty in monitoring low-level signals falling close or below the background noise floor and the necessity to attain enough energy to activate the nonlinear mechanisms involved in the emergence of the modulation sidebands. Moreover, it is also worth noticing that due to the small extent of the projected delaminated area and the comparable features of the impact-induced damage, in some of the considered testing

165

scenarios, the average amplitude of the first pair of modulation sidebands recorded at the severest level of damage was lower than the value measured at the other damage states.

In conclusion, the Nonlinear Vibro-Acoustic Modulation was shown to be effective in identifying the occurrence of barely visible impact damage in fiber-reinforced composite materials. Nonetheless, due to some critical issues related to the choice of excitation frequencies, the selection of the excitation amplitudes range, the type, and the positioning of the employed sensors, which make necessary further investigations, caution must be paid in interpreting the experimental data.

Conclusions

Despite the high specific strength and resistance to fatigue and corrosion, composite materials exhibit an equally high susceptibility to impact damage that may question their use in critical load-bearing structures. Hence, their safe employment in structural mechanics became subordinated to the ability to detect the occurrence of internal damage and monitor its progression, leading to the development of many non-destructive testing (NDT) techniques. However, since several proposed approaches are still laboratory demonstrations rather than reliable tools for practical engineering applications, a growing effort has recently been devoted to assessing the potential of classical and non-classical nonlinear acoustic phenomena for damage detection. In this perspective, this thesis aimed to investigate the applicability and the performance of two nonlinear acoustics approaches, namely the Scaling Subtraction Method (SSM) and the Nonlinear Vibro-Acoustic Modulation (VAM), and demonstrate their effectiveness in both damage detection and characterization.

After the brief introduction to the damage process occurring in composite laminated structures provided in Chapter 1, Chapter 2 gives an insight into Structural Health Monitoring (SHM), i.e., the emerging interdisciplinary field aimed to design tools and strategies to provide real-time diagnosis/prognosis on the component status, with a particular focus on the methods commonly applied to inspect composite materials. Among these approaches, those based on nonlinear acoustic/vibration phenomena have gained increasing attention being more sensitive to early-stage defects than their linear counterparts. Thus, Chapter 3 provides a description of the nonlinear acoustic phenomena arising in solids, i.e., contact acoustic nonlinearity, higher harmonic generation, resonance frequency shift, and frequency mixing. In this perspective, the lack of a deep understanding of the physics underlying these nonlinear phenomena has emerged as one of the main reasons behind

Conclusions

the difficulties in implementing reliable engineering tools for damage detection and characterization. Thus, aiming at further exploring the capability of the considered nonlinear acoustic approaches (i.e., SSM and VAM) to detect the onset of impact damage in composite materials, the remaining chapters illustrate the experimental campaign conducted to address some of the related critical issues that mainly concern the selection of the testing parameters.

Chapter 4 goes into an in-depth outline of the principle underlying the *Scaling Subtraction Method,* which provides information on the material integrity and its ability to withstand critical loads by accounting for the global nonlinear content of the inspected sample response. Although the Scaling Subtraction Method was shown to be effective in detecting the onset of internal damage in a wide range of different materials, two main drawbacks were pointed out: (1) the need for preliminary modal analysis and (2) the sensitivity to the interrogating frequency. In this thesis, a novel SSM-based methodology relying on driving the monitored structure with a broadband impulsive excitation has been proposed to overcome these limitations. The feasibility and the effectiveness of the proposed pulse-based SSM approach have been verified by alternatively exciting the inspected laminated composite beam through a pure harmonic excitation tuned at different natural frequencies of the system and an impulsive excitation. The obtained results allow drawing the following insights:

- The Scaling Subtraction Method managed to detect the onset of impact damage in laminated composite beams.

- The sensitivity of the Scaling Subtraction Method depends on the interrogating frequency

- The quality of the indications that the SSM provides does not significantly vary relative to the sensor positioning.

- The pulse-based SSM approach turned out to be a rather promising option for identifying the nonlinearities associated with the onset of impact-induced damage in composite materials.

- A global indicator, which considers the nonlinear contributions associated with all the considered testing frequencies, appears to improve both the effectiveness and the robustness of the SSM pulse-based approach.

Chapter 5 first provides the theoretical background of the ***Nonlinear Vibro-Acoustic Modulation***. Then, an in-depth review of its applications, especially those dealing with composite materials, pointed out the VAM's ability to detect the presence of small cracks in both metal and non-metallic structures. However, some critical issues must still be faced, such as the selection of both the frequency and amplitude of the pump and probe excitation waves, the characteristic of the testing setup, the actuators, and sensors. Therefore, making the Nonlinear Vibro-Acoustic Modulation a reliable and effective tool for practical engineering applications requires further investigations. As a contribution to address this matter, Chapter 5 illustrates the results obtained by applying the Nonlinear Vibro-Acoustic Modulation to detect the emergence of impact damage in three laminated composite beams. Although barely detectable at a visual inspection, the damage produced on the inspected samples by means of multiple low-velocity transverse impact loads induced the occurrence of a clear pattern of modulation sidebands around the probe frequency peak. According to the considered actuation/sensing scenarios and the outlined procedures, the beams were driven at several pump/probe frequency combinations in both pristine and damaged conditions, allowing to draw a few considerations:

- The results confirmed the effectiveness of the Nonlinear Vibro-Acoustic Modulation in detecting the occurrence of impact damage in laminated composites samples.

- The emergence of modulation sidebands was triggered by the applied impact loads, which caused the onset of delaminations and matrix cracks. The amplitude of these additional spectral components generally increased with the damage severity and the pump excitation level. Nonetheless, exceptions to this trend suggested the proper selection of both the probe and pump frequencies to be essential for reliable damage detection.

Conclusions

- The choice of the probe frequency appeared to affect the sensitivity of the Nonlinear Vibro-Acoustic Modulation, although picking its value among the sample natural frequencies did not necessarily enhance the damage detection efficacy.

- The quality of the indications provided was tendentially higher at the highest pump excitation amplitude, where the method managed to detect the occurrence of damage and, at once, correctly rank the damage severity. Conversely, low pump excitation levels generally resulted in a decay of the VAM performance owing to the difficulty in monitoring low-level signals or attaining the minimum amount of energy required to activate the nonlinear wave interaction mechanisms.

- The VAM capability to provide information on the material degradation slightly varied with the employed sensors and appeared to be affected by the sensor positioning relative to the excitation sources and the damaged area.

- The examined actuation scenarios, which alternatively combined the piezoceramic disk that provided the probe excitation with an electrodynamic shaker or a stack actuator for exciting the pump excitation, did not significantly affect the ability of the VAM approach to detect the damage.

In the end, both the Scaling Subtraction Method and the Nonlinear Vibro-Acoustic Modulation were able to reveal the occurrence of barely visible impact damage in fiber-reinforced composite materials. However, because the implementation of reliable tools for practical non-destructive testing applications requires a good comprehension of the mechanisms underlying the nonlinear acoustic phenomena, further investigations are still needed to gain a deep understanding of the effects of factors as the sample geometry, the stacking sequence, the operating and environmental conditions may have on the performance of the considered nondestructive testing methodologies. Moreover, since similar nonlinear effects may

arise from different mechanisms or inherent nonlinearities (e.g., overloads, boundary conditions, connections between transducers and monitored surfaces, and instrumentation), an extensive research effort is needed to distinguish between damage-related and non-damage-related nonlinear effects to improve the efficiency of the damage detection process and, at once, develop a robust algorithm to select the testing parameters (e.g., the interrogating frequency) with the highest sensitivity to damage detection.

Reference

[1]   C. Hood, Dealing with disaster in Japan: responses to the flight JL123 crash, London: Rotledge, 2013.

[2]   NTBS, "Aircraft accident report – Aloha Airlines, Flight 243, Boeing 737-200, N73711, near Maui, Hawaii, April 28, 1988.," Technical Report, National Transportation Safety Board Bureau of Accident Investigation, 1988.

[3]   W. L. Guan and K. Yong, "Ballistic trajectory analysis for the CI611 accident investigation. Technical Report," Aviation Safety Council, 2003.

[4]   P. O. Moore, Nondestructive testing handbook," Vol. 10, in Overview, 3rd ed., American Society for Nondestructive Testing, (2012)., Columbus, OH, 2012.

[5]   C. Hellier, Handbook of Nondestructive Evaluation, 2nd ed.,, New York: McGraw Hill Professional, 2012.

[6]   W. J. Staszewski, C. Boller and G. R. Tomlinson, Health monitoring of aerospace structures, Chichester: Wiley, 2004.

[7]   V. Giurgiutiu, Structural Health Monitoring with piezoelectric wafer active sensors (2nd edition), New York: Elsevier Accademic Press, 2008.

[8]   Boller C., F. K. Chang and Y. Fujino, Encyclopedia of Structural Health Monitoring, Chichester: Wiley, 2008.

[9]   D. Betterghor, S. Grihon and J. Morher, "Bilevel optimization of large composite structures based on lamination parameters and post-optimal sensitivities. Part 1: Theoretical aspects.," *ISAE-SUPAERO, Tuolose,* 2018.

Reference

[10]   T. Kundu, Nonlinear Ultrasonic and Vibro-Acoustical Techniques for Nondestructive Evaluation, Cham (Switzerland): Springer Nature Sweitzerland, 2019.

[11]   M. Daniel, "Failure mechanisms in fiber-reinforced composites.," in *Proceedings of the ARPA/AFML Review of Progress in Quantitative NDE, September 1976–June 1977*, 1978.

[12]   C. C. Chamis, "Micromechanics strength Theories," in *Fracture and fatigue. Vol 5*, New York, Broutman L. J. and Krock R. H., Academic Press, 1974.

[13]   B. W. Rosen and N. F. Dow, "Mechanics of failure of fibrous composites," *Fracture of Nonmetals and Composites,* pp. 611 - 674, 1972.

[14]   P. K. Mallick, Fiber-reinforced composites (Third Eeition), CRC Press (Taylor and Francis Group), 2008.

[15]   B. W. Rosen, "Mechanics of composite strengthening," in *Composite materials*, Metals Park, OH, American Society of Metals, 1965, pp. 37 - 75.

[16]   R. M. Jones, Mechanics of composite materials (Second edition), Taylor and francis, 1999.

[17]   R. Talreja, "Damage analysis for structural integrity and durability of composite materials," *Fatigue & Fracture of Engineering Materials & Structures,* vol. 29, pp. 481 - 506, 2006.

[18]   E. k. Gamstedt and B. A. Sjögren, "Micromechanisms in tension-compression fatigue of composite laminates containing transverse plies," *Composites Scince and Technology,* vol. 59, no. 2, pp. 167 - 178, 1999.

[19]   M. Talreja, "Multiscale modeling," in *Comprehensive Composite Materials II, Volume 2*, Elsevier, 2018, pp. 148 - 166.

[20]   P. A. Carraro and M. Quaresimin, "A damage based model for crack initiation in unidirectional composites under multiaxial cyclic loading," *Composites science and Technology,* vol. 99, pp. 154 - 163, 2014.

Reference

[21]   A. Matzenmiller, J. Lubliner and R. L. Taylor, "A constitutive model for anisotropic damage in fiber-composites A. Matzenmiller 1, J. Lubliner, R.L. Taylor Department of Civil Engineering, University of California at Berkeley, Berkeley, CA 94720, USA Received 19 March 1992, accepted 29 June 1994 Abstra," *Mechanics of Materials,* vol. 20, pp. 125 - 152, 1995.

[22]   R. Talreja, "PMC failure mechanisms," in *Comprehensive Composite Materials II, Volume 2*, Elsevier, 2018, pp. 107 - 117.

[23]   A. L. Highsmith and K. L. Reifsnider, "Stiffness-reduction mechanisms in composite laminates," in *Procedia ASTM - Conference on Damage in Compoiste Laminates*, 1980.

[24]   D. E. Bowles, "Effect of microcracks on the thermal expansion of composite laminates," *Journal of Composite Materials,* vol. 18, no. 2, pp. 173 - 187, 1984.

[25]   J. E. Lundgen and P. Gudmundson, "Moisture absorption in glass-fibre/epoxy laminates with transverse matrix cracks," *Composite Science and Technology,* vol. 59, no. 13, pp. 1983- 1991, 1999.

[26]   V. Birman and L. W. Byrd, "Effect of matrix cracks on damping in unidirectional and cross-ply ceramic matrix composites.," *ournal of Composite Materials,* vol. 36, no. 15, pp. 1859 - 1877, 2002.

[27]   V. Birman and L. W. Byrd, "Natural frequencies of cross-ply laminated panels with matrix cracks.," *AIAA Journal,* vol. 39, no. 1, 2001.

[28]   J. A. Nairn and S. Hu, "The initiation and growth of delaminations inducedby matrix microcracks in laminated composites," *International Journal of Fracture,* vol. 57, pp. 1 - 24, 1992.

[29]   J. Zhang, J. Fan and K. P. Herrmann, "Delaminations induced by constrained transverse crackingin symmetric composite laminates," *International Journal of Solids and Structures,* vol. 36, pp. 813 - 846, 1999.

Reference

[30]   M. R. Wisnom, "The role of delamination in failure of fibre-reinforced composites," *Philosoplhical transactions of the Royal Society A - Mathematical, physical and engineering science,* vol. 370, p. 1850 – 1870, 2012.

[31]   C. R. Farrar, S. W. Doebling and D. A. Nix, "Vibration-based structural damage identification," *Philosophical Transactions of the Royal Society A: Mathematical, Physical and Engineering Sciences,* vol. 359, no. 1778, pp. 131 - 149, 2001.

[32]   C. R. Farrar and K. Worden , "An introduction to Structural Health Monitoring," *Philosophical Transactions of the Royal Society A: Mathematical, Physical and Engineering Sciences,,* vol. 365, no. 1851, pp. 303 - 315, 2007.

[33]   T. Stsepinski, T. Uhl and J. W. Staszewski, Structural Damage Detection: from Theory to Engineering Applications, Wiley, West Sussex, 2013., Chichester: Wiley, 2013.

[34]   S. W. Doebling, C. R. Farrar, M. B. Prime and D. W. Shevitz, "Damage identification and health monitoring of structural and mechanical systems from changes in their vibration characteristics: a literature review.," Technical report, Los Alamos National Laboratory, NM, USA, 1996.

[35]   C. P. Fritzen and P. Kraemer, "Self-diagnosis of smart structures based on dynamical properties.," *Mechanical Systems and Signal Processing,* vol. 23, no. 6, p. 1830–1845, 2009.

[36]   K. Worden, C. R. Farrar, G. Manson and G. Park, "The fundamental axioms of Structural Health mMonitoring," *Proceedings of the Royal Society A: Mathematical, Physical and Engineering Sciences,* vol. 463, no. 2082, p. 1639–1664, 2007.

[37]   H. Sohn, "Effects of environmental and operational variability on Structural Health Monitoring," *Philosophical Transaction of the Royal Society of London A,* vol. 365, pp. 539 - 560, 2006.

[38]   S. B. Kim and H. Sohn, "Instantaneous reference-free crack detection based on polarization characteristics of piezoelectric materials," *Smart Materials and Structures,* vol. 16, pp. 2357 - 2387, 2007.

Reference

[39]   E. S. Sazonov, P. Klinkhachom, U. B. Halabe and H. V. S. Gangarao, "Non-baseline detection of small damages from changes in strain energy mode shapes," *Nondestructive Testing and Evaluation,* vol. 18, no. 3-4, pp. 91 - 107, 2002.

[40]   S. Park, C. Lee and H. Sohn , "Reference-free crack detection using transfer impedances," *Journal of Sound and Vibration,* vol. 329, no. 12, p. 2337 – 2348, 2010.

[41]   R. S. Gostautas, G. Ramirez, J. Peterman and D. Meggers, "Acoustic Emission monitoring and analysis of glass fiber-reinforced composites bridge decks," *Journal of Bridge Engineering,* vol. 10, no. 6, pp. 713 - 721, 2005.

[42]   M. Huang, L. Jiang, P. K. Liaw , C. R. Brooks, R. Seeley and D. L. Klarstrom, "Using acoustic emission in fatigue and fracture materials research," *Journal of the Minerals, Metals and Material Society,* vol. 50, no. 11, 1998.

[43]   J. Kaiser, Untersuchungen uber das auftreten Gerauschhen beim Zugversuuch, Munich : PhD Thesis, Technische Hochschule, 1950.

[44]   H. L. Dunegan, D. O. Harris and C. A. Tatro , "Fracture analysis by use of acoustic emission," *Engineering Fracture Mechanics,* vol. 1, pp. 105 - 122, 1968.

[45]   H. L. Dunegan and D. Harris, "Acoustic Emission - A new nondestructive testing tool," *Ultrasonic,* vol. 7, no. 3, pp. 160 - 166, 1969.

[46]   D. Hagemaier, H. J. McFaul and D. Moon, "Nondestructive testing of graphite fiber composite structures," *Materials Evaluation,* vol. 28, no. 9, pp. 194 - 204, 1971.

[47]   H. Y. Chou, A. P. Mouritz, M. K. Bannister and A. R. Bunsell, "Acoustic Emission analysis of composite pressure vessels under constant and cyclic pressure.," *Composites: Part A,* vol. 70, pp. 111 - 120, 2015.

[48]   M. Saeedifar M., M. Fotouhi, M. A. Najafabadi , H. H. Toudeshky and G. Minak, "Prediction of quasi-static delamiantion onset and growrg in

laminated composites by Acoustic Emission," *Composite Part B,* vol. 85, pp. 113 - 122, 2016.

[49]   T. H. Loutas , V. Kostopoulos , C. Ramirez-Jimenez and M. Pharaohc, "Damage evolution in center-holed Glass/Polyester composite under quasi-static loading using time/frequency analysis of Acoustic Emission monitored waveforms," *Compostes Science and Technology,* vol. 66, no. 10, pp. 1366 - 1375, 2006.

[50]   M. Saeedifar , M. A. Najafabadi , K. Mohammadi , M. Fotouhi, H. H. Toudeshky and R. Mohammaadi, "Acoustic Emission-based methodology to evaluate delamination crack growth under quasi-static and fatigue loading conditions," *Journal of Nondestructive Evaluation,* vol. 37, no. 1, 2018.

[51]   S. Benmedakhene , M. Kenane and M. L. Benzeggagh, "Initiation and growth of delamination on Glass/Epoxy composites subjected to static and dynamic Loading by Acoustic Emission monitoring," *Composite Science and Technology,* vol. 59, no. 2, pp. 201 - 208, 1999.

[52]   M. Saeedifar M and D. Zarouchas, "Damage characterization of laminated composites using Acoustic Emission: A review," *Composites Part B: Engineering,* vol. 195, no. 108039, 2020.

[53]   O. Ceysson, M. Salvia and L. Vincent, "Damage mechanisms characterisation of carbon fibre/epoxy composite laminates by both electrical resistance measurements and Acoustic Emission Analysis," *Scripta Mater,* vol. 34, pp. 1273 - 1280, 1996.

[54]   P. F. Liu , J. K. Chua , Y. L. Liu and J. Y. Zheng , "A study on the failure mechanisms of carbon/epoxy composite laminates using Acoustic Emission," *Material and Design,* vol. 37, pp. 228 - 235, 2012.

[55]   M. G. R. Sause , T. Müller, A. Horoschenkoff and S. Horn, "Quantification of failure mechanisms in mode-I loading of fiber reinforced plastic utilizing Acoustic Emission analysis," *Composite Science and Technology,* vol. 72, pp. 167 - 174, 2012.

[56]   A. J. Brunner, "Identification of damage mechanisms in fiber-reinforced polimer-matrix composite with Acoustic Emission and the challenge of

Reference

assessing structural integrity and service-life," *Construction and Building Materials* , vol. 173 , pp. 629 - 637, 2018.

[57]   M. Bourchak, I. R. Farrow, I. P. Bond , C. Rowland and F. Menana , "Acoustic Emission energy as a fatigue damage parameter for CFRP composites," *International Journal of Fatigue,* vol. 29, no. 3, pp. 457 - 470, 2007.

[58]   A. Marec , J. H. Thomas , El Guerjouma and R., "Damage characterization of polymer-based composite materials: Multivariable analysis and wavelet transform for clustering acoustic emission data," *Mechanical Systems and Signal Processing,* vol. 22, no. 6, pp. 1441 - 1464, 2008.

[59]   C. Liang, F. P. Sun and C. A. Rogers, "Coupled Electro – Mechanical analysis of adaptive material systems – Determination of the actuator power consumption and system energy transfer," *Journal of Intelligent Material Systems and Structures,* vol. 8, no. 4, pp. 335 - 343, 1994.

[60]   S. W. Zhou , C. Liang and C. A. Roger, "An Impedance – based system modeling approach for induced strain actuator – driven structures," *Journal of Vibration and Acoustics,* vol. 118, no. 3, pp. 323 - 331, 1996.

[61]   V. Giurgiutiu and A. N. Zangrai, "Embedded self-sensing piezoelectric active sensors for on-line structural identification (transaction of ASME)," *Journal of Vibration and Acoustics,* vol. 124, pp. 116 - 125, 2002.

[62]   F. P. Sun, Z. Chaudry, C. A. Rogers, M. Majmundar and C. Liang, "Automated real-time structure health monitoring via signature pattern recognition," *Proceedings of SPIE — The International Society for Optical Engineering Smart Structures and Materials: Smart Sensing, Processing, and Instrumentation,* vol. 2443, pp. 236 - 243, 1995.

[63]   Z. Chaudhry, T. Joseph, F. P. Sun and C. A. Rogers, "Local-area health monitoring of aircraft via piezoelectric actuator/sensor patches," *Proceedings, SPIE North American Conference on Smart Structures and Materials, San Diego, CA, 26 Feb–3 March, Vol 2443,* pp. 268 - 276, 1995.

[64]   V. G. M. Annamdas and C. K. Soh, "Embedded piezoeletric ceramic transducers in sandwiched beams," *Smart Materials and Structures,* vol. 12, pp. 538 - 549, 2006.

Reference

[65]   C. Bois, P. Herzog and C. Hochard, "Monitoring delamination in a laminated composite beam using in-situ measurements and parametric identification," *Journal of Sound and Vibration,* vol. 299, pp. 786 - 805, 2007.

[66]   W. Yan, J. B. Cai and W. Q. Chen, "Monitoring interfacial defects in a composite beam using impedance signatures," *Journal of Sound and Vibration,* vol. 326, pp. 340 - 352, 2009.

[67]   G. Park, H. Sohn and C. R. Farrar, "Overview of piezoelectric impedance-based health monitoring and path forward," *The Shock and Vibration Digest,* vol. 35, no. 6, 2003.

[68]   W. S. Na and J. Baek, "A review of the piezoelectric electromechanical impedance based structural health monitoring technique for engineering structures," *Sensors,* vol. 18, pp. 63 - 77, 2018.

[69]   H. Sohn , C. R. Farrar, F. M. Hemez and J. Czarnecki, "A Review of Structural Health Monitoring Literature: 1996-2001. Report no LA-13976-MS," Los Alamos National Laboratory, 2004.

[70]   E. P. Carden and P. Fanning, "Vibration based condition monitoring: a review," *Structural Health Monitoring,* vol. 3, no. 4, pp. 355 - 377, 2004.

[71]   D. Montalvão, N. M. M. Maia and A. M. R. Ribeiro, "A review on vibration-based structural health monitoring with special emphasis on composite materials," *The Shock and Vibration Digest,* vol. 38, no. 4, pp. 295 - 324, 2006.

[72]   W. Fan and P. Qiao, "Vibration-based Damage Identification Methods: A Review and Comparative Study," *Structural Health Monitoring,* vol. 10, no. 1, pp. 83 - 111, 2011.

[73]   J. S. Sakellariou, S. D. Fassois and S. Sakaris, "Vibration-based damage localization and estimation via the stochastic functional model based method (FMBM) – An overview," *Structural Health Monitoring,* vol. 17, no. 6, pp. 1335 - 1348, 2018.

Reference

[74]   R. D. Adams, P. Cawley, C. J. Pye and P. J. Stone, "A vibration technique for non-destructively assessing the integrity of structures," *Journal of Mechanical Engineering Science,* vol. 20, pp. 93 - 100, 1978.

[75]   P. Cawley and R. D. Adams, "The locations of defects in structures from measurements of natural frequencies," *Journal of Strain Analysis,* vol. 14, no. 2, pp. 49 - 57, 1979.

[76]   J. J. Tracy and G. C. Pardoen, "Effect of delamination on the natural frequencies of composite laminates," *Journal of Composite Materials,* vol. 23, pp. 1200 - 1215, 1989.

[77]   D. R. Sanders, Y. L. Kim and N. Stubbs, "Nondestructive evaluation of damage in composite structures using modal parameters," *Experimental Mechanics,* vol. 32, no. 3, pp. 240 - 251, 1992.

[78]   Z. Zhang, K. Shankar, E. V. Morozov and M. Tahtali, "Vibration-based delamination detection in composite beams through frequency changes," *Journal of Vibration and Control,* vol. 22, no. 2, pp. 496 - 512, 2014.

[79]   J. Pana, Z. Zhang , J. Wua, K. R. Ramakrishnan and H. K. Singh, "A novel method of vibration modes selection for improving accuracy of T frequency-based damage detection.ì," *Composites Part B,* vol. 159, pp. 437 - 446, 2019.

[80]   W. M. West, "Illustration of the Use of Modal Assurance Criterion to detect structural changes in an orbiter test specimen," *Procedia Air Force Conference on Aircraft Structural Integrity,* pp. 1 - 6, 1984.

[81]   A. K. Pandey, M. Biswas and M. M. Samman, "Damage detection from changes in curvature mode shapes," *Journal of Sound and Vibration,* vol. 145, pp. 321 - 332, 1991.

[82]   O. S. Salawu and C. Williams, "Damage location using vibration mode shapes," *International Modal Analysis Conference,* pp. 933 - 939, 1994.

[83]   C. H. J. Fox, "The location of defects in structures: A comparison on the use of natural frequency and mode shape data," in *Proceedings of the 10th*

International Modal Analysis Conference (IMAC X), San Diego, California, USA, pp. 522-528, 1992.

[84]   M. M. Abdel Wahab and G. De Roeck , "Damage detection in bridges using modal curvatures: Application to a real damage scenario," *Journal of Sound and Vibration,* vol. 226, pp. 217 - 235, 1999.

[85]   Y. K. Ho and D. J. Ewins, "On the structural damage identification with mode shapes," *. Proceedings of the European Conference on System Identification and Structural Health Monitoring, Madrid, Spain.,* p. 677 – 686, 2000.

[86]   S. Hanagud, Luo H. and W. Lestari, "Detection of an edge notch defect by using a single mode-based methods," *In: 43rd Structures, structural dynamics and materials conference, Denver, CO, 22–25 April 2002. Reston, VA: American Institute of Aeronautics and Astronautics (AIAA),* vol. 2, pp. 989 - 998, 2002.

[87]   C. S. Hamey, W. Lestari and P. Qiao, "Experimental damage identification of carbon/epoxy composite beams using curvature mode shapes," *Struct Health Monitoring,* vol. 3, no. 4, pp. 333 - 353, 2004.

[88]   W. Lestari and P. Qiao, "Damage detection of fiber-reinforced polymer honeycomb sandwich beams," *Composite Structures,* vol. 67, pp. 365 - 373, 2005.

[89]   P. Qiao, K. Lu, W. Lestari and J. L. Wang, "Curvature mode shape-based damage detection in composite laminated plates," *Composite Structures,* vol. 80, pp. 409 - 428, 2007.

[90]   W. Lestari, P. Qiao and S. Hanagud, "Curvature mode shape-based damage assessment of carbon/epoxy composite beams," *Journal of Intelligent Materials Systems and Structures,* vol. 18, pp. 189 - 208, 2007.

[91]   M. He, T. Yang and Y. Du, "Nondestructive identification of composite beams damage based on the curvature mode difference," *Composite Structures,* vol. 176, pp. 178 - 186, 2017.

Reference

[92]   L. Yam, Y. Yan and J. J., "Vibration-based damage detection for composite structures using wavelet transform and neural network identification," *Composite Structures,* vol. 60, no. 4, pp. 403 - 412, 2003.

[93]   M. S. Cao and P. Qiao, "Integrated wavelet transform and its application to vibration mode shapes for the damage detection of beam-type structures," *Smart Materials and Structures,* vol. 12, no. 055014, 2008.

[94]   W. Xu, M. S. Cao, W. Ostachowicz, M. Radzienski and N. Xia, "Two-dimensional curvature mode shape method based on wavelets and Teager energy for damage detection in plates," *Journal of Sound and Vibrations,* vol. 347, pp. 266 - 278, 2015.

[95]   R. Janeliukstis, S. Rucevskis, M. Wesolowski and A. Chate, "Experimental structural damage localization in beam structure using spatial continuous wavelet transform and mode shape curvature methods," *Measument,* vol. 102, pp. 253 - 270, 2017.

[96]   L. Rayleigh, "On waves propagated along the plane surface of an elastic solid," *Proceedings of the London Mathematical Society ,* vol. 17, no. 1, pp. 4 - 11, 1885.

[97]   H. Lamb, "On waves in elastic plate," *Proceedings of the Royal Society of London A,* vol. 95, pp. 114 - 128, 1917.

[98]   L. Ambrozinski, T. Stepinski and T. Uhl, "Efficient tool for designing 2D phased arrays in Lamb waves imaging of isotropic structures," *Journal of Intelligent Material Systems and Structures ,* vol. 26, no. 17, pp. 2283 - 2294, 2014.

[99]   M. Engholm and T. Stepinski, "Adaptative beamforming for array imaging of plate structures using Lamb waves," *IEEE Transactions on Ultrasonics, Ferroelectrics, and Frequency Control,* vol. 57, no. 12, pp. 2712 - 2724, 2010.

[100]   M. Engholm and T. Stepinski, "Direction of arrival estimation of Lamb waves using circular arrays," *Structural Health Monitoring,* vol. 10, no. 5, pp. 467 - 480, 2010.

Reference

[101]   T. Wandowski, P. H. Malinowski and W. M. Ostachowicz, "Circular sensing networks for guided waves based structural health monitoring," *Mechanical Systems and Signal Processing,* Vols. 66 - 67, pp. 248 - 267, 2016.

[102]   P. Malinowski, T. Wandowski, I. Trendafilova and W. M. Ostachowicz, "A phased-array-based method for damage detection and localization in thin plates," *Strucutral Health Monitoring,* vol. 8, no. 1, pp. 5 - 15, 2008.

[103]   Z. Su, L. Ye and Y. Lu, "Guided Lamb waves for identification of damage in composite structures: A review," *Journal of Sound and Vibration,* vol. 295, no. 3-5, pp. 753 - 780, 2006.

[104]   R. Chona, C. Suh and G. A. Rabroker, "characterizing defects in multi-layer materials using guided ultrasonic waves," *Optics and Lasers in Engineering,* vol. 40, no. 4, pp. 371 - 378, 2003.

[105]   H. Sohn, D. Dutta, J. Y. Yang, M. DeSimio, Olson S. and E. Swenson, "Automated detection of delamination and disbond from wavefield images obtained using a scanning laser vibrometer," *Smart Materials and Structures,* vol. 20, no. 4, p. 045017, 2011.

[106]   W. H. Leong, W. J. Staszewski, B. C. Lee and F. Scarpa, "Structural health monitoring using scanning laser vibrometry. Part III: Lamb waves for fatigue crack detection," *Smart Materials and Structures ,* vol. 14, no. 6, pp. 1387 - 1395, 2005.

[107]   K. Dziedziech, L. Pieczonka, P. Kijanka and W. J. Staszewski, "Enhanced nonlinear crack-wave interactions for structural damage detection based on guided ultrasonic waves," *Structural Control and Health Monitoring,* vol. 23, no. 8, pp. 1108 - 1120, 2016.

[108]   R. D. Mindlin, "Mathematical theory of Vibrations of elastic plates," *IEEE 11th Annual Symposium on Frequency Control - Asbury Park, NJ, USA ,* 1957.

[109]   D. E. Chimenti, "Guided waves in plates and their use in materials characterization," *ASME, Applied Mechanics Reviews,* vol. 50, no. 5, pp. 247 - 284, 1997.

Reference

[110]   I. A. Viktorov , Rayleigh and Lamb Waves - Physical theory and applications, Springer US, 1967.

[111]   D. C. Worlton, "Experimental confirmation of Lamb waves at megacycle frequencies," *Journal of Applied Physics,* vol. 32, pp. 967 - 971, 1961.

[112]   D. N. Alleyne and P. Cawley, "The interaction of Lamb waves with defects," *IEEE Transaction of Ultrasonic, Ferroelectris and Frequency Control,* vol. 39, no. 3, 1993.

[113]   P. Cawley and D. Alleyne, "The use of Lamb Waves for the long range inspection of large structures," *Ultrasonics,* vol. 34, pp. 287 - 290, 1996.

[114]   D. A. Saravanos, V. Birman and D. A. Hopkins, "Detection of delaminations in composite beams using piezoelectric sensors," *Proceedings of the 31st AIAA/ASME/ASCE/AHS/ASC/ Structures, Structural Dynamics and Materials Conference,* pp. 181 - 191, 1994.

[115]   M. D. Seale, B. T. Smith and W. H. Prosser, "Lamb wave assessment of fatigue and thermal damage in composites," *Journal of the Acoustical Society of America,* vol. 103, no. 5, pp. 2416 - 2424, 1997.

[116]   N. Toyama, J. Noda and T. Okabe, "Quantitative damage detection in cross-ply laminates using Lamb wave method," *Composite Science and Technology,* vol. 63, no. 10, pp. 1473 - 1479, 2003.

[117]   S. S. Kessler, S. M. Spearing and M. J. Atalla, "In-situ damage detection of composites structures using lamb waves methods," *Proceedings of the 1st European Workshop on Structural Health Monitoring, Ecole Noemale Supérieure, Cachan, Paris, France,* pp. 374 - 381, 2002.

[118]   Z. Su, L. Ye and X. Bu, "Evaluation of delamination in laminated composites based on Lamb waves methods: FEM simulation and experimental verification," *In Proceedings of the 1st European Workshop on Structural Health Monitoring, Ecole Noemale Supérieure, Cachan, Paris, France,* pp. 328 - 335, 2002.

Reference

[119]   H. Sohn, G. Park, J. R. Wait, N. P. Limback and C. R. Farrar, "Wavelet-based signal processing for detecting delamination in composite plates," *Smart Materials and Structures,* vol. 13, pp. 153 - 160, 2004.

[120]   A. D. Mitsheal, M. Diogo, D. Opukuro and H. George, "A review of Structural Health Monitoring techniques as applied to composite structures," *Structural Durability & Health Monitoring,* vol. 11, no. 2, pp. 91 - 147, 2017.

[121]   Y. Okabe, K. Fujibayashi, M. Shimazaki, H. Soejima and T. Ogisu, "Delamination detection in composite laminates using dispersion change based on mode conversion of Lamb waves," *Smart Materials and Structures,* vol. 19, no. 115013, 2010.

[122]   C. Ramadas, K. Balasubramaniam, M. Joshi and C. V. Krishnamurthy, "Interaction of guided Lamb waves with an asymmetrically located delamination in a laminated composite plate," *Smart Materials and Structures,* vol. 19, no. 065009, 2010.

[123]   W. Li, Y. Cho and J. D. Achenbach, "Detection of thermal fatigue in composites by second harmonic Lamb waves," *Smart Materials and Structures,* vol. 21, no. 085019, 2012.

[124]   B. Yang, F. Xuan, S. Chen, S. Zhou, Y. Gao and B. Xiao, "Damage localization and identification in WGF/epoxy composite laminates by using Lamb waves: Experiment and simulation," *Composite Structures,* vol. 165, pp. 138 - 147, 2017.

[125]   L. Pieczonka, L. Ambrozinski, J. W. Staszewski, D. Barnoncel and P. Pérès, "Damage detection in composite panels based on mode-converted Lamb waves sensed using laser scanning vibrometer," *Optics and Laser in Engineering,* vol. 99, pp. 80 - 87, 2017.

[126]   L. Zeng, L. Huang and J. Lin, "Damage imaging of composite structures using multipath scattering Lamb waves," *Composite Structures,* vol. 216, pp. 331 - 339, 2019.

[127]   J. D. Achenbach, Wave propagation in elastic solids, North-Holland Publishing COmpany, 1973.

Reference

[128]   I. Y. Solodov, N. Krohn and G. Busse, "CAN: an example of nonclassical acoustic nonlinearity in solids," *Ultrasonics,* vol. 40, no. 1-8, pp. 621 - 625, 2002.

[129]   C. Pecorari and I. Y. Solodov, "Nonclassical nonlinear dynamics of solid surfaces in partial contact for NDE applications," *Springer,* pp. 309 - 326 , 2006.

[130]   J. H. Cantrell and W. Yost, "Nonlinear ultrasonic characterization of fatigue microstructures," *Interantion Journal of Fatigue,* vol. 23, no. 1, pp. 487 - 490, 2001.

[131]   J. Frouin, S. Sathish, T. E. Matikas and J. K. Na, "Ultrasonic linear and nonlinear behavior of fatigued Ti–6Al–4V," *Journal of Materials Research,* vol. 14, no. 4, pp. 1295 - 1298, 1999.

[132]   J. K. Na, J. H. Cantrell and W. T. Yost, "Linear and nonlinear ultrasonic properties of fatigued 410Cb stainless steel," in *Thompson DO, Chimenti DE, editors. Review of progress in quantitative nondestructive evaluation, vol. 14*, vol. 14, New York: Plenum, 1996, pp. 1347 - 1353.

[133]   D. C. Hurley, D. Balzer, P. T. Purtscher and K. W. Hollman, "Nonlinear ultrasonic paramter in quenched martensitic steels," *Journal of Applied Physics,* vol. 83, pp. 4584 - 4588, 1998.

[134]   P. B. Nagy, "fatigue damage assessment by nonlinear ultrasonic material characterization," *Ultrasonics,* vol. 36, pp. 375 - 381, 1998.

[135]   I. Solodov, K. Pfleiderer and G. G. Busse, "Nonlinear acoustic approach to material characterisation of polymers and composites in tensile tests," *Ultrasonics,* vol. 42, no. 1-9, pp. 1011 - 1015, 2004.

[136]   N. Rauter and R. Lammering, "Impact damage detection in composite strucutres considering nonlinear Lamb wave propagation," *Mechanics of Advanced Materials and Structures,* vol. 22, no. 1 - 2, pp. 1647 - 1654, 2015.

[137]   R. Guyer and P. A. Johnson, "Nonlinear mesoscopic elasticity: evidence for a new class of materials," *Physics Today,* vol. 52, no. 4, pp. 30 - 36, 1999.

Reference

[138]   L. K. Zarembo, V. A. Krasil'nikox and I. E. Shkol'nik, "Nonlinear acoustics in a problem of diagnosing the strength of solids," *Problemy Prochnosti,* vol. 21, no. 11, pp. 86 - 92, 1989.

[139]   M. Meo, U. Polimeno and G. Zumpano, "Detecting damage in composite material using nonlinear elastic wave spectroscopy methods," *Applied Composite Materials,* vol. 15, no. 3, pp. 115 - 126, 2008.

[140]   S. K. Chakrapani and D. J. Barnard, "Determination of acoustic nonlinearity parameter (β) using nonlinear resonance ultrasound spectroscopy: Theory and experiment," *The Journal of the Acoustical Society of America,* vol. 141, no. 919, 2017.

[141]   K. Van Den Abeele and K. Van De Velde, "Correlation between dynamic nonlinearity and static mechanical properties of corroded E-glass reinforced polyester composites," *AIP Conference Proceedings,* vol. 509, no. 1, pp. 1359 - 1365, 2000.

[142]   K. Van Den Abeele, P. Y. Le Bas, B. Van Damme and T. Katkowski, "Quantification of material nonlinearity in relation to microdamage density using nonlinear reverberation spectroscopy: Experimental and theoretical study," *The Journal of the Acoustical society of America,* vol. 126, no. 3, pp. 963 - 972, 2009.

[143]   Q. Wie, Z. Liyong, J. zhu, L. Zhuo, W. Hao and W. Xie, "Characterization of impact fatigue damage in CFRP composites using nonlinear acoustic resonance method," *Composite Structures,* vol. 253, no. 112804, 2020.

[144]   U. Ingard and D. C. Pridmore-Brown, "Scattering of sound by sound," *The Journal of the Acoustical Society of America,* vol. 28, no. 3, pp. 367 - 369, 1956.

[145]   L. A. Ostrovsky, S. N. Gurbatov and J. N. Didenkulov, "Nonlinear acoustic in Nizhni Novgorod (A review)," *Acoustical Pysics,* vol. 51, no. 2, pp. 114 - 127, 2005.

[146]   K. E. A. Van Den Abeele, P. A. Johnson and A. Sutin, "Nonlinear elastic Wave Spectroscopy (NEWS) techniques to discern material damage.

Reference

Part I: Nonlinear Wave Modulation Spectroscopy," *Research in Nondestructive Evaluation,* vol. 12, no. 1, pp. 17 - 30, 2000.

[147]   H. Sohn, H. J. Lim, M. P. DeSimio, K. Brown and M. Derriso, "Fatigue crack detection using guided waves nonlinear modulation," *SPIE Proceedings,* vol. 8695, 2013.

[148]   V. Y. Zaitsev, A. M. Sutin, I. Y. Belyaeva and V. E. Nazarov, "Nonlinear interaction of acoustical waves due to cracks and its possible usage for cracks detection," *Journal of Vibration and Control,* vol. 1, no. 3, pp. 335 - 344, 1995.

[149]   A. M. Sutin and D. M. Donskoy, "Vibro-Acoustic Modulation nondestructive evaluation technique," *SPIE Proceedings - The International Society for Optical Engineering,* vol. 3397, pp. 226 - 237, 1998.

[150]   A. S. Koroktov, M. M. Slavinskii and A. M. Sutin, "Variations of acoustic nonlinear parameters with the concentration of the defects in steel," *Acoustical Physics,* vol. 40, no. 1, pp. 71 - 74, 1994.

[151]   A. M. Sutin and V. E. Nazarov, "Nonliear Acoustic Methods of crack diagnostic," *Radiophysics and Quantum Electronics,* vol. 39, no. 3-4, pp. 109 - 120, 1995.

[152]   V. Zaitsev and P. Sas, "Nonlinear response of a weakly damaged metal sample: A dissipative modulation mechanism of vibro-acoustic interaction," *Journal of Vibration and Control,* vol. 6, pp. 803 - 822, 2000.

[153]   N. A. Chrysochoidis, T. T. Assimakopoulou and D. Saravanos, "Nonlinear wave structural health monitoring method using an active nonlinear piezoceramic sensor for matrix cracking detection in composites," *Journal of Intelligent Material Systems and Structures,* vol. 26, no. 15, pp. 2108 - 2120, 2015.

[154]   F. Aymerich and J. W. Staszewski, "Impact damage detection in composite laminates using nonlinear acoustics," *Composites Part A: Applied Science and Manufacturing,* vol. 41, no. 9, pp. 1084 - 1092, 2010.

[155]   N. A. Chrysochoidis, A. K. Toulitsis and D. A. Saravanos, "Impact damage detection in composites using an active nonlinear acousto-ultrasonic

piezoceramic sensor," *Proceedings of SPIE - The International Society for Optical Engineering,* vol. 7981, 2011.

[156]   M. Meo and G. Zumpano, "Nonlinear elastic wave spectroscopy identification of impact damage on a sandwich plate," *Composite Structures,* vol. 71, no. 3, pp. 469 - 474, 2005.

[157]   A. Klepka, W. J. Staszewski, D. Di Maio and F. Scarpa, "Impact damage detection in composite chiral sandwich panels using nonlinear vibro-acoustic modulations.," *Smart Materials and Structures,* vol. 22, no. 8, p. 084011, 2013.

[158]   V. Y. Zaitsev, V. Gusev and B. Castagnede, "Observation of the "Luxemburg-Gorky effect" for elastic waves," *Ultrasonics,* vol. 40, no. 1-8, pp. 627 - 631, 2002.

[159]   B. D. H. Tellegen, "Interacrion between radiowaves?," *Nature,* vol. 131, no. 840, 1933.

[160]   V. Y. Zaitsev, V. E. Nazarov, V. Tournat, V. E. Gusev and B. Castagnede, "Luxemburg-Gorky effect in a granular medium: Probing perturbations of the material state via cross-modulation of elastic waves," *EPL (Europhysics Letters),* vol. 70, no. 5, pp. 607 - 613, 2005.

[161]   L. Fillinger, V. Y. Zaitsev, V. E. Gusev and B. Castagnede, "Nonlinear relaxational absorption/ transparency for acoustic waves due to thermoelastic effect," *Acta acustica united with acustica,* vol. 92, no. 1, pp. 24 - 34, 2006.

[162]   D. Donskoy, A. Zagrai, A. Chudnovsky, E. Golovin and V. Agarwala, "Nonlinear Vibro-Acoustic Modulation technique for lLife prediction of aging aircraft components," in *Structural Health Monitoring 2006: Proceedings of the Third European Workshop*, 2006, pp. 251 - 258.

[163]   C. J. Lissenden, Y. Liu, G. W. Choi and X. Yao, "Effect of localized microstructure evolution on higher harmonic generation of guided waves.," *Journal of Nondestructive Evaluation,* vol. 33, pp. 178 - 186, 2014.

Reference

[164]   A. A. Shaha and Y. Ribakov, "Non-linear ultrasonic evaluation of damaged concrete based on higher order harmonic generation," *Material and Design,* vol. 30, pp. 4095 - 4102, 2009.

[165]   P. B. Dao, A. Klepka, L. Pieczonka, F. Aymerich and W. J. Staszewski, "Impact damage detection in smart composites using nonlinear acoustics - cointegration analysis for removal of undesired load effect," *Smart Materials and Structures,* vol. 26, no. 035012, 2017.

[166]   L. Pieczonka, L. Zietek, A. Klepka, W. J. Staszewski and F. Aymerich, "Damage imaging in composites using nonlinear vibro-acoustic wave modulations.," *Structural Control and Helath Monitoring,* vol. 25, no. e2063, 2018.

[167]   M. Scalerandi, A. S. Gliozzi, C. L. E. Bruno, D. Masera and D. Bocca, "A scaling method to enhance detection of a nonlinear elastic response," *Applied Physics Letters,* vol. 92, p. 101912, 2008.

[168]   C. L. E. Bruno, A. S. Gliozzi, M. Scalerandi and P. Antonaci, "Analysis of elastic nonlinearity using the scaling subtraction method," *Physical Review B,* vol. 79, no. 6, p. 064108, 2009.

[169]   P. Antonaci, C. L. E. Bruno, P. G. Bocca, M. Scalerandi and A. S. Gliozzi, "Nonlinear ultrasonic evaluation of load effect on discontinuities in concrete," *Cement and Concrete research,* vol. 40, no. 2, pp. 340 - 346, 2010.

[170]   P. Antonaci, C. L. E. Bruno, A. S. Gliozzi and M. Scalerandi, "Monitoring evolution of compressive damage in concrete with linear and nonlinear ultrasonic methods," *Cement and Concrete Research,* vol. 40, no. 7, pp. 1106 - 1113, 2010.

[171]   M. Scalerandi, M. Griffa, P. Antonaci, M. Wyrzykowski and P. Lura, "Nonlinear elastic response of thermally damaged consolidated granular media," *Journal of Applied Physics,* vol. 113, no. 154902, 2013.

[172]   M. C. Porcu, L. Pieczonka, A. Frau, W. J. Staszewski and F. Aymerich, "Assessing the Scaling Subtraction Method for Impact damage detection in composite plates," *Journal of Nondestructive Evaluation,* vol. 36, no. 33, 2017.

Reference

[173]   G. Loi, M. C. Porcu and F. Aymerich, "Impact damage detection in composite beams by analysis of non-linearity under pulse excitation," *Journal of Composite Science,* vol. 5, no. 2, p. 39, 2021.

[174]   M. A. Ouarabi, P. Antonaci, F. Boubenider, A. Gliozzi and M. Scalerandi, "Ultrasonic monitoring of the interaction between cement matrix and alkaline silicate solution in self-healing systems," *Materials,* vol. 10, no. 46, 2017.

[175]   A. Frau, L. Pieczonka, M. C. Porcu, J. W. Staszewski and F. Aymerich, "Analysis of elastic nonlinearity for impact damage detection in composite laminates," *Journal of Physics: Conference Series,* vol. 628, no. 012103, 2015.

[176]   N. C. Yoder and D. E. Adams, "Vibro-Acoustic modulation utilizing a swept probing signal for robust crack detection," *Structural Health Monitoring,* vol. 9, no. 2, pp. 257 - 267, 2010.

[177]   H. Sohn, H. J. Lim, M. P. DeSimio, K. Brown and M. Derriso, "Nonlinear ultrasonic wave modulation for online fatigue crack detection," *Journal of Sound and Vibration,* vol. 333, pp. 1473 - 1484, 2013.

[178]   K. Klepka, W. J. Staszewski, K. Dziedziech and F. Aymerich, "Non-linear Vibro-Acoustic Wave Modulation - Analysis of different types of low-frequency excitation," *Key Engineering Materials,* Vols. 569 - 570, pp. 924 - 931, 2013.

[179]   L. Pieczonka, A. Klepka, M. Adamczyk, W. J. Staszewski, F. Aymerich and T. Uhl, "Optimal selection of parameters for impact damage detection in composites based on nonlinear vibro-acoustic modulation," in *ECCM16 - 16th European conference on Composite Materials*, Seville, Spain, June 2014.

[180]   A. J. Hillis, S. A. Neild, B. W. Drinkwater and P. D. Wilcox, "Global crack detection using bispectral analysis," *Proceedings of the Royal Society A: Mathematichal, Physical and Engineering Sciences,* vol. 462, no. 2069, pp. 1515 - 1530, 2006.

[181]   A. M. Sutin and P. A. Johson, "Nonlinear elastic wave NDE II. Nonlinear Wave Modulation Spectroscopy and nonlinear time reversed acoustics," *AIP Conference Proceedings,* vol. 760, pp. 385 - 392, 2005.

Reference

[182]   T. J. Ulrich, A. M. Sutin, R. A. Guyer and P. A. Johnson, "Time reversal and non-linear elastic wave spectroscopy (TR NEWS) techniques," *International Journal of Non-Linear Mechanics,* vol. 43, no. 4, pp. 209 - 216, 2008.

[183]   K. Dziedziech, L. Pieczonka, M. Adamczyk, A. Klepka and J. W. Staszewski, "Efficient swept sine chirp excitation in the non-linear vibro-acoustic wave modulation technique used for damage detection," *Structural Health Monitoring,* vol. 17, no. 3, pp. 565 - 576, 2017.

[184]   P. B. Dao, A. Klepka, L. Pieczonka, F. Aymerich and J. W. Staszewski, "Impact damage detection in smart composites using nonlinear acoustics—cointegration analysis for removal of undesired load effect," *Smart Materials and Structures,* vol. 26, no. 035012, 2017.

[185]   M. Morbidini, P. Duffour and P. Cawley, "Vibro-Acoustic Modulation NDE technique. Part 2: experimental study," *AIP Conference Proceedings,* vol. 760, no. 616, 2005.

[186]   P. Duffour, M. Morbidini and P. Cawley, "A study of the vibro-acoustic modulation technique for the detection of cracks in metals," *The Journal of the Acoustical Society of America,* vol. 119, no. 1463, 2006.

[187]   A. Klepka, J. W. Staszewski, R. B. Jenal, M. Szwedo, J. Iwaniec and T. Uhl, "Nonlinear acoustics for fatigue crack detection – experimental investigations of vibro-acoustic wave modulations," *Structural helath Monitoring,* vol. 11, no. 2, pp. 197 - 211, 2012.

[188]   J. Jiao, L. Zheng, G. Song, C. he and B. Wu, "Vibro-acoustic modulation technique for micro-crack detection in pipeline," *Proc. SPIE 8321, Seventh International Symposium on Precision Engineering Measurements and Instrumentation,* vol. 83213X, 2011.

[189]   A. Zagrai, D. Donskoy, A. Chudnovsky and E. Golovin, "Micro- and macroscale damage detection using the nonlinear acoustic vibro-modulation technique," *Research in Nondestructive Evaluation,* vol. 19, no. 2, pp. 104 - 128, 2008.

[190]   F. Aymerich and J. W. Staszewski, "Experimental study of impact-damage detection in composite laminates using a Cross-Modulation Vibro-Acoustic technique," *Strctural Health Monitoring,* vol. 9, no. 6, pp. 541 - 553, 2010.

[191]   A. Klepka, L. Pieczonka, W. J. Staszewski and F. Aymerich, "Impact damage detection in laminated composites by non-linearvibro-acoustic wave modulations," *Composites: Part B,* vol. 65, pp. 99 - 108, 2014.